Catalytic Gasification and Assessment of Dimethyl Ether Synthesis from Victorian Brown Coal

by

Kazi Bayzid Kabir

A thesis submitted in fulfillment of the requirements
for the degree of Doctor of Philosophy

in the

Department of Chemical Engineering
Faculty of Engineering
Wellington Road, Clayton
VIC-3800, Australia

July 2014

This page intentionally left blank

General Declaration

I hereby declare that this thesis contains no material which has been accepted for the award of any other degree or diploma at any university or other equivalent institution. To the best of my knowledge and belief, this thesis contains no material previously published or written by another person, except where due reference is made in the text of the thesis.

Kazi Bayzid Kabir

This page intentionally left blank

"Knowledge is indivisible. When people grow wise in one direction, they are sure to make it easier for themselves to grow wise in other directions as well. On the other hand, when they split up knowledge, concentrate on their own field, and scorn and ignore other fields, they grow less wise - even in their own field."

ISAAC ASIMOV, *The Roving Mind*

This page intentionally left blank

Abstract

This is the first ever study assessing the possibility of dimethyl ether (DME) production through gasification of Victorian brown coal. This project involves gasification of Victorian brown coal and catalyst development for syngas to DME conversion process.

Victoria has large reserves of brown coal, 430 billion tonnes at current estimate. Use of Victorian brown coal is currently limited mostly to mine-mouth power generation because of high moisture content of the as-mined coal and high reactivity of the dried coal; both these properties make Victorian brown coal, raw or dried, unexportable. Gasification based alternative processing paths can provide export market for brown coal derived products, and more energy efficient application of brown coal. Syngas from Victorian brown coal can be catalytically converted into DME with higher energy efficiency and at potentially lower CO_2 emission. DME is a non-toxic, non-carcinogenic and non-corrosive compound. In addition, it has wide application as a fuel in cars, gas turbines, fuel cells and household applications.

A process simulation for as-mined Victorian brown coal to DME was performed using ASPEN Plus. The simulation study shaped the experimental matrix as it provided a realistic range of operating conditions (e.g. gasification temperature and syngas H_2 to CO ratio). CO_2 Gasification kinetics for raw parent coal as well as demineralised and catalyst-loaded (Ca, Fe) coals were studied using a thermogravimetric analyser. Pyrolysis and gasification of the coal was performed in an entrained flow reactor (EFR) and the solid, liquid and gaseous products were characterised. DME synthesis experiments were performed in a high pressure fixed-bed reactor, using commercial and developed catalysts, and synthetic syngas consisting H_2 and CO. A 3^2 factorial experimental design was used to optimise catalyst composition and syngas ratio (H_2 to CO). The developed catalysts were prepared based on the information generated from preliminary experiments with commercial catalysts. Physical mixing and coprecipitation-impregnation methods were used for the preparation of bi-functional DME synthesis catalysts. Performance (CO conversion, DME yield and DME selectivity) of the developed catalysts was compared with that of commercial catalysts. Effects of sulphur poisoning on CO-conversion, DME yield and DME selectivity were also studied.

Process simulation using ASPEN plus showed that the low temperature gasification at 900°C can produce syngas with appropriate H_2 to CO ratio. The ratio was found

to be 0.81 at the gasifier outlet (before the recycle stream) and 1.41 at the DME reactor inlet (after the recycle stream). The overall process efficiency was found to be $\sim$ 32% after considering the energy penalty for CO_2 separation, higher than the power generation efficiency of 28% (without CO_2 separation).

Two kinetic models (Grain model and random pore model) were used to find the intrinsic CO_2 gasification kinetics. Random pore model predicted the experimental results better than the grain model. The activation energy for char-CO_2 gasification was $\sim$189 kJ/mol. Ca-loaded coal char showed better gasification reactivity. However, addition of iron did not show any improvement. The results indicate that the effect of minerals become insignificant at 1000 °C or above and catalytic gasification showed be carried out below this temperature. EFR studies showed that the tar yield rapidly decreased as the gasification temperature was increased. The residence time and gasification temperature in the EFR were not enough for complete carbon conversion.

In situ synchrotron radiation X-ray diffraction on methanol and DME synthesis catalysts showed rapid catalyst deactivation at temperatures above 300°C, resulted from phase mobility and thermal sintering. The extent of deactivation was higher for the bi-functional DME catalyst compared to the methanol synthesis catalyst.

Regression analysis on the yield data, obtained using commercial catalysts, showed that a H_2 to CO ratio of 1.45 and a catalyst consisting 58% methanol synthesis component results maximum DME yield.

Among the four developed catalysts (DSC-1, DSC-2, DSC-M, DSC-1-PRE), three catalysts (except DSC-1-PRE) showed performance similar or better than the commercial catalyst mixture M1A1. CO conversion was between 67-70% for the DSC-1 catalyst, best among the developed catalysts, compared to 58-60% conversion for the M1A1 catalyst. DME yield was 36-40% and 35-38% for the DSC-1 and M1A1, respectively.

A 10 hour exposure of the catalyst to 103 ppm H_2S showed at least 12% reduction in conversion and yield, indicating rapid deactivation in the catalyst activity.

All the results were at least duplicated, and triplicated in most of the cases. The obtained results positively indicate that the conversion of syngas from Victorian brown coal to DME is a feasible option.

Acknowledgements

The author expresses his sincere thanks to Professor Sankar Bhattacharya for accepting him as a PhD student. The author would also like to express his profound respect to Professor Bhattacharya for his valuable guidance and supervision throughout the entire work.

The author also appreciates valuable advice from Dr David Harris and Dr Daniel Roberts of CSIRO in the early stage, and from Professor Klaus Hein at various stages of the research.

The author greatly appreciates the support he has received from Mr Chiranjib Saha, Mr David Stokie, Ms Kathryn Waldron, Ms Niema Allen and Ms Yao Zeng for helping him to settle down in his early days at Monash Univesity. The author would like to thank Post Doctoral research fellows in the research group: Dr Ali Akhavan, Dr Luguang Chen, Dr Anthony Auxilio, Dr Wei Lit Choo and Dr Srikanth Chakravartula Srivatsa for helping him with the training, experiment design and performance, and analysis throughout the PhD tenure.

The author would like to gratefully acknowledge the help and contribution from two fellow PhD students, Mr Kawnish Kirtania and Mrs Joanne Tanner, with whom he closely worked in the laboratory. Critical discussions with them over cups of Assam tea are invaluable to the author.

The author would like to thank his office mate Ms Sunaina Dayal for sharing her joy and cheerfulness.

The author thanks Ms Helen Maynard-Casely (Australian Synchrotron; currently working in ANSTO) for helping him with the analysis of the synchrotron radiation XRD data. He would also like to thank Mrs Joanne Tanner, Ms Sunaina Dayal, Ms Luguang Chen, Mr Sharmen Rajendran and Mr Kawnish Kirtania for helping him in the experiments performed at Australian Synchrotron. Special thanks to Dr Arash Tahmasebi (Associate Professor, University of Science and Technology Liaoning, China) for helping the author with TGA experiments.

The author would like to acknowledge Ms Lilyanne Price for her guidance regarding the academic issues and Mrs Jill Crisfield for helping with the administrative matters. The author would like to thank Mr Garry Thunder for fast forwarding the purchase requisitions, and Mr Ronald Graham and Ms Kim Phu for educating him with the safety and laboratory procedures at Monash University. Thanks to Mr Ross Ellingham for preparing the coal sample. Special thanks goes Daniel Campbell and Martin Watkins for helping him to set up the experimental rig. The author also gratefully acknowledges help from Mr Harry Bouwmeester for fabrication and machining of the reactor. Thanks to Mr Gamini Ganegoda for electrical and computer related work.

Brown Coal Innovation Australia (BCIA), Department of State Development, Business and Innovation, and Monash University are acknowledged for the financing the project. Experimental facilities at Monash Centre for Electronic Microscopy (MCEM) and Australian Synchrotron (AS) were also used for analysis.

This page intentionally left blank

Contents

List of Figures

This page intentionally left blank

List of Tables

This page intentionally left blank

Abbreviations

AAEM	Alkaline and alkaline earth metals
ASAP	Accelerated surface area and porosimetry system
ASU	Air separation unit
ATR	Auto-thermal reforming
BET	Brunauer-Emmett-Teller
BPR	Back pressure regulator
CC	Combined cycle
CCS	Caron capture and storage
CEC	California Energy Commission
CGRT	Chemically recuperated gas turbine
CLC	Chemical looping combustion
CI	Compression-ignition
CPR	Curie-point reactor
COED	Char Oil Energy Development
CP	Co-precipitation
COP	Coefficient of performance
CPI	Co-precipitation impregnation
CPS	Co-precipitation sedimentation
daf	Dry ash free
D-R	Dubinin-Radushkevich
DCL	Direct coal liquefaction
DDEFC	direct dimethyl ether fuel cell
DFT	Density functional theory
DICI	Direct injection compression-ignition
DLFC	Direct liquid-feed fuel cell
DLN	Dry-Low-NO_x
DME	Dimethyl ether
DTG	Differential thermogravimetry
DTO	DME-to-olefins
DTP	DME to propylene
DTR	Drop-tube reactor

EDX	Energy-dispersive X-ray spectroscopy
EFR	Entrained-flow reactor
EGR	exhaust gas recirculation
ETBE	Ethyl tert-butyl ether
FBR	Fluidised-bed reactor
FC	Fuel cell
FEG	Field emission gun
FR	Fuel ratio
FTD	Fischer-Tropsch diesel
FTIR	Fourier transform infrared spectroscopy
FTL	Fischer-Tropsch liquid
FTS	Fischer-Tropsch synthesis
FWHM	full width at half maximum
GCR	Generalised comprehensive reactor
GHG	Greenhouse gas
GM	Grain model
GWP	Global warming potential
HC	Hydrocarbons
HRSG	Heat recovery steam generator
HTXRD	High temperature X-ray diffraction
ICL	Indirect coal liquefaction
IDGCC	Integrated drying and gasification combined cycle
IGCC	Integrated gasification combined cycle
IMP	Impregnation
IPCC	Intergovernmental panel on climate change
IRM	Infrared Microspectroscopy
LCA	Life cycle analysis
LHHW	Langmuir-Hinshelwood-Hougen-Watson
LHV	Lower heating value
LPDME	Liquid-phase DME
LPG	Liquified petroleum gas
LY	Loy Yang
MCFC	Molten carbonate fuel cell
MCT	Mercury Cadmium Telluride
MDC	Methanol dehydration catalyst
MFC	Mass flow controller

MGT	Micro gas turbines
MHI	Mitsubishi Heavy Industries
MSC	Methanol synthesis catalyst
MTBE	Methyl tert-butyl ether
MTG	Methanol to gasoline
MTO	Methanol to olefins
MW	Morwell
NG	Natural gas
PAFC	Phosphoric acid fuel cell
PCF	Pulverised coal-fired
PEC	Primary energy consumption
PEMFC	Proton exchange membrane fuel cell
PISI	Plug-injection spark-ignition
PM	Physical mixing
POX	Partial oxidation
PR	Peng-Robinson
RK	Redlich-Kwong
RPM	Random pore model
SDY	Steam dealuminated Y
SECV	State Electricity Commission of Victoria
SEM	Scanning electron microscopy
SG	Sol-gel
SGI	Sol-gel impregnation
SI	Spark-ignition
SIGT	Steam-injected gas turbine
SNG	Synthetic natural gas
SOFC	Solid oxide fuel cell
SR	Steam reforming
SRK	Soave-Redlich-Kwong
STD	Syngas to DME
TAME	Tert-amyl methyl ether
TEM	Transmission electron microscopy
TGA	Thermogravimetric analyser
TPD	Temperature programmed desorption
TPR	Temperature programmed reduction
TTW	Tank-to-wheels

XRD	X-ray diffraction
WGS	Water gas shift
WMR	Wire-mesh reactor
WTT	Well-to-tank
WTW	Well-to-wheel
WWF	World Wide Fund for nature
YL	Yallourn

Symbols

ΔG	Gibbs energy of reaction	kJ/mol
ΔH	heat of reaction	kJ/mol
λ	wavelength	m
θ	angle of reflection	
A_i	ash content	g /g
B	D-R structural constant	K^{-2}
c	BET constant	
E_a	activation energy	kJ/mol
f_i	fugacity of component i	N/m^2
F_{IN}	molar flow of reactor feed	mol/h
F_{OUT}	molar flow of reactor outlet	mol/h
k	specific reaction constant	s^{-1}
k_0	transfer number	s^{-1}
K_{f_i}	equilibrium constant of the reaction i	
K_i	adsorption constant of component i	
n_i	number of moles of component i	mol
p	partial vapour pressure of adsorbate gas	N/m^2
p_0	saturated pressure of adsorbate gas	N/m^2
R^2	Coefficient of determinations	
T	temperature	K
t	time	s
v	adsorbed gas quantity	m^3
v_0	micropore capacity	m^3
v_m	monolayer adsorbed gas quantity	m^3
W	mass	g
x	char conversion	g/g
X_i	mole fraction of species i in the reactor inlet stream	mol/mol
Y_i	mole fraction of species i in the reactor outlet stream	mol/mol
YI_{DME}	Yield of DME	mol/mol

This page intentionally left blank

Chapter 1

Introduction

1.1 Background

Secure and sustainable energy source is a major requirement for the economic stability and development. Fossil fuels are still the major source of world's primary energy supply. In 2009, oil, natural gas and coal's share to the total global energy consumption were 34.8, 23.8 and 29.4%, respectively [1]. With sharp rise in the energy demand in developing countries (e.g. China, India), the scenario is not going to change in near future.

The problems associated with the extensive use of fossil fuels are predominantly environmental. Between 2007 and 2008, CO_2 emission from coal, oil and natural gas consumption increased by 3.0, 0.7 and 2.6%, respectively [2]. Since the growing energy demand is currently met by coal, a substantial increase in the CO_2 emission is expected if proper measures are not taken. In this current trend, global CO_2 emission is expected to be doubled by 2050 [3]. CO_2 is one of the long-lived greenhouse gases (GHG), it has consequential effects on climate. Increase in the average air and ocean temperature could result widespread melting of ice cap, leading to a rise in the sea level. Intergovernmental Panel on Climate Change (IPCC) predicts increased stress on coastal communities and habitats, freshwater scarcity, loss of bio-diversity, more frequent drought, floods and wildfires all over the world due to anthropogenic warming of the atmosphere [4]. However, it is very unlikely that the consumption of fossil fuels will reduce in the near future. Development of advanced and novel technologies are necessary to make sure that there is a net reduction in anthropogenic GHG emission without hindering necessary economic activities.

Section 1.1 is excerpted from: Bhattacharya S, Kabir KB and Hein K, *progress. energy combust. sci*, 39: 577-605

Table 1.1: Typical properties of Victorian brown coals [9]

Carbon[1]	65-70 wt%
Oxygen[1]	25-30 wt%
Hydrogen[1]	4.0-6.0 wt%
Nitrogen[1]	0.36-0.85 wt%
Sulphur[1]	0.14-5.36 wt%
Ash[2]	0.5-12.8 wt%
Moisture	43.7-71.0 wt%
Energy value (gross dry)	25-29 MJ/kg
Energy value (net wet)	5.24-13.87 MJ/kg

[1]dry ash free basis
[2]dry basis

Victoria has an abundance of fossil fuels: oil, gas and coal. As a result, energy system in Victoria is heavily dependent on indigenous cheap primary energy sources (e.g. coal and gas). Among them, brown coal currently contributes 47% of Victoria's total energy needs. The power generation sector is heavily dependent on coal. In 2008-2009, 90% of total electricity was generated in brown coal-fired power plants [1].

Brown coals, also referred to as lignite in literature, are of the lowest rank among different coals. Victorian brown coals are distributed in three different basins: the comparatively shallow Murray basin and the deeper Otway and Gippsland basins. The coal reserve in the Murray and Otway basins are 19,600 and 15,500 million tonnes respectively [5]. The Gippsland basin is larger than the other two and has an estimated reserve of 65,000 million tonnes of brown coal [6]. Brown coal seams in the Gippsland basin are typically located under 10-20 metres of overburden. The shallow depth of overburden combined with high coal to overburden ratio (between 0.5:1 and 5:1) make it one of the low cost energy source in the world [7].

Victorian brown coals have low carbon content, 25-35% (65-70%, dry ash free (daf) basis) of raw coal. More than half of the carbon present in the coal is of aromatic nature. Rest of the carbon is present in aliphatic chains and in various functional groups. Brown coals have high oxygen content. Oxygen is present as $-COOH$, $-OH$, ether or carbonyl forms. The sulphur content in as-mined Yallourn (YL) and Morwell (MW) coals ranges between 0.2-0.4% on dry basis. Sulphur present in Victorian brown coals is mostly organic [8]. Typical properties of Victorian brown coal are shown in Table 1.1 [9].

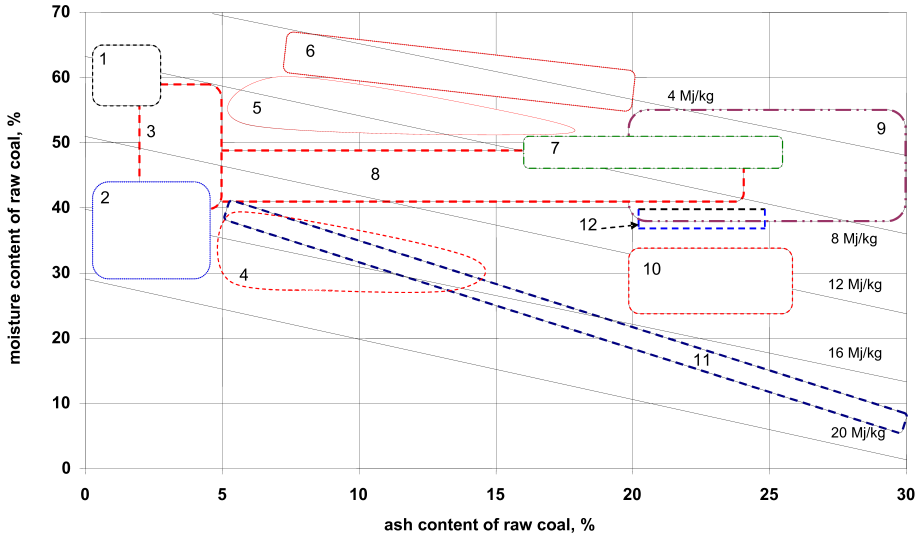

FIGURE 1.1: Comparison of different low rank coals 1: Australia; 2: Indonesia; 3:India; 4: USA (Texas, North Dakota); 5: Germany; 6: Greece; 7: Spain; 8: Poland; 9: Czech Republic; 10: China; 11: Turkey; 12: Romania [10]

A comparison of the properties of the low rank coals around the world is shown in Figure 1.1 [10]. It shows the unique nature of Victorian brown coals with high moisture and low ash content compared to other low ranked coals (Located in the top right).

Another notable feature of Victorian brown coals is the presence of significant amount of alkaline and alkaline earth metal (AAEM). Though the total content of the AAEM is less than 1% of as-mined coal, they play a very important role in coal utilisation. If sodium to ash yield ratio is greater than 0.12 then there is a chance of fouling in the boilers [11]. Volatilisation of the AAEM species can lead to severe corrosion problems for downstream equipment such as turbine blades [12]. On the other hand, if AAEM species are retained in the char after pyrolysis they can potentially act as catalysts for gasification/combustion of the char [13].

Due to the high moisture content and high reactivity of the dried brown coals, these cannot be readily transported. As a result, brown coal is currently used in mine-mouth power generation plants. Table 1.2 shows an energy balance on Victorian power sector for 2008-2009.

Since efficiency of brown coal-fired power plants is low [12], CO_2 emissions from these plants are much higher than comparable bituminous coal power plants, as shown in Figure 1.2. Hazelwood power station in the Latrobe valley, using coal from the Morwell open cut mine, was once listed as the most polluting of all the power plants in the world by World Wide Fund for nature (WWF), Australia [15]. High GHG

TABLE 1.2: Victorian power sector: 2008-2009 energy balance [14]

Items	Energy, PJ
Fuels consumed	
Brown coal	645.3
Brown coal briquettes	0.9
Petroleum products	1.5
Wood, waste wood	5.6
Automotive diesel oil	0.3
Fuel oil	0.3
Natural gas	28.1
Electricity	28.1
Thermal electricity generated	201.9
Net energy consumed	508
Energy efficiency	28.40%

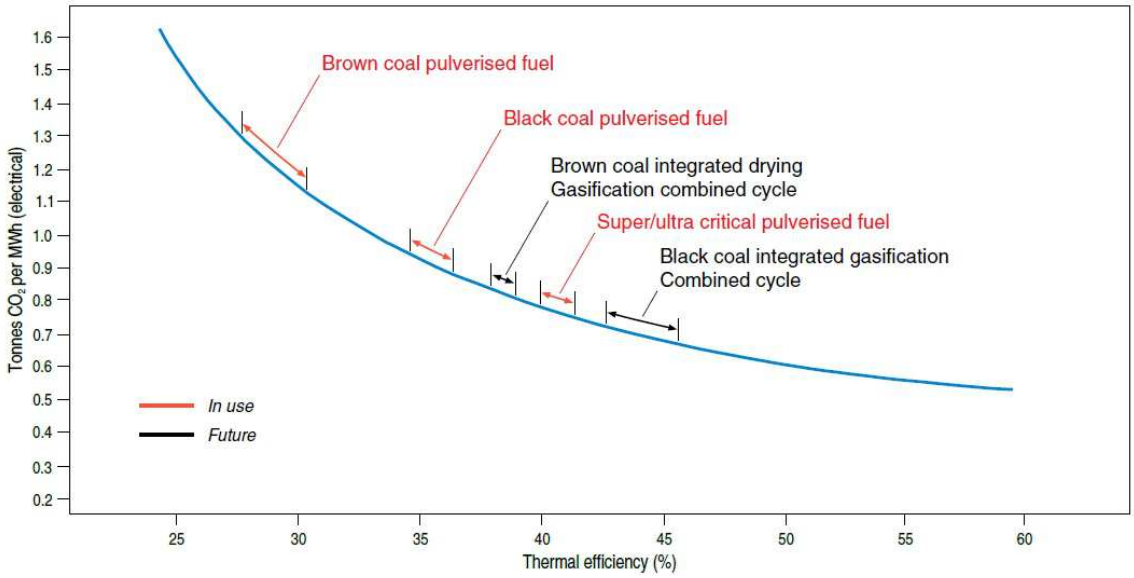

FIGURE 1.2: Thermal efficiencies and carbon dioxide emissions from various coal-fired power generation technologies (without Carbon capture and storage) [14]

emission is now considered as the single biggest threat for the future utilisation of Victorian brown coal.

The production and consumption of Victorian brown coal has gradually increased between 1960 and 1990, as shown in Figure 1.3. However, the consumption has not seen much change in the last 15 years. With the increased concern about climate change, it is likely to have an uncertain future with current application trend outlined in the Victorian Government's progressive framework for energy policy planning towards 2030, as shown in Figure 1.4 [14]. Most of the 700 PJ energy input in the power generation sector current comes from brown coal. By 2030, this energy consumption

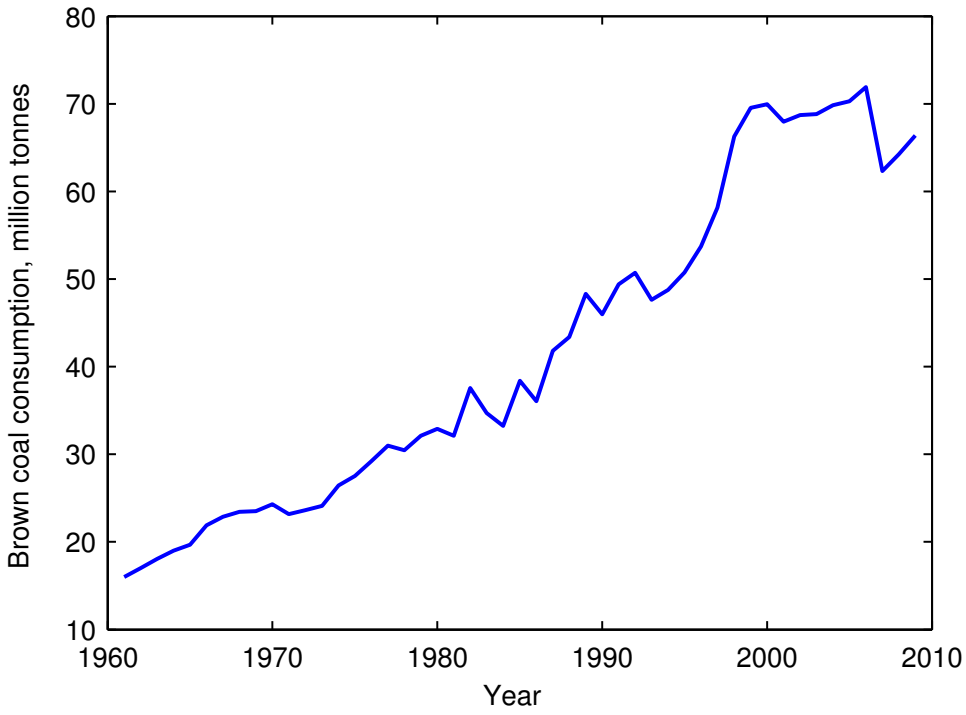

FIGURE 1.3: Annual production of Victorian brown coal [14]

will further increase by 30%. However, brown coal will not be the major contributor according to the projected future usage pattern. Therefore, use of brown coal other than power generation leading to production of liquid fuels or value-added chemicals holds the key to the future utilisation of Victorian brown coal.

Liquefaction and gasification of brown coals can provide alternate application routes. Liquid fuels can be produced from coal by three alternative routes: coal pyrolysis, direct coal liquefaction (DCL) and indirect coal liquefaction (ICL). Coal pyrolysis is a destructive distillation process yielding gas, liquid and solid products. In DCL, coal is hydrogenated in a slurry-phase to produce partially refined synthetic crude oil, which can be further refined to obtain liquefied petroleum gas (LPG), petrol and diesel. Gasification is the first step of ICL. Syngas produced via gasification can be catalytically converted into various liquid fuels. A variety of chemicals other than fuels can also be produced via gasification. Integration of coal gasification with combined cycle power generation (IGCC) is also a high efficiency and environmentally preferable process.

Methanol yield from syngas is thermodynamically limited at industrial operating temperatures and pressures. Synthesis of dimethyl ether (DME) from syngas removes the equilibrium constraints in methanol synthesis by in situ conversion of methanol to

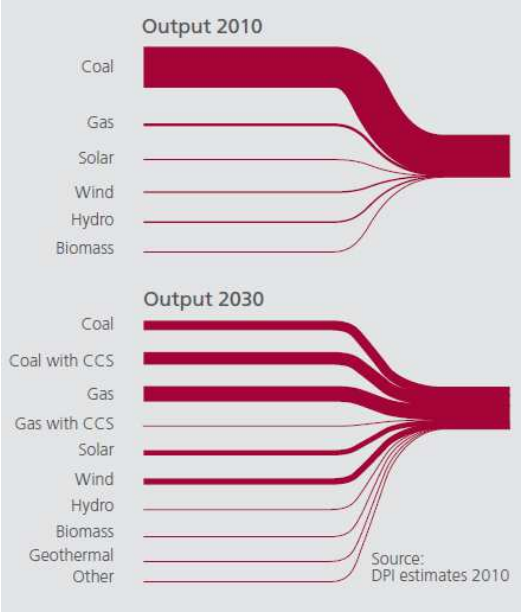

FIGURE 1.4: Electricity output from different energy sources in Victoria: Current and future outlook [14]

DME. Therefore the process yield improves significantly [16–18]. Moreover, a syngas to DME production facility can be used for co-production of methanol and DME by changing the catalyst composition only. Both DME and methanol are value-added chemicals that can be used as fuel and chemical feedstock. DME-fueled engines have shown better emission characteristics than the other diesel engine fuels in terms of soot, particulate and NO_x emission [19]. Therefore, DME synthesis from Victorian brown coal can be a win-win situation from both resource utilisation and environmental point of view.

1.2 Objectives, methodology and outcomes

The objective of this research is to identify issues related to the production of DME from Victorian brown coal through gasification in a laboratory scale equipment. The following aspects are covered in this project:

- Study of the gasification of brown coal at low temperatures
- Identification of catalyst components with high activity and selectivity towards DME synthesis
- Preparation of the bi-functional catalyst for direct conversion of syngas to DME

- Study of the effect of impurities on the bi-functional catalysts
- Process modeling of coal to DME production in a process simulator
- Study of the effect of syngas composition, temperature and space velocity on the yield of DME

The proposed project has three distinct parts:

- development of a process simulation model
- gasification experiments using Victorian brown coal
- assessment and development of catalysts for synthesis of DME from brown coal syngas

1.2.1 Process model for brown coal to DME

1.2.1.1 Approach and methodology

A process model was developed for brown coal to DME production using Aspen Plus. As-mined Victorian brown coal was used as the feed material for the process. In this model, the coal was dried to the equilibrium moisture before gasification. The syngas produced from the gasifier was subjected to gas cleaning prior to synthesis. For the gasification block, a Gibbs reactor model was used. On the other hand, the synthesis reactor was a kinetic plug-flow reactor. The product stream from the synthesis reactor was treated in downstream units for product separation and recycling purposes.

1.2.1.2 Outcomes

The developed model was used to set the baseline conditions for the experimental studies. It provided valuable information about the gasification temperature and product composition. An optimised gasification condition was also proposed from the model calculation to maximise DME yield. The process model also provided information about the effect of process operating condition on DME yield. The developed process model can be utilised for process optimization and study of process input variations on the overall process.

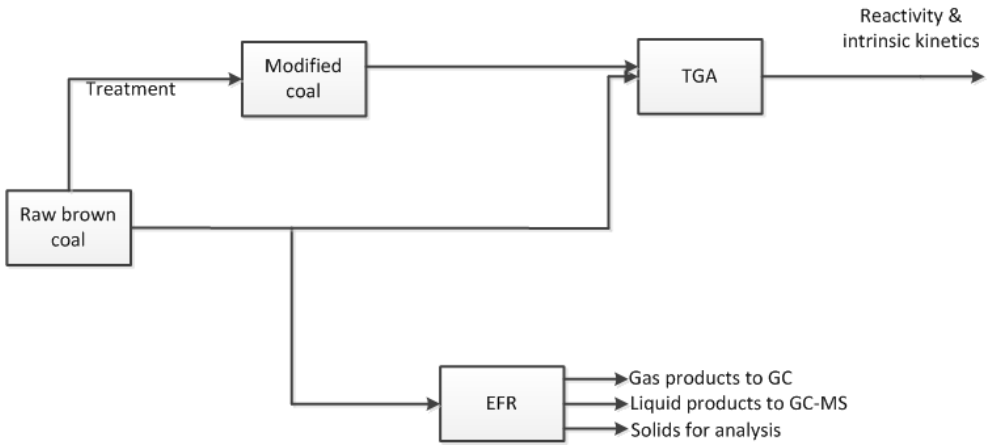

FIGURE 1.5: Experimental scheme: brown coal gasification

1.2.2 Gasification experiments

1.2.2.1 Approach and methodology

Gasification experiments involved collection and preparation of brown coal samples followed by a series of gasification experiments in a Thermogravimetric analyser (TGA) and laboratory scale entrained flow reactor (EFR). Thermogravimetric analyses were performed on brown coal and treated coal samples. Experimental data obtained from the TGA were used to study the reactivity and kinetics of the gasification process with CO_2 as the gasification agent.

Coal samples were also used in an EFR. The coal samples were pyrolysed in a nitrogen environment to prepare char. The char samples were then fed to the EFR for a second time for the gasification experiments with CO_2 as the gasification agent. The pyrolysis experiments provided information about the solid (char), liquid (tar) and gaseous products generated during the process. The gasification experiments provided the syngas compositions as well as char conversions at different temperatures. The experimental scheme for the gasification studies are shown in Figure 1.5.

1.2.2.2 Outcomes

The kinetic data obtained from the TGA studies provided a comparison between the non-catalytic and catalytic gasification processes for the selected coal sample. The comparative study of the kinetic data provide information regarding effectiveness of the loaded catalysts. The chemically controlled zone of the CO_2 gasification was also

identified from the study. Catalytic gasification beyond this temperature has shown not be advantageous when compared to that of non-catalytic gasification.

Pyrolysis and gasification experiments in the EFR provided conversion and syngas composition in realistic conditions. The variation in char yield, gas yield and tar composition with varying temperature were obtained. The experiments on the parent coal showed that the residence time used for the reactor was not long enough for complete conversion of coal char.

1.2.3 Assessment and development of catalysts for DME synthesis

1.2.3.1 Approach and methodology

In the early stages, DME synthesis experiments were conducted using commercial catalysts. A methanol synthesis catalyst and a methanol dehydration catalyst were selected for the purpose. The commercial catalyst mixtures were used in a high pressure rig for DME synthesis studies using simulated syngas consisting of CO and H_2. Experimental results were aimed to optimise the process conditions and catalyst composition for maximum DME yield and selectivity. The catalyst samples were also subjected to different characterisation techniques:

- physisorption for surface area and pore size distribution
- acidity by temperature programmed desorption (TPD) of ammonia
- reducibility by temperature programmed reduction (TPR)
- scanning electron microscopy for surface morphology
- x-ray powder diffraction (XRD) for phase analysis

Based on the performance of the commercial catalyst mixture, more catalysts were synthesised in the laboratory. The catalysts were then used in the high pressure reactor to obtain the corresponding DME selectivity and yield. Physical characterisation of the synthesised catalysts were also performed.

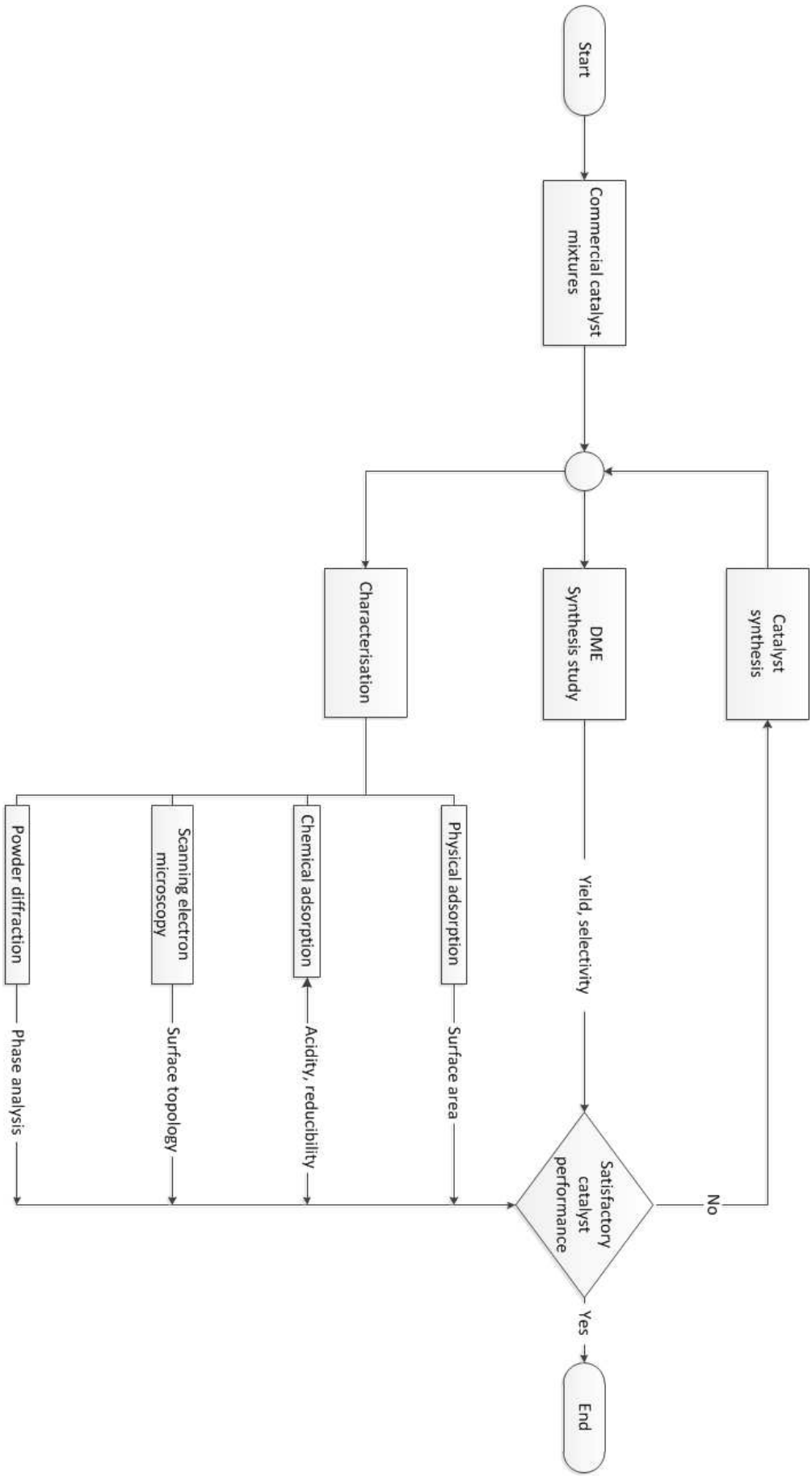

FIGURE 1.6: Experimental scheme: DME synthesis

Effects of contaminants, such as COS and H_2S on the catalyst performance were also studied using in situ reaction cell using Fourier transform infrared spectroscopy (FTIR) and XRD.

1.2.3.2 Outcomes

Analysis of conversion, yield and selectivity data using regression analysis provided optimum process conditions (catalyst composition and syngas composition) for maximising DME yield. A suitable operating temperature was also obtained for maximum yield.

The results obtained from commercial catalyst mixture along with characterisation of the catalyst mixes led to synthesis of new catalysts. The performance of these catalysts at optimum temperature and syngas composition was obtained. Performance of these catalysts with time on-stream was also determined.

Structural changes in the catalyst on exposure to two sulphur containing gases were determined. The effect of poisoning on the DME yield was also evaluated.

1.3 Thesis organisation

Chapter 1 is the introduction to this thesis. The background of the study, methodology and outcomes, and the overall thesis organization are also included in this chapter.

Chapter 2 provides an overview of the current and potential applications of Victorian brown coal. Out of all potential applications gasification and indirect liquefaction has been given preference. Developments in the gasification of Victorian brown coal has been discussed in details.

Chapter 3 focuses on the reported work DME in open literature. The chapter provides a brief introduction on DME and its applications. In the later part of the chapter chemistry and technology involved in the synthesis of DME have been discussed in details.

Chapter 4 provides a summary of the Chapters 2 and 3. It provides rationale for the production of DME from Victorian brown coal. The research and development needs for producing DME are also summarised.

Chapter 5 includes experimental methods and materials. Material specifications and the description of the experimental rigs are provided. Analytical techniques and experimental methods used during this study are also summarised.

Chapter 6 presents results from the equilibrium modelling and process modelling. Equilibrium yield and product composition are discussed. A process model in Aspen plus are presented here. The model includes drying and gasification of Victorian brown coal, and DME synthesis. Effect of pressure and temperature on the gasification products are discussed. The model was also used to study the effect of various operating parameters on DME yield and CO conversion. These results are presented in this chapter.

Chapter 7 contains findings of the gasification studies. Gasification experiments using a TGA have been used to find the intrinsic gasification kinetics. A comparative study of the catalytic and non-catalytic gasification kinetics has been presented here. Finding for the pyrolysis and gasification of coal and char samples in an EFR has also been included.

Chapter 8 reports performance of the commercial catalyst mixes. A factorial experimental design was used for the optimisation of catalyst composition and syngas composition. This chapter includes results from this 3^2 factorial design. The regression analysis, used to find the conditions, has been discussed here.

Chapter 9 includes preparation and characterisation of the developed catalysts. The performance of the catalysts during synthesis reaction was discussed. Finally, a comparison of these catalysts with the commercial mixes are presented.

Chapter 10 covers FTIR and XRD studies conducted on the sulphur poisoned catalysts. Effect of poisoning on the catalyst performance is also discussed in this chapter.

Chapter 11 draws an overall conclusion to the research work. Major conclusions obtained from the modelling and experimental work are presented here. The conclusion drawn from the work also provided the scope of future work required in this and other related fields, which is discussed in the latter section of the chapter.

References

[1] BP, 2010, Statistical review of world energy. British Petroleum

[2] IEA, 2010, Energy technology perspectives 2010: scenarios & strategies to 2050. International Energy Agency

[3] IEA, 2010, CO_2 emissions from fuel combustion 2010 - highlights. International Energy Agency

[4] IPCC, 2007, Climate change 2007: synthesis report. Intergovernmental Panel for Climate Change

[5] Li CZ, 2004, *In:* Advances in the science of Victorian brown coal, Li CZ, editor, 1 – 10, Elsevier Science, Amsterdam

[6] Barton C, Gloe C, Holdgate G, 1993, International Journal of Coal Geology, **23**: 193 – 213

[7] DPI, 2010, *Brown coal - Victoria, Australia: A principal brown coal province.* Cited: 17 October 2010. Available from: http://www.dpi.vic.gov.au/

[8] Li CZ, 2004, *In:* Advances in the science of Victorian brown coal, Li CZ, editor, 286 – 359, Elsevier Science, Amsterdam

[9] Perry GJ, Allardice DJ, Kiss LT, 1984, *In:* The chemistry of low-rank coals, Schobert HH, editor, 3–14, American Chemical Society, Washington, D.C.

[10] Burnard K, Bhattacharya S, 2011, Power generation from coal: ongoing developments and outlook. International Energy Agency, Paris

[11] Anderson B, Ledger RC, Ottrey AL, 1987, Study of long-term fouling behaviour of low rank coal, Vol. 1: overview. State Electricity Commission of Victoria, Melbourne

[12] Li X, Wu H, Hayashi JI, Li CZ, 2004, Fuel, **83**: 1273–1279

[13] Ohtsuka Y, Asami K, 1997, Catalysis Today, **39**: 111 – 125

[14] ABARE, 2010, Australian energy resource assessment. Geoscience Australia and ABARE, Canberra

[15] WWF-Australia, 2005, *Hazelwood tops international list of dirty power stations.* Cited: 17 October 2010. Available from: http://www.wwf.org.au/

[16] Fujimoto K, Asami K, Shikada T, Tominaga H, 1984, Chemistry Letters, **13**: 2051–2054

[17] Jia G, Tan Y, Han Y, 2005, Journal of Natural Gas Chemistry, **14**: 47–53

[18] Zahner JC, 1977, *Conversion of modified synthesis gas to oxygenated organic chemicals (US Patent 4011275)*

[19] Arcoumanis C, Bae C, Crookes R, Kinoshita E, 2008, Fuel, **87**: 1014 – 1030

Chapter 2

Review of Gasification of Victorian Brown Coal

2.1 Introduction

This chapter reviews current and potential future applications of Victorian brown coal. A comparison between various potential applications has been discussed. Latter part of the chapter includes a review on the gasification of Victorian brown coal.

2.2 Current applications of Victorian brown coal

Victorian brown coal is currently used in mine-mouth power generation plants. Production of brown coal briquettes, which is used for heating and cooking, is the only other major application of Victorian brown coal.

2.2.1 Pulverised coal-fired (PCF) power plants

Power generation is currently the primary use of Victorian brown coal. Table 2.1 shows operational coal-fired power plants in Victoria. These plants are located close to the mine sites. Coals are transported to the plant by belt conveyors.

High moisture coals are first dried in the pulverisers by recovering some of the heat from the boiler flue gas. The coal is then pulverised and blown into the boiler furnace for combustion. Because of the high moisture content, a special firing system called separation firing is used in the boilers. A portion of the flue gas is recycled through the pulveriser. About 80% of the pulverised coal and 30% of the gas is fed to the main burners to achieve a stable flame. The remaining 20% coal is carried in the 70% recycled flue gas plus the evaporated coal moisture vapour and fed to the vapour

Excerpted from: Bhattacharya S, Kabir KB and Hein K, *progress. energy combust. sci*, 39: 577-605

TABLE 2.1: List of operational brown coal-fired power plants in Victoria (2013)

Power plant	Start-up	Turbine(s)	Capacity,MW	Operator
Anglesea	1969	1	150	Alcoa
Hazelwood	1964	8	1675	International Power
Loy Yang A	1984	4	2210	AGL Limited
Loy Yang B	1993	2	1026	GDF SUEZ Energy International
Yallourn W	1973	4	1480	Energy Australia
Energy Brix	1956	5	170	HRL

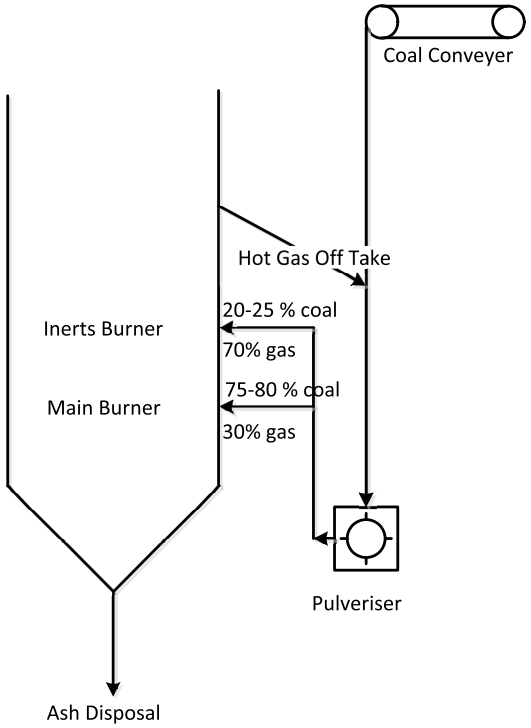

FIGURE 2.1: Separation firing system of Victorian brown coal

burners, higher in the furnace. A simplified scheme of the firing system is shown in Figure 2.1. Since Morwell coal has a lower moisture content than both Loy Yang (LY) and Yallourn coals, it does not require separate firing [1].

Because of the high inert gas loading (water vapour and recycled flue gas) furnace gas temperature and flame temperature of brown coal-fired boilers are several hundred degrees lower than the comparable black coal units. A brown coal-fired boiler is therefore larger compared to a black coal-fired boiler of same capacity [2, 3]. As a result, brown coal-fired power plants are more capital intensive.

2.2.2 Briquetting

Long distance transport of Victorian brown coal is not practical and economical due to its high moisture content. Briquetting is an agglomeration process for brown coal to remove moisture and to reduce its volume for transportation and storage. Briquette production is the only other major application of brown coal apart from power generation.

For briquetting brown coal is crushed, ground and screened to a particular size range. The coal is then dried to reduce moisture content from about 60% to about 15% before being cooled and sent to a press to form hard compacts. Briquettes produced from brown coals are comparable to higher rank coals in terms of energy density. Large scale briquetting of brown coal started in 1920s at Yallourn followed by another plant at Morwell in 1959. The briquettes were used for cooking and heating, both domestic and industrial, as well as in some of the base load power plants in the Latrobe valley. Use of the briquette dropped with the introduction of natural gas in Victoria. Currently only the Morwell plant (Energy Brix) is in operation.

2.3 Potential Uses of Victorian Brown Coal

Installation of new coal-based power stations is possible only through implementation of low emission technologies, such as use of brown coal coupled with carbon capture and storage (CCS) technology. Current government policies in Victoria encourage efficient utilisation of brown coal. The Government of Victoria is attempting to attract new investments in low emission coal technologies other than electricity generation [4]. Production of value-added chemicals and fuels from brown coal will deliver a larger economic benefit compared to power generation alone, since electricity is a relatively low-value commodity. Development of such processes could lead to large investments in brown coal producing zones in Victoria.

Coal pyrolysis, DCL and gasification can provide alternate means of coal utilisation. These are further discussed in the following sections.

2.3.1 Direct coal liquefaction (DCL)

This can be classified as pyrolysis and hydrogenation process.

2.3.1.1 Pyrolysis

There are several commercially available pyrolysis processes (e.g. COED [5], TOSCOAL [6]). Reaction temperature and pressure greatly vary from process to process. Pyrolysis of coal yields char, condensable tar and oil, water vapour, and non-condensable gases. All the products need further treatment for nitrogen and sulphur containing compounds. Composition of the synthetic crude produced from pyrolysis can vary depending on the properties of coal and pyrolysis conditions [7].

2.3.1.2 Hydrogenation

Hydrogenation of coal can be a single stage or two stage process. Hydrogenation processes have a long history with first commercial process in Germany in 1910s. Most of the coal rich countries used hydrogenation of coal to produce synthetic crude oil. However, currently there are no commercial plants using any of the hydrogenation processes [8]. One of the major problems with these processes is the source of hydrogen, which should be produced either by steam reforming of natural gas or by coal gasification.

2.3.2 Gasification and indirect coal liquefaction (ICL)

Coal gasification refers to the reaction of coal with air or oxygen and steam. During gasification some additional reactions also take place between the gaseous products and carbon. Composition of the product gas, also referred to as syngas, depends considerably on type of the coal and the gasifying agent, as well as the reaction conditions.

Coal undergoes devolatilisation when fed to a gasifier producing char and volatiles. Subsequently in the gasification step, reactions occur between the gasifying agents (e.g. steam), and the volatiles and char. Major reactions involved during coal gasification are as follows:

$$C + O_2 \longrightarrow CO_2 \tag{R2.1}$$

$$C + \tfrac{1}{2}O_2 \longrightarrow CO \tag{R2.2}$$

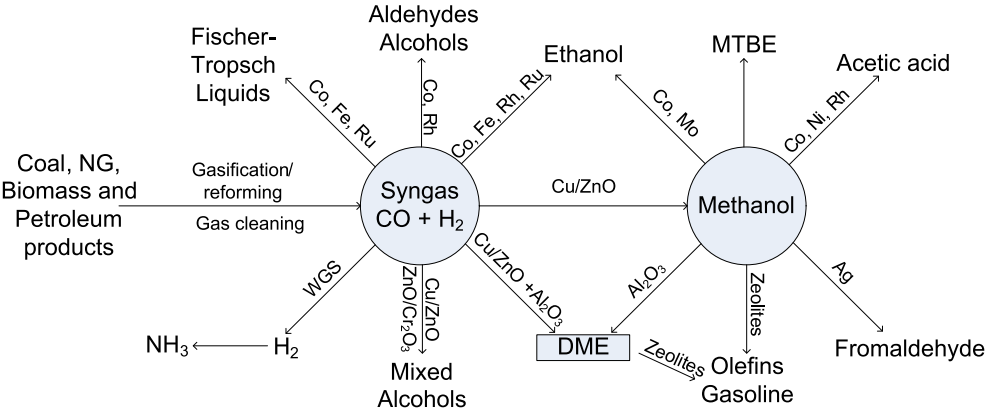

FIGURE 2.2: Syngas to fuels and chemicals

$$\mathrm{C} + \mathrm{H_2O} \longrightarrow \mathrm{CO} + \mathrm{H_2} \tag{R2.3}$$

$$\mathrm{C} + \mathrm{CO_2} \longrightarrow 2\,\mathrm{CO} \tag{R2.4}$$

$$\mathrm{C} + 2\,\mathrm{H_2} \longrightarrow \mathrm{CH_4} \tag{R2.5}$$

$$\mathrm{CO} + \mathrm{H_2O} \longrightarrow \mathrm{CO_2} + \mathrm{H_2} \tag{R2.6}$$

$$\mathrm{CO} + 3\,\mathrm{H_2} \longrightarrow \mathrm{CH_4} + \mathrm{H_2O} \tag{R2.7}$$

The major components of the syngas are carbon monoxide and hydrogen. Syngas can be used as a fuel in gas turbines or as a precursor to many chemicals. Catalysts play a pivotal role in the reaction between CO and H_2. Based on the reaction on the catalyst surface, the same mixture can lead to variety of products, as shown in Figure 2.2.

Currently, largest use of syngas is in hydrogen production. The produced hydrogen is currently used either in NH_3 production or in petrochemical sectors [9]. Hydrogen itself is a fuel and its combustion produces water. Therefore, significant amount of research work is going on hydrogen fuelled internal combustion engines and fuel cells [10]. However, the technology (production, transport and storage of H_2) is not yet ready to be commercialised. In addition, handling of large quantity of CO_2, and high operation cost are some of the major problems for hydrogen-based energy system.

Fischer-Tropsch synthesis (FTS) is one of the commercial operating processes for indirect liquefaction of coal. In FTS, carbon monoxide and hydrogen react to form wide range of hydrocarbons.

$$n\mathrm{CO} + (2n+1)\mathrm{H_2} \longrightarrow \mathrm{C_nH_{2n+2}} + n\mathrm{H_2O} \tag{R2.8}$$

where n is a positive integer and dependent on the product (for methane $n = 1$).

FT liquid (FTL) products are similar to fuel products from crude oil. FTL does not contain sulphur and has better emission characteristics compared to the conventional diesel.

FT process requires high capital cost, and high maintenance and operating costs. Gas based FT process is currently favoured over coal-based process because of their lower clean-up requirements [11].

One of the major disadvantages of FT process is that it produces a wide range of products. The selectivity towards any particular product is hard to control. Again, the products are similar to those produced in a crude oil refinery. Therefore, the economic acceptability of FT process heavily depends on the uncertain and volatile price of crude oil. FTS also has lower thermal and carbon efficiency compared to methanol/DME synthesis [12].

Methanol synthesis from coal via gasification is a mature and proven technology. Methanol can be used as a fuel or as a precursor to many other chemicals. Petrol additives, such as methyl tertbutyl ether (MTBE), ethyl tert-butyl ether (ETBE), tert-amyl methyl ether (TAME) etc., are made from methanol. Methanol is also a feedstock for several processes, such as MTO [13], MOGD [14], MTG [13], TIGAS [15] and etc.

While methanol can be used as a petrol substitute, DME can be a diesel fuel alternative. DME has many other potential uses. DME is currently produced from methanol by catalytically removing one molecule of water from two molecules of methanol. In situ dehydration of methanol to DME, during production of methanol from syngas, is found to increase the overall carbon conversion to methanol and DME. Therefore, researchers are now more focussed on direct synthesis of DME from syngas.

Selection of appropriate process path depends on a variety of factors such as process yield, economics, demand, etc. Nowadays, environmental acceptability and sustainability are also considered as critical selection criteria. Life cycle analysis (LCA) of the competitive processes can assess environmental impacts associated with their production, transport and usage. A brief review of LCA studies for coal to fuel production via gasification is presented in the following section.

2.3.2.1 LCA of coal to liquid fuels process

A well-to-wheels (WTW) study of coal-based DME (indirect; coal to methanol and methanol to DME) and Fischer-Tropsch diesel (FTD) for urban buses in China was carried out by Zhang and Huang [16]. The study estimated total primary energy consumption (PEC) and global warming potentials (GWP) for both the processes. PEC was 14% less for DME pathway than that of FTD pathway. At the same time, DME process had 25% less GHG emission compared to the FTD process. Inclusion of CCS in the fuel production step greatly reduced emission from FTD pathway, though it was still 12% more than the corresponding DME pathway [16].

TOTAL Gas & Power performed a cradle-to-gate analysis on five different processes from coal: methanol, DME (indirect), DME (direct; syngas to DME), synthetic natural gas (SNG) and FTD. All these pathways included CCS. The study considered PEC, GHG emission and water consumption. FTD pathway found to have maximum PEC and GHG emission while direct DME had maximum water usage (0.54 kg/MJ). Normalised ranking of the processes showed that SNG is the most environmentally friendly while FTD was the least attractive option. Methanol, direct and indirect DME pathways showed similar impact results [17].

Another WTW analysis was performed by European Commission combining their well-to-tank (WTT) and tank-to-wheels (TTW) studies for various feedstock producing automotive fuels [18]. WTT energy consumption and GHG emission for coal-based fuels are shown in Figure 2.3. The WTT analysis compared electricity generation to other alternative options for coal use. Electricity generation using conventional coal combustion process required more energy than other processes except compressed H_2 production (with CCS). It also showed maximum emission among all the studied processes. Electricity production through gasification reduced process energy consumption and net GHG emission. Among the liquid fuels methanol process consumed least energy with lowest GHG emission. GHG emission from DME was slightly higher than that of FTD. FTD production required slightly higher energy than DME. Adapting CCS with FPD significantly reduced GHG emission. CCS integrated DME or methanol facilities were not considered in this study.

A comparison of WTW analysis for automotive fuels produced coal is shown in Figure 2.4. Efficiency of a direct injection compression-ignition (DICI) engine efficiency was used for FTD and DME, while efficiency of a plug-injection spark-ignition (PISI) engine was used for H_2 calculations.

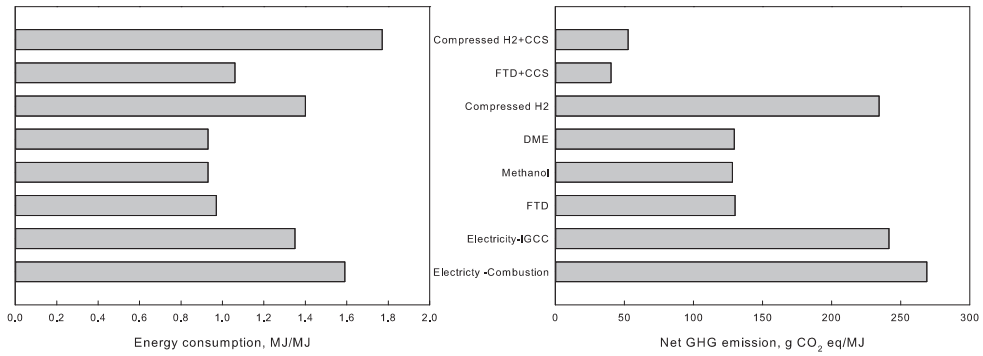

FIGURE 2.3: WTT energy consumption and GHG emission for coal to X (X denotes electricity, FTD, methanol, DME and H_2) [18]

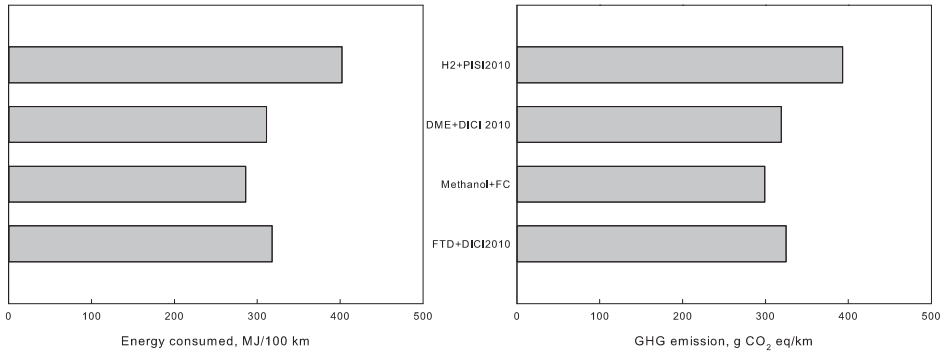

FIGURE 2.4: WTW energy consumption and GHG emission coal-based automotive fuels [18]

Efficiency of a fuel cell (FC) driven vehicle was used for the methanol calculations.Methanol gave the best results in terms of energy consumed and GHG emission while H_2 showed the worst performance. DME and FTD were ranked second and third respectively. FC driven vehicles have higher efficiency than conventional engines and hence resulted lower emission and energy consumption for methanol [18]. In a different WTW study, conducted on buses in China, SI engine running on coal-based methanol found to have more GHG emission and higher energy consumption than CI engine running on coal-based DME [19].

2.3.3 Comparison of DCL and ICL

DCL and ICL technologies are at different stages of development. ICL technologies have either been commercialised or comprise of components that have been commercialised already. On the other hand, DCL technologies do not have a long history of commercial performance.

Few studies have been performed to compare these two groups of technologies [20, 21]. The findings can be summarised as below:

- Both DCL and ICL are capital intensive [20].
- ICL technologies producing methanol and DME have 58.3% and 55.1% efficiency respectively [21]. On the other hand, DCL technologies have higher energy efficiency, between 60 and 70% [21]. However, DCL makes a partially refined synthetic crude oil. The synthetic crude oil needs to be refined into synthetic diesel/petrol. Therefore, ICL is as energy efficient as DCL when end-use is considered [20, 21].
- Some DCL processes require hydrogen. Hydrogen is not readily available and needs to be synthesised either from natural gas (NG) or coal. ICL processes use only coal as the feedstock.
- ICL technologies offer better prospects for GHG mitigation than DCL technologies [20, 21].
- The infrastructure and technological support is available for ICL technologies. DCL technologies are not there yet in terms of scale-up and commercialisation.

In Conclusion, ICL technologies are more feasible for future utilisation of coal than DCL technologies. Coal-based methanol and DME have better process energy efficiency and lower GHG emission than other ICL technologies such as FTD and compressed H_2.

2.4 Brown coal gasification

In a gasifier, coal is partially combusted to achieve the required temperature for pyrolysis and gasification. During pyrolysis, oxygen-containing functional groups present in the coal (e.g. carboxyl, phenol), decompose to produce H_2O, CO and CO_2. In addition, small amounts of H_2, light hydrocarbons (mainly CH_4), H_2S, HCN and NH_3 are also formed. Hydrocarbons with larger molecules and their derivatives form the tar. The non-volatile residue, i.e. char, is composed of fixed carbon and inorganic matters. In the gasification step, char reacts with gasifying agents (e.g. O_2, CO_2, H_2O) to produce CO, H_2 and CO_2. At the same time, the volatiles and tar, evolved

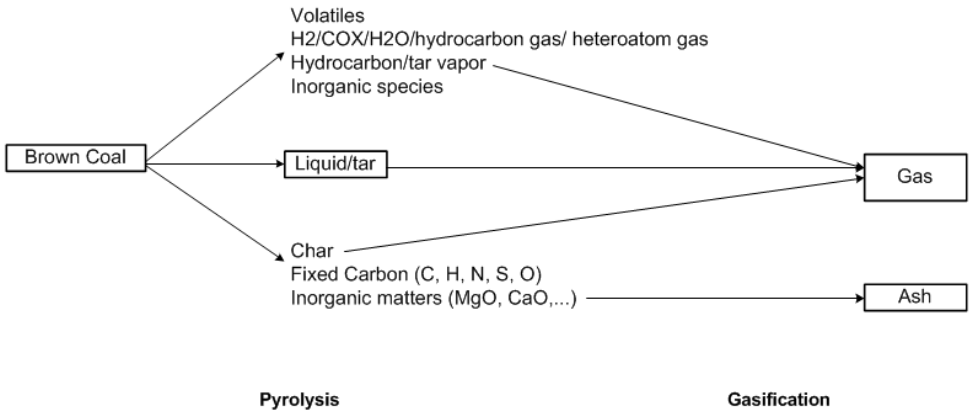

FIGURE 2.5: Brown coal gasification scheme(modified from Ref. [22])

TABLE 2.2: Typical concentration of alkaline and alkaline-earth metals in Victorian brown coal, wt% (dry basis)

	Coals		
	Loy Yang	Yallourn	Morwell
Na	0.128	0.12	0.34
K	0.012	Not reported	0.03
Ca	0.0034	0.29	0.81
Mg	0.058	0.70	0.52

during pyrolysis, undergo secondary reactions or cracking to produce more CO, H_2 and CO_2. Inorganic matters present in the coal produce ash. A simplified pathway for brown coal gasification is shown in Figure 2.5.

An important feature of Victorian brown coal is the presence of significant amount of AAEM (Table 2.2) [23–25]. AAEM can be present in soluble form within the coal moisture (as NaCl, $CaCl_2$ etc.) or may be associated with the carboxylic and functionalities in the coal structure [26]. Though total content of AAEM is less than 1% of as-mined coal, they can play a very important role in coal utilisation. Volatilisation of AAEM species can lead to severe corrosion problems for downstream equipment such as turbine blades [23]. On the other hand, if AAEM species are retained in the char after pyrolysis they can act as excellent catalyst for gasification/combustion of the char [27].

In the following sections, major studies on Victorian brown coal gasification, including pyrolysis, char gasification and other secondary reactions, have been summarised. Afterwards, properties of Victorian brown coal are discussed in view of an appropriate gasifier selection.

2.4.1 Pyrolysis

Pyrolysis is the initial step of coal gasification and can be classified into primary and secondary pyrolysis. Primary pyrolysis involves formation of volatiles and chars due to intra-particle thermochemical reactions. Gaseous products of primary pyrolysis are usually H_2, CO, CO_2, H_2O, CH_4 and other low hydrocarbons. Primary tar is defined as any product that is heavier than C6 compounds [28]. Thermal cracking of primary tar at higher temperature is termed as the secondary pyrolysis resulting in the formation of more light gases and carbonaceous solid termed as soot. Yield of pyrolysis products (primary and secondary) depends on many factors such as physico-chemical properties of coal, heating rate, operating pressure, holding time etc. Brown coal macromolecules have aromatic clusters consisting of mono or poly aromatic rings with peripheral functional groups and inter-cluster linkage [26]. Aromatic ring systems are believed to be the precursor of tarry materials while peripheral groups and inter-cluster linkages break down to give up light non-aromatic gases.

A number of reactor systems have been used to study pyrolysis behaviour of Victorian brown coal over a wide range of operating conditions: fixed-bed reactors, wire-mesh reactors (WMR), curie-point reactors (CPR), drop-tube reactors (DTR) and fluidised-bed reactors (FBR) [28].

Flash pyrolysis of Loy Yang coal was performed by Tyler [29] in a small scale FBR. Analysis of product composition showed that the maximum tar was produced at 580 °C. At higher temperatures, cracking of tar produced more C1-C3 hydrocarbons. Agglomeration between coal char and bed material was observed, with a maximum at 700 °C. Reason behind lower agglomeration above 700 °C was not provided [29]. Similar tar and gas yields were observed with Yallourn coal in the same FBR [30].

Variation in tar and gas yield over heating rate 0.167-2000 °C s^{-1} has been studied [25, 31–33]. All these studies showed that yield of total volatile (tar and gas) increases with higher heating rate. Though rapid pyrolysis lowers yield of CO, CO_2 and H_2O it increases tar yield. Sathe et al. [32], using WMR for pyrolysis of Loy Yang coal, found that the tar yield was more than three times at 1000 °C s^{-1} than that of at 1 °C s^{-1}. Studies on Morwell and Loy Yang coals also showed that tar yield was almost unchanged after 600 °C for various heating rates [25, 32–35]. Tar yield was also found to be unaffected by holding time above this temperature indicating that the tar yield was completed before the particle temperature reached 600 °C [32, 36].

This asymptotic tar yield from Loy Yang coal has a linear relationship with logarithm of heating rate [32].

Kershaw et al. [31] performed fluorescence spectroscopic analysis on tars from Loy Yang coal pyrolysis in a WMR, to study the effect of process variables on the tar composition. The intensity of fluorescence emission from brown coal tars was significantly lower than higher rank coals, which indicates low concentrations of 3-6 ring polycyclic aromatic compounds. It was reported earlier by Kershaw [37, 38] that single and two ring aromatic structures predominate the aromatic part of brown coal tar. However, rapid pyrolysis of brown coal has been found to have increased concentration of larger aromatic rings in tar [31].

Effect of heating rate on tar yield can be explained by two different and independent aspects: first, shortened residence time of coal tar precursors inside coal particles and second, enhancement of bridge breaking relative to cross-linking [28]. Higher heating rate results higher concentration gradient across the matrix of pyrolysing coal particle which enhances intra-particle transport of volatiles by diffusion or convection. Therefore, higher heating rate can shorten residence time and thereby suppress further thermal cracking and polymerisation of tar precursors. As a result higher heating rate encourages release of larger aromatic rings, higher yield and higher molecular mass of tar.

The second reasoning evolved from the experimental observations of Hayashi et al. [25]. Molar yields of CO, CO_2, H_2O and hydrocarbon gases were evaluated as function of aliphatic to aromatic carbon conversion during pyrolysis. Aliphatic to aromatic conversion was determined from the difference in the content of aliphatic carbon between the coal and the primary pyrolysis products. It was found that yield of H_2O decreased with higher heating rate for each values of aliphatic to aromatic conversion. Fast heating during pyrolysis enhanced bridge breaking consuming donatable hydrogen from aliphatic groups which in turn suppressed H_2O formation and cross-linking of tar precursors. Net increase in depolymerisation of coal macromolecules resulted higher tar yield.

Unlike bituminous coal, pressure effect on pyrolysis of brown coal is complicated. Sathe et al. [39] studied the effect of pressure (1-61 bar) on pyrolysis of Loy Yang coal in a WMR at a heating rate of 1000 °C s^{-1}. Effect of pressure of char yield was insignificant. Variations in tar yield were compensated by increase/decrease in yield of light gaseous products. Tar yield decreased for the pressure range of 1-11 bar,

then increased by several percentage for pressures 11-20 bar and finally decreased gradually for 20-61 bar. The change in tar yield pattern was explained by transition from diffusion flow of volatile precursors to forced convection flow. Increased external pressure suppresses diffusion and hence increases residence time of volatile precursors. As a result, enhanced thermal cracking produces larger amount of light gaseous. This might be the reason for decreased tar yield from 1 bar to 11 bar. However, significant production of light gaseous products can result rapid build-up of pressure inside the particle. The volatile precursors then flow out of the particle upon build-up of sufficient pressure to overcome the external pressure resistance. Transition from bulk diffusion to forced convective flow can explain increased tar yield from 11 to 20 bar. Further increase in pressure lowers the pressure gradient and therefore a gradual decrease in tar yield was observed.

At a heating rate of 1 °C s^{-1}, tar yield increased from 6 wt%-daf to 10 wt%-daf for when the pressure was inceased from 1 to 20 bar [39].

Inherently present AAEM species also affects pyrolysis. To study the effect, Sathe et al. [32] removed AAEM species from Loy Yang coal by acid washing. Subsequent pyrolysis of the acid-washed coal resulted increased tar yield for heating rates of 1 °C s^{-1} and 1000 °C s^{-1}, and at 1-20 bar compared to raw coal. Though Ca-, Mg- and Na-carboxylate present in the coal undergoes thermal decomposition during pyrolysis they may rebonded with coal/char matrix.

$$(-\mathrm{COO}-\mathrm{Ca}-\mathrm{OOC}-) + (-\mathrm{CM}) \longrightarrow (-\mathrm{OOC}-\mathrm{Ca}-\mathrm{CM}) + \mathrm{CO_2} \tag{R2.9}$$

$$(-\mathrm{COO}-\mathrm{Ca}-\mathrm{CM}) + (-\mathrm{CM}) \longrightarrow (\mathrm{CM}-\mathrm{Ca}-\mathrm{CM}) + \mathrm{CO_2} \tag{R2.10}$$

$$(-\mathrm{COO}-\mathrm{Na}) + (-\mathrm{CM}) \longrightarrow (\mathrm{CM}-\mathrm{Na}) + \mathrm{CO_2} \tag{R2.11}$$

It is apparent from Reactions (R2.9)-(R2.11), that the AAEM species enhance cross-linking during pyrolysis and thereby suppresses tar yield from brown coal.

Average molecular weight of brown coal tar has been reported to be 200-300 [40, 41]. Based on this value and elemental analysis Tomita et al. [42] estimated chemical formula of tar as $(C_8H_{11}O)_n$ with n ≈ 2-3.

Pyrolysis conditions (e.g. peak temperature, heating rate, residence time) determine the char surface area and pore structure. Therefore, pyrolysis condition plays a significant role is subsequent char gasification [43, 44].

2.4.2 Char gasification

Rapid pyrolysis is usually followed by slower char gasification. Char gasification has been extensively studied and reviewed by many workers. General conclusion of these reviews is that the gasification of char is mainly dependent on three factors: intrinsic reactivity of char, catalytic effect of minerals present in the coal, and pore structure [45]. These factors can also be strongly correlated with each other.

Several workers have studied the gasification reactivity of different grades of coal in oxygen, steam and CO_2 environment. Similar results were observed for all gasifying agents. Coals with lower fixed carbon showed greater reactivity. Jenkins et al. [46] studied oxygen gasification of 21 char samples and concluded that the catalytic effect of CaO and MgO in the char was responsible for varied reactivity. Knight et al. [47] found decreasing char reactivity in CO_2 with increasing fixed carbon. Development of pore structure and increase of active site caused by stripping of volatile matter during pyrolysis and initial stage of char gasification was attributed to the higher reactivity of lower rank coals. Kasaoka et al. [48] found that the CO_2 reactivity decreased with increase of fuel ratio (FR = fixed carbon/volatile matter), reaching a minimum at $FR = 3$ and then increasing gradually. Fujita et al. [49] studied CO_2 reactivity at 900-1200 °C with respected to amount of Fe_2O_3, CaO, MgO, Na_2O and K_2O present in the char. Dum of the amounts of Fe_2O_3 and K_2O showed better correlation with char reactivity. Hashimoto et al. [24] also found steam-gasification reactivity of chars increase with increase of Na, Ca and K in char. Reason behind higher reactivity can be related to the high dispersion of the cations in the char after pyrolysis. K, Ca and Na in highly dispersed form can catalyse char gasification with steam and CO_2. Therefore, coals with higher AAEM found to be more reactive than the others. It can be seen from Table 2.2. that Morwell brown coal has more catalytic mineral than both Loy Yang and Yallourn. As a result, Morwell coal is more reactive [50].

Use of catalysts during gasification can lower the gasification temperature. Therefore, catalytic gasification can be an alternative for high temperature gasification provided that cheap and highly active catalyst is available [51]. AAEM and some of the transition metals (e.g. Ni, Fe) have shown catalytic activity for coal gasification.

Veraa and Bell [52] studied the effects of LiCl, NaCl, KCl, RbCl, CsCl, KOH and K_2CO_3 on the steam-gasification of sub-bituminous coal. K_2CO_3 and KOH showed almost identical effect and were significantly more active than the chloride salts. KOH and K_2CO_3 showed similar behaviour since it is easily converted to carbonate in presence of CO_2:

$$2\,KOH + CO_2 \longrightarrow K_2CO_3 + H_2O \tag{R2.12}$$

Mckee et al [53] performed similar study on alkali metal salts, but only with the carbonate salts in steam and carbon dioxide environment for temperatures 600-1000 °C. Though observed gasification rates were much higher for low-ranked coals, catalytic activity was more for the higher ranked coals. Based on catalyst loading, K_2CO_3 was most and Li_2CO_3 was least active for low-rank coal for CO_2-gasification. No apparent difference between activities was observed for high-rank coal. In case of steam-gasification, both Li_2CO_3 and Cs_2CO_3 showed decreased activity with time at temperatures above 800 °C due to hydrolysis of the salts and vaporisation of the hydroxides produced. Similar mechanism of inter-conversion between metal and metal carbonate for both CO_2-and steam-gasification was proposed.

Though K_2CO_3 showed most activity, potassium catalysts undergo deactivation in presence of alumino-silicate compounds which are present in most of the coals [54]. The deactivation reactions are as follows:

$$K_2CO_3 + SiO_2 \longrightarrow K_2SiO_3 + CO_2 \tag{R2.13}$$

$$K_2CO_3 + Al_2Si_2O_5(OH)_4 \longrightarrow 2\,KAlSiO_4 + 2\,H_2O + CO_2 \tag{R2.14}$$

Steam-gasification of Ca-loaded YL brown coal samples were performed by Ohtsuka and Tomita [55]. They used six different Ca-salts as precursor for Ca-loading of coal samples. Gasification experiments were studied at 923 and 973 K. All except $CaSO_4$ showed significant improve in gasification rate. High temperature X-ray diffraction (HTXRD) patterns in N_2 showed presence of $CaSO_4$ on coal which is inactive for gasification. No diffraction peaks were observed for $Ca(NO_3)_2$, $Ca(OOCCH_3)_2$, $Ca(OH)_2$ and $CaCl_2$ loaded coal samples indicating very fine dispersion throughout the coal surface. However increasing temperature to 1023 K of loaded coals showed distinct peaks

of CaO. Increase in crystal size with heat treatment also resulted lower gasification rates.

Though potassium and calcium show enhanced gasification at higher temperatures they are not active at temperatures below 900 K. Tomita el al [56, 57] studied gasification of YL coal by nickel impregnation at 773 K. Aqueous solution of Hexammine nickel (II) nitrate was used as nickel precursor. Ni-loading was found to lower the gasification temperature by 200 K compared to 150 K by K_2CO_3 [56]. No catalytic activity was observed at low-loading which may be resulted from deactivation of nickel catalyst by coal-derived sulphur. Sharp increase in activity was observed between 4 wt% and 10 wt% and seemed to level off after 10 wt% Ni loading. Presence of nickel also resulted in-situ desulfurization. Most of the sulphur-containing gases were adsorbed by nickel. Only one tenth of the coal sulphur was measured as H_2S in the syngas [57]. Takarada et al. [50] studied reactivity of 34 coals from 8 different countries under Ni-loading. It was observed that reactivity was strongly dependent on type of coal, low-rank coals being more reactive. Some of the low-rank coals (e.g. MW, YL, Rheinsh brown, Malaysia peat) showed two-stage gasification, with extent of gasification in the first stage being extremely high.

In comparison to non-catalytic gasification, in which 25% of coal was converted to non-gaseous products (e.g. tar, liquid and water), Ni-loaded coal suppressed tar formation as tarry material was gasified without any soot formation [42]. Attempt of recovering spent Ni-recovery was also made by NH_3-leaching. Catalysts recovery at 323 K was 90% for single-stage and 94% for two-stage extraction. At 393 K, 98% of Ni was recovered with first leaching [42].

Scanning electron microscopy (SEM) studies could not recognize any Ni particles on Ni-loaded LY, even at high loading of 10.5% [58]. Transmission electron microscopy (TEM) studies were able to find out the nickel particle size in the size range of 3-10 nm. After 2 h of gasification only some of the particle size increased above 30 nm. It must be noted that, Ni particles become catalytically inactive when size exceeds 30 nm. Energy-dispersive X-ray spectroscopy (EDX) study confirmed high dispersion of Ni throughout the coal surface [58]. Presence of large number of oxygen-containing functional groups in low-rank coals act as cation exchange sites for Ni and resulted high dispersion on Ni on the chars derived from these coals.

Ohtsuka et al. [59] investigated the effect of nickel precursors on activity using YL coal. Some trend of reactivity was observed for both steam and hydro-gasification:

$Ni(NH_3)_6CO_3$, $Ni(NO_3)_2$ > $Ni(CH_3COO)_2$ >> $NiCl_2$, $NiSO_4$, no catalyst.

It was found that $Ni(NH_3)_6CO_3$, $Ni(NO_3)_2$ and $Ni(CH_3COO)_2$ was easily reduced to metallic Ni with size of 10 nm at 773-873 K. Though $NiCl_2$ was easily reducible, particle size was much higher, 35 nm. On the other hand, reduction of $NiSO_4$ was difficult. Ohtsuka et al. [59] also tried to load chars with nickel precursors. However their attempt resulted formation of larger Ni particles. Since carboxyl group in devolatilised char is nearly zero it also caused ill-dispersion of Ni particles.

Addition of small amount of potassium with nickel (1% K, 10% Ni) showed enhanced gasification rate. Presence of potassium somehow reduced the rate of crystallite size growth resulting more activity. However, similar effect with addition of 1% Ca was not observed [55].

Catalytic activity of iron was evaluated in order to develop a cheaper catalyst for low temperature gasification [60]. $Fe(NO_3)_3$, $(NH_4)_3Fe(C_2O_4)_3$, $FeCl_3$ and $Fe_2(SO_4)_3$ were used to load YL coal with iron. Ni- and Co-loaded YL were also used for comparison. Hydro-gasification of LY with 10-wt% metal loading at 873 K showed activity sequence of: Co > Ni > Fe. For Fe-loading reactivity enhancement was not significant at low loadings up to 6-wt%. 16-wt% iron loading showed comparable coal conversion with 10-wt% Ni. Among the precursors both $Fe(NO_3)_3$ and $(NH_4)_3Fe(C_2O_4)_3$ showed good activity. However, for $FeCl_3$ and $Fe(SO_4)_3$ average crystal size of iron metal in the coal was greater than 100 nm and they showed no/low catalytic activity. Similar results were obtained for steam-gasification at 923 K. Sulphur content in coal plays an important role for iron's activity since the catalyst is poisoned by H_2S. North Dakota lignite, which has high sulphur content (2.9 wt%) compared to LY(0.3 wt%) no char gasification was observed at 873 K even with 16 wt% iron loading [60].

Additives like K and Ca greatly enhanced gasification rates when added with iron. However, 1 wt% K showed more improvement than 1 wt% Ca. Similar result was obtained by Suzuki et al. [61] using $Na[HFe(CO)_4]$ with YL. In all these cases, Ca/K/Na interacts with iron and make sure that it remains in a lower oxidation state (e.g. FeO instead of Fe_3O_4). FeO seems to be more active than magnetite and therefore resulting better gasification rates.

Based on their earlier unsuccessful attempt to use $FeCl_3$ as catalyst precursors, Ohtsuka et al. [62] used a buffer solution (NH_3/NH_4Cl) to precipitate iron at pH 8-9. Removal of chlorine was ensured by repeated washing with deionized water. This new chlorine free catalyst from $FeCl_3$ showed significant improvement over the previous

one. Other methods to precipitate iron on the coal were also performed by using urea, $Ca(OH)_2$ and by high temperature hydrolysis [63]. Each of these cases resulted fine dispersion of iron in coal. Among them, use of $Ca(OH)_2$ gave the most active catalyst even at low loadings of iron (1-5 wt%). This iron catalyst has added benefit of presence of calcium from the $Ca(OH)_2$ used for precipitation. Urea precipitated catalyst was the second most active. Not much significant difference in catalytic activity was observed for catalysts prepared by using of buffer solution and high temperature. High performance was also observed for iron loading, from $FeCl_3$ by using NH_4OH, on H-form LY [64].

2.4.3 Secondary reactions of volatiles

Comparative study on YL coal pyrolysis and steam-gasification indicated that tar formed during pyrolysis goes through steam reforming to produce H_2 and CO_2 through the following reaction [42]:

$$(C_8H_{11}O)_n + 15nH_2O \longrightarrow 41(n/2)H_2 + 8nCO_2 \qquad \text{(R2.15)}$$

Pyrolysis of Ca- and Ni-loaded YL showed lower weight loss and the product gas was comparatively CO richer compared to the YL without Ca loading [22, 42]. Presence of Ca and Ni in the coal catalysed decomposition of tar by the following reaction:

$$(C_8H_{11}O)_n \longrightarrow 7nC + nCO + 11(n/2)H_2 \qquad \text{(R2.16)}$$

Deposition of C may be the reason for decrease in weight loss. Weight loss for Ni-loaded LY was much more than the raw coal and Ca-loaded coal indicating the Ni considerably catalysed tar decomposition reaction.

Presence of steam in metal-loaded LY induced steam-gasification of tar along with decomposition reaction, resulting gas with high H_2 and CO_2 content. However, Ni is known to catalyse direct synthesis of CH_4 according to the following reaction:

$$2\,C + 2\,H_2O \longrightarrow CH_4 + CO_2 \qquad \text{(R2.17)}$$

Based on the significant increase of H_2 in final gas Tomita and Ohtsuka [22] concluded that in place of deposited carbon, nascent carbon precursors (CH_x) formed by tar decomposition must have reacted with steam:

$$2\,CH_x + 2\,H_2O \longrightarrow CH_4 + CO_2 + xH_2 \qquad \text{(R2.18)}$$

At 875 K in presence of steam weight loss of Ni-loaded LY doubled compared to that of in absence of steam. Under these conditions, steam-gasification of char as well as the decomposition of tar proceeds to a large extent. Increasing steam to coal ratio did not show significant change in weight loss but resulted in lower CH_4 yield, as CH_4 goes through steam reforming in presence of excess steam [22]

$$CH_4 + 2\,H_2O \longrightarrow CO_2 + 4\,H_2 \qquad \text{(R2.19)}$$

Hayashi et al. [65] reported that the steam evolved during pyrolysis can also react with hydrocarbons and tar to produce hydrogen. Hydrogen balance on the experimental systems revealed that there is a trade-off between H_2O, gaseous hydrocarbon and tar with hydrogen. Increase in H_2 concentration at higher temperature was accompanied by considerable increase in CO and CO_2 indicates that hydrocarbons and tarry materials react with the evolved steam during pyrolysis.

2.4.4 Fate of the pollutant-forming elements

Nitrogen, sulphur and chlorine are the major pollutant-forming elements present in Victorian brown coals.

Nitrogen exists in hetero-aromatic ring systems (e.g. pyrrole, pyridine) in coals [66]. Conversion of coal-N during pyrolysis and gasification has been extensively studied by Li and co-workers. Depending on the reaction condition coal-N can be converted to NH_3, HCN, N_2 and various oxides of nitrogen. However, since NH_3 and HCN were the major products most of the works were focused on the production of these two gases. NH3 can formed either by hydrogenation of char-N by H redicals or thermal cracking of N-containing stable volatile compounds in the gas phase. HCN is mainly generated from thermal cracking of unstable volatile compounds in the gas phase [67, 68]. Availability of H-radicals plays a critical role in formation of NH_3 and to

a lesser extent for HCN. Gasification of LY coal in 15% steam (balance Ar) at 800 °C resulted conversion of 75% coal-N to NH_3 [68]. However, production of HCN increased marginally. O_2-gasification alone (2000 ppm O_2) at the same temperature showed only 20% Coal-N to form NH_3. Presence of both 2000 ppm O_2 and 15%-steam showed conversion of 65% coal-N to NH_3.

In comparison to steam-gasification, this reduction in NH_3 formation can be attributed to partial oxidation of some char-N sites. CO_2-gasification studies showed that presence of CO_2 suppress both formation of NH_3 and HCN [69].

Victorian brown coal contains two types of organic sulphur compounds: thermally unstable aliphatic (sulphides, mercaptans and disulfides)and stable aromatic compounds (sulphides and mercaptans) [70]. H_2S is the major sulphur containing species in the gasification products. Heating LY coal at 6.7 K min^{-1} to 1000 °C released about 48% of Coal-S as H_2S. 55% of sulphur converted to H_2S when the same coal was heated to 800 °C at a faster heating rate. It was concluded that heating rate does not significantly affect H_2S formation. Difference in yield can be attributed to re-incorporation of some H2S into the char surface at higher temperature (700-1000 °C) [71]. Presence of metallic species in the coal can significantly reduce formation of H_2S during pyrolysis and gasification. Calcium as well as nickel can retain significant amount of sulphur as sulfides during gasification of Victorian brown coals [42, 72].

Information about the fate of chlorine in Victorian brown Coal is scarce in the literature. Studies on other coals identified the release of HCl into two temperature zones. Release of HCl below 450 °C is more prominent and can be evolved from hydrated $CaCl_2$ and NaCl as well as organic hydrochlorides present in the coal. Release of HCl at higher temperatures (>450 °C) was attributed to the decomposition of unstable compounds that are formed by secondary reactions of HCl formed at lower temperature with the nascent char [73, 74]. Tsubouchi et al. [74] found a linear and reverse correlation between char-Cl and HCl which indicates that HCl formation from tar-Cl is negligibly small. During CO_2-gasification of a sub-bituminous coal at 1000 °C and 2.5 MPa HCl yield was less than the detection limit of 0.05 ppm all the time. Residual char retained 92% of coal-Cl and only 8% coal-Cl was released as volatile inorganic chlorides other than HCl [75].

2.4.5 Volatile-char interactions

Volatiles evolved during the devolatilisation process include hydrogen, oxides of carbon and hydrocarbon vapours (Figure 2.5). Interactions between volatiles and char are unavoidable for moving- bed, fluidised-bed and entrained-flow gasifiers. Victorian brown coals have more volatiles than higher rank coals. Therefore, volatile-char interactions are important phenomena for brown coal gasification.

Inhibition of char gasification by hydrogen [76], carbon dioxide [77] and carbon monoxide [78] is a well-known phenomenon. Less stable volatiles undergo thermal cracking to produce free radicals. Interactions between the char and these highly reactive radicals were studied in a two-stage quartz reactor [79], a combination of fluidised- and fixed-bed reactors.

Volatile-char interaction is responsible for volatilisation of monovalent AAEM species (e.g. Na). Sodium present in chloride form release chlorine as HCl [80]:

$$\mathrm{CM} + \mathrm{NaCl} \longrightarrow \mathrm{CM{-}Na} + \mathrm{HCl} \tag{R2.20}$$

Here, CM denotes the char matrix. Sodium present in carboxylate form also breaks down during pyrolysis [81]:

$$\mathrm{CM{-}COONa} \longrightarrow \mathrm{CM{-}Na} + \mathrm{CO_2} \tag{R2.21}$$

H- or R-radicals formed from thermal cracking of volatiles then reacts with the char matrix resulting release of sodium in the gas phase [79]:

$$\mathrm{CM{-}Na} + \mathrm{H} \longrightarrow \mathrm{CM{-}H} + \mathrm{Na} \tag{R2.22}$$

$$\mathrm{CM{-}Na} + \mathrm{R} \longrightarrow \mathrm{CM{-}R} + \mathrm{Na} \tag{R2.23}$$

Volatilisation of Ca or Mg requires simultaneous breakage of two bonds between the metal and the char matrix. Therefore, Ca or Mg volatilisation is lesser compared to that of Na [79, 82].

A comparative study on demineralised, Na- and Ca-loaded LY coal has shown that the volatile-char interactions also lead to the formation of soot on the char surface [82]. The soot then undergoes catalytic destruction if Na or Ca is present. At temperatures above 700 °C, net soot production was zero because of the catalytic effect of Na. Ca showed lower catalytic effect towards soot destruction [82].

Retention of Na in char matrix, due to its volatilisation during volatile-char interactions, can be as low as 10% of its initial amount [83]. Na is well dispersed throughout the char matrix [82]. This observation indicates that the radicals can penetrate deep into the char matrix release Na. At the same time, the radicals also enhance ring condensation reactions inside the char matrix, changing the char structure [84]. The volatile-char interactions, therefore, reduces the char reactivity by volatilising the inherently present catalytic species (e.g. Na) and changing the char structure to more orderly and non-reactive form [85, 86].

2.4.6 Kinetics of brown coal/char gasification

A summary of the kinetic study of brown coal/char gasification is shown in Table 2.3. Studies have been performed on different Victorian brown coal/char samples, with different gasifying agents for wide ranges of sample size and particle size. The activation energies obtained, therefore, varied a great deal from one study to the others. O_2 gasification/combustion reaction had lowest activation energy. For CO_2 and steam activation energies were similar. Doping samples with iron decreased the activation energy, since iron catalyses steam-gasification. Iron is also known to catalyse CO_2-gasification and combustion. However, effect of iron addition to coal on these reactions was not considered for the study. Transfer numbers for most of these studies were not reported.

2.4.7 Brown coal properties and gasifier selection

Gasifiers can be grouped into three generic types, namely moving-bed, fluidised-bed and entrained-flow gasifier. Depending on the type of gasifier the syngas composition can vary a great deal. A comparison of major features of the three major types of gasifiers is shown in Table 2.4.

TABLE 2.3: Victorian brown coal/char gasification kinetics

Coal/char	Particle size (μm)	Gasifying agents	Reactor	Sample	Temperature range	Activation energy (kJ/mol)	Transfer number (s^{-1})
LY [62]	150-250	Steam	TB	20 mg	873-1073 K	160	-
LY (14% Fe loaded)[62]	150-250	Steam	TB	20 mg	873-1073 K	120	-
LY [63]	150-250	Steam	TB	20 mg	873-1073 K	190	-
LY-Fe loaded [63]	150-250	Steam	TB	20 mg	873-1073 K	110-160	-
MW-char [87]	700-1000	CO_2/N_2	FB	1-5 g	873-1073 K	230	-
MW-char [87]	700-1000	Steam/N_2	FB	1-5 g	773-973 K	225	-
MW-char [87]	700-1000	O_2/N_2	FB	1-5 g	773-873 K	127	-
LY-char [88]	<250	CO_2	TB	20 mg	1143-1559 K	170	6.60×10^3
LY [89]	150-250	20% CO_2/N_2	TR	0.5 g	773-1223 K	160	1.31×10^3
YL-briquettes [90]	74-150	Steam/N_2	TB	20 mg	1198-1348 K	170	1.31×10^3
YL [72]	1000-2000	Steam/N_2	TB	20 mg	873-973 K	160	-

TB: Thermobalance; FB: Fluidised-bed; TR: Tubular reactor

TABLE 2.4: Characteristic features of generic types of gasifiers [91]

	Moving bed	Fluidised bed	Entrained flow
Preferred feedstock	Lignite, reactive bituminous coal, wastes	Lignite, bituminous coal, cokes, wastes, biomass	Lignite, reactive bituminous coal, petcokes
Coal feed size (mm)	5-80	< 6	< 0.1
Ash content	No limitation; <25% for slagging type	No limitation	<25% preferred
Scale	Small	Small to medium	Large
CO_2 in dry raw gas	26-29	18	6-16
CH_4 in dry raw gas	8-10	6	<0.3
H_2/CO ratio	1.7-2.0	0.7	0.7-0.9
Tars produced	Co-current: low counter-current: moderate to high	Intermediate	Absent
Ash conditions	Dry/slagging	Dry/agglomerating	Slagging
Key technical issues	Utilisation of fines and hydrocarbon liquids	Carbon conversion	Raw gas cooling

Moving-bed gasifiers require good bed permeability to ensure efficient heat and mass transfer between the solid and the gas phase. Moving-bed gasification of brown coal was commercialised in Victoria in 1956 [92] to supply town gas to Melbourne. The Lurgi gasification plant near Morwell had a rated capacity of 425,000 m^3/day town gas and used raw coal and briquettes as feedstock. The average heating value was 16.4 MJ m^{-3}. The purified product gas contained 23.3% CO, 52.2% H_2, 18.4% CH_4, 4.2% CO_2, 1% N_2 and 1% higher hydrocarbons [92]. In the early years, operation of the plant was hindered by problems in fuel feeding, water spray system in the gas outlet and corrosion in cooler circuit. These problems were gradually solved and reliable operation was achieved. However, operation of the gasification plant ceased in 1969, with the discovery of low cost natural gas in Bass Strait and its recirculation in Melbourne [92].

The syngas from moving-bed gasifiers has high hydrocarbon concentration. Hydrocarbons act as inert during the production of methanol or DME. Hence, moving-bed gasifiers are not appropriate for such processes.

The operating temperatures for fluidised-bed gasifiers are low (900-1050 °C) [93]. Therefore, fluidised-bed gasification requires reactive coal as feedstock. Victorian brown is highly reactive [50] and hence can be used in fluidised-bed gasifiers. Considerable work has been done assessing the viability of fluidised-bed gasification of Victorian brown coals under various conditions. Hydro-gasification of brown coal was studied by CSIRO in 1960s and 1970s in both fixed- and fluidised-bed reactors [94]. A wet brown coal variant of IGCC was developed by State Electricity Commission of Victoria (SECV) and later by HRL Limited oer the period 1989- 1998. The process, integrated drying gasification technology (IDGCC), allows the wet coal to come into direct contact with the hot fuel gas coming from the circulating fluidised-bed gasifier. The hot gas dries the feed coal containing 60-67% moisture [93]. Carbon conversion of 75-90% was reported from the process development unit for IDGCC [95, 96]. Details of the process can be found elsewhere [93, 95]. Fluidised-bed gasification was also extensively studied in laboratories and already been discussed in the preceding sections.

Bed agglomeration is considered as a major operating problem for fluidised-bed gasifiers [97]. Though Victorian brown coal in non-caking [29], bed agglomeration has been observed during gasification. Presence of low temperature silicates (melting point around 850 °C) along with halite (NaCl) are believed to cause agglomeration

[96, 97]. Bed agglomeration along with low carbon conversion has been identified as impediments for wider application of this technology with Victorian brown coal [96].

LY coal has been studied in transport reactor development unit [98]. Transport reactor is a high velocity adaptation of circulating fluid-bed process. Exit gas temperature in transport reactor is similar to that of fluidised-bed gasifier. However, the residence time, 5-30 s [99], is shorter than that of fluidised-bed gasifiers (10-100 s [91]). For LY coal, carbon conversion was 77.3% and 83% for air- and oxygen-blown gasification, respectively [98].

Entrained-flow gasifiers can use both pulverised coal and coal- water slurry as feed. Rheological study on brown coal-water slurry indicated that economic pipeline transport is not possible [100]. However, feeding of dry pulverised coal is still viable. Low ash content and ash melting point below 1400 °C [101] indicate that brown coal is suitable for entrained-flow gasification. However, work on entrained-flow gasification of Victorian brown coal is limited and not available in open literature.

References

[1] Allardice DJ, Young BC, 2001, *In:* Annual international Pittsburgh coal conference, Newcastle, Australia

[2] St Baker TC, Juniper LA, 1982, Australian Coal Geology, **4**: 187

[3] Kumar KS, Sommerland RE, Feldman PL, 1991, Power, **135**: 31–38

[4] Campbell R, 2012, Undermined or overburdened Victoria's brown coal: an economic perspective a report for Environment Victoria. Economists at Large, Melbourne

[5] Speight JG, 2012, The chemistry and technology of coal. CRC Press, Boca Raton

[6] Atwood MT, Schulman BL, 1977, American Chemical Society Divison of Fuel Chemistry Preprints, **22**: 233–252

[7] Lee JG, Kim JH, Lee HJ, Park TJ, Kim SD, 1996, Fuel, **75**: 1035 – 1042

[8] Shui H, Cai Z, Xu C, 2010, Energies, **3**: 155–170

[9] Pant K, Gupta RB, 2009, *In:* Hydrogen fuel: production, transport, and storage, Gupta RB, editor, 3–32, CRC, Boca Raton

[10] Midilli A, Ay M, Dincer I, Rosen MA, 2005, Renewable and sustainable energy reviews, **9**: 255–271

[11] Zennaro R, 2013, *In:* Greener Fischer-Tropsch processes for fuels and feedstocks, Maitlis PM, de Kler A, editors, 149–169, Wiley-VCH Verlag GmbH & Co. KGaA, Weinheim

[12] Fleisch T, Sills R, 2007, *In:* Natural gas conversion symposium 8, Natal, Brazil

[13] Olah GA, Goeppert A, Prakash GKS, 2009, Beyond oil and gas: the methanol economy. 2nd ed., WILEY-VCH Verlag GmbH & Co. KGaA, Weinheim

[14] Tabak SA, Avidan AA, Krambeck FJ, 1986, American Chemical Society DIvision of Fuel Chemistry Preprints, **31**: 293–299

[15] Topp-Jørgensen J, 1988, *In:* Methane conversion proceedings of a symposium on the production of fuels and chemicals from natural gas, Bibby D, Chang C, Howe R, Yurchak S, editors, vol. 36 of *Studies in Surface Science and Catalysis*, 293 – 305, Elsevier

[16] Zhang L, Huang Z, 2007, Energy, **32**: 1896 – 1904

[17] Nissing C, Coënt L, Girault N, 2011, *In:* Towards Life Cycle Sustainability Management, Finkbeiner M, editor, 469–480, Springer Netherlands

[18] Edwards R, Larive JF, Beziat JC, 2011, Well-to-wheels analysis of future automotive fuels and powertrains in the European context. Tech. rep., European Commission Joint Research Centre, Luxembourg

[19] Ou X, Zhang X, Chang S, 2010, Energy Policy, **38**: 406 – 418

[20] Höök M, Aleklett K, 2010, International Journal of Energy Research, **34**: 848–864

[21] Williams RH, Larson ED, 2003, Energy for Sustainable Development, **7**: 103 – 129

[22] Tomita A, Ohtsuka Y, 2004, *In:* Advances in the science of Victorian brown coal, Li CZ, editor, 223 – 285, Elsevier Science, Amsterdam

[23] Li CZ, Sathe C, Kershaw JR, Pang Y, 2000, Fuel, **79**: 427 – 438

[24] Hashimoto K, Miura K, Ueda T, 1986, Fuel, **65**: 1516 – 1523

[25] Hayashi JI, Takahashi H, Doi S, Kumagai H, Chiba T, Yoshida T, Tsutsumi A, 2000, Energy & Fuels, **14**: 400–408

[26] Hayashi JI, Li CZ, 2004, *In:* Advances in the Science of Victorian Brown Coal, Li CZ, editor, 11 – 84, Elsevier Science, Amsterdam

[27] Ohtsuka Y, Asami K, 1997, Catalysis Today, **39**: 111 – 125

[28] Hayashi JI, Miura K, 2004, *In:* Advances in the Science of Victorian Brown Coal, Li CZ, editor, 134 – 222, Elsevier Science, Amsterdam

[29] Tyler RJ, 1979, Fuel, **58**: 680 – 686

[30] Cliff DI, Doolan KR, Mackie JC, Tyler RJ, 1984, Fuel, **63**: 394 – 400

[31] Kershaw JR, Sathe C, Hayashi Ji, Li CZ, Chiba T, 2000, Energy & Fuels, **14**: 476–482

[32] Sathe C, Pang Y, Li CZ, 1999, Energy & Fuels, **13**: 748–755

[33] Xu WC, Tomita A, 1987, Fuel, **66**: 632 – 636

[34] Xu WC, Tomita A, 1987, Fuel, **66**: 627 – 631

[35] Miura K, Mae K, Asaoka S, Yoshimura T, Hashimoto K, 1991, Energy & Fuels, **5**: 340–346

[36] Jamil K, Hayashi JI, Li CZ, 2004, Fuel, **83**: 833 – 843

[37] Kershaw JR, 1985, Liquid Fuels Technology, **3**: 205–228

[38] Kershaw J, 1989, Spectroscopic analysis of coal liquids. Coal science and technology, Elsevier

[39] Sathe C, Hayashi JI, Li CZ, 2002, Fuel, **81**: 1171 – 1178

[40] Wailes PC, Bell AP, Triffett AC, Weigold H, Galbraith M, 1980, Fuel, **59**: 128 – 132

[41] Kershaw JR, Kelly BA, 1983, Fuel Processing Technology, **7**: 145 – 159

[42] Tomita A, Watanabe Y, Takarada T, Ohtsuka Y, Tamai Y, 1985, Fuel, **64**: 795 – 800

[43] Gale TK, Bartholomew CH, Fletcher TH, 1996, Energy & Fuels, **10**: 766–775

[44] Wang X, Chen H, Yang H, Ju F, Zhang S, 2012, Asia-Pacific Journal of Chemical Engineering, **7**: S171–S176

[45] Miura K, Hashimoto K, Silveston PL, 1989, Fuel, **68**: 1461 – 1475

[46] Jenkins RG, Nandi SP, Walker Jr PL, 1973, Fuel, **52**: 288 – 293

[47] Knight AT, Sergeant GD, Stubington JF, 1983, *In:* International conference on coal science, 468–471, Pittsburgh

[48] Kasaoka S, Sakata Y, Tong C, 1983, Journal of the Fuel Society of Japan, **62**: 335–348

[49] Fujita H, Uba M, Nishida S, 1982, Journal of the Fuel Society of Japan, **61**: 301–305

[50] Takarada T, Tamai Y, Tomita A, 1985, Fuel, **64**: 1438 – 1442

[51] Nishiyama Y, 1986, Fuel, **65**: 1404 – 1409

[52] Veraa MJ, Bell AT, 1978, Fuel, **57**: 194 – 200

[53] McKee DW, Spiro CL, Kosky PG, Lamby EJ, 1983, Fuel, **62**: 217 – 220

[54] McKee DW, Spiro CL, Kosky PG, Lamby EJ, 1982, American Chemical Society DIvision of Fuel Chemistry Preprints, **27**: 74–86

[55] Ohtsuka Y, Tomita A, 1986, Fuel, **65**: 1653 – 1657

[56] Tomita A, Tamai Y, 1981, Fuel, **60**: 992 – 994

[57] Tomita A, Ohtsuka Y, Tamai Y, 1983, Fuel, **62**: 150 – 154

[58] Higashiyama K, Tomita A, Tamai Y, 1985, Fuel, **64**: 1157 – 1162

[59] Ohtsuka Y, Tomita A, Tamai Y, 1986, Applied Catalysis, **28**: 105 – 117

[60] Ohtsuka Y, Tamai Y, Tomita A, 1987, Energy & Fuels, **1**: 32–36

[61] Suzuki T, Mishima M, Takahashi T, Watanabe Y, 1985, Fuel, **64**: 661 – 665

[62] Ohtsuka Y, Asami K, 1991, Industrial and Engineering Chemistry Research, **30**: 1921–1926

[63] Asami K, Ohtsuka Y, 1993, Industrial and Engineering Chemistry Research, **32**: 1631–1636

[64] Yu J, Tian FJ, Chow MC, McKenzie LJ, Li CZ, 2006, Fuel, **85**: 127 – 133

[65] Hayashi JI, Takahashi H, Iwatsuki M, Essaki K, Tsutsumi A, Chiba T, 2000, Fuel, **79**: 439 – 447

[66] Li CZ, 2004, *In:* Advances in the science of Victorian brown coal, Li CZ, editor, 286 – 359, Elsevier Science, Amsterdam

[67] Tian FJ, Yu J, McKenzie LJ, Hayashi Ji, Li CZ, 2007, Energy & Fuels, **21**: 517–521

[68] McKenzie LJ, Tian FJ, Guo X, Li CZ, 2008, Fuel, **87**: 1102–1107

[69] Chang L, Xie Z, Xie KC, Pratt KC, ichiro Hayashi J, Chiba T, Li CZ, 2003, Fuel, **82**: 1159 – 1166

[70] Taghiei MM, Huggins FE, Shah N, Huffman GP, 1992, Energy & Fuels, **6**: 293–300

[71] Tan LL, Li CZ, 2000, Fuel, **79**: 1891 – 1897

[72] Ohtsuka Y, Asami K, 1995, Energy & Fuels, **9**: 1038–1042

[73] Tsubouchi N, Ohtsuka S, Hashimoto H, Ohtsuka Y, 2004, Energy & Fuels, **18**: 1605–1606

[74] Tsubouchi N, Ohtsuka S, Nakazato Y, Ohtsuka Y, 2005, Energy & Fuels, **19**: 554–560

[75] Takeda M, Ueda A, Hashimoto H, Yamada T, Suzuki N, Sato M, Tsubouchi N, Nakazato Y, Ohtsuka Y, 2006, Fuel, **85**: 235 – 242

[76] Lussier M, Zhang Z, Miller DJ, 1998, Carbon, **36**: 1361 – 1369

[77] Roberts DG, Harris DJ, 2007, Fuel, **86**: 2672–2678

[78] Huang Z, Zhang J, Zhao Y, Zhang H, Yue G, Suda T, Narukawa M, 2010, Fuel Processing Technology, **91**: 843–847

[79] Wu H, Quyn DM, Li CZ, 2002, Fuel, **81**: 1033–1039

[80] Quyn DM, Wu H, Li CZ, 2002, Fuel, **81**: 143–149

[81] Quyn DM, Wu H, Bhattacharya SP, Li CZ, 2002, Fuel, **81**: 151–158

[82] Li X, Wu H, Hayashi Ji, Li CZ, 2004, Fuel, **83**: 1273–1279

[83] Li CZ, 2007, Fuel, **86**: 1664 – 1683

[84] Zhang S, Hayashi JI, Li CZ, 2011, Fuel, **90**: 1655–1661

[85] Wu H, Li X, Hayashi Ji, Chiba T, Li CZ, 2005, Fuel, **84**: 1221–1228

[86] Zhang S, Min Z, Tay HL, Asadullah M, Li CZ, 2011, Fuel, **90**: 1529–1535

[87] Harris DJ, Smith IW, 1991, Symposium (International) on Combustion, **23**: 1185–1190

[88] Osafune K, Marsh H, 1988, Fuel, **67**: 384–388

[89] Asami K, Sears P, Furimsky E, Ohtsuka Y, 1996, Fuel Processing Technology, **47**: 139–151

[90] Takarada T, Nabatame T, Ohtsuka Y, Tomita A, 1989, Industrial & Engineering Chemistry Research, **28**: 505–510

[91] Wagner NJ, Coertzen M, Matjie R, van Dyk J, 2008, *In:* Applied Coal Petrology, Suárez-Ruiz I, Crelling JC, editors, 119 – 144, Elsevier, Burlington

[92] Chan W, Urie R, 1985, Review of gasification studies on Victorian brown coal. Coal Corporation of Victoria, Melbourne, Victoria, Australia

[93] Higman C, van der Burgt M, 2003, Gasification. Gulf Professional Publishing, Burlington

[94] Birch T, 1970, Hydrogasification of Brown Coal: Experiments with a two-stage reactor. CSIRO, Division of Chemical Engineering, Clayton, Victoria, Australia

[95] Johnson TR, 2001, *In:* EPRI-VGB Conference on Lignites and Low-rank Coals, 972–983, Wiesbaden, Germany

[96] Bhattacharya SP, 2006, Process Safety and Environmental Protection, **84**: 453–460

[97] Collot AG, 2006, International Journal of Coal Geology, **65**: 191–212

[98] Swanson ML, 2005, Advanced High-Temperature, High-Pressure Transport Reactor Gasification. Tech. rep., University Of North Dakota

[99] Shadle LJ, Monazam ER, Swanson ML, 2001, Industrial & Engineering Chemistry Research, **40**: 2782–2792

[100] Leong YK, Creasy DE, Boger DV, Nguyen QD, 1987, Rheologica Acta, **26**: 291–300

[101] DPI, 2010, *Latrobe Valley brown coal submission: Green Global Technologies. Cited: 20 April 2013. Available from: http://www.dpi.vic.gov.au/*

Chapter 3

Review: Dimethyl ether synthesis

3.1 Introduction

DME is the simplest form of ether with a chemical formula of CH_3OCH_3. It is a colourless gas with typical ether-like sweet smell. DME is a non-toxic, non-carcinogenic and non-corrosive compound. DME has been used as an aerosol propellant [1], refrigerant [2] and precursor to many important chemicals [3–5]. DME can be used as a diesel substitute since it has high cetane number (55-60) [6]. It undergoes almost smoke-free combustion because of its low auto-ignition temperature, high oxygen content and absence of C−C bond in the molecular structure [7].

DME is also an environmentally benign fuel. DME has a lifetime of 5.1 days in the troposphere and has global warming potential (GWP) of 1.2, 0.3 and 0.1 for 20, 100 and 500-year time horizon respectively [8].

3.2 Applications of DME

DME can be used for various applications: as household and transportation fuel, in gas turbines and fuel cells. The following section includes major applications of DME.

3.2.1 DME for household use

Natural gas (NG) and LPG are the two most prevalent fuels for household application in developed countries. Major component of NG is methane (CH_4) while LPG is a mixture of propane (C_3H_8), butane (C_4H_{10}) and other minor constituents. For household application NG is supplied via pipeline while LPG is used from high-pressure

Excerpted from: Bhattacharya S, Kabir KB and Hein K, *progress. energy combust. sci*, 39: 577-605

Table 3.1: Physical properties of DME and main constituents of NG and LPG

	Methane	Propane	Butane	DME
Chemical formula	CH_4	C_3H_8	C_4H_{10}	C_2H_6O
Normal boiling point (°C)	-161.5	-42.1	-0.6	-24.9
Explosion limit (%)	5-15	2.1-9.5	1.9-8.5	3.4-17
Lower heating value (kJ/kg)	49,900	46,350	45,740	28,620
Auto ignition temperature (°C)	595	450	405	235
Specific gravity to air	0.55	1.53	2.01	1.6
Vapour pressure at 20 °C (bar)	-	8.4	2.1	5.1

cylinders. A comparison of properties of methane, propane, butane and DME is shown in Table 3.1. It is apparent that the physical properties of DME are similar to that of major components of LPG. Like LPG, DME can be liquefied at mild pressure. Vapour pressure of DME at 37.8 °C is approximately 8.4 bar [9], less than the LPG maximum vapour pressure specification of 13.8 bar [10]. Therefore LPG infrastructure can readily be used for DME without any modification. DME has lower heating value than other fuels presented here. Therefore, more DME would be required for equal quantity of heat generation.

Emission characteristics of DME were studied by Central Station for Environmental monitoring of Shanxi province of China to evaluate its applicability as a household cooking fuel. The study showed that the CH_3OH and CO concentrations in the exhaust gas were much lower than the permissible value while NO_x concentration was slightly higher [11, 12]. A comparative study of CO and NO emissions from propane, n-butane and DME in a co-flow burner giving laminar premixed flames were studied by Frye et al. [13]. They compared these fuels on the basis of constant mass flow, constant C-atom flow, and constant energy release rate. For a wide range of fuel-to-air ratio, CO and NO emissions for DME were lower than that for other fuels. In the worst case, emissions from DME flame were equal to that of propane/n-butane.

DME has a huge potential as LPG alternative, especially for non-petroleum producing countries like China and Japan. Global LPG demand is expected to be 260 million tonnes by 2015 [14] and DME can have its share with no/slight change in the existing infrastructure.

Table 3.2: Physical properties of transportation fuels

	Gasoline	Diesel	Ethanol	Methanol	DME
Chemical formula	C_4-C_{12}	C_{10}-C_{15}	C_2H_5OH	CH_3OH	CH_3OCH_3
Normal boiling point (°C)	38-204	125-240	78.8	64.0	-24.9
Explosion limit (%)	0.6-7.5	1.4-7.6	3.5-19	5.5-30	3.4-17
Lower heating value (kJ/kg)	41,660	43,470	26,870	19,990	28,620
Auto ignition temperature (°C)	246-280	210	365	385	235
Octane number	82-92	25	113	123	-
Cetane number	-	40-55	-	5	55-60
Sulphur content (ppm)	∼200	∼250	-	-	-

3.2.2 DME as a transportation fuel

A comparison of the properties of various transportation fuels is shown in Table 3.2. Methanol has high octane rating while DME has high cetane number. Therefore, methanol and DME are appropriate for spark-ignition (SI) and compression-ignition (CI) engines, respectively. DME has several advantages as a transportation fuel. It is a sulphur-free, zero aromatic fuel. DME has a low boiling point and therefore it is readily vaporized when injected into the engine. DME molecule has approximately 34.8% oxygen content. Absence of C-C bonds and high oxygen content enhances oxidation rate and thus DME undergoes almost smoke-free combustion. C-O bond being weaker than the CeH bond facilitates dissociation of DME molecule at relatively low temperatures and results in high cetane number and shorter ignition delay [7]. Therefore, DME engines run with reduced combustion noise [15]. Major disadvantages of DME are lower energy density and low viscosity, and DME requires higher compression work than diesel [7].

Emission characteristics from DME-fuelled engines have been reported by several researchers [16–18]. Studies show that soot emissions from engines disappear if the oxygen concentration in the fuel is greater than 30% [19, 20]. DME having 34.8% oxygen gives soot free emission. Particulate emission from DME-fuelled engines was found to be lower than that of other fuels for CI engines [20]. NO_x emission is also found to be lower [16–18]. Since DME engines do not need a trade-off between NO_x-soot emissions they can operate at higher exhaust gas recirculation (EGR). With optimised EGR ratio, DME engines can meet EURO IV NO_x limit [21]. However, studies on emission of hydrocarbons (HC) and CO showed varied results [7]. Studies on formaldehyde emission showed increased concentration compared to that of diesel engines [22].

Though DME has very favourable combustion properties, its physical properties are the main barrier for its application as a transportation fuel. Low liquid density and viscosity, lower heating value and necessity of engine modification are going to be major problem areas. However, DME is still expected to be a major part of the sustainable and more environment friendly transportation system in the future.

3.2.3 DME use in gas turbines

DME can be used in Dry-Low-NO_x (DLN) turbines [23, 24]. Performance analysis of combined cycle power plants fuelled with DME, NG and naphtha was carried out using GE PG9117E gas turbines. Instead of pure DME, Fuel-grade DME composed of 88-89 wt% DME, 7-8% methanol, 2.9-3.5% water and 0.3-0.5% other oxygenates was used. NOx and CO emissions from DME-fuelled turbine were lower compared to that of NG and naphtha fuelled turbines. However, higher carbon content in DME produced more CO_2 for per unit of energy generated. Heat rate for DME-fuelled turbine was 1.6% lower than the NG turbine since the heat rate was calculated for liquid DME lower heating value (LHV) instead of its gaseous form. Low temperature heat of flue gas was utilised to vaporise the DME. As a result stack temperature of DME-fuelled turbine was 15 °C lower than that of NG [23, 24]. Lee et al. [25] studied the performance of DME in a commercial gas turbine (GE7EA). The results show that DME is an efficient and clean fuel for gas turbine. However, they concluded that small modification of this NG fuelled turbine would provide better performance if DME is used as a fuel. Cocco et al. [26] evaluated the performance of chemically recuperated gas turbine (CRGT) power plants fuelled by DME. CRGT is a novel gas turbine cycle promoted by California Energy Commission (CEC). Although CRGT is not commercialised yet, it holds great prospect due to its potential for ultra-low NO_x emissions ($\sim$1 ppm) [27]. In a CRGT, heat recovery steam generator (HRSG) used in the steam-injected gas turbine (SIGT) and combined cycle (CC) is replaced with a steam reformer. The steam produced from the exhaust heat, instead of making superheated, is mixed with the fuel in the reformer. The mixture is heated by the exhaust heat and goes through endothermic reaction producing a mixture of CO, H_2, CO_2 and unconverted fuel and H_2O. However, the problem of using NG in CRGT is high reforming temperature of methane (about 600-800 °C) compared to commercial gas turbine exhaust temperature. On the other hand, DME is more suitable for CRGT with reforming temperature of about 300-350 °C [26]. DME-fuelled CRGT

power plant can achieve efficiency equal to combined cycle DME-fuelled power plant, which is not the case for NG [28].

3.2.4 Fuel cells using DME

Fuel cells (FCs) are designed to convert chemical energy into electrical energy. The fuel (usually H_2) is fed continuously to the anode while an oxidant (i.e. oxygen) is fed to the cathode. Hydrogen and oxygen give an overall electrochemical reaction:

$$H_2 + \tfrac{1}{2}O_2 \longrightarrow H_2O \qquad \text{(R3.1)}$$

with a theoretical electrochemical potential of 1.23 V.

Quality of the fuel (hydrogen) supplied to the anode significantly affects the performance of the fuel cell. Proton exchange membrane fuel cell cannot operate in presence of CO in the fuel gas due to poisoning of the Pt-anode. Phosphoric acid fuel cell (PAFC) can tolerate high level of CO (1-2%). Though both proton exchange membrane fuel cell (PEMFC) and PAFC can tolerate CO_2 alkaline fuel cell cannot perform with CO_2 due to carbonate formation with the electrolyte (NaOH or KOH). Increasing operating temperature of the fuel cells can also increase impurity tolerance limit in fuel gas. Molten carbonate fuel cell (MCFC) and solid oxide fuel cell (SOFC) can tolerate CO, CO_2 and small amount of hydrocarbons, especially CH_4.

Hydrogen storage is still a major challenge [29–33]. Steam reforming (SR), partial oxidation (POX) or a combination of these two, auto-thermal reforming (ATR) of primary fuels can be used for on-demand hydrogen generation [34]. Like methanol, DME can be reformed at lower temperatures than the hydrocarbon. Thermodynamic aspects of DME steam reforming both at lower [35, 36] and higher temperatures [37] show that DME can decompose to form CH_4 during SR and therefore development of catalysts leading to higher hydrogen and lower methane selectivity is necessary. According to current understanding, catalytic SR of DME is a two-step mechanism [38–40]: DME dehydration to methanol followed by SR of methanol. Here, the DME hydrolysis step is rate-limiting [41, 42]. Therefore, current research on DME reforming is highly focused on the DME hydration catalyst as well as catalyst for the subsequent step for higher H_2 and reduced CO yield to match the requirement of fuel cells [40, 43, 44]. Cocco and Tola [45, 46] also evaluated possibility of replacing methane with

DME for Solid oxide fuel cell-Micro gas turbines (SOFC-MGT). Lower reforming temperature of DME allows better heat recovery from the exhaust gas. With 280 °C SR of DME and SOFC operating at 1000 °C provided 69% plant efficiency.

Direct liquid-feed fuel cell (DLFC) can eliminate the requirement of expensive catalytic reformer system for hydrogen production. Demirci [47] reviewed the thermodynamic and environmental aspects of 14 DLFCs. Methanol is the most studied liquid fuel for DLFC. However, major problem with direct methanol fuel cell (DMFC) is the toxicity. Compared to methanol DME is a safer choice with no apparent health and environmental hazard. In a direct dimethyl ether fuel cell (DDEFC) DME get oxidised to produce CO_2 and H_2O. The individual electrode and overall reactions are as follows:

$$\text{Anode:} CH_3OCH_3 + 3\,H_2O \longrightarrow 2\,CO_2 + 12\,H^+ + 12\,e^- \tag{R3.2}$$

$$\text{Cathode:} 3\,O_2 + 12\,H^+ + 12\,e^- \longrightarrow 6\,H_2O \tag{R3.3}$$

$$\text{Overall:} CH_3OCH_3 + 3\,O_2 \longrightarrow 2\,CO_2 + 3\,H_2O \tag{R3.4}$$

These reactions also show that DME can donate 12 electrons, twice as much as from methanol. Therefore, 1 mol of DME and 2 mol of methanol would produce equivalent amount of energy.

A comparative study between DMFC and DDEFC showed that DDEFC can be more efficient than DMFC under certain conditions [48]. Though, development of DDEFC is still at its infancy it can be said that DME is a promising fuel for FC not only performance-wise but also from environmental and hazard point of views.

3.2.5 Other potential applications of DME

DME has been used as an aerosol propellant for many years [49]. DME is preferable than CFC propellants because it has significantly less impact on ozone layer and lower GWP.

DME is designated as refrigerant E170 by ASHRAE. Studies show that performance of DME as a refrigerant is similar to that of R134a. The coefficient of performance (COP) of DME was found to be greater than that of R134a. Therefore, DME can be one of the alternatives after R12 and R22 are completely phased out. A ranking

of 40 refrigerants based on ozone depletion potential, global warming potential and atmospheric lifetime was done by Restrepo et al. [50] by applying the Hasse diagram technique. DME was found to be the least problematic refrigerant along with ammonia among those 40 refrigerants.

DME can be used as a chemical feedstock. DME is the starting chemical for DME-to-olefins (DTO) process. Product range of DTO varies depending on the nature and selectivity of the catalyst towards specific olefins [3, 51]. Feasibility study of DME to propylene (DTP) is underway through construction of a demonstration plant in Mitsubishi Chemical's Mizushima plant [52]. The process and the zeolite-based catalyst are developed jointly by JGC Corporation and Mitsubishi Chemicals. JGC also developed a process for SNG production process from DME [53]. This process is intended for town gas production to cope with increased gas demand. Using DME as a feedstock instead of LPG would make the process insensitive to the frequent price fluctuations of LPG feedstocks.

Few recent communications also mentioned about power generation systems with CO_2 recovery using DME-fuelled chemical looping combustion (CLC) [54, 55]. Research is also underway to assess possibility of producing other chemicals such as ethanol [56–58] from DME.

3.3 Chemistry of DME production

3.3.1 Feedstock and pathway

First step in DME production is to produce the syngas. Syngas can be produced from a wide range of fuels: coal, biomass, petroleum coke, natural gas, and solid and liquid wastes. Composition of the syngas would depend on the conditions of gasification and/or reforming steps. However, the feedstock itself plays the most significant role since their composition covers a wide range of atomic hydrogen-to-carbon (H/C) and oxygen-to-carbon (O/C) ratio. Among them NG has highest H/C ratio while coals have lowest H/C ratios. Coal itself has a wide spectrum of H/C ratio. Low-rank coals such as Victorian brown coal has higher H/C ratio compared to the high-rank coals.

Depending on these ratios the produced syngas will be either rich in CO or in H_2. In both cases, the produced syngas needs to be upgraded to the suitable H_2 to CO

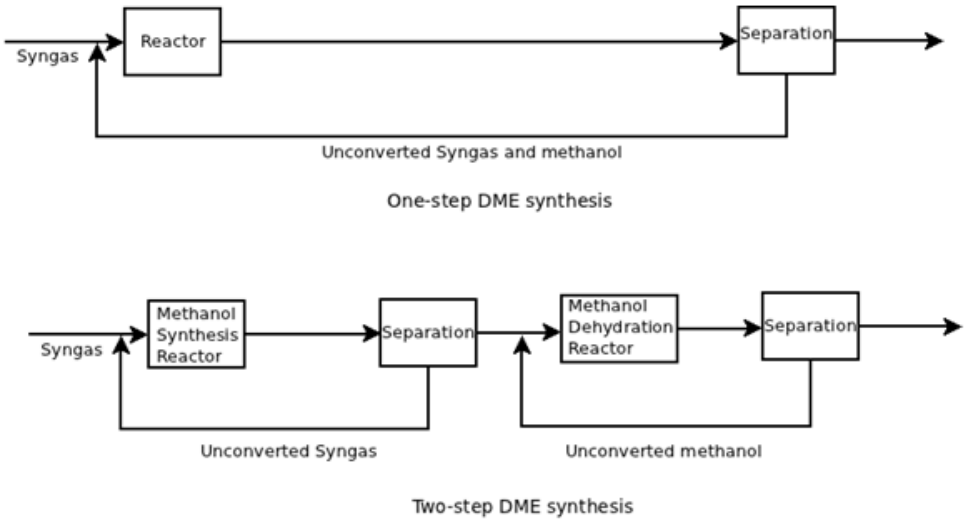

FIGURE 3.1: Syngas to DME pathway

ratio for the DME synthesis. Another important issue is the amount of polluting gases (e.g. H_2S, HCl, HCN) generated during production of syngas, which also varies from feedstock to feedstock. These gas species can poison the catalysts used in the synthesis process and needs to be removed.

Simulation studies on the DME production systems based on bituminous coal and NG showed that co-feeding of coal and NG is advantageous than either of the coal or NG-based feeding [59, 60]. Mixing a high H/C fuel (NG) with a low H/C fuel (coal) balances the CO to H_2 ratio and hence has higher resource utilisation efficiency. Similar study on the Victorian brown coal [61] showed that it suits the purpose even better since it falls in between the bituminous coal and NG in terms of H/C ratio.

Syngas to DME can follow an indirect or a direct pathway (Figure 3.1). Indirect or two-step synthesis involves production of methanol, purification of methanol and then dehydration of methanol to DME. On the other hand, for direct or single-step synthesis both the methanol synthesis and dehydration takes place simultaneously inside the same reactor. Now-a-days, direct conversion of syngas to DME (STD) is getting more attention due to higher conversion of CO and higher DME yield.

Both indirect synthesis and STD have their advantages and disadvantages. The STD process combines both reactions in the same reactor and has higher yield compared to the yield of indirect process. On the other hand, the separation of the product DME for STD is more complex. The gas stream contains CO, CO_2, H_2O, H_2 and methanol in addition to DME. The separation process is more cost intensive than

that of indirect process [6]. Therefore optimising the reaction system for greater productivity is essential to make STD process cost effective.

A variation of the STD process has also been reported. These polygeneration systems use unconverted portion of syngas from the DME reactor for power generation in gas turbine cycle/combined cycle [62–64].

3.3.2 Synergy of the STD process

Conversion of syngas to DME involves CO-hydrogenation to methanol (R3.5), methanol dehydration to DME (R3.6) and water gas shift (WGS) reaction (R3.7):

$$CO + 2\,H_2 \longrightarrow CH_3OH \tag{R3.5}$$

$$2\,CH_3OH \longrightarrow CH_3OCH_3 + H_2O \tag{R3.6}$$

$$CO + H_2O \longrightarrow CO_2 + H_2 \tag{R3.7}$$

In addition to the three reactions above CO_2-hydrogenation to methanol (R3.8) also takes place:

$$CO_2 + 3\,H_2 \longrightarrow CH_3OH + H_2O \tag{R3.8}$$

Early works by Zahner [65] and Fujimoto et al. [66] showed a synergy in the STD reaction system. Methanol synthesis by CO hydrogenation (R3.5) is thermodynamically limited. However removal of the product (i.e. methanol) via dehydration reaction (R-3.6) removes the thermodynamic limitation. Water produced during reaction (R3.6) could limit the reaction rate. However, water is consumed by WGS reaction (R3.7) which in turn produces more hydrogen, one of the reactants for the methanol synthesis reaction. Therefore, the synergistic effect of these three reactions allows higher syngas conversion compared to methanol synthesis process alone.

Thermodynamic investigation on DME synthesis from syngas confirmed the synergy of the reactive system. There is a lack of consensus between researchers about how

methanol is derived from syngas: CO hydrogenation, CO_2 hydrogenation or both [67]. However, a reactive system containing CO, H_2, CO_2, CH_3OH, H_2O and C_2H_6O has only three independent reactions. Some researchers used CO hydrogenation, methanol dehydration and WGS reaction for their model while the others used CO_2 hydrogenation, methanol dehydration and reverse WGS reaction for their study [67–72].

Jia et al. [67, 70, 71] compared three separate models to study the synergy of the reaction system. Model 1 consisted of the methanol synthesis reaction (R3.5) only. Model 2 had methanol dehydration reaction (R3.6) in addition to (R3.5), while Model 3 had (R3.7), (R3.5) and (R3.6). Comparative study at 260 °C, 5 MPa and CO_2-free feed stream showed that Model 2 is preferable when both methanol and DME are the desirable products. On the other hand, Model 3 is the best in CO-rich syngas when only DME is considered as the final product. Increasing temperature caused a reduction in CO conversion, DME yield and DME selectivity due to exothermic nature of the involved reactions. CO conversion, DME yield and DME selectivity increased with increasing pressure [71]. Jia et al. [67] also studied the influence of the presence of CO_2 in the syngas on the yield. Molar ratio of CO_2 output to input is greater than 1 for low CO_2 concentration in the feed. Therefore, CO_2 cannot be recycled back and excess CO_2 is needed to be separated. With higher CO_2 concentration in the feed, CO_2 becomes the reactant while CO becomes the product and results reversal of the WGS reaction. The process then can be considered as the CO_2 hydrogenation rather than the CO hydrogenation [72, 73]. However, DME synthesis from CO_2 hydrogenation has no advantage when compared with methanol synthesis [71].

Thermodynamic analysis of the synergy, though provides valuable information, is not enough to explain the industrial catalytic systems, far away from the equilibrium and are kinetically driven. Peng et al. [5] studied chemical synergy under liquid-phase DME (LPDME) condition for once through application (e.g. once through coal gasification combined cycle [74]). The synergy is better realised in CO rich condition where methanol synthesis is the rate-limiting step. However, trade-off between the synergistic effect and optimal condition for methanol synthesis gives H_2 to CO ratio between 2:1 and 1:1 for maximum productivity.

A simulation study of DME synthesis with recycling of the unreacted gas was also performed for optimisation of DME productivity [75]. Optimal condition for best kinetics and carbon utilisation found to occur at the same feed composition of H_2 to CO molar ratio of 1:1. Probable utilisation of generated CO_2 was proposed by integration of syngas-generation facility with the DME synthesis reactor. Several

syngas production schemes were analysed. CO_2 reforming of CH_4 enables syngas generation with required H_2 to CO ratio and thus can be a basis for commercial DME processes with minimal emission and optimal productivity.

3.3.3 Catalysts

Since DME synthesis from syngas involves two reactions (methanol synthesis and methanol dehydration), catalysts for direct synthesis of DME from syngas must have both metallic active sites (e.g. copper) for methanol production and acidic sites (solid acid) for methanol dehydration. Therefore, direct DME synthesis is done essentially over a mixture of methanol synthesis and methanol dehydration catalysts (MDC). Copper-based methanol synthesis catalyst (MSC) has been used predominantly with few of the dehydration catalysts (e.g. γ-Al_2O_3, ZSM-5). The mixed catalyst with dual functionality it is termed as bi-functional catalyst.

Methanol production from syngas came into streamline in 1923 with BASF's zinc oxide/chromia catalyst [76]. Disadvantages of this catalyst were low activity and high temperature requirements. To compensate the equilibrium conversion the process has to be run at higher pressures. It was used until mid-1960s when the importance of the Cu-based catalysts was realised [77].

Catalytic ability of copper/zinc oxide was known well before it was used commercially [78, 79]. Poor catalyst life, low thermal stability and poisoning by the sulphur containing gas in the coal-derived syngas were the main barriers for the commercial application. However, inclusion of aluminium or chromium into the catalyst and shift from coal to naptha/NG-based processes resolved these deficiencies [77]. Aluminium was found to impart more stability than chromium [80] and further improved catalyst was achieved through modification in the preparation method [81]. Since then, extensive work is going on the modification of the $CuO/ZnO/Al_2O_3$ catalyst for better performance. There have been many claims of improvement in the catalytic performance by incorporating additives such as boron [82], silver [83], manganese [84], cerium [85], tungsten [86], chromium [86], vanadium [87], magnesium [88] and palladium [89].

Methanol dehydration reaction is catalysed by the weak solid acid sites of Lewis or Brønsted nature [90]. The nature and strength of the surface acid sites and the interaction of methanol with these sites determine the reaction path, yield and selectivity [91]. Study of the methanol dehydration from the mechanistic point of view has been

presented by several researchers. Results of these studies show that the reaction of methanol over the solid-acid catalyst can either lead to the formation of DME, olefins, paraffins or aromatics. Higher reaction temperature usually favours the formation of hydrocarbons [92, 93].

Alumina has catalytic activity for methanol dehydration since Lewis acid-base pair forms during calcination [94]. Sung et al. [95] carried out experiments involving dehydration of methanol with different crystalline phases of alumina as catalyst. η-Al_2O_3 and γ-Al_2O_3 showed the highest activity for methanol to DME conversion, while α- and κ-Al_2O_3 showed lowest activity.

Other mixed metal oxides also show activity towards methanol dehydration. Brønsted sites on silica-alumina surface can be converted into Lewis sites after treating at elevated temperatures [96]. Silica-alumina shows greater selectivity when the stronger sites are inhibited by introduction of a weak base at controlled level [97]. Inclusion of NiO on alumina and silica-alumina also found to reduce the acidity of both catalysts [98]. Though iron oxide has been known for its dehydrogenation activity, in presence of alumina it shows considerable dehydration activity [91]. Some other reported dehydration oxide catalysts are ZnO/Al_2O_3 [91], TiO_2/SiO_2 [99], TiO_2/ZrO_2 [100], TiO_2/Al_2O_3 [4] and $MgAl_2O_4$ [101].

Members of zeolite group have wide range of acid strengths, high active site density and availability. In addition, the surface characteristics of zeolite can be varied by alteration of the type of cation and amount of water in the structure. As a result, zeolites have been widely studied as MDC. De Canio et al. [102] examined dehydration of methanol over HY, H-ZSM-5 and various dealuminated Y zeolite. All of these catalysts showed activity towards DME formation. Though, HY has large number of acid sites the activity was much less than as expected. Among all these catalysts steam dealuminated Y (SDY) showed highest dehydration at 275 °C. However, at higher temperatures the reaction went further to form hydrocarbons instead of DME. Bandiera and Naccache [93] used dealuminated H-mordenite at atmospheric pressure and temperatures between 200 and 300 °C and found that the yield is approximately 16%. Current research work are focused on modifying zeolite surface to impart better activity and selectivity towards DME [103–106].

Pure aluminophosphates, though microporous, do not have ion exchange capability for being charge neutral. However, substitution of some of the cations by foreign cations can introduce acidic sites on the surface. Pyke et al. [107] produced 25

different catalysts and found that those containing B^{3+}, Ga^{3+}, Fe^{3+}, Ti^{4+}, Mn^{4+} and V^{5+} cations in galloaluminophosphate and ferroaluminophosphate framework yielded DME at 380 °C.

3.3.3.1 Preparation of catalysts

Bi-functional catalysts contain active sites for both CO hydrogenation and methanol dehydration. Dual functionality is achieved by combining two types of catalysts together. Bi-functional catalysts can be synthesised by several different preparation methods.

1. Physical mixing (PM). It is the simplest preparation method. MSC and MDC are prepared first. The catalysts are then mixed together in appropriate ratio to get the bi-functional catalyst. Dry mixing of catalysts can be either low-dispersion or high-dispersion [108]. In low-dispersion mixing MSC is crushed and sieved to a particular size and then mixed with dehydration catalyst of similar size range. For high-dispersion mixing the two catalysts are mixed and ground together, tableted, crushed and then sieved to particular size range.

Wet mixing method involves mixing of the components in water followed by stirring, filtering, drying, calcination and moulding under pressure to form tablets. On the other hand, LPDME process using bubbling slurry reactor uses a suspension of both the catalysts in an inert mineral oil.

2. Co-precipitation (CP). Na_2CO_3 solution is added drop wise to a mixed solution of nitrates of copper, aluminium and zinc in a controlled pH and temperature. The formed precipitates are aged, filtered, washed and dried. The catalyst is then calcined at higher temperature. Finally, the resultant power is then moulded under pressure into tablets which is then crushed into granules and sieved into specific size range [108–110].

Another variation of this method is to use $NaAlO_2$ for coprecipitates of copper and zinc [108–110]. The AlO_2^- ions reacts with the copper and zinc cations to form a mixed precipitates of copper, zinc and aluminium oxides.

$$M^{2+} + 2\,AlO_2^- + 4\,H_2O \longrightarrow M(OH)_2 + 2\,Al(OH)_3 \qquad \text{(R3.9)}$$

where, M = Cu, Zn. Post-treatment of the precipitates is similar to that of co-precipitation by Na_2CO_3.

3. Impregnation (IMP). The bi-functional catalyst is prepared by impregnation of γ-alumina with appropriate volume of copper- and zinc nitrate solution [111]. The impregnated catalyst is then dried, calcined, moulded and crushed into specific size.

4. Co-precipitation impregnation (CPI). Sodium carbonate is added to the mixed nitrate solution to form the precipitation in a water suspension containing the dehydration component (e.g. γ-alumina, HZSM-5) [109]. Post-treatment of the impregnated precipitate is the same as in other methods.

5. Co-precipitation sedimentation (CPS). Precipitates of MSC if formed and aged, filtered and washed. The separated precipitates are added to a suspension containing dehydration component. The mixture is then stirred, filtered, dried and calcined. The powder is then formed into tablets and crushed to required size range.

6. Sol-gel (SG). A sol is prepared from the catalyst precursors instead of the precipitates [110]. Solution of nitrate salts are prepared in ethanol and cooled in an ice bath. Oxalic acid in ethanol is added, while stirring, to the mixture to form the sol. The sol is then heated to 70 °C for removal of ethanol by evaporation. The gel is then dried and calcined.

7. Sol-gel impregnation (SGI). γ-Al_2O_3 is added to a mixed solution of copper and zinc nitrates in ethanol. The sol is then formed by addition of oxalic acid in ethanol in an ice bath. The following procedure is the same as the sol-gel method [110].

8. Liquid-phase synthesis. This preparation method is applicable for the slurry-phase DME synthesis only. A Cu/Zn/Al gel is obtained from $(C_3H_7O)_3Al$, copper nitrate and zinc nitrate. The gel is then treated with acetone and dispersed in parrafin by mechanical stirring. The slurry catalyst is obtained after heat treating the gel in N_2 flow [112].

Studies have shown that the activity, selectivity and deactivation characteristics of the catalyst are dependent on the method of preparation. Comparative studies between the various preparation methods were performed and conclusions have been made on the preferred method of preparation [108–110]. However, a broad consensus is yet to be established among the researchers on the choice of the preparation method.

Performance of the bi-functional catalysts with different methanol synthesis and dehydration component and varying composition under different operating conditions was evaluated by various researchers. The optimised operating condition and proper catalyst composition has not been worked out yet. A brief review of the preparation method of bi-functional catalysts, operating conditions, CO conversion and DME selectivity is given in Table 3.3.

Table 3.3: Bi-functional catalysts for syngas to DME synthesis

MSC + MDC		Preparation method
$CuO/ZnO/Al_2O_3$		CP [108, 109]
$CuO/ZnO/Al_2O_3$		CPI [108, 109]
$CuO/ZnO/Al_2O_3$		CPS [109]
$CuO/ZnO/Al_2O_3$		IMP [109, 111]
$CuO/ZnO/Al_2O_3$		SG [110]
$CuO/ZnO/Al_2O_3$		SGI [110]
$CuO/ZnO/Al_2O_3$		Slurry mixing [109]
$CuO/ZnO/Al_2O_3$		Slurry phase synthesis [112]
$CuO/ZnO/Al_2O_3$		Mechanical milling and combustion synthesis [113]
Cu- and Zn-pillared ilerites		HTS [114]
ZnO/Cu-ilerites		HTS+IMP [114]
CuO/Zn-ilerites		HTS+IMP [114]
$Pd/ZnO/Al_2O_3$		Incepient wetness impregnation [115]
Mesoporous $Cu/\gamma\text{-}Al_2O_3$		evaporation-induced self-assembly [116]
MSC	MDC	Preparation method
CuO/MnO	Y	CPI [117]
CuO/MnO	$\gamma\text{-}Al_2O_3$	IMP [118]
CuO/MnO/ZnO	Y and derivatives	CPI [119], PM [120]

CuO/MnO/ZnO	γ-Al_2O_3	IMP [121]
CuO/ZnO	H-ferrierite	CPI, CPS [122]
CuO/ZnO	γ-Al_2O_3	PM [65]
CuO/ZnO/Al_2O_3	Al-phosphate	PM [123]
CuO/ZnO/Al_2O_3	HZSM-5 and derivatives	PM [124, 125], CPI [126], CPS [109]
CuO/ZnO/Al_2O_3	HA	CPS [109]
CuO/ZnO/Al_2O_3	H-ferrierite and derivatives	CPI [126], CPS [122]
CuO/ZnO/Al_2O_3	H-MCM-22	PM [127]
CuO/ZnO/Al_2O_3	H-MFI-90	PM [104, 128]
CuO/ZnO/Al_2O_3	HSY	CPS [109]
CuO/ZnO/Al_2O_3	HX	CPS [109]
CuO/ZnO/Al_2O_3	HY and derivatives	CPS [109], PM [124], CPI [126]
CuO/ZnO/Al_2O_3	HZSM760	CPS [109], PM [124]
CuO/ZnO/Al_2O_3	SAPO	PM [129]
CuO/ZnO/Al_2O_3	SiO_2	CPS [109]
CuO/ZnO/Al_2O_3	SiO_2-Al_2O_3	CPS [109], PM [130]
CuO/ZnO/Al_2O_3	SO_4^{2-}-ZrO_2	CPS [109]
CuO/ZnO/Al_2O_3	S-ZrO_2	PM [131]
CuO/ZnO/Al_2O_3	W-ZrO_2	PM [131]
CuO/ZnO/Al_2O_3	γ-Al_2O_3	CPI [132], CPS [133] PM [128]
CuO/ZnO/Al_2O_3-M (M=Ga, La, Y, Zr)	Al_2O_3	CPI [134]
CuO/ZnO/Al_2O_3/Cr_2O_3/Ga_2O_3	SiO_2-Al_2O_3	PM [135]
CuO/ZnO/Al_2O_3/Cr_2O_3/Ga_2O_3 +Pd/Al_2O_3	SiO_2-Al_2O_3	PM [135]
CuO/ZnO/Al_2O_3/MnO	γ-Al_2O_3	PM [136]
CuO/ZnO/Al_2O_3/SiO_2	γ-Al_2O_3	PM [137, 138]
CuO/ZnO/Al_2O_3/ZrO_2	Ferrierite	PM [139]
CuO/ZnO/Al_2O_3/ZrO_2	HZSM-5	CPS [140], PM [106, 141]
CuO/ZnO/Cr_2O_3	γ-Al_2O_3	PM [142]
CuO/ZnO/ZrO_2	Al-modified H-mordenite	CPS [143]

$CuO/ZnO/ZrO_2$	Ferrierite	PM [139]
$CuO/ZnO/ZrO_2$	HZSM-5	CPS [144]
Mg-$CuO/ZnO/Al_2O_3$	HZSM-5	CPS [145]
Mn-$CuO/ZnO/Al_2O_3$	HZSM-5	CPS [145]
Mn-$CuO/ZnO/Al_2O_3$	γ-Al_2O_3	PM [136]
Pd-SiO2	γ-Al_2O_3	PM [66]
Pd-$CuO/ZnO/Al_2O_3/ZrO_2$	HZSM-5	CPS+IMP, CPS+PM, Sequential Precip. [139]
Zr-$CuO/ZnO/Al_2O_3$	HZSM-5	CPS [145]
$CuO/ZnO/Al_2O_3$	NH_4ZSM-5	PM [146]
$CuO/ZnO/Al_2O_3$	MgO-ZSM-5	PM [146]
Au/ZnO/γ-Al_2O_3	γ-Al_2O_3	PM [147]
$CuO/ZnO/Al_2O_3$	Zr-ferrierite	CPI [148]

3.4 Process simulation studies

Performance of STD process plants is greatly affected by factors such as starting feedstock, gasification condition, configuration of the DME synthesis reactor, and the catalyst used for the syngas to DME conversion. Process modelling and simulation of DME plants can be used for analysing and optimizing operating condition for such a plant.

Simulation studies on DME production can be classified into categories based on the type of reactor used for DME production: fixed-bed, slurry-phase and fluidised-bed reactors.

All reactions occurring inside DME reactor are exothermic. Heat generated during these reactions will increase the reactor temperature. Temperatures above 300 °C lead to deactivation of the catalyst. Hence, heat removal is essential for high yield. Therefore, fixed-bed reactors are usually modelled using a shell-and-tube heat exchanger [149, 150]; the tube side acts a packed bed reactor and the coolant in the shell side removes heat generated from reactions. A simulation study on the arrangement of the MSC and MDC beds of inside a fixed-bed reactor was performed by McBride et al. [151]. The study was performed both for equilibrium and kinetic cases. For a single layer of MSC followed by a single layer of MDC, which is the same arrangement as

two-step DME production, the conversion was lowest. The conversion increased with an increase in the number of layers of each catalyst and reached a maximum for an infinite number of layers, approaching a physical mixture of two catalysts. Comparison between a physical mixture of MSC and MDC catalysts and a hybrid catalyst (consisting both metallic and acidic function) was done introducing effectiveness factor calculations in the simulation [150]. Productivity for hybrid catalyst was found to be higher. The simulation study was well supported by pilot-plant reactor data [152]. Effect of in situ H_2O removal on DME synthesis using a fixed-bed membrane reaction was simulated by Iliuta et al. [153] .The retentate section of the reactor was packed with bi-functional catalyst and permeate section was an empty cavity continually swept by an inert gas. The simulation studies showed that in situ H_2O removal is more productive than that without H_2O removal especially for CO_2 rich syngas.

Slurry-phase or three-phase reactor (e.g. LPDME) is of great interest since the configuration is expected to work better at highly exothermic condition with better heat removal capability of the liquid media. A mathematical model of slurry-phase reactor considering liquid-phase back-mixing and grain sedimentation was developed by Liu et al. [154]. Based on the simulation results, dimensions for an industrial reactor producing 10,000 tonnes per annum DME was proposed. Coal syngas to DME was simulated by Han et al. [155]. Simulation of DME production from biomass gasification was also reported. The model included biomass gasification, WGS reaction, gas purification and single-step DME synthesis [156]. An optimised polygeneration process without WGS reaction and simplified gas clean-up was proposed. Three systems based on coal, natural gas, and coal and natural gas co-feeding were studied by Zhou et al. [60]. A Chinese bituminous coal and NG were used for the simulation study. These models were composed of air separation unit, coal gasification and/or NG reforming, WGS, syngas cleaning, synthesis, distillation and power generation. The results showed that co-feeding system is superior compared to coal-based or NG-based systems. Bituminous coal-based system had higher C/H ratio while NG-based system was lean in carbon content than that needed for producing DME [60].

Though fluidized-bed reactor for DME production is still under development, few simulation studies have been reported for such reactors. Lu et al. [157] considered presence of two-phases in a fluidised-bed reactor: the bubble phase and surrounding dense phase. Plug-flow was assumed for the bubble phase while both plug-flow (P-P) and back-mixed (P-M) assumptions were applied for the dense phase. Experimental validation of the simulation results showed P-M model gives better result than P-P

model. The generalised comprehensive reactor (GCR) model was used by Kumar and Srivastava [158] for simulating fluidised-bed reactor. The GCR model assumed two pseudo-phases containing both solids and gas, one is high-density phase and the other low-density phase and reaction occurs in both phases. Kumar and Srivastava [158] validated there model using data from [157] and found reasonable agreement.

References

[1] Moradi G, Ahmadpour J, Yaripour F, 2008, Energy and Fuels, **22**: 3587–3593

[2] Arkharov AM, Glukhov SD, Grekhov LV, Zherdev AA, Ivashchenko NA, Kalinin DN, Sharaburin AV, Aleksandrov AA, 2003, Chemical and Petroleum Engineering, **39**: 330–336

[3] Cai G, Liu Z, Shi R, Changqing H, Yang L, Sun C, Chang Y, 1995, Applied Catalysis A: General, **125**: 29–38

[4] Xu M, Lunsford JH, Goodman D, Bhattacharyya A, 1997, Applied Catalysis A: General, **149**: 289–301

[5] Peng X, Toseland B, Tijm P, 1999, Chemical Engineering Science, **54**: 2787–2792

[6] Yoon ES, Han C, 2009, *In:* 10th International symposium on process systems engineering: Part A, de Brito Alves RM, do Nascimento CAO, Biscaia EC, editors, vol. 27, 169–175, Elsevier

[7] Arcoumanis C, Bae C, Crookes R, Kinoshita E, 2008, Fuel, **87**: 1014–1030

[8] Good DA, Francisco JS, Jain AK, Wuebbles DJ, 1998, Journal of Geophysical Research, **103**: 28181–28186

[9] Wu J, Yin J, 2008, Journal of Chemical and Engineering Data, **53**: 2247–2249

[10] Parkash S, 2010, Petroleum fuels manufacturing handbook. McGraw-Hill

[11] Yizhuo H, Yisheng T, Yuqin N, Zhenghua C, 2004, Energy for Sustainable Development, **8**: 129–130

[12] Chen Z, Niu Y, 1996, Coal Conversion (in Chinese), **19**: 37–42

[13] Frye CA, Boehman AL, Tijm PJA, 1999, Energy and Fuels, **13**: 650–654

[14] Fleisch T, 2002, *In:* IBS Gas to Liquid Conference, Milan, Italy

[15] Mills G, 1994, Fuel, **73**: 1243–1279

[16] Fleisch TH, Basu A, Gradassi MJ, Masin JG, 1997, *In:* Natural Gas Conversion IV, de Pontes M, Espinoza RL, Nicolaides CP, Scholtz JH, Scurrell MS, editors, vol. 107, 117–125, Elsevier, Amsterdam

[17] Kim MY, Lee JH, Lee CS, 2008, Energy and Fuels, **22**: 4206–4212

[18] Kim MY, Yoon SH, Ryu BW, Lee CS, 2008, Fuel, **87**: 2779–2786

[19] Beatrice C, Bertoli C, Giacomo ND, Lazzaro M, 1996, *In:* IMechE Conference Transactions, 261–272, IMechE, London, UK

[20] Miyamoto N, Ogawa H, Nurun NM, Obata K, Arima T, 1998, SAE transactions, **107**: 171–177

[21] Song R, Li K, Feng Y, Liu S, 2009, Energy and Fuels, **23**: 5460–5466

[22] Jie L, Shenghua L, Yi L, Yanju W, Guangle L, Zan Z, 2010, Energy and Fuels, **24**: 2465–2469

[23] Basu A, Gradassi M, Sills R, Fleisch T, Puri R, 2001, *In:* ASME Turbo-Expo, New Orleans

[24] Basu A, Wainwright JM, 2001, *In:* Petrotech-2001, New Delhi

[25] Lee MC, Seo SB, Chung JH, Joo YJ, Ahn DH, 2009, Fuel, **88**: 657–662

[26] Cocco D, Pettinau A, Cau G, 2006, Proceedings of the Institution of Mechanical Engineers, Part A: Journal of Power and Energy, **220**: 95–102

[27] Abdallah H, Harvey S, 2001, International journal of thermal sciences, **40**: 372–384

[28] Kesser KF, Hoffman MA, Baughn JW, 1994, Journal of Engineering for Gas turbines and Power, **116**: 277

[29] Felderhoff M, Weidenthaler C, von Helmolt R, Eberle U, 2007, Physical Chemistry Chemical Physics, **9**: 2643–2653

[30] Mori D, Hirose K, 2009, International journal of hydrogen energy, **34**: 4569–4574

[31] Chalk SG, Miller JF, 2006, Journal of Power Sources, **159**: 73–80

[32] Zhou L, 2005, Renewable and Sustainable Energy Reviews, **9**: 395–408

[33] Harris R, Book D, Anderson PA, Edwards PP, 2004, The fuel cell review, 17–23

[34] Hoogers G, 2003, *In:* Fuel cell technology handbook, CRC Press, Boca Raton

[35] Semelsberger TA, Borup RL, 2005, Journal of Power Sources, **152**: 87–96

[36] Semelsberger TA, Borup RL, 2006, Journal of Power Sources, **155**: 340–352

[37] Sobyanin VA, Cavallaro S, Freni S, 2000, Energy and Fuels, **14**: 1139–1142

[38] Galvita VV, Semin GL, Belyaev VD, Yurieva TM, Sobyanin VA, 2001, Applied Catalysis A: General, **216**: 85–90

[39] Matsumoto T, Nishiguchi T, Kanai H, Utani K, Matsumura Y, Imamura S, 2004, Applied Catalysis A: General, **276**: 267–273

[40] Kawabata T, Matsuoka H, Shishido T, Li D, Tian Y, Sano T, Takehira K, 2006, Applied Catalysis A: General, **308**: 82–90

[41] Takeishi K, Suzuki H, 2004, Applied Catalysis A: General, **260**: 111–117

[42] Tanaka Y, Kikuchi R, Takeguchi T, Eguchi K, 2005, Applied Catalysis B: Environmental, **57**: 211–222

[43] Zhang L, Huang Z, 2009, Journal of Shanghai Jiaotong University, **14**: 210–214

[44] Badmaev SD, Snytnikov PV, 2008, International Journal of Hydrogen Energy, **33**: 3026–3030

[45] Cocco D, Tola V, 2009, Energy, **34**: 2124–2130

[46] Cocco D, Tola V, 2009, Energy Conversion and Management, **50**: 1040–1048

[47] Demirci UB, 2007, Journal of Power Sources, **169**: 239–246

[48] Muller JT, Urban PM, Holderich WF, Colbow KM, Zhang J, Wilkinson DP, 2000, Journal of The Electrochemical Society, **147**: 4058–4060

[49] Sciarra JJ, Sciarra CJ, 2000, *In:* Kirk-Othmer Encyclopedia of Chemical Technology, John Wiley & Sons

[50] Restrepo G, Weckert M, Brüggemann R, Gerstmann S, Frank H, 2008, Environmental Science and Technology, **42**: 2925–2930

[51] Zhao TS, Takemoto T, Tsubaki N, 2006, Catalysis Communications, **7**: 647–650

[52] JGC, 2011, *DTP (Dominant technology for Propylene production) process. Cited: 21 March 2011. URL: http://www.jgc.co.jp/en/04tech/11dme/dtp.html*

[53] JGC, 2011, *Synthetic natural gas (SNG) production process from DME. Cited: 21 March 2011. URL: http://www.jgc.co.jp/en/04tech/11dme/sng.html*

[54] Han T, Hong H, Jin H, Zhang C, 2011, Journal of Energy Resources Technology, **133**: 012201–7

[55] Han T, Hong H, He F, Jin H, 2012, Combustion and Flame, **159**: 1806–1813

[56] San X, Yang G, Zhang Y, Li X, Tsubaki N, 2009, Journal of the Japan Petroleum Institute, **52**: 357–358

[57] San X, Zhang Y, Shen W, Tsubaki N, 2009, Energy and Fuels, **23**: 2843–2844

[58] Yang G, San X, Jiang N, Tanaka Y, Li X, Jin Q, Tao K, Meng F, Tsubaki N, 2011, Catalysis Today, **164**: 425–428

[59] Zhou L, Hu S, Li Y, Zhou Q, 2008, Chemical Engineering Journal, **136**: 31–40

[60] Zhou L, Hu S, Chen D, Li Y, Zhu B, Jin Y, 2009, Ind Eng Chem Res, **48**: 4101–4108

[61] Kabir KB, Grills G, Walter J, Bhattacharya S, 2011, *In:* International Conference on Coal Sicence and Technology (ICCS&T), Oviedo

[62] Liu P, Pistikopoulos EN, 2009, *In:* Optimization in the energy industry, Kallrath J, Pardalos PM, Rebennack S, Scheidt M, editors, Energy Systems, 167–191, Springer Berlin Heidelberg

[63] Adams II TA, Barton PI, 2011, Fuel Processing Technology, **92**: 639–655

[64] Bin C, Hongguang J, Lin G, 2008, International Journal of Energy Research, **32**: 722–734

[65] Zahner JC, 1977, *Conversion of modified synthesis gas to oxygenated organic chemicals (US 4011275)*. Mobil Oil Corporation

[66] Fujimoto K, Asami K, Shikada T, Tominaga H, 1984, Chemistry letters, **13**: 2051–2054

[67] Jia G, Tan Y, Han Y, 2005, Journal of natural gas chemistry, **14**: 47–53

[68] An X, Li JL, Wang JF, 2007, Natural Gas Chemical Industry, **32**: 5–7

[69] Grzesik M, Skrzypek J, 1999, *In:* Reaction kinetics and the development of catalytic processes, proceedings of the international symposium, Froment GF, Waugh KC, editors, vol. 122, 407–410, Elsevier

[70] Jia G, Tan Y, Han Y, 2005, Coal Conversion, **28**: 92–96

[71] Jia G, Tan Y, Han Y, 2006, Industrial and Engineering Chemistry Research, **45**: 1152–1159

[72] Meshcheryakov V, Kirillov V, 2000, Theoretical Foundations of Chemical Engineering, **34**: 85–89

[73] Shen WJ, Jun KW, Choi HS, Lee KW, 2000, Korean Journal of Chemical Engineering, **17**: 210–216

[74] Brown DM, Bhatt BL, Hsiung TH, Lewnard JJ, Waller FJ, 1991, Catal Today, **8**: 279–304

[75] Peng XD, Wang AW, Toseland BA, Tijm PJA, 1999, Industrial and Engineering Chemistry Research, **38**: 4381–4388

[76] Klier K, 1982, *In:* Advances in Catalysis, Vol.31, vol. 31, 243–313, Elsevier

[77] Chinchen GC, Denny PJ, Jennings JR, Spencer MS, Waugh KC, 1988, Applied Catalysis, **36**: 1–65

[78] BASF, 1925, *A process for transforming oxides of carbon into oxygenated organic compounds (GB 237030)*

[79] Lormand C, 1925, Industrial and Engineering Chemistry, **17**: 430–432

[80] Gallagher JT, Kidd JM, 1969, *Methanol synthesis (GB 1159035)*. ICI Ltd.

[81] Cornthwaite D, 1972, *Methanol synthesis and catalyst composition therefor (GB 1296212)*. ICI Ltd.

[82] Asakawa K, Yamamoto Y, Ebata S, Nakamura T, 1980, *Process for preparing a catalyst composition containing oxides of copper zinc and aluminum (GB 2047556)*. Mitsubishi Gas Chemical Co, Inc.

[83] Magoon EF, 1973, *Process for the production of methanol (GB 1371638)*. Shell International Research

[84] Kotowski W, Lach J, Mazurek F, Gorka F, Kuszka W, Marquardt M, 1980, *Methanol from synthesis gas (GB 2025418)*. Instytut Ciezkiej Syntezy Organicznej Blacjownia

[85] Herman RG, Simmons GW, Klier K, 1981, *In:* New horizons in catalysis, proceedings of the 7th International congress on catalysis, Seivama T, Tanabe K, editors, vol. 7, Part 1, 475–489, Elsevier

[86] Bondar PG, Goroshko ON, Suschaya LE, Lavrova VV, Leleka VE, Ilko EG, 1978, *Catalyst for the synthesis of methanol and method for preparing same (US 4107089)*

[87] Asakawa K, 1982, *Process for the preparation of methanol (GB 2095233)*. Mitsubishi Gas Chemical Co, Inc.

[88] Herbert R, Liebgott H, 1972, *A catalyst for use in the production of methanol, its production and use (UK Patent 1827327)*

[89] Melin-Cabrera I, Granados ML, Fierro JLG, 2002, Journal of Catalysis, **210**: 285–294

[90] Pines H, Haag WO, 1960, Journal of the American Chemical Society, **82**: 2471–2483

[91] Spivey JJ, 1991, Chemical Engineering Communications, **110**: 123–142

[92] Kubelkov L, Novkov J, Nedomov K, 1990, Journal of Catalysis, **124**: 441–450

[93] Bandiera J, Naccache C, 1991, Applied Catalysis, **69**: 139–148

[94] Gates BC, Katzer JR, Schuit GCA, 1979, Chemistry of catalytic processes. McGraw-Hill

[95] Sung D, Kim Y, Park E, Yie J, 2010, Research on Chemical Intermediates, **36**: 653–660

[96] Satterfield CN, 1980, Heterogeneous catalysis in practice. McGraw-Hill

[97] Tanabe K, 1970, Solid acids and bases: their catalytic properties. Kodansha

[98] Viswanathan VN, Yeddanapalli LM, 1974, Zeitschrift fÃijr anorganische und allgemeine Chemie, **407**: 98–108

[99] Itoh M, Hattori H, Tanabe K, 1974, Journal of Catalysis, **35**: 225–231

[100] Vishwanathan V, Roh HS, Kim JW, Jun KW, 2004, Catalysis Letters, **96**: 23–28

[101] Narasimhau CS, Swamy CS, 1976, Current Science, **45**: 759–760

[102] DeCanio SJ, Sohn JR, Fritz PO, Lunsford JH, 1986, Journal of Catalysis, **101**: 132–141

[103] Hassanpour S, Yaripour F, Taghizadeh M, 2010, Fuel Processing Technology, **91**: 1212–1221

[104] Moradi GR, Yaripour F, Vale-Sheyda, 2010, Fuel Processing Technology, **91**: 461–468

[105] Wang J, Cheng X, Guo J, Chen X, He H, Long Y, 2010, Chinese Journal of Chemistry, **28**: 183–188

[106] Zhang L, Wang J, Wu P, Hou Z, Fei J, Zheng X, 2010, Chinese Journal of Catalysis, **31**: 987–992

[107] Pyke DR, Whitney P, Houghton H, 1985, Applied catalysis, **18**: 173–190

[108] Li JL, Zhang XG, Inui T, 1996, Applied Catalysis A: General, **147**: 23–33

[109] Ge Q, Huang Y, Zhang T, 1996, Natural Gas Chemical Industry (C1 Chemistry and Technology), **21**: 19–22

[110] Moradi G, Nosrati S, Yaripor F, 2006, *In:* International Conference on Science & Technology: Application in Industry & Education, Pulau Pinang, Malaysia

[111] Slaugh LH, 1983, *Catalyst for the preparation of dimethyl ether (US 4375424).* Shell Oil Company

[112] Gao Zh, Hao Lf, Huang W, Xie Kc, 2005, Catalysis Letters, **102**: 139–141

[113] Lei H, Nie Rf, Fei Jh, Hou Zy, 2012, Journal of Zhejiang University - Science A, **13**: 395–406

[114] Ahn SH, Kim SH, Hahm HS, 2008, Research on Chemical Intermediates, **34**: 793–801

[115] Lebarbier VM, Dagle RA, Kovarik L, Lizarazo-Adarme JA, King DL, Palo DR, 2012, Catalysis Science and Technology, **2**: 2116–2127

[116] Jiang H, Bongard H, Schmidt W, Schüth F, 2012, Microporous and Mesoporous Materials, **164**: 3–8

[117] Tang XJ, Fei JH, Hou ZY, Zheng XM, Lou H, 2008, Energy and Fuels, **22**: 2877–2884

[118] Qi GX, Fei JH, Zheng XM, Hou ZY, 2001, Catalysis Letters, **72**: 121–124

[119] Fei JH, Yang MX, Hou ZY, Zheng XM, 2004, Energy and Fuels, **18**: 1584–1587

[120] Fei J, Hou Z, Zhu B, Lou H, Zheng X, 2006, Applied Catalysis A: General, **304**: 49–54

[121] Zheng XM, Fei JH, Hou ZY, 2001, Chinese Journal of Chemistry, **19**: 67–72

[122] Flores JH, da Silva MI, 2008, Colloids and Surfaces A: Physicochemical and Engineering Aspects, **322**: 113–123

[123] Peng XD, Parris GE, Toseland BA, Battavio PJ, 1998, *Use of Aluminum phosphate as the dehydration catalyst in single step dimethyl ether process: US Patent 5753716*

[124] Sofianos AC, Scurrell MS, 1991, Industrial and Engineering Chemistry Research, **30**: 2372–2378

[125] Yang G, Tsubaki N, Shamoto J, Yoneyama Y, Zhang Y, 2010, Journal of the American Chemical Society, **132**: 8129–8136

[126] Sai Prasad PS, Bae JW, Kang SH, Lee YJ, Jun KW, 2008, Fuel Processing Technology, **89**: 1281–1286

[127] Mao D, Xia J, Chen Q, Lu G, 2009, Catalysis Communications, **10**: 620–624

[128] Moradi GR, Nazari M, Yaripour F, 2008, Fuel Processing Technology, **89**: 1287–1296

[129] Yoo KS, Kim JH, Park MJ, Kim SJ, Joo OS, Jung KD, 2007, Applied Catalysis A: General, **330**: 57–62

[130] Naik SP, Du H, Wan H, Bui V, Miller JD, Zmierczak WW, 2008, Industrial and Engineering Chemistry Research, **47**: 9791–9794

[131] Ramos FS, de Farias AMD, Borges LEP, Monteiro JL, Fraga MA, Sousa-Aguiar EF, Appel LG, 2005, Catalysis Today, **101**: 39–44

[132] Bae JW, Potdar HS, Kang SH, Jun KW, 2008, Energy and Fuels, **22**: 223–230

[133] Hadipour A, Sohrabi M, 2008, Chemical Engineering Journal, **137**: 294–301

[134] Kang SH, Bae JW, Kim HS, Dhar GM, Jun KW, 2010, Energy and Fuels, **24**: 804–810

[135] Takeguchi T, Yanagisawa Ki, Inui T, Inoue M, 2000, Applied Catalysis A: General, **192**: 201–209

[136] Tan Y, Xie H, Cui H, Han Y, Zhong B, 2005, Catalysis Today, **104**: 25–29

[137] Gogate MR, Lee S, Kulik CJ, 1991, Petroleum Science and Technology, **9**: 653–679

[138] Kim HJ, Jung H, Lee KY, 2001, Korean Journal of Chemical Engineering, **18**: 838–841

[139] Flores JH, Peixoto DPB, Appel LG, de Avillez RR, da Silva MIP, 2011, Catalysis Today, **172**: 218–225

[140] Sun K, Lu W, Wang M, Xu X, 2004, Catalysis Communications, **5**: 367–370

[141] An X, Zuo YZ, Zhang Q, Wang Dz, Wang JF, 2008, Industrial and Engineering Chemistry Research, **47**: 6547–6554

[142] Manara G, Notari B, Fattore V, 1979, *Catalyst for the preparation of dimethyl Ether (US 4177167)*. Snamprogetti

[143] Khandan N, Kazemeini M, Aghaziarati M, 2009, Catalysis Letters, **129**: 111–118

[144] Jia M, Li W, Xu H, Hou S, Ge Q, 2002, Applied Catalysis A: General, **233**: 7–12

[145] Ge Q, Huang Y, Qiu F, Li S, 1998, Applied Catalysis A: General, **167**: 23–30

[146] Abu-Dahrieh J, Rooney D, Goguet A, Saih Y, 2012, Chemical Engineering Journal, **203**: 201–211

[147] Kalala MG, 2012, Synthesis gas conversion into dimethyl ether and light hydrocarbons via methanol over a hybrid gold-based catalyst. Msc thesis, University of the Witwatersrand, Johannesburg

[148] Jung JW, Lee YJ, Um SH, Yoo PJ, Lee DH, Jun KW, Bae JW, 2012, Applied Catalysis B: Environmental, **126**: 1–8

[149] Shim H, Lee S, Yoo Y, Yun Y, Kim H, 2009, Korean J Chem Eng, **26**: 641–648

[150] Lee SB, Cho W, Park DK, Yoon ES, 2006, Korean Journal of Chemical Engineering, **23**: 522–530

[151] McBride K, Turek T, Güttel R, 2012, AIChE Journal, **58**: 3468–3473

[152] Song D, Cho W, Lee G, Park DK, Yoon ES, 2008, Industrial and Engineering Chemistry Research, **47**: 4553–4559

[153] Iliuta I, Larachi F, Fongarland P, 2010, Industrial and Engineering Chemistry Research, **49**: 6870–6877

[154] Liu D, Hua X, Fang D, 2007, Journal of Natural Gas Chemistry, **16**: 193–199

[155] Han Y, Zhang H, Ying W, Fang D, 2009, Chinese Journal of Chemical Engineering, **17**: 108–112

[156] Ju F, Chen H, Ding X, Yang H, Wang X, Zhang S, Dai Z, 2009, Biotechnology advances, **27**: 599–605

[157] Lu W, Teng L, Xiao W, 2004, Chemical Engineering Science, **59**: 5455–5464

[158] Kumar M, Srivastava VC, 2010, Chemical Engineering and Technology, **33**: 1967–1978

Chapter 4

Summary of the Review and Research Scopes

4.1 Introduction

Current applications of Victorian brown coal have been discussed in Chapter 2. The true potential of Victorian brown has not yet been realised due to its high moisture content and high reactivity of the dried coal. The coal *per se* is not exportable and therefore the scope of its use is rather limited. Moreover, higher CO_2 emission than that of comparable bituminous coal-fired power plants also impeded its wider use.

The potential future applications of Victorian brown coal have also been discussed in Chapter 2. Synthesis of value-added chemicals through gasification can revive the future of brown coal. DME stands out among the other chemicals because of its wide applicability and environmental acceptability as discussed in Chapter 3. Rationale for producing DME from Victorian Brown Coal as are as follows:

- DME can be used as a transportation, cooking or generator fuel. WTW LCA studies showed that DME production consumes less energy and emits less GWG than other comparable processes [1]. CO_2 separation from the syngas is an integral part of the DME synthesis process. High purity CO_2 stream is beneficial from sequestration point of view. Separated CO_2 can be also used as feedstock for methane reforming, methanol synthesis or even DME synthesis itself.
- Brown coal is not exportable because of its moisture content and high reactivity when dried. On the other hand, DME has a huge and expanding market in regions without significant crude oil, especially in China and Japan. DME synthesis would therefore provide a pathway for brown coal to produce exportable commodity.

- Use of DME as alternative fuel is beneficial because of its similarity with LPG. For DME, existing land- and ocean-based LPG infrastructure can be utilised without any modification.
- DME is a sulphur-free low aromatic fuel, and burns smokeless. Environmental pollution from combustion of DME is lower than other comparable fuels.

4.2 Research needs

DME synthesis from Victorian brown coal would involve drying and gasification of coal followed by syngas to DME conversion. All these steps still require significant unmet research needs.

Coal gasification and polluting species: Important issues in coal gasification are the conversion of coal, the quality of syngas and agglomeration of solid materials inside the gasifier. Minerals present in the brown coal have catalytic activity towards gasification reactions. Externally added metal species can also improve gasification characteristics. Significant research is needed to find the roles of the inherent and extraneous metal species on the coal conversion and syngas composition.

Targeted work is also required to identify the volatiles species during gasification, their reforming in the gas phase and on the catalyst surface. Ability of the gasification catalysts to reduce pollutant species in the final gas product (i.e. NH_3, H_2S, HCN, HCl) as well as the AAEM species also needs attention. Both pollutant gases and AAEM species can cause substantial problems in downstream units depending on their amount if not removed. The amount of pollutant gas also dictates the extent of gas cleaning that is required before synthesis step.Discussion on brown coal gasification in previous sections revealed the status of brown coal gasification in different types of gasifiers. Entrained-flow gasification of Victorian brown coal is yet to be reported in open literature. Studies on pyrolysis, char structure development and char gasification under different operating conditions in an entrained-flow gasifier would provide basis for scale-up and process development. Experimental studies on Victorian brown coal under entrained-flow conditions are currently underway [2, 3].

Agglomeration behaviour of ash components and its slagging characteristics is also unknown under entrained-flow conditions. Analysis of solid and molten ash phases

and its viscosity measurement is necessary for the proper design of the entrained-flow gasifier. Initial studies on slag composition and Viscosity can be found here [4].

Brown coal syngas to DME synthesis: To our knowledge, there is no reported work on brown coal syngas to chemicals. Therefore, work needs to be done using commercially available catalysts with the syngas generated from Victorian brown coal. Syngas from brown coal contains impurities such as NH_3, HCN, HCl, H_2S. The effect of H_2S on methanol catalyst is known for a long time. However, not much information is available on the effect of the other polluting gas species present in brown coal syngas. Their effect on the methanol dehydration catalyst and the bi-functional catalyst as a whole is still unknown. Effect on the activity and selectivity of bi-functional catalyst by the pollutant species would set the extent of purification necessary for commercial DME plants.

Catalyst development and characterisation: Catalysts for methanol and DME production still pose major challenges to the researchers. Though catalysts for individual processes are well established, development of the bi-functional catalysts is relatively new. Deactivation characteristics, interaction between the active components, interaction with the feed and products are needed to be explored. Modification of acidic component of the bi-functional catalyst to reduce further dehydration of DME into olefins is also an important area needed to be explored.

Effect of process parameters (e.g. pressure, temperature, varying feed composition) on yield and selectivity of DME need to be studied extensively. Results obtained from these studies will lead to development of kinetic models for the individual catalysts. Comparison of the developed catalyst with the commercially available catalysts would provide valuable information regarding further modification and development of catalysts.

Moreover, there are still scope for development of novel active components, supports and promoters to enhance overall conversion of syngas to DME. Computation techniques such as DFT calculations can aid in developing novel catalysts as well as modification of the existing catalyst.

An important area for focused research is to establish the extent to which the polluting gaseous species can be tolerated by the bi-functional catalysts.

Process simulation: Commercialisation of a process plant producing DME from brown coal is an idea for the time being since the path has never been explored before. However, process simulation studies linked with the laboratory based experiments can provide valuable information about the process scale-up and optimisation.

4.3 Scope of the thesis

From the literature review, the critical research issues are identified and discussed in Section 4.2. Some of this issues are addressed in this study. The objectives of the current study are:

1. To develop a process model using a process simulator. The process model will use as-mined brown coal as input and produce DME through drying, gasification and single step conversion of syngas.
2. To study char gasification in an entrained flow reactor and analyse the pyrolysis and gasification products: solid, liquid and gas.
3. To study gasification kinetics of the dried Victorian brown coal and demineralised coal.
4. To study the effect of catalyst loading on the gasification kinetics
5. To prepare bi-functional catalysts from commercially available catalysts. The catalysts will then be characterised using different techniques: x-ray diffraction, temperature programmed reduction and desorption, physisorption, and electron microscopy.
6. To study the effect of temperature, catalyst composition and syngas H_2 to CO ratio on the CO conversion, DME yield and selectivity. The optimum condition for the DME synthesis will be determined
7. To prepare bi-functional catalysts from the information generated on the performance and composition of the commercial catalysts. The developed catalysts will be characterised using analytical techniques. The catalysts will be used to find the catalysts activity and selectivity. The performance of the developed catalysts will be compared with the commercial catalysts.

8. To study the effect of sulphur poisoning on the CO conversion, and DME yield and selectivity for the developed catalysts.

References

[1] Edwards R, Larive JF, Beziat JC, 2011, Well-to-wheels analysis of future automotive fuels and powertrains in the European context. Tech. rep., European Commission Joint Research Centre, Luxembourg

[2] Alam MS, Kabir KB, Wijayanta AT, Nakaso K, Fukai J, Bhattacharya S, 2012, *In:* AIChE annual meeting, Pittsburgh

[3] Kabir KB, Moore J, Hein K, Bhattacharya S, 2012, *In:* International workshop on clean technologies of coal and biomass utilization (CTCBU), Anshan, China

[4] How HHH, Roy B, Bhattacharya S, 2010, *In:* Chemeca, Adelaide

This page intentionally left blank

Chapter 5

Materials and Methods

5.1 Introduction

This project involves assessment of DME synthesis from Victorian brown coal through gasification.

Brown coal from the Morwell mine was used for the study. The coal sample was characterised and used for the pyrolysis and gasification studies.

Commercially available methanol synthesis and methanol dehydration catalysts were used for the preliminary DME synthesis experiments. The catalysts have been characterised and used in the synthesis experiments.

Based on the preliminary results, composition of bi-functional catalyst for DME synthesis was formulated, and a preparation method was devised. The developed catalysts have also been characterised and used for the synthesis experiments

This chapter provides a brief description of the materials, analytical techniques and experimental methods used during this project.

5.2 Coal preparation, characterisation, pyrolysis and gasification

This section describes the analytical techniques and experimental methods used for the pyrolysis and gasification studies.

5.2.1 Collection and preparation of coal samples

As-mined Morwell coal was collected in large drums from the coal mine and transported back to the laboratory. The collected sample was high in moisture. The coal was air-dried at 35 °C to reduce the moisture content to the equilibrium moisture content.

The air-dried sample was crushed in a roller mill. Size-reduced sample was then passed through a stack of laboratory tests sieves (SO 03310-1, Endecott Laboratories, England). A RO-TAP sieve shaker (W.S. Tyler, USA) with 278 ± 10 oscillations per minute was used for shaking. The size fractions were stored in sample containers, with the headspace filled with nitrogen. The samples were stored below 4 °C to minimise surface oxidation.

5.2.2 Proximate and ultimate analysis

The proximate analysis of Morwell coal was performed according to the Australian standard [1]. Moisture was determined by calculating the mass loss from the sample after exposing it at 105 °C for 3 hours. The mass loss of the dried sample, after heating the sample in N_2 at 900 ± 10 °C for 7 minutes, was recorded as the volatile matter. For ash determination, a known mass of coal was heated in air to 500 °C in 30 minutes, maintained at this temperature for 30 minutes and then heated to 815 °C until the incineration of the sample was complete. The percentage of ash was calculated from the residual solid mass. Finally, fixed carbon was calculated by subtracting ash, moisture and volatile matter. The ash, fixed carbon and volatile matter were reported on dry basis.

A PerkinElmer 2400 Series II CHNS/O elemental analyser was used for the determination of carbon, hydrogen, nitrogen and sulphur. The instrument was operated in CHNS mode. A known mass of sample (ca. 1-2 mg) was introduced into the analyser. The sample was combusted in pure oxygen environment. The resultant combustion gases were separated using frontal chromatography. As the gases elute, a thermal conductivity detector was used to analyse the product gases [2]. Oxygen content was calculated by subtraction method. Ultimate analysis was reported on dry ash free dry basis.

5.2.3 Surface area

Usually surface area of prorous materials are determined from the N_2 adsorption isotherms measured at -196 °C. However, as the adsorption of N_2 on coals at -196 °C involves activated diffusion into the pores, nitrogen adsorption at this temperature does not measure the toal surface area of coals [3].

Adsorption of gases with smaller molecular size and high critical temperatures are therfore can be used for adsorption at a higher temperature. CO_2 has a smaller kinetic diameter than N_2 and has a critical temperature of of 31.5 °C. Adsorption of CO_2 at 0 °C (273.15 K) has been demonstrated to work for surface area measurement of carbonaceous samples [4].

Dubinin-Radushkevich (D-R) [5] equation describes the adsorption of gases by microporous structures:

$$\log v = \log v_0 - \left(\frac{BT}{\beta}\right)\left(\log \frac{p_0}{p}\right)^2 \tag{5.1}$$

where v is the amount adsorbed at equilibrium pressure p, v_0 the micropore capacity, p_0 the saturation vapor pressure of the adsorbate, β the affinity coefficient of the adsorbate relative to N_2, and B a constant which is a measure of the micropore size.

Accelerated surface area and porosimetry system (ASAP 2010, Micromeritics) was used for the surface area measurements. In a typical run, 100-300 mg of sample was loaded in a sample tube. The sample was degassed at 150 °C. This was followed by CO_2 adsorption at 273.15 K (0 °C).plot between $\log v$ and $[\log(p_0/p)]^2$ gives the micropore capacity v_0. Multiplying this number the cross-sectional area of the adsorbed molecule (e.g. CO_2), gives the micropore surface area.

5.2.4 Coal demineralisation and catalyst loading

A three step washing process was used for coal demineralisation [6]. In step 1, the coal sample was washed with alkali. A 10% solution of NaOH was used. The washing conditions were: 80 °C, 40 minutes and liquor to coal ratio 6 ml g^{-1}. The purpose of the alkali was step was to dissolve silica and alumina in the coal in form of silicate and aluminate. The organic and pyritic sulphur also react with caustic soda forming precipitates, which can be dissolved in latter steps.

Caustic washing was followed by sulphuric acid leaching. 4% H_2SO_4 solution was used with a liquor to coal ratio of 2.5 ml g^{-1}. The leaching was carried out at 80 °C for 40 minutes. Finally the sample was leached with 20% nitric acid solution at 80 °C for 40 minutes. A liquor to coal ration 4 ml g^{-1} was maintained. The purpose of the acid leaching steps was to dissolve the mineral species as well as the precipitates from step 1.

In between the washing steps, the sample was filtered to remove the spent liquor. The sample was then washed with demineralised water to remove any trapped solvent. The sample was then oven dried prior to further treatment. The demineralised sample was then stored in an appropriate sample container. More details about the washing procedure can be found here [6].

Catalysts (Ca, Fe) were loaded to the parent coal by incipient wetness method [7]. In incipient wetness method, small volume of solvent containing salts of Ca and Fe were added to the coal sample. The volume of the solvent was maintained as such that it was enough to wet the sample. The slurry was maintained in a well stirred condition overnight. The slurry was then dried and stored in the appropriate sample containers.

5.2.5 Thermogravimetric analysis

A thermogravimetric analyser (TGA) (NETZSCH STA 449 F3 Jupiter) was used for thermogravimetric studies. This TGA is designed to operate up to 1250 °C for heating rates between 0.1 and 50 °C min^{-1}.

Alumina crucibles were used for the TGA experiments. The dimension (ID 18 mm, Wall thickness 1 mm) of the crucibles were matched to fit in the sample stage. The depth of the crucibles were kept to 2 mm to ensure that the gas phase can interact with the sample without any diffusion problem.

In a typical pyrolysis experiment ca 10-11 mg coal sample was loaded in a alumina crucible. The sample was then heated up in 100 ml min^{-1} N_2 at 5 °C min^{-1} heating rate up to 200 °C. When the system temperature reached to 200 °C, the heating rate was changed to 10 °C min^{-1}. Final temperature of the sample was 1000 °C.

In a typical gasification experiment, the coal sample was pyrolysed according to the method mentioned above. As the sample temperature reached 1000 °C, the sample was then cooled to the gasification temperature. Gasifying agent was introduced as

the temperature stabilised. In a typical run, a mixture of 90 ml min^{-1} of CO_2 and 10 ml min^{-1} of N_2 was introduced. The sample was then exposed to this environment up to 6 hours.

Gasification experiments were carried out at 700, 750, 800, 850, 900 and 1000 °C with 90% CO_2 concentration for Four samples. Experiments were triplicated to ensure the reproducibility of the results. To understand the effect of CO_2 concentration, additional gasification was carried out at 800 °C for 10, 30, 50 and 70% CO_2 concentration.

5.3 Entrained flow pyrolysis and gasification

An electrical vertical tube furnace was used for pyrolysis and gasification experiments. The furnace is 2.0 metre long and has six heating zones that can be controlled individually.

A tubular quartz reaction was used as the pyrolysis/gasification reactor. The tube consists of an inner reaction chamber of 50 mm diameter and an outer annulus of 80 mm diameter. The reactor has two inlets and one outlet. The inlet at the top is used to introduce coal/char sample. 10% of the total feed gas is also introduced from the top inlet, which entrains the coal coming from the vibratory feeding system located at the top of the furnace. The remaining 90% of the feed gas is introduced from the bottom inlet to the annular space. The gas going into the annular space gets preheated as it goes up before entering the inner reaction chamber through a sintered plated. In a typical run, 5 l min^{-1} of total gas was used, 4.5 l/min from the bottom inlet an 0.5 l min^{-1} from the top inlet. N_2 and different mixes of CO_2 and N_2 were used for pyrolysis and gasification experiments, respectively. A schematic of the reactor is shown in Figure 5.1.

The pyrolysis/gasification products (solid, liquid and gas) come out of the reactor from the bottom. The sampling system consists of a solids collection vessel, a series of tar traps, a particulate filter. The clean gas from the system then passes through another membrane-based moisture guard before passing to a micro-GC gas analysis system (Varian 490-GC). The micro-GC is equipped with a Molsieve-5A and PoraPlot Q columns an a dual thermal conductivity detector and can measure H_2, CO, CO_2 and hydrocarbons. The total volume of gas was calculated using N_2 as the internal standard.

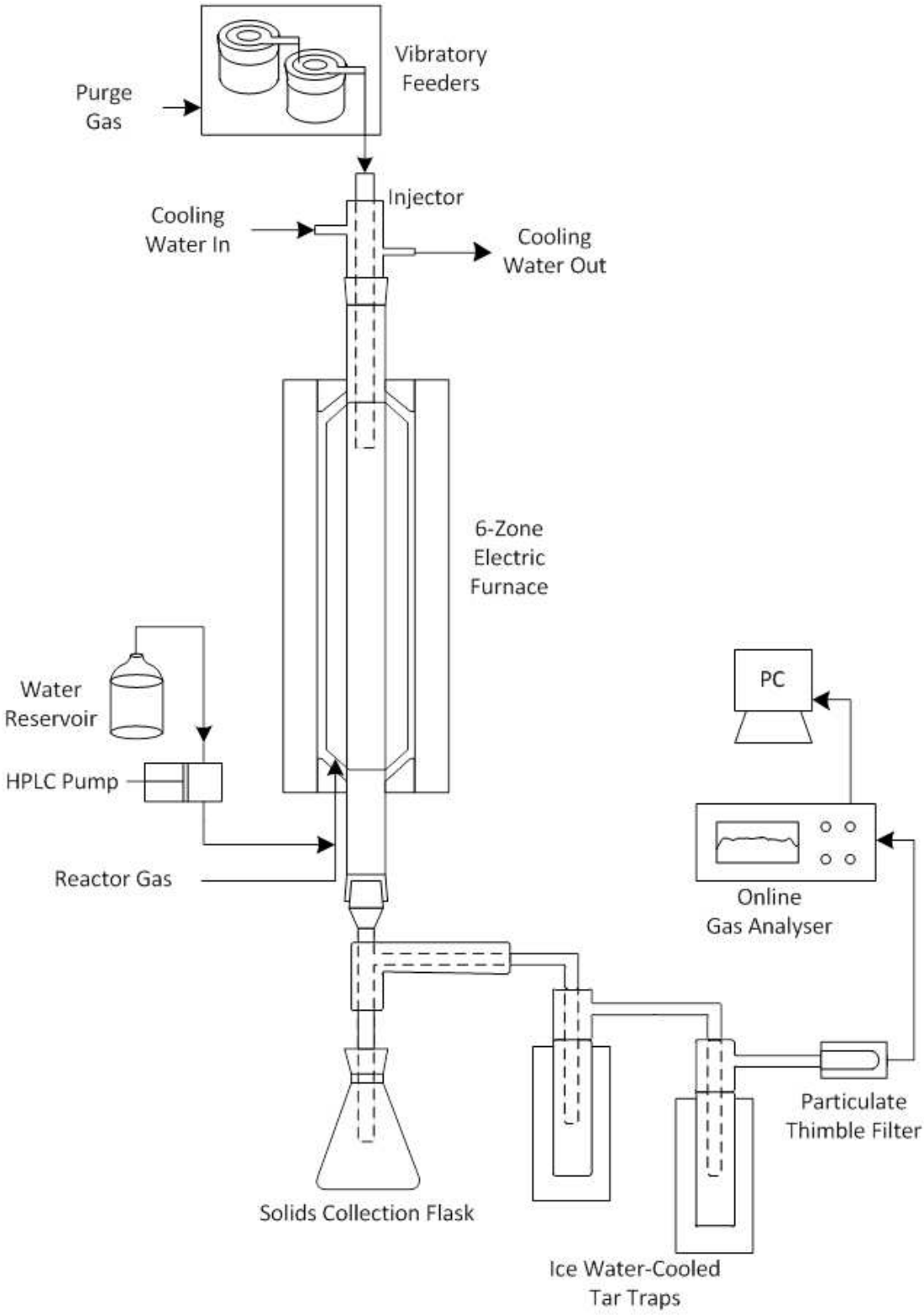

FIGURE 5.1: Drop tube reactor arrangement

Collected tar sample was dissolved in dicholoromethane. The solution was then analysed using a PerkinElmer Clarus 600 GC coupled with a Clarus 600S mass spectroscopy.

Ash tracer method [8] was used to calculated the coal/char conversion:

$$\frac{\Delta W}{W} = 1 - \frac{A_1}{A_2} \tag{5.2}$$

where, A_1 and A_2 are the ash contents before and after conversion.

5.4 Assessment and development of DME synthesis catalysts

This section includes materials and methods used for the DME synthesis studies.

5.4.1 Commercial catalysts

Initially, one commercial methanol synthesis catalyst (Alfa Aesar, Product No. 45776) and one methanol dehydration catalyst (Alfa Aesar, Product No. 12867). were used. Methanol synthesis and methanol dehydration catalysts were in pellet form with 5.8 and 3.2 mm diameter, respectively. Before using, the catalysts were curshed and sieved. Only particles between 20-40 mesh (425-850 μm) were used for these studies. The two catalysts were physically mixed together prior to synthesis experiments.

5.4.2 Catalyst characterisation

Catalyst samples were characterised to obtain their physical and chemical properties.

5.4.2.1 X-ray diffraction: bench top and synchrotron raidation

X-ray diffraction technique was used to bulk phase identification. A laboratory based as well as synchrotron radiation based instrument were used for this purpose.

A Rigaku MiniFlex 600 benchtop X-ray diffraction instrument was used for most of the samples. The instrument has a copper X-ray tube. A $k\beta$ filter and a monochromator installed in the instrument makes sure that the sample interacts with Cu-$K\alpha 1$ radiation. The sample was finely ground and packed into the sample holder. The diffraction intensity was obtained against scattering angle at a rotation speed of 2° min^{-1}.

Synchrotron radiation XRD measurements were carried out for in situ examination of structural changes during catalyst reduction and DME synthesis processes. These experiments were conducted in the powder diffraction beam line end station (10-BM-1) at the Australian Synchrotron [9]. In a typical experiment, ca. 50 mg of catalyst was loaded into 0.7 mm OD (0.5 mm ID) quartz capillary. The catalyst loaded quartz capillary was then inserted into the flow cell as shown in Figure 5.2 (a). The flow cell was then installed on to the beamline end station as shown in Figure 5.2 (b). The beam size at the sample was 1 mm (horizontal) × 1.2 mm (vertical). The beam was focused at the centre of the quartz capillary. The catalyst was reduced by flowing 10% H_2 in He gas through the flow cell from room temperature to 250°C using a gas manifold. The sample holder and the flow cell were allowed to oscillate by 10 degrees to ensure maximum interaction between the bulk sample and the X-ray source. A Cyberstar hot air blower was used to heat up the sample inside the capillary at a heating rate of 10°C min^{-1}. Diffraction patterns from the capillary were collected with the MYTHEN-II strip detector [10] at a wavelength of 0.7743 Å (approximately 16000 keV). The wavelength was determined from the refinement of a NIST LaB_6-660b standard. Before collecting the diffraction patterns the catalyst was held at a given temperature for 20 min. At 250°C the gas was changed from H_2-He mixture to CO-H_2-CO_2 mixture. Figure 5.3 shows the temperature profile and times for the 12 diffraction spectra collected during the course of the experiment. Each diffractogram was collected for 10 minutes. No further analysis of the exhaust gas from the flow cell was performed.

5.4.2.2 Chemisorption

Chemisorption experiments included temperature programmed desorption (TPD) and temperature programmed reduction (TPR). Chemisorb 2720 (Micromeritics) has been used for these techniques.

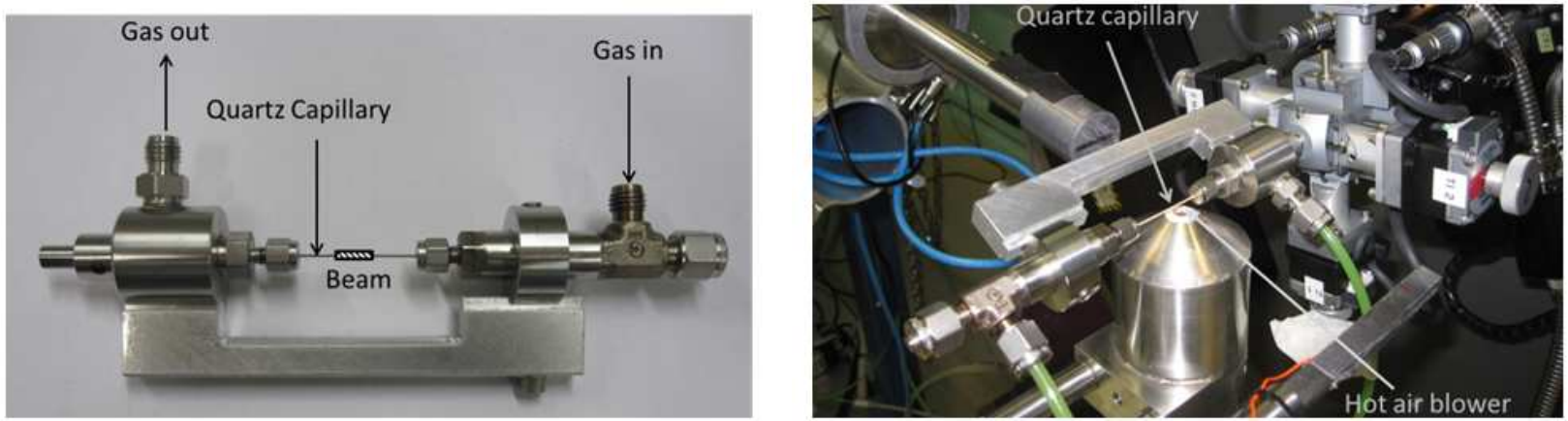

(a) (b)

FIGURE 5.2: (a) Flow cell with sample inside the quartz capillary, (b) Flow cell-Hot air blower configuration

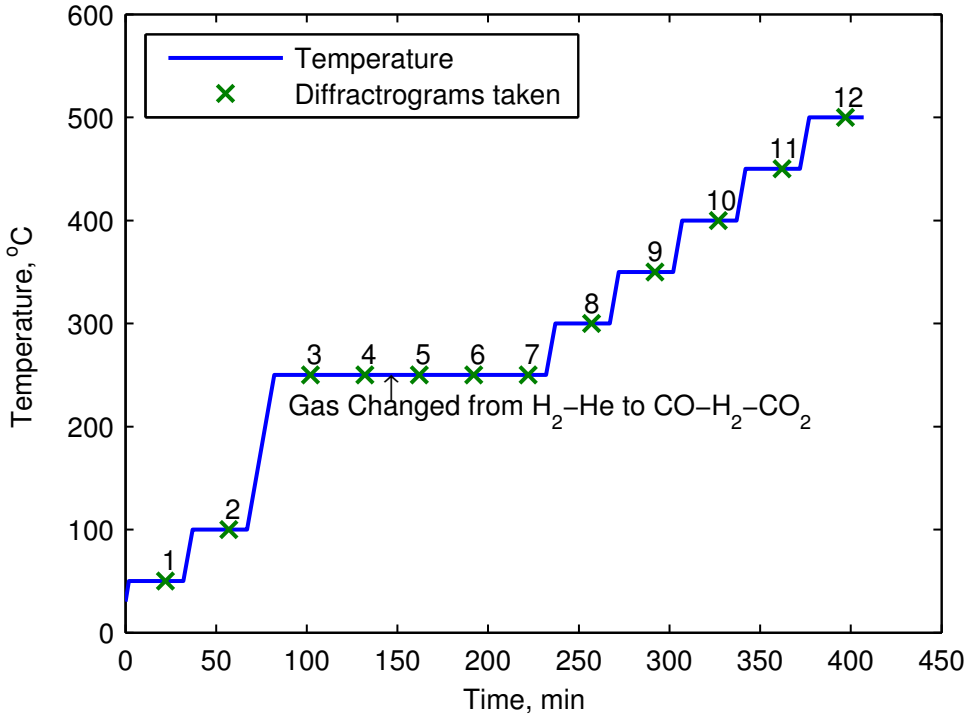

FIGURE 5.3: Temperature profile for XRD measurements (measurement times are indicated by x)

Making this test is accomplished by injecting small quantities of the reactive gas into an inert gas stream that is passing over the catalyst and determining the quantity of reactive gas that is eluted. The test is typically performed with the sample at ambient or elevated temperature so that only chemisorption and not physisorption occurs.

As the sample temperature is linearly increased, the ChemiSorb 2720 is capable of revealing at what temperature a previously chemisorbed component is desorbed (TPD), oxidized (TPO), or reduced (TPR) [11].

For TPD experiments, the sample was degassed by heating up to 300 °C in helium. The sample was then cooled down. A 10% NH_3 in Helium was then passed through the sample. As the sample surface was saturated with NH_3, the gas was changed to pure helium. This enables removal of any physirobed NH_3 on the catalyst surface. The sample temperature was then increased at a rate of 10 °C min^{-1} and the corresponding thermal conductivity was measured. Any variation in the intensity from the baseline at this stage indicates desorption of NH_3 from the catalyst surface.

For TPR experiments, samples were degassed following the same steps as TPD. When the sample was cooled down to 100 °C, the gas was changed to 5% H_2 in N_2. The temperature was also increased at a rate of 10 ° min^{-1}. As soon as the reduction

process started, H_2 was consumed by the catalyst. Differences in thermal conductivity of the inlet and outlet gas was recorded. Any variation in the intensity from the baseline at this stage indicates consumption of H_2 by the catalyst surface.

5.4.2.3 Physisorption

Brunauer-Emmett-Teller (BET) [12] equation of physical adsorption of gas molecules on a solid surface was used for the measurement of the specific surface area of the catalysts:

$$\frac{1}{v[(p_0/p)-1} = \frac{c-1}{v_m c}\left(\frac{p}{p_0}\right) + \frac{1}{v_m c} \tag{5.3}$$

where p and p_0 are the equilibrium and the saturation pressure of adsorbates at the temperature of adsorption, v is the adsorbed gas quantity, and v_m is the monolayer adsorbed gas quantity and c is the BET constant. BET surface area of the sample is determined using v_m.

Accelerated surface area and porosimetry system (ASAP 2010, Micromeritics) was used for the surface area measurements. In a typical run, 100-300 mg of sample was loaded in a sample tube. The sample was degassed at 300 °C. This was followed by nitrogen adsorption at 77.355 K (-195.795 °C). From the pressure versus adsorbed gas volume data, $1/v[(p_0/p) - 1]$ versus (p_0/p) was plotted. The slope and intercept of the plot were then used to calculated the surface area of the catalyst.

5.4.2.4 Electron microscopy

Scanning electron microscopy (SEM) and energy dispersive x-ray (EDX) analyses of the samples were performed using either a JEOL 7001F Field emission gun (FEG) SEM.The SEM images are taken at 15 keV and 10 mm working distance. Samples were prepared by mounting onto a metal stub with double-sided carbon tape and then these are platinum coated to improve conductivity.

5.4.2.5 Synchrotron radiation infra-red spectroscopy

The infre-red spectroscopy measurements were carried out using the Infrared Microspectroscopy (IRM) Beamline at Australian Synchrotron, Melbourne, Australia.

The IRM beamline combines the high brilliance and high collimation of the synchrotron beam with a Bruker V80v FTIR spectrometer and a Hyperion 2000 IR microscope [13].

Both the microscope and the spectrometer were controlled via Bruker OPUS software, version 7.2 including data acquisition, sample stage position and automated multipoint data collection. Measurements were performed using a narrow-band, high sensitivity, liquid nitrogen cooled Mercury Cadmium Telluride (MCT) detector. It was optimised for detection and data collection at a wavelength range of 3800-900 cm^{-1}. The aperture was set to $\sim 10\mu m \times 10\mu m$ and the resolution was 4 cm^{-1}.

A Linkam FTIR600 sample stage was used. The central aperture through the sample stage is 3 mm in diameter. Samples below 100 μm were dispersed on the windowCaF_2 (diameter: 16 mm, 0.5-1 mm thick) to measure the transmittance. An optical microscope was used to capture the images of the particle. A spectrum ollected from an area without any sample was used as the background.

5.4.3 Catalyst preparation

Alumina was prepared from aluminium nitrate using either sodium carbonate or aqueous ammonia as the precipitating agent. To prepare the alumina precursor, initially aluminium nitrate nonahydrate [$Al(NO_3)_3 \cdot 9\,H_2O$; Sigma Aldrich 237973] was dissolved in demineralised water to produce $\sim\ 0.25M$ solution. Then the precipitation was carried out using aqueous ammonia and Na_2CO_3 solution. A 2-l three-neck round bottom flask with 200 mL of demineralised water was placed in a magnetic stirrer hotplate. The content of the flask was heated to 70 °C while heating continuously. The aluminium nitrate and the base solutions were then added drop by drop to the stirred solution in the flask in a manner that the pH of the solution stays close to 8. The precipitate was aged at 70 °C for 4-hours. After that, the precipitate was filtered, washed and dried at 105 °C overnight. The solid is the alumina precursor. The alumina precursor was then calcined in air from room temperature to 550 °C with a heating rate of 2 °C. min^{-1}, and kept at this temperature for 6 hours.

Methanol synthesis catalyst was prepared from a solution of nitrates of copper, zinc by co-precipitation method using sodium carbonate as the precipitating agent. The precipitation method was similar to that of alumina. The final pH of the solution was

maintained close to 7. The catalyst was prepared from the precursor by calcining at 550 °C.

Bi-functional catalysts were prepared using physical mixing [14] and co-precipitation impregnation [15].

5.4.4 DME synthesis

A high pressure rig was used for the DME synthesis experiments. A schematic of the rig is shown in Figure 5.4.

Gas feed to the reactor was controlled by electronic mass flow controllers (MFC). These controllers compare the actual flow rate delivered to set point, and automatically adjust an integral control valve to maintain a constant gas flow.

The reactor (Parr 5403 tubular reactor) has a inner diameter of 25 mm and 826 mm long. The rector is made out of stainless steel (SA479 T 316SS). Elements present in stainless steel are known to act as poisons for methanol synthesis catalyst. Therefore, a brass liner was used inside the reactor. A split-tube furnace, with three separate heating zones, provided the required heat for the reactor. A single movable thermocouple measured the temperatures at points along the catalyst bed. Three external thermocouples were used for control of each zone of the heater.

The reactor was kept at a constant pressure by using a back pressure regulator (BPR). The pneumatically controlled BPR along with electronically controlled MFCs ensured that a constant flow of gas was passing through the reactor, which was held at a constant pressure.

The BPR installed in the rig can not handle liquid. Therefore, a cooling condenser (double-pipe heat exchanger) and gas/liquid separator (Parr 4544 pressure vessel) were provided in between the reactor and the BPR.

In a typical experiment, ca. 3 g of catalyst was loaded inside the reactor. The catalyst was reduced at 190 °C for 8 hours before use. Reduction was carried out at room temperature. The reactor was then pressurised using N_2. As the required pressure was achieved, synthesis gas (CO and H_2) was introduced to the reactor.

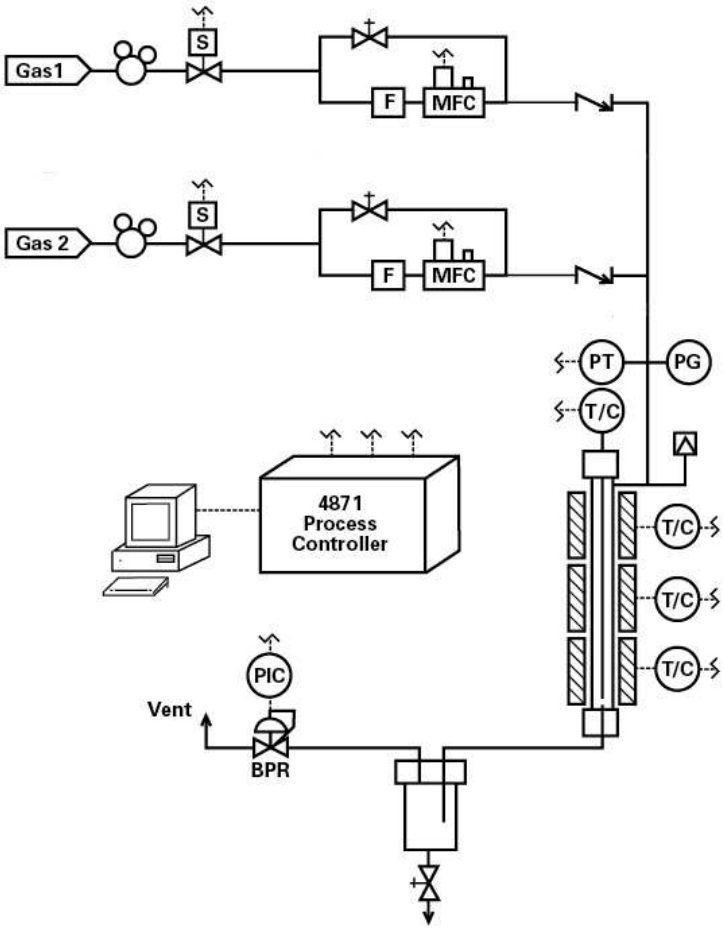

(a) Schematic

(b) Photograph

FIGURE 5.4: High pressure DME synthesis rig: (a) Schematic (b) Photograph

Online analysis of the outlet gas was carried out using Agilent 7890A (G3440A) GC equipped with four columns (HayeSep N, MolSieve 5A, Porapak Q and Sulfinert) and three detectors (TCD, FID and FPD).

References

[1] Standards Australia, 2002, *Methods for the analysis and testing of low rank coal and its char (AS 2437.4-2002)*

[2] PerkimElmer, 2003, *2400 Seris II CHNS/O analyzer user's guide*

[3] Mahajan OP, 1991, Carbon, **29**: 735–742

[4] Lozano-Castello D, Cazorla-Amoros D, Linares-Solano A, 2004, Carbon, **42**: 1233–1242

[5] Mahajan O, Jr PW, 1978, *In:* Analytical Methods for Coal and Coal Products, Karr C, editor, 125 – 162, Academic Press, New York

[6] Yang RT, Das SK, Tsai B, 1985, Fuel, **64**: 735–742

[7] Augustine RL, 1996, Heterogeneous catalysis for the synthetic chemist. Marcel Dekker, New York

[8] Kobayashi H, Howard J, Sarofim A, 1977, Symposium (International) on Combustion, **16**: 411 – 425

[9] Wallwork KS, Kennedy BJ, Wang D, 2007, AIP Conference Proceedings, **879**: 879–882

[10] Bergamaschi A, Cervellino A, Dinapoli R, Gozzo F, Henrich B, Johnson I, Kraft P, Mozzanica A, Schmitt B, Shi X, 2010, Journal of Synchrotron Radiation, **17**: 653–668

[11] Micromeritics Instrument Corporation, 2009, *ChemiSorb 2720 Operator's manual*

[12] Brunauer S, Emmett PH, Teller E, 1938, Journal of the American Chemical Society, **60**: 309–319

[13] Australian Synchrotron, 2014, *Technical information (IR)*. Cited: 26 June 2014. Available from: http://www.synchrotron.org.au/

[14] Li JL, Zhang XG, Inui T, 1996, Applied Catalysis A: General, **147**: 23–33

[15] Ge Q, Huang Y, Zhang T, 1996, Natural Gas Chemical Industry (C1 Chemistry and Technology), **21**: 19–22

Chapter 6

Equilibrium Modelling and Process Simulation

6.1 Introduction

The first section of the chapter includes equilibrium modelling of DME synthesis from syngas. Thermodynamic treatment of the reactions involved in the syngas to DME synthesis provided information about spontaneity and change of energy of the system at different temperatures (25-400 °C). The effect of H_2 to CO ratio on the equilibrium product composition is also presented. Finally, the pressure and temperature effects on DME yield are also calculated.

Thermodynamic modelling was followed by a steady-state process model, developed using Aspen Plus, for drying and gasification of Victorian brown coal and subsequent conversion of the syngas to DME with recycling of the unreacted gas. This study involves assessment of DME production from brown coal and identification of the major process constraints. The evaluated results were then used as one of the basis for the experimental work.

6.2 Thermodynamic simulation of DME synthesis

Conversion of syngas to DME involves CO-hydrogenation to methanol (R6.1), methanol dehydration to DME (R6.2) and water gas shift (WGS) reaction (R6.3):

$$CO + 2\,H_2 \longrightarrow CH_3OH \qquad \text{(R6.1)}$$

Excerpted from: Bhattacharya S, Kabir KB and Hein K, *progress. energy combust. sci*, 39: 577-605; Kabir KB, Hein K and Bhattacharya S, *Comput. Chem. Eng.*, 48:96-104

$$2\,CH_3OH \longrightarrow CH_3OCH_3 + H_2O \tag{R6.2}$$

$$CO + H_2O \longrightarrow CO_2 + H_2 \tag{R6.3}$$

In addition to the three reactions above CO_2-hydrogenation to methanol (R6.4) also takes place:

$$CO_2 + 3\,H_2 \longrightarrow CH_3OH + H_2O \tag{R6.4}$$

Figure 6.1 shows variation in the Gibbs free energy for reactions (R6.1), (R6.2), (R-6.3) and (R6.4). CO-hydrogenation is thermodynamically favourable at temperatures below 150 °C. The Gibbs free energy ∼140 °C becomes positive. CO_2-hydrogenation is thermodynamically unfavourable for the temperature range shown in Figure 6.1. Therefore, CO-hydrogenation above 140 °C and CO_2 hydrogenation for all temperatures would require high pressure to make these reactions more favourable in forward direction producing methanol. It is also clear from Figure 6.1 that both methanol dehydration and WGS reactions are thermodynamically feasible for the plotted temperature range.

Figure 6.2 shows enthalpy of reaction for the temperature range of 25-400 °C. All four reactions are exothermic. For both the hydrogenation reactions heat of reaction becomes more negative while for WGS and dehydration reactions ΔH slightly increases.

Thermodynamic analysis of the system involving these four reactions is useful since this provides preliminary understanding of the conversion process: effect of pressure, temperature and feed composition. However, a reactive system with the above mentioned species (six in total: CO, H_2, CO_2, H_2O, CH_3OH and CH_3OCH_3) has only three independent reactions and taking any three reactions from R6.1, R6.2, R6.3 and R6.4 would give the same equilibrium composition. Presence of species such as N_2 or CH_4 would not have any impact on the reactive system since they can be considered as inert for the syngas to DME conversion. However, their presence in the system would lower the partial pressure of the reactants hence will alter the equilibrium composition.

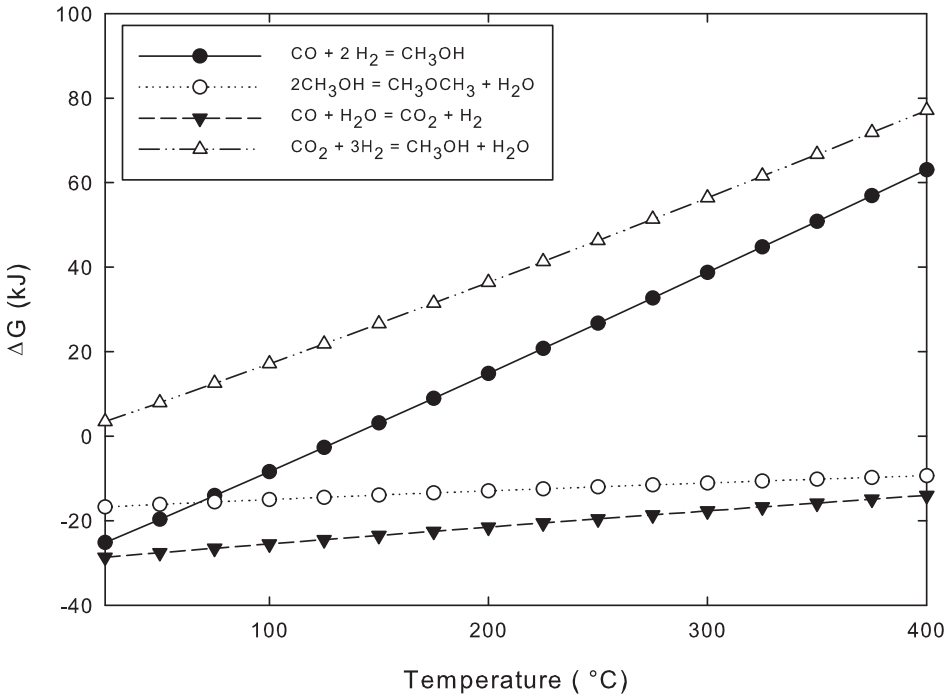

FIGURE 6.1: Gibbs free energy of reaction at different temperatures

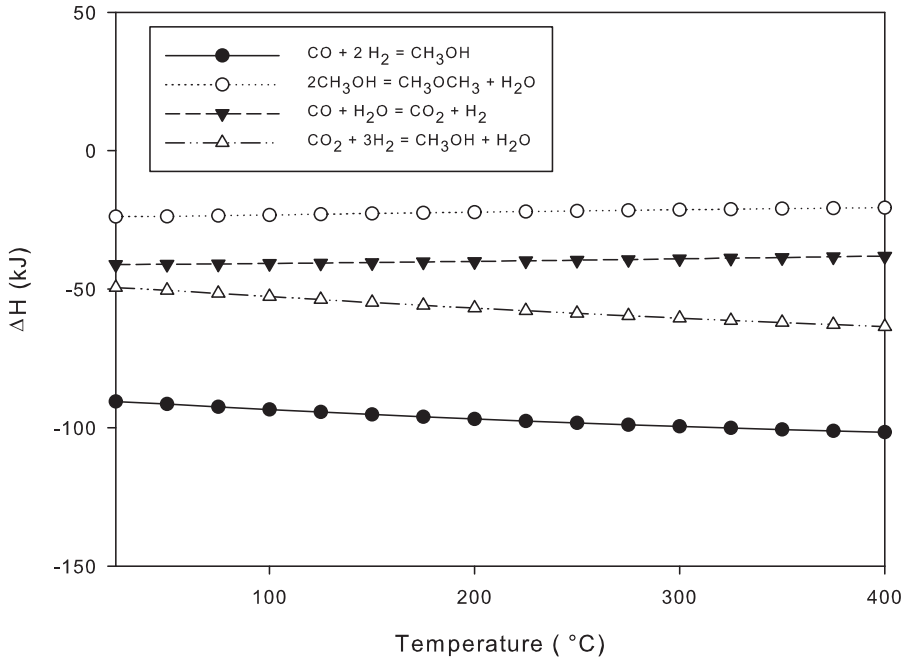

FIGURE 6.2: Enthalpy of reaction at different temperatures

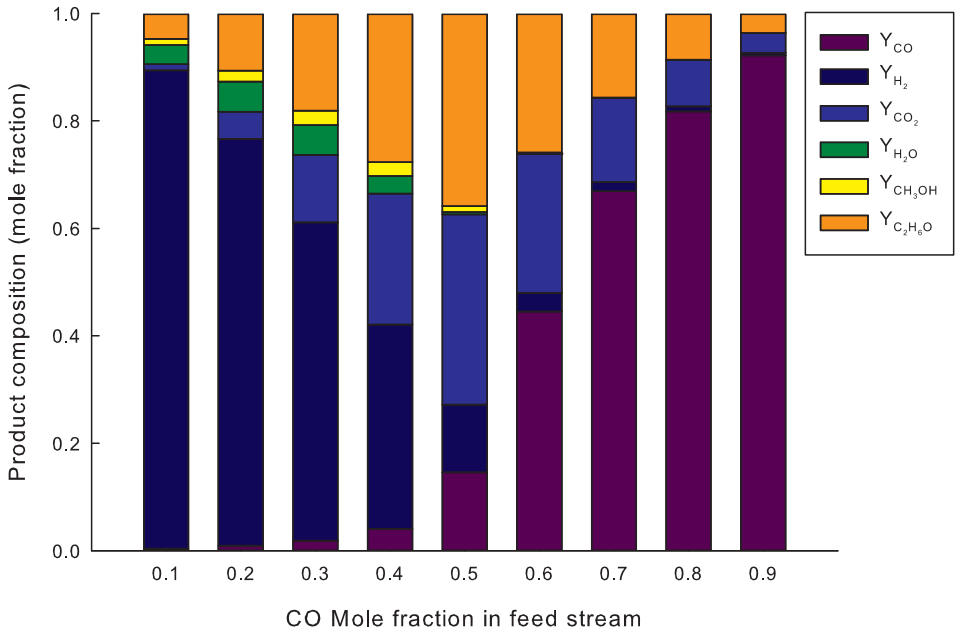

FIGURE 6.3: Equilibrium product composition with varying CO mole fraction in the feed stream (balance is H_2)

Equilibrium yield for a CO and H_2 mixed stream feed to the reactor at 260 °C and 5 Mpa is shown in Figure 6.3. The mole fraction of CO in the feed stream was varied from 0.1 to 0.9. Equilibrium product composition for six involved species shows that an equimolar mixture of CO and H_2 gives maximum DME and minimum methanol concentrations in the product stream. CO_2 is the other major product for this condition.

Effect of temperature and pressure on the equilibrium yield of DME for an equimolar mixture of CO and H_2 is shown in Figure 6.4. Equilibrium DME yield is defined by the following equation:

$$YI_{DME} = \frac{2F_{OUT}Y_{DME}}{F_{IN}X_{CO}} \tag{6.1}$$

where YI_{DME} is DME yield, Y_{DME} is mole fraction of DME in the product, X_{CO} is the mole fraction of CO in the feed stream, and F_{IN} and F_{OUT} are the molar flow rate of feed and product streams, respectively.

As shown in Figure 6.4, high pressure and low temperature conditions in the reactor would increase equilibrium yield. However, increasing temperature would significantly increase the reaction rates. Hence a trade-off between the yield and reaction rate is necessary.

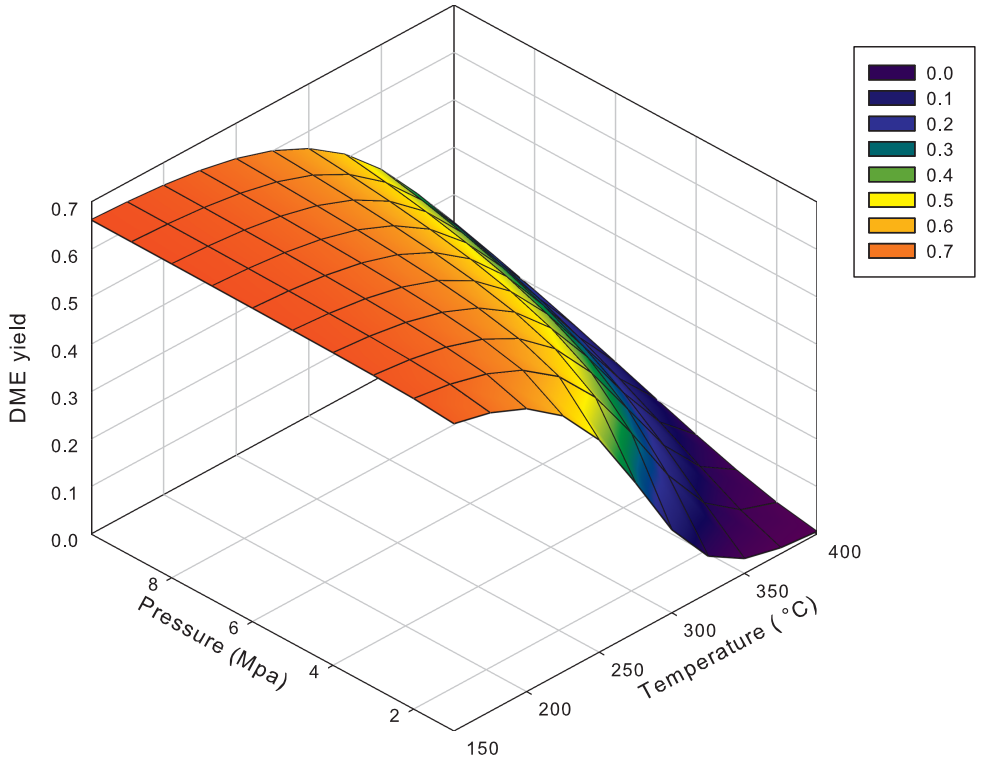

FIGURE 6.4: Equilibrium yield of DME at different temperatures and pressures

Thermodynamic analysis of the DME synthesis process shows a synergistic effect on total conversion of syngas to useful products.

6.3 Process simulation

Process simulation can shed insights into the conceptual design of the chemical processes by finding out the best process flowsheet and optimum design conditions [1]. Process performance for DME synthesis can greatly vary with factors such as the source of syngas, gasification conditions, configuration of the DME reactor, and catalyst functionality. Simulation of a fluidized-bed DME reactor was performed by Lu et al [2] assuming both bubble and dense phase in plug flow (P-P model). In a later study, Lu et al. [3] showed that fully back-mixed back flow (P-M model) performs better than the P-M model for fluidized-bed reactor modelling. Kumar and Srivastava [4] employed generalized comprehensive reactor (GCR) model for simulating fluidized-bed reactor. Fixed-bed DME synthesis reactors were simulated using both

shell-and-tube [5, 6] and adiabatic reactors [7]. There had also been some attempts to simulate co-generation of DME and electricity from various feedstocks [8–11]. Most of these simulation studies used once-through reactor for DME synthesis.

This current work involves development of a steady-state process model in Aspen Plus for Victorian brown coal gasification and subsequent conversion of the syngas to DME with recycling of the unreacted gas. This study involves assessment of DME production from brown coal and identification of major process constraints. The evaluated results will feed into our experimental work required for development and commercialization of such process.

6.3.1 Description of the process

The schematic of the steady state process model for DME synthesis from Victorian brown coal is shown in Figure 6.5 and 6.6. As-mined brown coal is dried to 12% moisture content (which is close to equilibrium moisture content) before feeding to the gasifier. Oxygen and steam is also fed to the gasifier. Syngas is then cleaned by removing all nitrogen, sulphur and chlorine containing compounds, compressed to the DME reactor pressure and cooled before feeding to the reactor.

Product stream from the reactor is flashed and the gaseous product from the flash separator is further washed with a methanol-water mixture to recover any residual DME. A fraction of this stream is purged and the rest is recycled back to the DME reactor. Liquid streams from the absorption column and flash separator is mixed together before feeding into the DME column. Distillate from this column is taken as the product. A portion of the bottom product from the DME column is fed to the absorption column while the remaining portion is sent to the methanol column. Recovered methanol from the column is recycled back to the DME synthesis reactor. Bottom product from the methanol column is mostly water with small amount of methanol and therefore requires further treatment.

6.3.2 Simulation basis

50 kg/hr as-mined Loy Yang coal was used as basis for this simulation study. Proximate and ultimate analysis of the as-received coal is shown in Table 6.1. Soave-Redlich-Kwong (SRK) equation of state was selected for the simulation, since it has

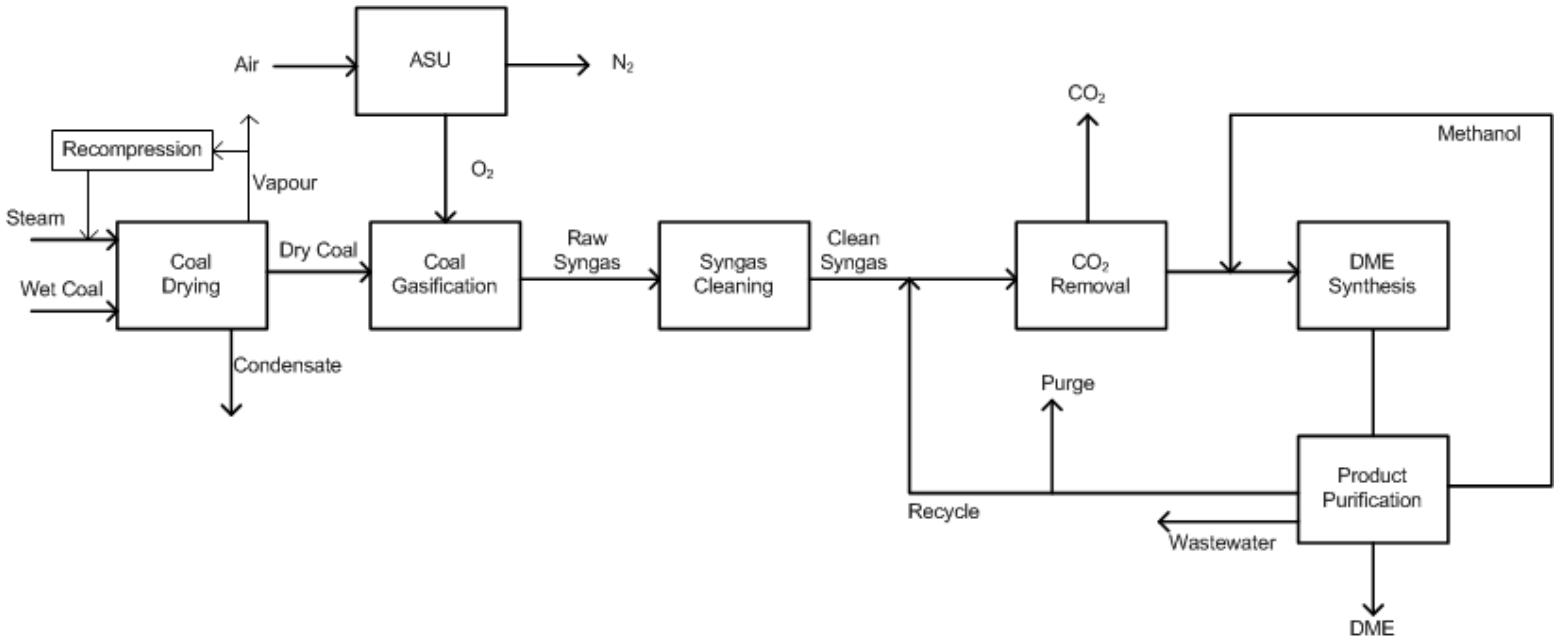

FIGURE 6.5: Block diagram of the process used for DME production from Loy Yang Coal

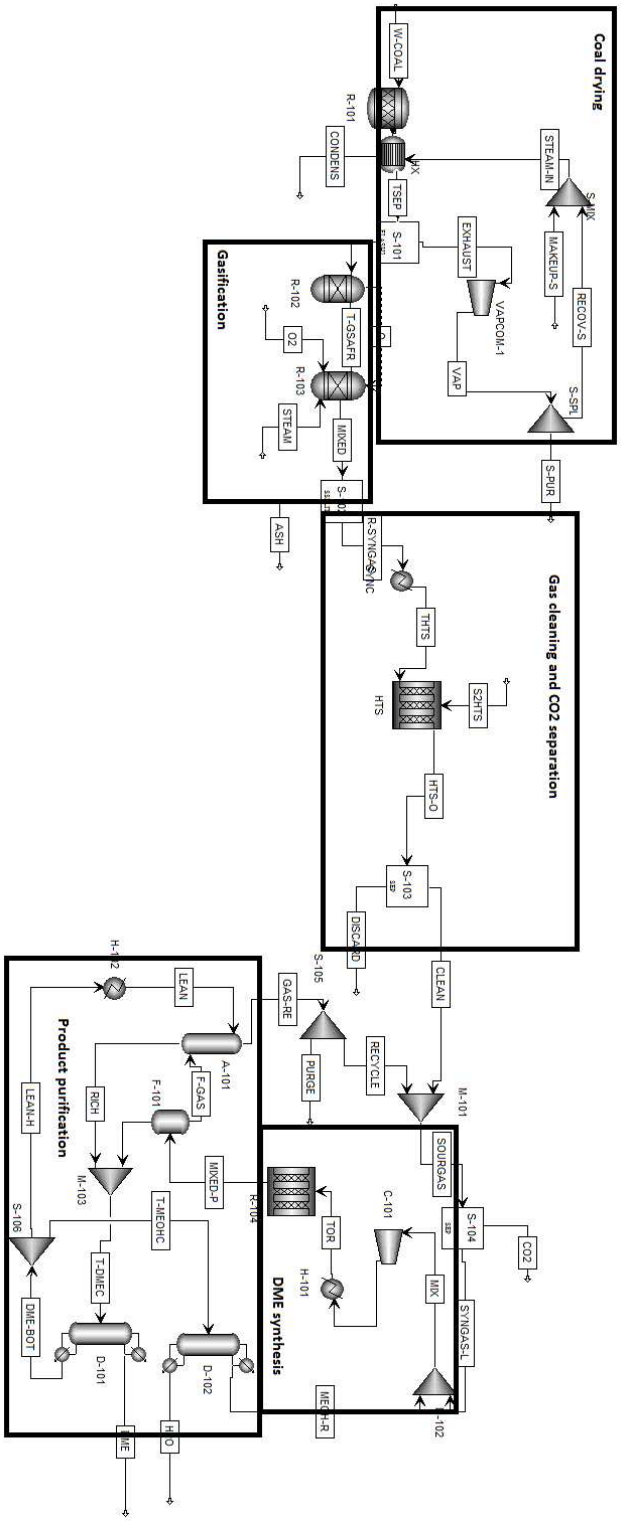

FIGURE 6.6: Brown coal to DME flowsheet in Aspen Plus

Table 6.1: Analysis of Loy Yang coal

Proximate analysis (% dry basis)		Ultimate analysis (% dry basis)		Ash Analysis	
Fixed carbon	49.5	Ash	1.5	SiO_2	56.5
Volatile matter	49	Carbon	68.5	Al_2O_3	20.5
Ash	1.5	Hydrogen	4.6	Fe_2O_3	4.6
		Nitrogen	0.6	K_2O	1.3
		Sulphur	0.31	MgO	3.6
		Oxygen	24.38	Na_2O	4.7
				CaO	1.6
		Other Elements		SO_3	5
		Chlorine	0.11	P_2O_5	0.2
Moisture content (as-mined coal) 62.8%					
Net heating value (as-mined coal) 7.9 MJ/kg					

been reported to give better property estimation than Redlich-Kwong (RK) or Peng-Robinson (PR) for methanol synthesis, water gas shift (WGS) reaction [12]) and dimethyl ether synthesis [6].

The gasifier model comprised of a yield reactor for the pyrolysis of coal followed by a Gibbs reactor for the conversion of the pyrolysis products (e.g. volatiles and char). A Gibbs reactor models chemical equilibrium by minimising Gibbs free energy. Coal is considered as a non-conventional component in Aspen and Gibbs free energy of coal cannot be calculated. Therefore, a yield reactor was placed before the Gibbs reactor to decompose coal into its constituent elements. The heat of reaction associated with coal decomposition was considered into the gasification step as shown in Figure 6.6. The gas species considered for the gasification model is shown in Table 6.2. A Gibbs model was used to predict the gasifier behaviour since many gasifiers produce near equilibrium products [13]. Gasifier pressure was varied from 30 to 60 bar.

A plug flow reactor with Langmuir-Hinshelwood-Hougen-Watson (LHHW) kinetic model was used as the DME synthesis reactor. Out of six possible reactions for the reactive system [14], three independent reactions were selected for the simulation. Kinetic data for the syngas to DME bi-functional catalyst were taken from the work of Nie et al [14, 15]. Reactions involved and corresponding kinetic expressions are shown in Table 6.2. Numerical values of the model parameters can be found in Nie et al [14]. An isothermal plug-flow reactor (Rplug; $\varnothing 0.2m \times L6.0m$; L/D ratio of 30 for turbulent flow condition) was used for the simulation. Selection of the reactor size was governed by the catalyst loading and the space velocity.

TABLE 6.2: Simulation basis for brown coal gasification and DME synthesis

Process	Model used	Operating condition and Gas species considered and reactions involved
Gasification	Gibbs energy minimisation (RYield, RGibbs)	Temperature: 900 °C, Pressure: 30-60 bar H_2O, N_2, O_2, H_2, CO_2, CO, H_2S, COS, S, HCl, HCN, SO_2, SO_3, NH_3, CH_4
DME synthesis	LHHW (RPlug)	Temperature: 240 °C, Pressure: 60 bar, SV= 800 ml/g_{cat}.h $CO + 2\,H_2 \longleftrightarrow CH_3OH$ $r_{CO} = k_1 f_{CO} f_{H2}^2 \frac{(1-f_{CH3OH}/K_{f1} f_{CO} f_{H2}^2)}{(1+K_{CO} f_{CO}+K_{CO2} f_{CO2}+K_{H2} f_{H2})^3}$ $CO_2 + 3\,H_2 \longleftrightarrow CH_3OH + H_2O$ $r_{CO2} = k_2 f_{CO2} f_{H2}^3 \frac{(1-f_{CH3OH} f_{H2O}/K_{f2} f_{CO2} f_{H2}^3)}{(1+K_{CO} f_{CO}+K_{CO2} f_{CO2}+K_{H2} f_{H2})^4}$ $2\,CH_3OH \longleftrightarrow CH_3OCH_3 + H_2O$ $r_{DME} = k_3 f_{CH3OH} \frac{(1-f_{DME} f_{H2O}/K_{f3} f_{CH3OH}^2)}{(1+\sqrt{K_{CH3OH} f_{CH3OH}})^2}$

note: f_i is the fugacity of component i, K_{fi} is the equilibrium constant of the reaction i, K_i is the adsorption constant of component i

6.3.3 Simulation results

6.3.3.1 Drying of brown coal

Drying of brown coal is an important issue because of its high reactivity and spontaneous combustibility. Brown coal is, therefore dried preferably in absence of oxygen, i.e. using nitrogen or steam. Both nitrogen and steam drying at 160 °C of Loy Yang coal was modelled during this study. Nitrogen provides completely inert condition, suitable for brown coal drying. In this model, a nitrogen stream is fed to the drier along with the wet coal. The product streams from the drier are dried coal stream and moist nitrogen stream. An Air separation unit (ASU) can provide the necessary nitrogen for the drying process. However, the ASU is usually installed for supplying the oxygen in the gasifier and a rated ASU of such a scale would be able to provide only $\sim 6\%$ of the required nitrogen for drying Loy Yang coal to 12% moisture content.

A different configuration was used for modelling steam drying, which is similar to RWE's WTA steam fluidised bed dryer [16]. Low pressure steam at 160 °C was used to dry the coal is a fluidised-bed. The simulation result showed that this option is a far better option than the nitrogen drying. The moisture evolved from the coal can be compressed and re-used in the steam heated coils inside the fluidised-bed. Vapour

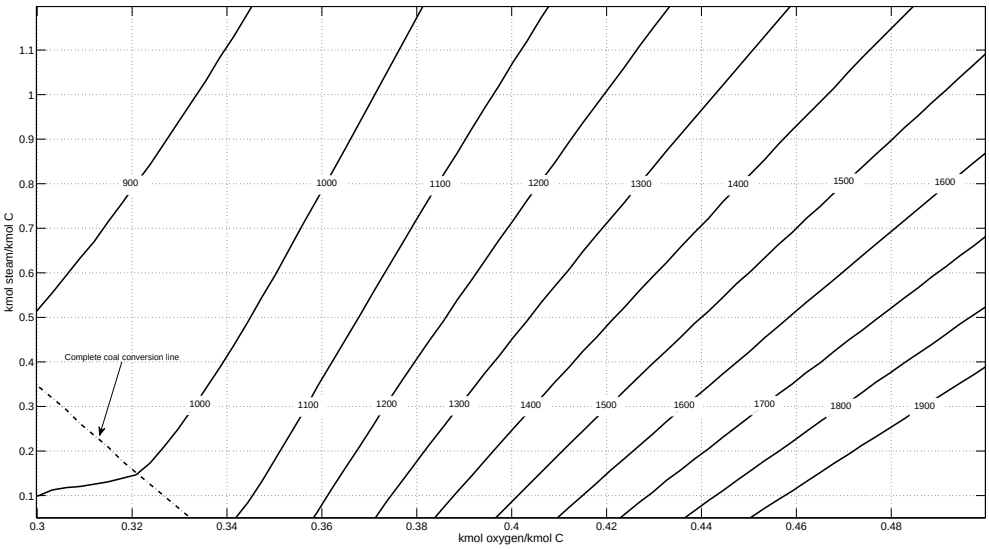

FIGURE 6.7: Gasification temperature as a function of steam and oxygen fed to the reactor

re-compression can provide ∼75% of the required steam while the rest can potentially be generated from waste heats in the DME synthesis process.

6.3.3.2 Brown coal gasification

A series of two reactors, one yield reactor followed by a Gibbs reactor, were used for the simulation of coal gasification. Air, oxygen or oxygen-steam mixture can be used as gasifying agent. However, air gasification produces syngas with significant amount of nitrogen making the product gas dilute. In addition, presence of such a high quantity of nitrogen also makes separation of CO_2 more difficult and costly [13]. Therefore, air gasification was excluded from further studies and oxygen-steam mixture (auto thermal reforming - ATR) was used as gasifying agents.

Figure 6.7 shows temperatures in the gasifier with varying flowrates of oxygen and the steam. Steam act as a moderator and hence reduce the temperature. Isotherms shown in the figure indicate that same temperature can be achieved for different combinations of oxygen and steam flowrate. The dotted line in the left bottom corner is the boundary line for complete conversion of coal into gas. To the left of this line supplied oxygen and steam is not sufficient to convert the solid fed to the gasifier. Figure 6.7 is very important in the sense that it provides information regarding the footprint of the gasification process. Depending on the operating point selected for the gasification, the amount of oxygen and steam consumed as well as CO_2 produced from the gasification can vary to a great extent.

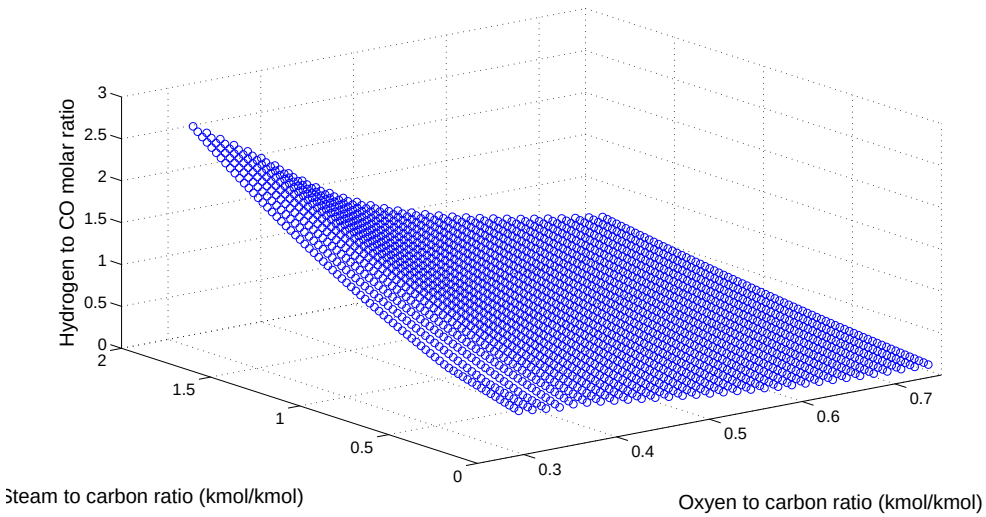

FIGURE 6.8: Hydrogen to CO molar ratio as a function of steam and oxygen feed rate to the gasifier

Composition of the syngas, especially hydrogen to CO ratio, is another important issue for the gasification process. Thermodynamic study of DME synthesis showed that for once-through synthesis of DME from syngas a H_2 to CO ratio of 1 is appropriate.

Variations of H_2 to CO molar ratio with oxygen and steam feed rate are shown in Figure 6.8. For a particular oxygen to carbon ratio, increasing amount of steam supplied to the gasifier gradually increases the amount of H_2 in the syngas and hence the corresponding H_2 to CO ratio. Changes are more prominent at lower oxygen to carbon ratio with more CO present in the gas to be converted to CO_2 and H_2 through water gas shift reaction.

From Figures 6.7 and 6.8, it can be concluded that fixing the gasification temperature and H_2 to CO molar ratio in the syngas would also fix the required oxygen and steam for the gasification process. Earlier simulation work by the authors on Victorian brown coal-simulation has shown that at higher temperatures alkaline species (chlorides and hydroxides of sodium and potassium) go into the gas phase which could be troublesome for the downstream processing units because of corrosive nature of those species [17]. Therefore, low temperature gasification (∼900 °C) would be beneficial. The temperature is in the range of fluidised bed gasifiers and justifies development of fluidised bed gasifier for the Victorian brown coal. Around this gasification temperature the H_2 to CO molar ratio would be governed by the optimum process output (i.e., DME yield) which is discussed in the following section. Oxygen and steam flow into the gasifier is therefore fixed by fixing the temperature and the H_2 to CO ratio.

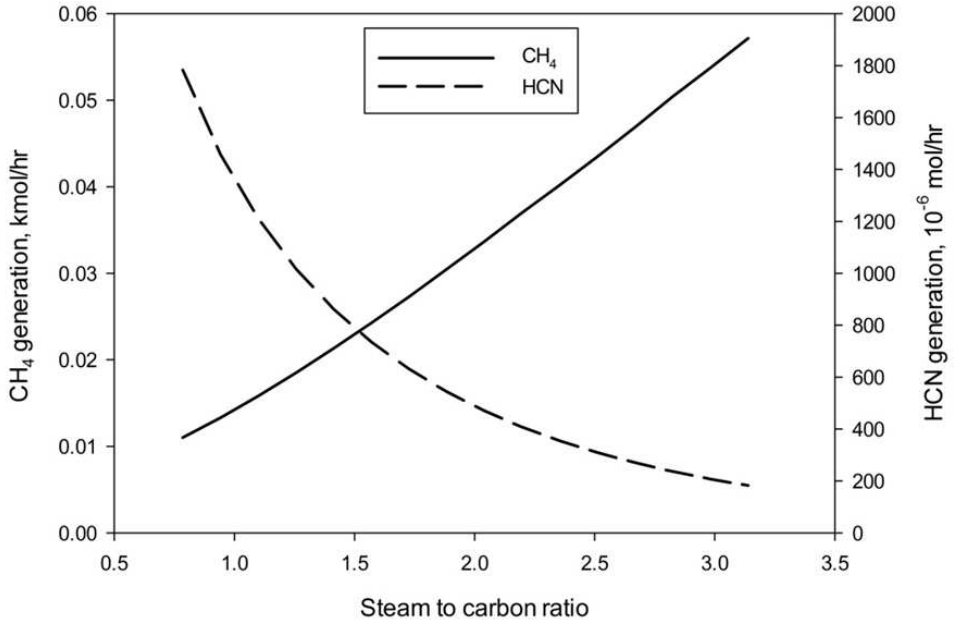

FIGURE 6.9: CH_4 and HCN generation in syngas at 30 bar

Sulphur, chlorine and nitrogen containing species (e.g. NH_3, H_2S, COS, HCl, HCN) act as poison for methanol synthesis catalyst while CH_4 is an inert for the synthesis reaction. Effect of steam feed on the formation of these species was evaluated and shown in Figures 6.9, 6.10 and 6.11. HCl and H_2S generation slightly decreased with increased steam feed. COS concentration decreased twofold when the steam to carbon ratio was increased from 1 to 3. However, NH_3 generation was found to increase instead. HCN generation in syngas found to be most sensitive to steam feed and decreased a order-of-magnitude with increased steam. Increased steam also found to favour formation of methane, as shown in Figure 6.11.

Pressure in the gasifier was varied from 30 bar to 60 bar. A steam to carbon ratio of ∼1.7 (kmol/kmol) was maintained while evaluating the pressure effect. Increasing pressure did not had any significant effect on H_2 to CO ratio or concentrations of species like COS, HCl and H_2S (Figure 6.12, 6.13). However, NH_3, HCN and CH_4 concentrations gradually increased with increasing pressure (Figure 6.14).

Oxy-gasification (partial oxidation-POR) followed by one/two WGS reactor can also be used in the process. During POR, oxygen is used as gasifying agent. A comparative study of both ATR and POR followed by WGS was performed to access the necessity of WGS reactor in the process. If the required gas composition (i.e. H_2 to CO molar ratio) can be achieved with the shift reaction, it would essentially save both the capital and operating costs associated with the shift reactor. To simulate WGS

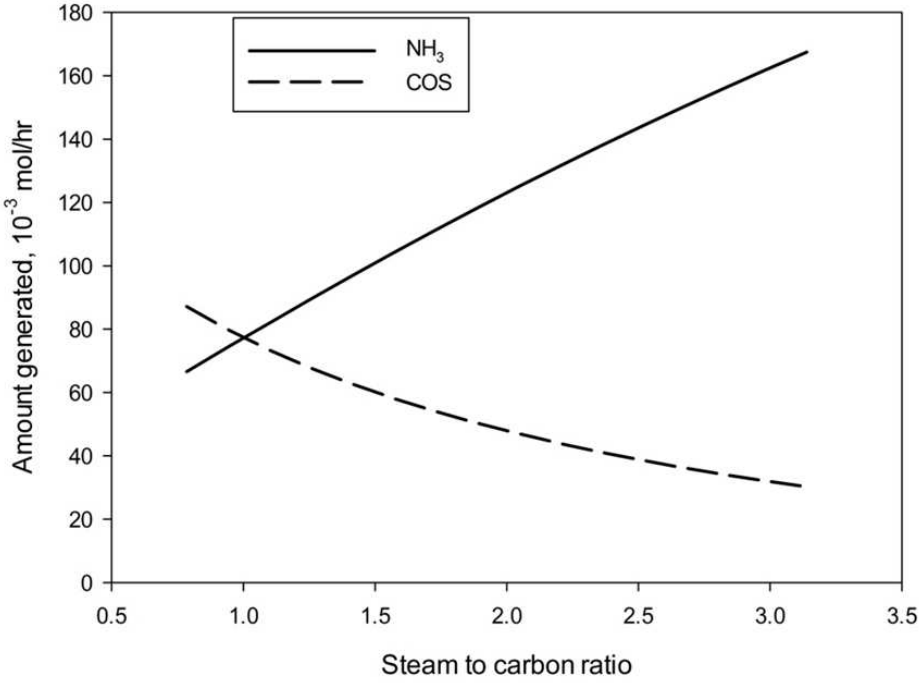

FIGURE 6.10: NH_3 and COS generation in syngas at 30 bar

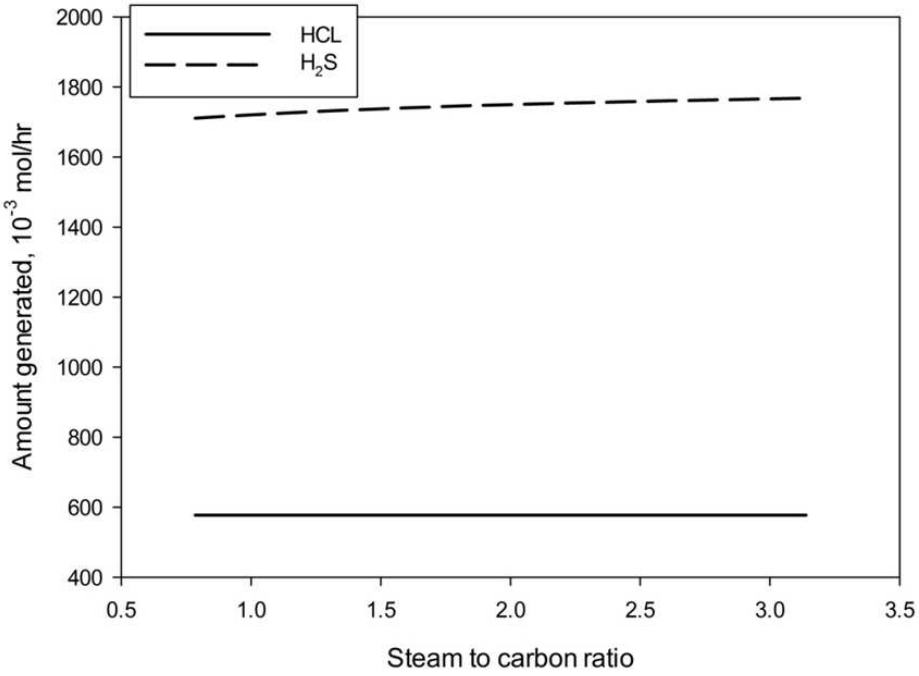

FIGURE 6.11: HCl and H_2S generation in syngas at 30 bar

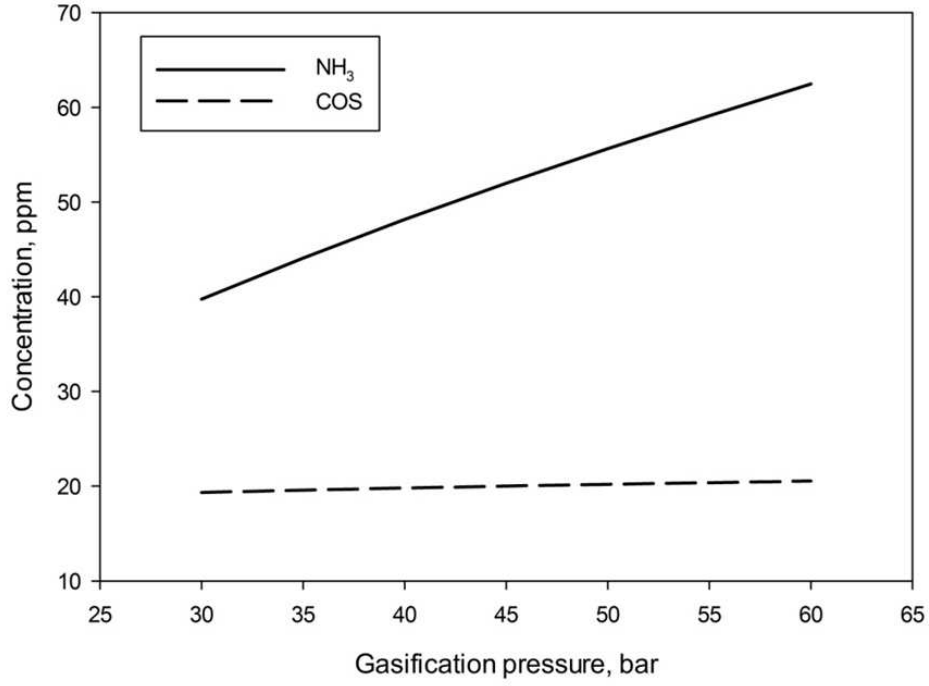

FIGURE 6.12: Pressure effect on NH_3 and COS concentration

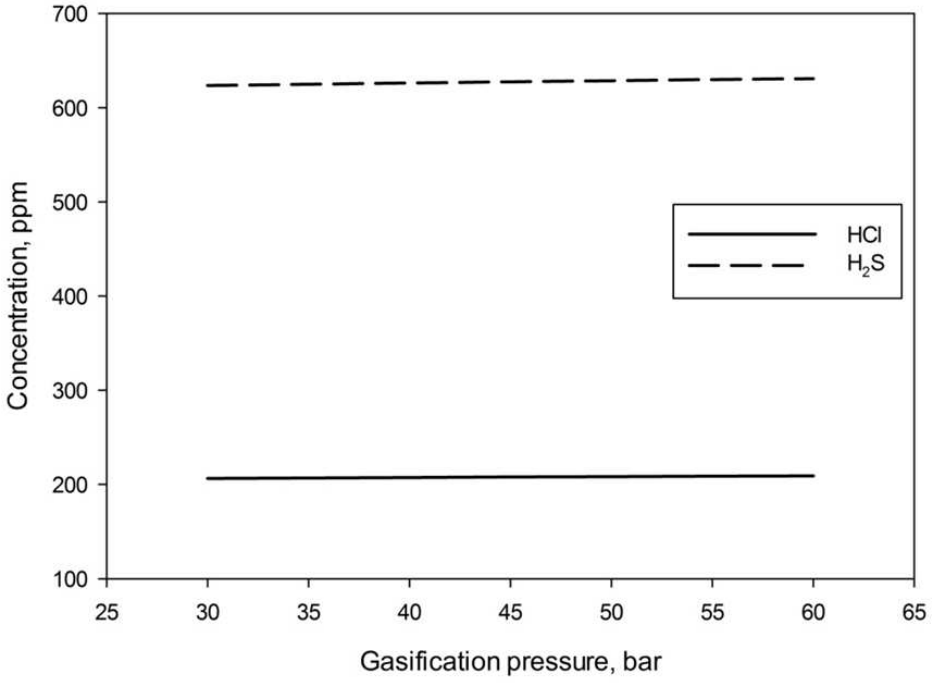

FIGURE 6.13: Pressure effect on HCl and H_2S concentration

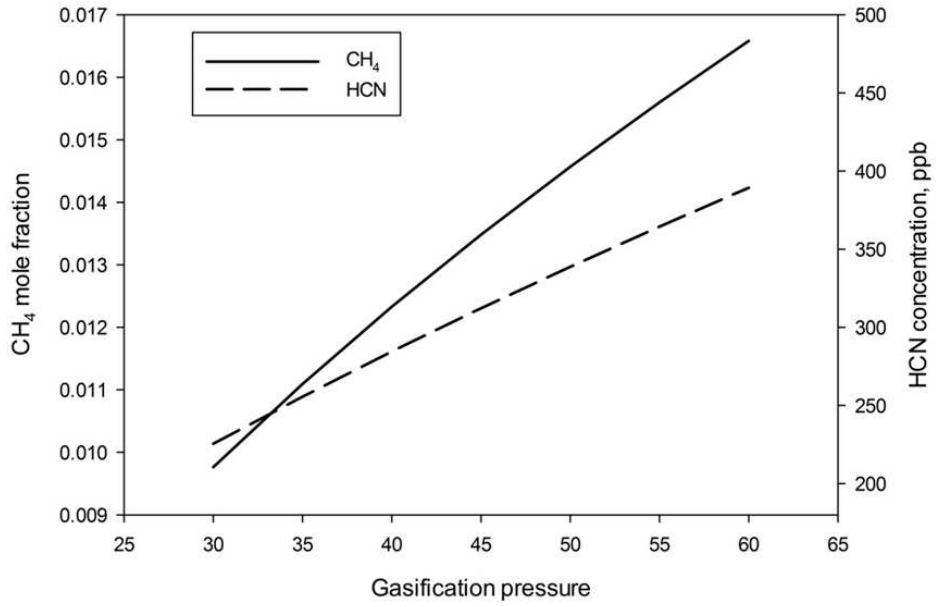

FIGURE 6.14: Pressure effect on CH_4 and HCN concentration

TABLE 6.3: Syngas composition at 900 °C and 30 bar

Gas species	Mole fraction	Gas species	PPM
H_2O	0.319	H_2S	622
H_2	0.296	NH_3	38
CO	0.209	COS	19
CO_2	0.165	HCl	206
CH_4	0.008	HCN	229

reactor a plug-flow reactor with LHHW kinetic model was used [18]. The combination of POR at 900 °C and WGS can only save 5-10% steam compared to ATR at the same temperature. It can be explained from the fact that the carbon-to-hydrogen ratio is lower for brown coal compared to black coal and hence the ideal syngas composition for DME can be easily obtained for brown coal. On the other hand, black coal would require additional hydrogen-rich feedstock (i.e. natural gas) because of high carbon-to-hydrogen ratio [11]. This is a definite positive aspect for brown coal compared to black coal as a DME synthesis feedstock.

Composition of the gasifier outlet (900 °C , 30 bar) gas is shown in Table 6.3.

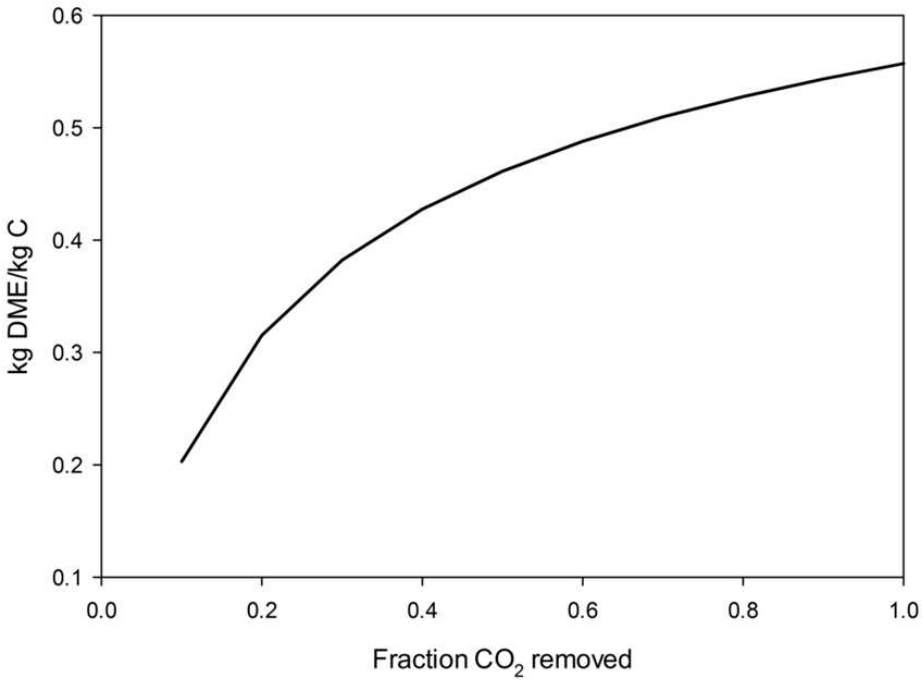

FIGURE 6.15: Effect of CO_2 removal on DME productivity

6.3.3.3 DME synthesis

Effect of CO_2 removal from the syngas before feeding to the DME reactor is shown in Figure 6.15. It is clear that reduced CO_2 concentration in the syngas greatly improves the DME yield. It was reported that CO_2 might compete for both the hydrogenation and acidic sites of a bi-functional catalyst [19]. Therefore CO_2 can decrease methanol dehydration rate and destroy the synergy of the reactive system. Figure 6.15 shows that complete CO_2 removal from syngas can increase the DME yield three-folds. However separation of CO_2 at this stage would increase the capital investment as well as the operating cost. Therefore economies of CO_2 removal prior to DME synthesis are needed to be evaluated. Meanwhile, CO_2 separation at this stage can also benefit from carbon capture and storage (CCS) viewpoint. For this current study, all simulations discussed from this point on were carried out assuming that CO_2 was completely removed from the syngas prior to feeding to the DME reactor.

DME yield is a strong function of H_2 and CO ratio in the reactor feed gas. Since the steam feed rate in the gasifier controls the H_2:CO ratio, influence of steam feed rate on final DME production rate was also evaluated; the results are shown in Figure 6.16. From this figure it can be concluded that DME yield increases with increasing steam feed rate and reaches a maximum for the steam to carbon ratio of approximately 1.1

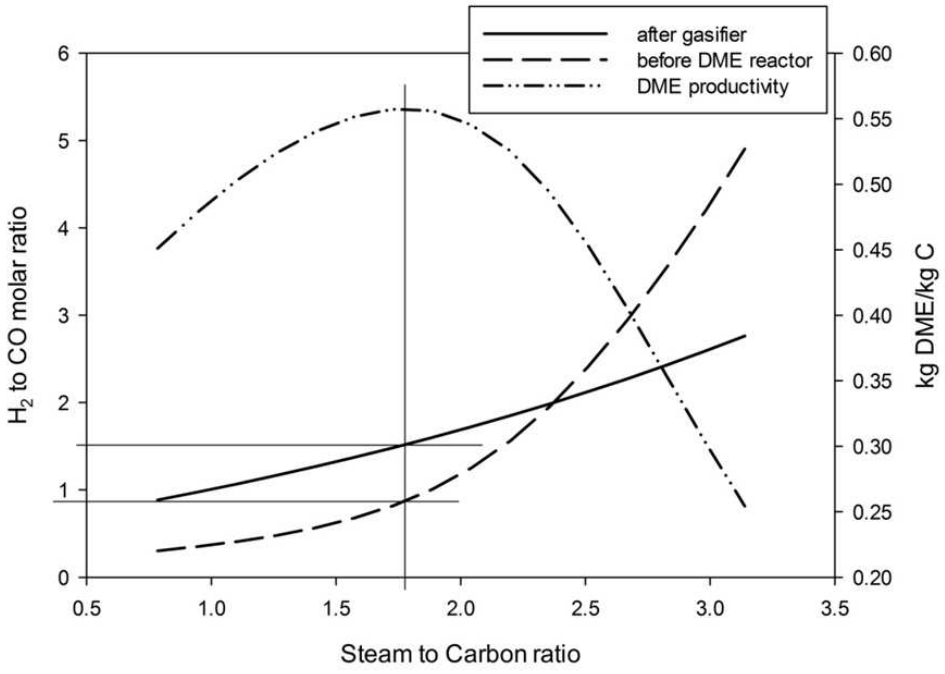

FIGURE 6.16: Effect of steam feed in the gasifier to H_2 to CO molar ratio and DME productivity at 30 bar pressure

(kmol/kmol). Further addition of the steam, though increases H_2:CO ratio in syngas, destroys the synergy effect by mis-balancing the feed ratio for DME synthesis. At the optimum level H_2 to CO molar ratio at the gasifier outlet and DME reactor inlet was 1.41 and 0.81, respectively.

Kinetic parameters for bi-functional catalyst prepared by physical mixing of commercial methanol synthesis catalyst and γ-Al_2O_3 in 1:1 ratio [14, 15] were used for this current study. Changes in either CO hydrogenation or methanol dehydration functionally of this catalyst can significantly affect the final product. Effect of changes in pre-exponential factors of LHHW kinetic model for both CO-hydrogenation and methanol dehydration (k_{CO} and k_{DME} respectively) are shown in Figure 6.17. For this purpose, CO conversion per single pass and DME yield is defined as follows:

$$\%CO \text{ conversion} = \frac{n_{CO,in} - n_{CO,out}}{n_{CO,in}} \times 100 \tag{6.2}$$

$$\text{DME yield} = \frac{2(n_{DME,in} - n_{DME,out})}{n_{CO,in} + n_{CH3OH,in}} \tag{6.3}$$

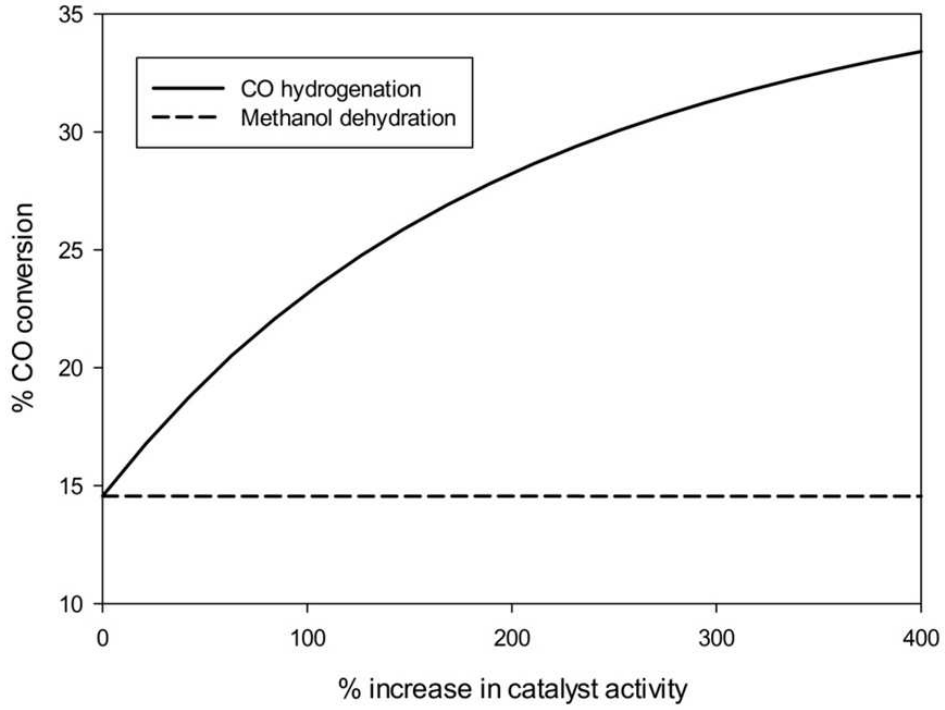

FIGURE 6.17: Influence of catalytic activity on CO conversion

From the observed results, it can be concluded that for the current process configuration methanol synthesis is the rate limiting step. Changes in k_{DME} did not effect CO conversion per single pass at all, while slight change in k_{CO} showed better CO conversion. These results also confirmed that change of composition of bi-functional catalyst is essential for better performance of the catalytic system. Though the catalyst had adequate dehydration active sites it certainly lacked CO hydrogenation sites.

Influence of the temperature on the single pass CO conversion and DME yield is shown in Figure 6.18. Though all the reactions occurring in the reactor are highly exothermic both CO conversion and DME yield was favoured with increased reaction temperature. The reactions considered here are kinetically driven and therefore showed increased rate with higher temperature.

Both the CO conversion and DME yield increased with the pressure (Figure 6.19). Under the simulation conditions, methanol synthesis (Reaction R6.1) is the rate limiting step.

Since the molar extent of this reaction is negative (-2) increased pressure favoured more methanol production and the produced methanol was readily converted to DME due to high availability of acidic sites in the catalyst surface. Combined effect of the pressure and temperature on the conversion of CO to DME is shown in Figure 6.20.

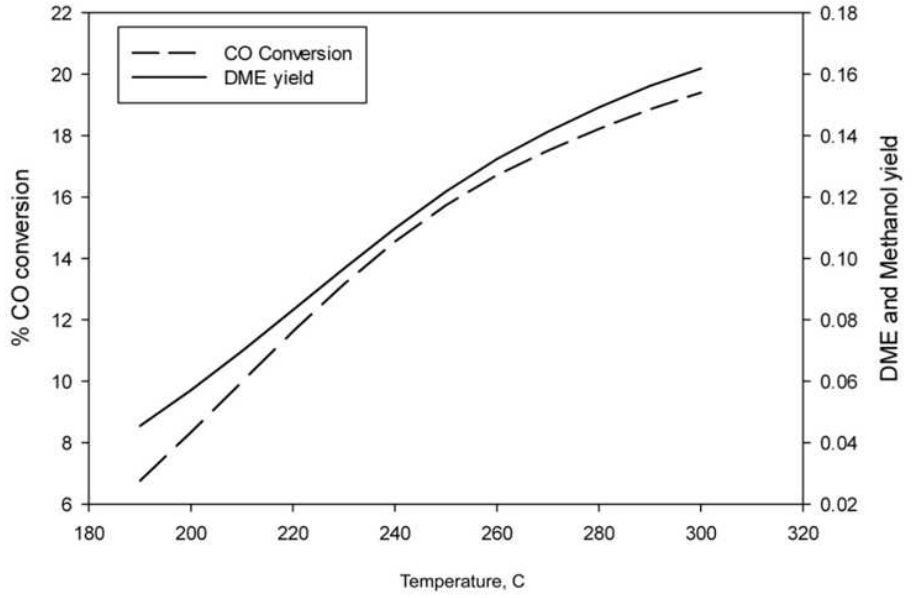

FIGURE 6.18: Influence of temperature on CO conversion and DME yield (Pressure: 60 bar; SV = 800 ml/g_{cat}.h)

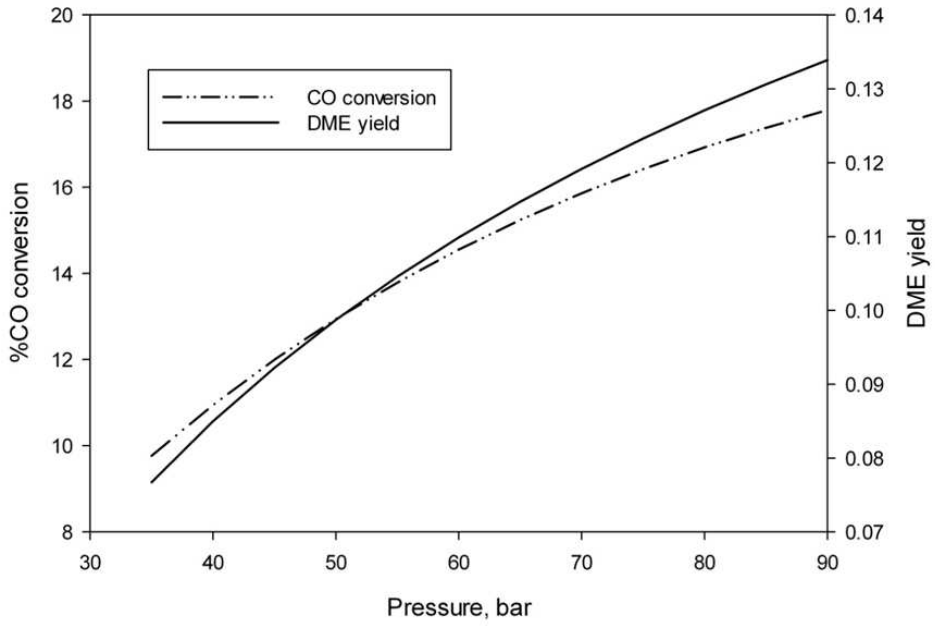

FIGURE 6.19: Influence of pressure on CO conversion (Temperature: 240 °C; SV= 800 ml/g_{cat}.h)

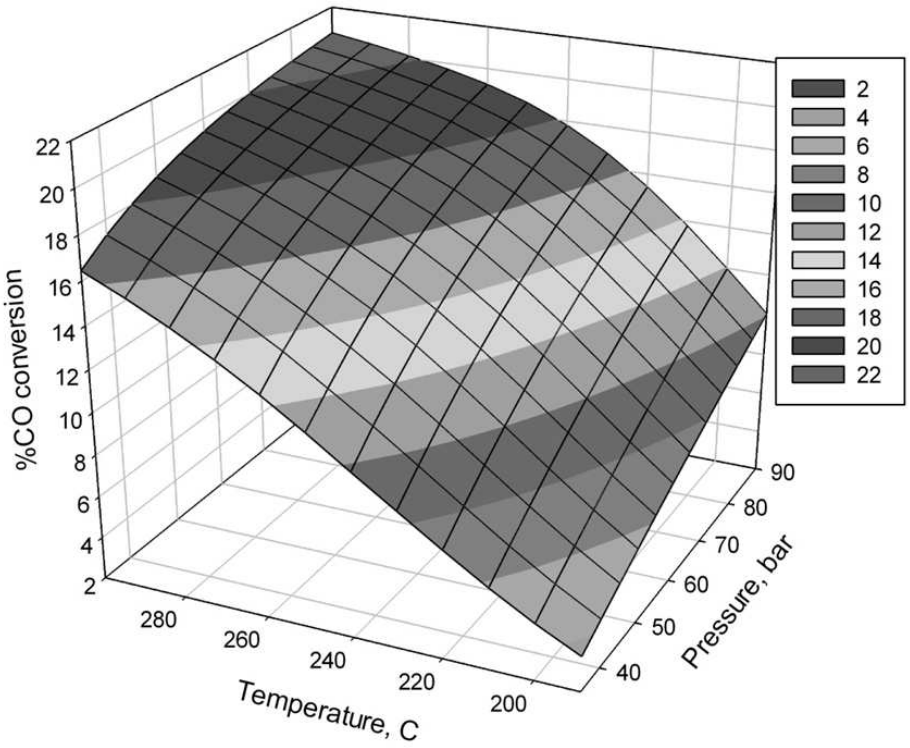

FIGURE 6.20: Combined temperature and pressure effect on CO conversion

With increase in temperature and pressure, the effect on CO conversion appear to level-off.

Effect of the syngas space velocity on the DME yield and CO conversion is shown in Figure 6.21. Increase in the space velocity leads to the decrease of CO conversion and DME yield. With higher space velocity contact time between the gas and the catalyst bed decreased which can be accounted for the lower CO conversion and DME yield. However, it must be noted that the simulated reactor here shows the performance in an ideal situation of complete removal of the generated heat during exothermic reactions. In real case, lower space velocity would result higher heat generation due to higher conversion of the reactants. Ineffective heat removal can then lead to lower DME yield due to catalyst deactivation. Therefore determination of optimum space velocity would require consideration of other factors such heat removal capacity of the cooling system.

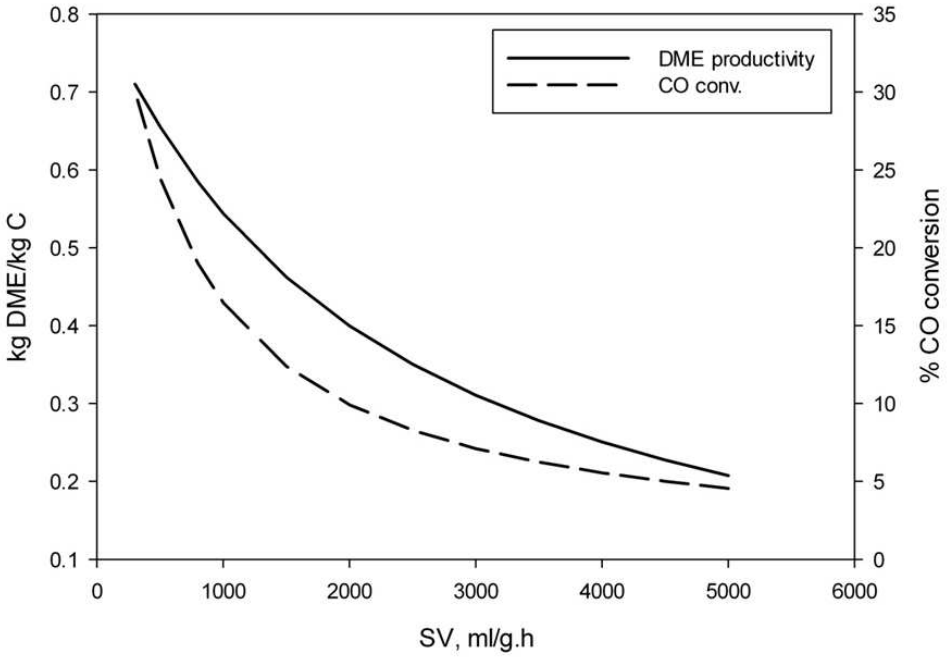

FIGURE 6.21: Effect of space velocity on CO conversion and DME yield (Pressure: 60 bar; Temperature: 240 °C

6.3.3.4 Overall process performance

The process model for producing DME from Loy Yang coal involves drying (steam fluidised bed), gasification (ATR) and DME synthesis. The process uses coal as a feedstock and steam, oxygen and cooling water as utilities and produces DME and CO_2 as well as wastewater from one of the distillation columns. Considering the base process condition (Coal drying with steam; Gasification temperature 900 °C, pressure 30 bar; DME synthesis temperature 240 °C, pressure 60 bar) the overall process efficiency is ∼32% considering the CO_2 separation energy requirement. The net CO_2 generation is 2.91 kg/ kg of DME or 0.37 tonnes/MW. Process steam requirement can be easily met from the waste heats. It must be mentioned, the calculation presented here still does not include waste heats from several location (e.g. inter-stage cooling). This efficiency is still higher than the pulverised coal combustion based power generation which is typically 28% for Victorian brown coal [20]. From the CO_2 emission view point it is far clearer than the conventional application. Moreover, since the CO_2 stream is highly pure (>90%) it can be readily sequestered and then the process can run with zero carbon emission.

However, it must be noted the process model is far from optimum in terms of catalyst as well as reaction temperature and pressure and hence there are still plenty of scope

to improve the efficiency. Design of bi-functional catalyst with higher DME selectivity (hence lower CO_2 selectivity) would be beneficial.

6.4 Conclusion

A steady state model for DME synthesis from Victorian brown coal has been developed integrating key processes drying, gasification, and the synthesis. Influence of various process parameters on the process performance has been evaluated.

Victorian brown coal is low in sulphur content. Therefore, syngas from Victorian brown coal gasification has low concentration of sulphur containing gases. On the other hand, HCN and HCl concentration in the Victorian brown coal syngas is usually known to be higher than that in other coals. It is a well known fact that cleaning of syngas is necessary to avoid poisoning of methanol synthesis catalyst. This cleaning operation imposes additional capital and operating cost. Development and use of the appropriate catalyst in gasification step can be one of the ways for minimizing the concentration of these gases. Another solution can be the design and development of a bi-functional catalyst that can handle higher concentrations of these poison gases.

It was found that CO_2 removal prior to DME reactor greatly enhance the yield. Separation at this stage would also provide high purity CO_2 and therefore will be beneficial for sequestration.

Steam drying of brown coal is beneficial than drying using nitrogen for the process. Steam can be sourced in large part ($\sim$75%) from the moisture evaporated from coal, and generated from waste heat in the process.

Proper formulation of the bi-functional catalyst is also important for better process performance. Separation of the final product from the unconverted feed gas is another area that needs proper attention. The yield of the DME was found to be a maximum for H_2 to CO molar ratio of 1.41 and 0.81 at the gasifier outlet and the DME reactor inlet, respectively. Process heat integration, and design of appropriate catalyst for gasification and DME synthesis can result in further improvements in the process.

6.4.1 Further work

Results from the process model indicate that low temperature gasification can provide appropriate syngas ratio. Therefore, low temperature gasification of Victorian brown coal will be studied to determine the conversion and product composition. Victorian brown coal is highly reactive. Low temperature gasification can be appropriate if complete conversion can be achieved. Catalytic gasification can improve conversion and reactivity at low temperature. Therefore, catalytic gasification of brown coal char will be studied to determine the reaction kinetics.

The simulation results also show that a syngas H_2 to CO ratio of 1.41 (for single pass) would maximise the DME yield. This finding will be verified using commercial catalysts.

References

[1] Babu B, 2004, Process plant simulation. Oxford University Press

[2] Lu W, Teng L, Xiao W, 2003, International Journal of Chemical Reactor Engineering, **1**: 1086

[3] Lu WZ, Teng LH, Xiao WD, 2004, Chemical Engineering Science, **59**: 5455 – 5464, iSCRE18

[4] Kumar M, Srivastava VC, 2010, Chemical Engineering & Technology, **33**: 1967–1978

[5] Lee S, Cho W, Park D, Yoon E, 2006, Korean Journal of Chemical Engineering, **23**: 522–530

[6] Shim H, Lee S, Yoo Y, Yun Y, Kim H, 2009, Korean Journal of Chemical Engineering, **26**: 641–648

[7] Chen YS, Lin JD, Lee JR, Shieu AL, Lan JJ, Wang GB, 2008, *In:* AIChE Annual Meeting, Philadelphia, PA

[8] Bin C, Hongguang J, Lin G, 2008, International Journal of Energy Research, **32**: 722–734

[9] Ju F, Chen H, Ding X, Yang H, Wang X, Zhang S, Dai Z, 2009, Biotechnology Advances, **27**: 599 – 605

[10] Zhou L, Hu S, Li Y, Zhou Q, 2008, Chemical Engineering Journal, **136**: 31 – 40

[11] Zhou L, Hu S, Chen D, Li Y, Zhu B, Jin Y, 2009, Industrial & Engineering Chemistry Research, **48**: 4101–4108

[12] Graaf G, Sijtsema P, Stamhuis E, Joosten G, 1986, Chemical Engineering Science, **41**: 2883 – 2890

[13] Bell DA, Towler BF, Fan M, 2011, Coal Gasification and Its Application. Elsevier, Amsterdam

[14] Nie ZG, Liu DH, Ying WY, Fang DY, 2003, Computers and Applied Chemistry, **20**: 662–666, [in Chinese]

[15] Nie Z, Liu H, Liu D, Ying W, Fang D, 2005, Journal of Natural Gas Chemistry, **14**: 22–28

[16] RWE, 2008, *The WTA Technology: An Advanced method for processing and drying lignites.* Website: http://www.rwe.com/web/cms/contentblob/2978/data/8735/DL-WTA-Technology.pdf, Cited: 8 June 2011

[17] Kabir KB, Hein K, Bhattacharya S, 2011, *In:* Proceedings of the 36th International Technical Conference on Clean Coal & Fuel Systems, Clearwater

[18] Hla SS, Park D, Duffy G, Edwards J, Roberts D, Ilyushechkin A, Morpeth L, Nguyen T, 2009, Chemical Engineering Journal, **146**: 148 – 154

[19] Brown DM, Bhatt BL, Hsiung TH, Lewnard JJ, Waller FJ, 1991, Catalysis Today, **8**: 279 – 304

[20] ABARE, 2010, Australian Energy Resource Assessment. Geoscience Australia and ABARE, Canberra

This page intentionally left blank

Chapter 7

Gasification of Victorian Brown Coal

7.1 Introduction

The primary objective of gasification is twofold: to convert the non-ash fraction of coal to gas and to produce gases that preserve, as much as possible, energy content of the feedstock [1]. Gasification of coal involves two essential steps: devolatilisation (or pyrolysis) of the coal followed by char gasification. As pyrolysis is a spontaneous and fast process, char gasification is the rate limiting step. Char gasification involves reaction between the fixed carbon in coal char and the gasifying agent, usually one or a mixture of oxygen, steam or carbon dioxide. The coal gasification scheme is shown in Figure 2.5.

Char gasification is heterogeneous in nature and its rate depends on various factors such as chemical processes, mass and heat transfer, impurities in the carbon, and nature of heat treatment prior to gasification [2].

Non-catalytic gasification is virtually non-existent as all carbon sources have inorganic impurities, which act as catalysts. Victorian brown coals are low in ash. The ash is composed of metallic species that catalyses gasification and combustion reactions. These make Victorian brown coals highly reactive during gasification.

Almost all existing metals catalyse the gasification reactions [3]. However, the catalytic gasification is still an emerging technology as it cannot compete with non-catalytic gasification processes. The catalytic gasification can only be competitive for a reactive coal (for example Victorian brown coal), if a cheap, active, selective and recoverable catalyst can be used.

The purpose of this study is to find out the intrinsic gasification kinetics of a Victorian brown coal char (Morwell) using a thermogravimetric analyser. The TGA studies were used to study the effect of inherently present metallic species in Morwell coal as well

Table 7.1: Analysis of Morwell coal

Proximate analysis		Ultimate analysis		Ash Analysis	
Moisture (as-mined)	60.1	Carbon	61.68	SiO_2	2.03
Fixed carbon	45.88	Hydrogen	4.69	Al_2O_3	0.97
Volatile matter	51.82	Nitrogen	1.57	Fe_2O_3	15.28
Ash	2.3	Sulphur	0.87	K_2O	0.48
		Oxygen	31.09	MgO	19.63
				Na_2O	1.26
				CaO	35.49
		Other Elements		SO_3	24.76
		Chlorine	0.1	P_2O_5	0.1

as the effect of loaded catalysts. Two catalysts were used: calcium and iron. They were selected since they are easily available and cheaper than other alternatives.

TGA studies involve slow heat treatment. They provide a basis for comparing the catalyst reactivity. However, industrial processes involve rapid heating and hence the intrinsic kinetics is not applicable in such conditions. Therefore, pyrolysis and gasification studies were also carried out using a low temperature (up to 1000 °C) entrained flow reactor. At these temperatures, an entrained flow reactor can simulate conditions similar to those in a fluidised bed.

7.2 Sample Preparation

A Victorian brown coal, from Morwell, was used for the study. The as-mined coal sample was air-dried at approximately 35 °C to remove most of the moisture. The air-dried coal was then pulverised and sieved to different size fractions. The obtained size fractions were then stored in different sample containers. The coal properties are shown in Table 7.1. The as-mined coal was high on moisture, approximately 60%, which is one of characteristic features of Victorian brown coals. The proximate and ash analyses are reported on dry basis. The ultimate analysis presented here does not include moisture or ash.

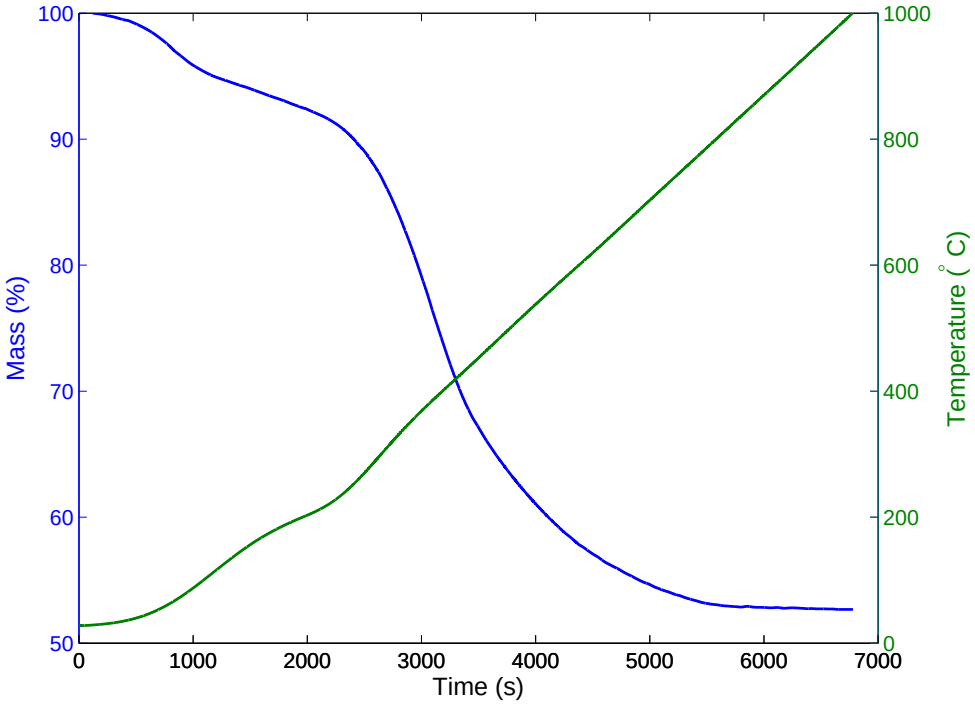

FIGURE 7.1: Mass loss curve during pyrolysis of Morwell coal

7.3 Pyrolysis in a thermogravimetric analyser (TGA)

Thermogravimetric analysis of Morwell coal samples were performed in NETZSCH STA 449 F3. Approximately 10 mg coal sample (45-53 μm) were heated up to 1000 °C in high purity N_2 for in situ char preparation. Mass loss curve during char preparation, i.e. pyrolysis, is shown in Figure 7.1.

Figure 7.1 shows both mass loss and the temperature with respect to time. Initial small change is mass was observed around 10 minutes, due to loss of moisture from the coal sample. At around 2000 s, with a corresponding temperature of ∼200 °C, the sample experienced a bigger mass loss due to start of the devolatilisation process. At the end of the devolatilisation step, the mass change curve flattened out as volatile components were completely removed from the coal sample. The observed mass loss was approximately 48-49%, which corresponds to complete removal of moisture from the sample. The residual solid, i.e. char, after the devolatilisation process is composed of the fixed carbon and ash fractions of the coal.

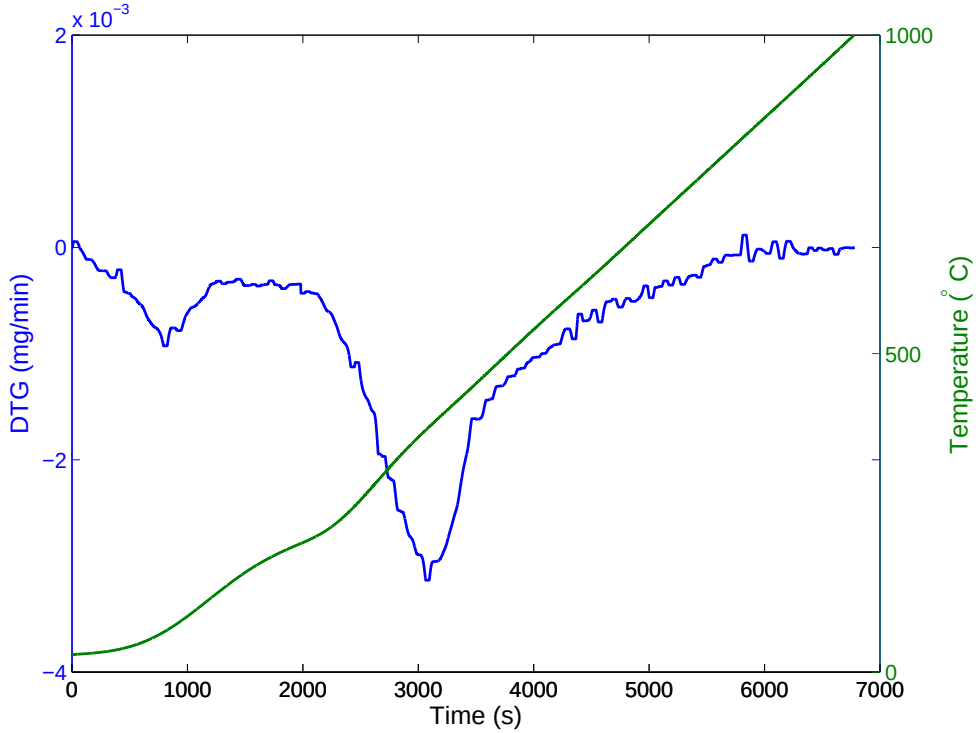

FIGURE 7.2: DTG curve during pyrolysis of Morwell coal

Differential thermogravimetric (DTG) curve for the Morwell pyrolysis is shown in Figure 7.2. This is calculated from the mass loss data using the following equation:

$$\text{DTG (mg/min)} = \frac{\Delta W}{\Delta t} \tag{7.1}$$

where W is the mass of the remaining sample at time t.

It shows two major peaks. The smaller peak at lower temperature indicates drying of coal sample. The sample used for the study was left in air before putting into the TGA. As Morwell coal is hygroscopic, the sample absorbed moisture and reached to its equilibrium moisture content, between 8-12% depending on the ambient temperature and humidity (∼9% for the sample as shown in Figure 7.1). When the sample was heated up, the moisture was removed between 80-150 °C. When the sample was heated further, volatile matters present in the coal started to evolve in gaseous form. Devolatilisation is an endothermic process and hence the rate of devolatilisation increased with temperature. The rate of devolatilisation showed its peak at 425 °C and then decreased gradually. This steady decline in rate was a result of insufficient volatile matter in the sample after this point. At around 800 °C, devolatilisation process was completed, as indicated by the DTG value returning back to 0.

The residual samples from the pyrolysis are the Morwell coal char, containing only fixed carbon and inorganic ash components. The char samples were then used for the gasification experiments. The char samples were cooled in situ in the TGA to the gasification temperatures and then gasified with 90% CO_2. The gasification results are discussed in the next section.

7.4 Gasification in a TGA

Gasification studies were carried out with CO_2 as the oxidant. The purpose of the gasification studies were to find out the CO_2 gasification reactivity of Morwell coal char. The intrinsic kinetics of CO_2 gasification was also determined from the reactivity data.

The reaction between CO_2 and char, as well as reactions of char with other oxidants (e.g. steam, O_2), is heterogeneous (gas-solid) in nature. The reaction involves three major steps [2]:

1. Bulk mass transfer: transport of reacting and product species across the viscous stagnant gas film from/to the surface of the solid
2. Mass transfer in the pores: transport of the reacting gases from the bulk surface to the active sites in pores and transport of the products from the pores to the surface
3. Chemical processes: Involves active reaction sites and includes chemisorption of the reactants, elementary reactions and desorption of products.

The gas-carbon reactions are largely dependent on the rate controlling step or steps as the reaction orders, activation energies and specific reaction rates are affected by it [2]. At lower temperatures, the reaction rate is low enough to make sure that the overall process is controlled by step 3. Hence, the reactivity data at lower temperature would provide information about intrinsic kinetics. Therefore, the gasification studies were performed at temperatures between 700-1000 °C. Also, a high concentration of CO_2 (90% CO_2 in nitrogen) with a shallow and thin-walled crucible was used for these experiments to make sure the mass transfer limitation is not present during the reaction. Larger particle size can cause diffusional problem and results in a temperature gradient across the particle cross-section. Use of small particles (usually <500 μm

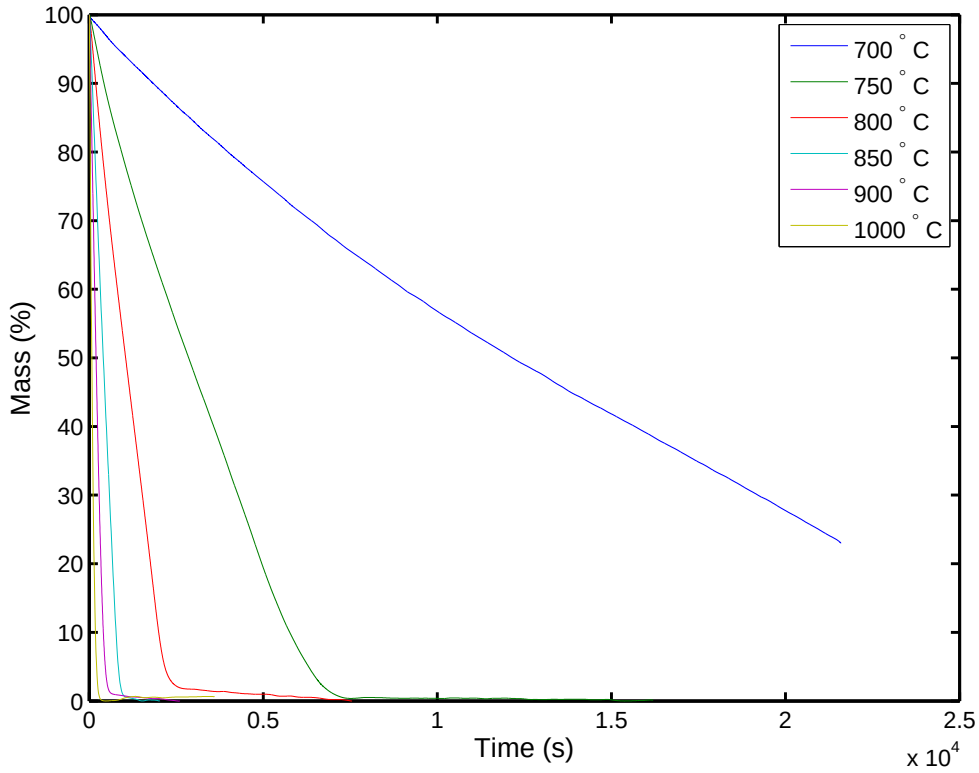

FIGURE 7.3: Mass loss during gasification of Morwell coal char

[4])are therefore more appropriate for char-CO_2 kinetic study. Kwon et al [5] showed that the char-CO_2 reactivity increased with a decrease in particle size within the range of 180-1000 μm. Here, a much smaller size of coal particles (45-53 μm) were used to prepare the char.

Changes in mass during CO_2 gasification of Morwell char are shown in Figure 7.3. The numbers plotted in Figure 7.3 were calculated on ash-free basis and only includes reactive portion of the char. Char-CO_2 reaction ($C + CO_2 \longrightarrow 2\,CO$) was very slow at lower temperatures. Gasification of Morwell char at 700 °C indicated that the complete conversion of char was not achieved, even after 21600 s (6 hours). With a 50 °C increase in temperature, complete conversion of char was achieved in approximately 2 hours. The reaction time decreased as the rate increased, as indicated by the curves shifting towards left, with increase in the gasification temperature. At 1000 °C, complete char conversion was achieved in less than 5 minutes. The changes in reaction rates from 900 °C to 1000 °C were not as significant as it was for lower temperatures. This observation suggests that the rate of reaction above 900 °C was no longer controlled by the chemical reactivity of the solid alone and the mass transfer effects gradually took control. Hence, only reactivity data up to 900 °C were used for finding the intrinsic reaction kinetics.

The general kinetic expression for char-gas reaction rate can be written as [3]:

$$\frac{dx}{dt} = k(C_g, T)f(x) \tag{7.2}$$

where x is the char conversion, t is time, k is the reaction rate and a function of temperature (T) and oxidant concentration (C_g). $f(x)$, in Equation 7.2, describes the structure factor and dependence on conversion.

Two widely used models for gas-char reactive systems are the grain model (GM) and the random pore model (RPM). The grain model [6], also known as the shrinking core model, assumes an assembly of nonporous grains. The space between the grains forms the porous network. In the chemically control regime the model considers only spherical particle as feedstock and the reaction rate expression takes the following form:

$$\frac{dx}{dt} = k_{GM}(1-x)^{2/3} \tag{7.3}$$

where, k_{GM} is the reaction rate constant.

The linear form of the GM can be obtained after separation of the variables and integration:

$$3[1-(1-x)^{1/3}] = k_{GM}t \tag{7.4}$$

The random pore model [7] considers development of pore structure during gasification. As the reaction progresses, the pore becomes larger as carbon is consumed. However, after a certain stage the pores merge resulting in a net loss of reactive surface area. Hence, a maximum for the reaction rate is observed, which is followed by a declining reaction rate. The rate expression according to RPM is:

$$\frac{dx}{dt} = k_{RPM}(1-x)\sqrt{(1-\psi\ln(1-x))} \tag{7.5}$$

The RPM model equation contains two parameters. K_{RPM} is the reaction rate constant. The second parameter, ψ, is a dimensionless structural property and given by:

$$\psi = \frac{4\pi L_0(1-\epsilon_0)}{S_0^2} \tag{7.6}$$

where, S_0 is the initial char surface area per unit volume, L_0 is the initial length of all of the pores in the particle per unit volume and ϵ_0 is the initial particle porosity. In practice, only S_0 and ϵ_0 can be measured. Therefore, ψ is used as a fitting parameter

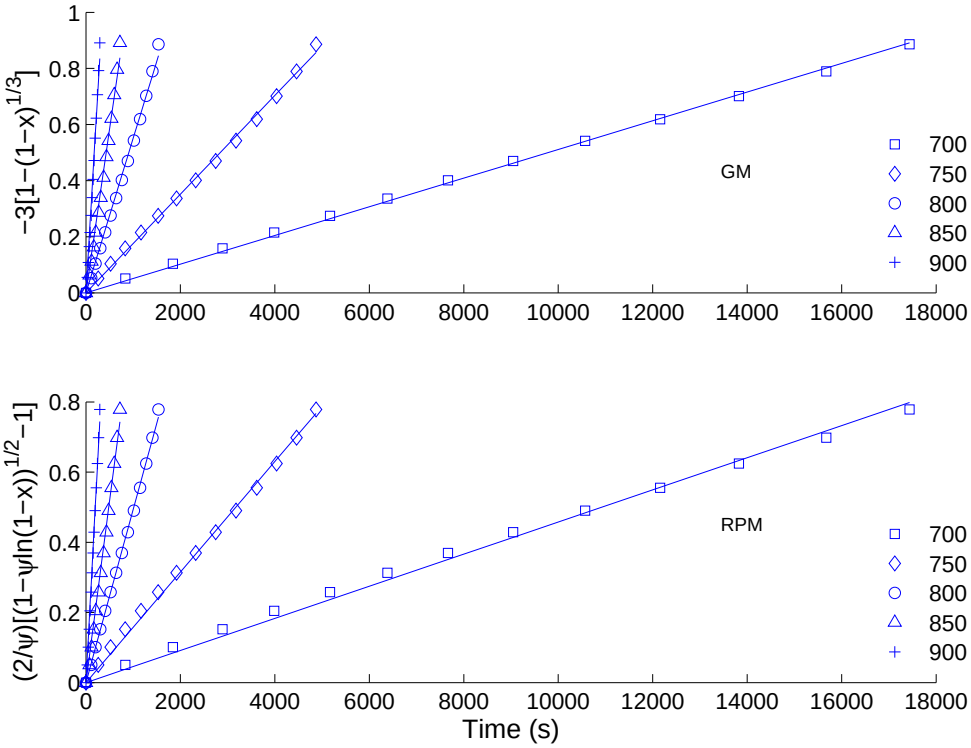

FIGURE 7.4: Plots of the grain and random pore linearised models at tempertures 700-900 °C

for the model [1]. The linearised form the RPM is:

$$(2/\psi)[\sqrt{(1-\psi\ln(1-x))}-1] = k_{RPM}t \tag{7.7}$$

By plotting the experimental results using equations 7.4 and 7.7, the reaction rate constants for grain and random pore models can be calculated. The slope of the plotted straight lines give the reaction rate constants, i.e. k_{GM} and k_{RPM}. Figure 7.4 shows the linear forms of both grain and random pore models for temperatures between 700 and 900 °C. For this study a range of conversion from 0.05 to 0.70 was used. Five values of reaction rate constants were obtained for five different temperatures.

A constant concentration of 90% CO_2 in N_2 was used for during these experiments. Since the gas concentration remained constant, the rate constants were only dependent on the temperature. This temperature dependence can be expressed using Arrhenius equation:

$$k = k_0 e^{-E_a/RT} \tag{7.8}$$

where, k_0 and E_a are the pre-exponential factor and activation energy, respectively.

TABLE 7.2: Grain and random pore model parameters for Morwell coal char

	E_a, kJ/mol	k_0, s^{-1}	ψ	R^2
Grain model	188.99	7.67×10^5	-	0.9822
Random pore model	189.05	7.23×10^5	1.32	0.9831

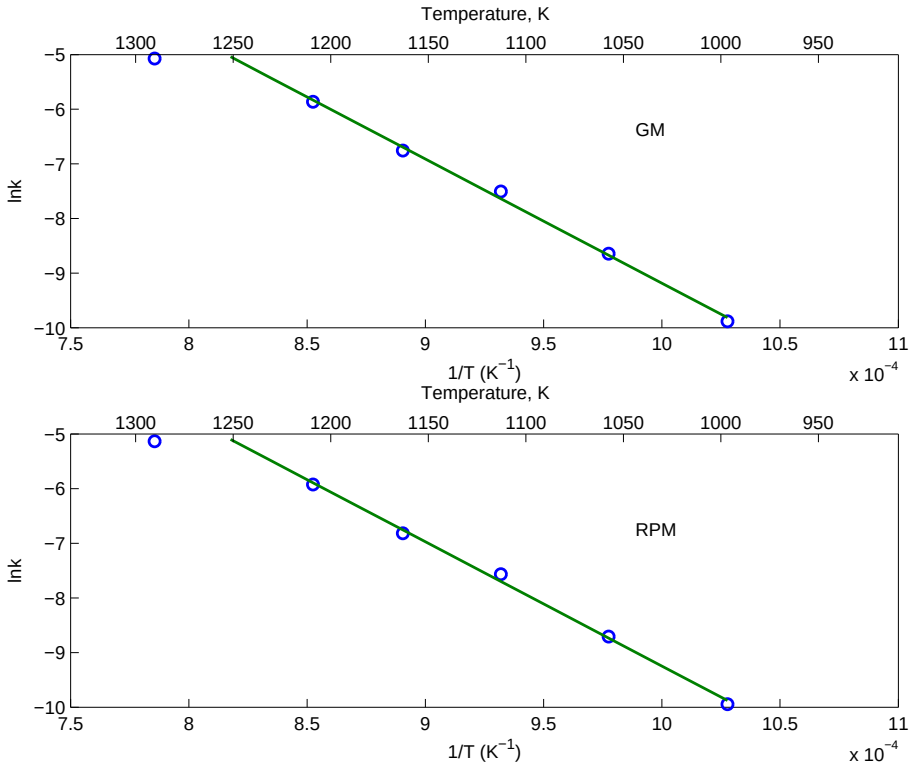

FIGURE 7.5: Arrhenius plots for grain and random pore models

Figure 7.5 shows the Arrhenius plot ($\ln k$ vs $1/T$) for both models. The kinetic parameters derived from the plots are listed in Table 7.2. For the random pore model, ψ was used as a fitting parameter, which was found to be 1.32. For both models, activation energy values are similar, but not the pre-exponential factors.

Only experimental data obtained for 700-900 °C were used for the Arrhenius plot and for the determination of the kinetic parameters. The rate constants obtained for 1000 °C was not used, but plotted in Figure 7.5, located at the top left corner for both models. This data point does not fall into the Arrhenius plot. This indicates that the gasification reaction was no longer chemically controlled. This temperature falls into zone II (or transition zone) [2]. At this temperature the reaction rate is controlled by steps 2 and 3.

To check the validity of the models, the models were used to predict the conversion

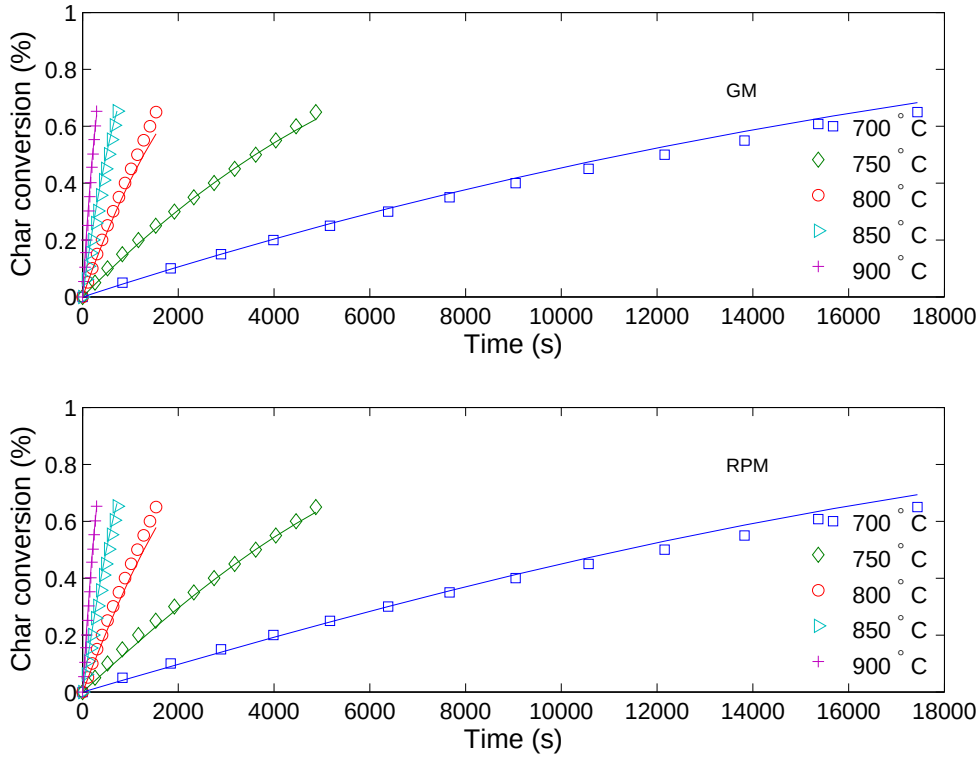

FIGURE 7.6: Comparison between the experimental and predicted conversion

and matched with the experimental conversion. A comparison of the experimental and predicted values is shown in Figure 7.6. Both models showed a good prediction of the experimental data. Both the models deviated slightly from the experimental values at higher conversions. At 700 °C, both models slightly overpredicted the conversion. At other temperatures, the models underpredicted the conversion. Coefficients of determinations, R^2, are shown in Table 7.2. Though both models gave acceptable performance, the random pore model predicts the conversion data slightly better than the grain model.

To find the effect of CO_2 concentration, gasification tests were carried out at CO_2 concentrations of 10, 30, 50, 70 and 90%. If the order of the reaction is n with respect to CO_2 concentration, the concentration dependence can be described as:

$$k = k' C_{H_2O}^n \tag{7.9}$$

Plotting equation 7.9 on log-log scale, the reaction order can be determined from the slope of the straight line. Plots for grain and random pore models are shown in Figure 7.7. The slopes of these lines are identical and found to be 0.34.

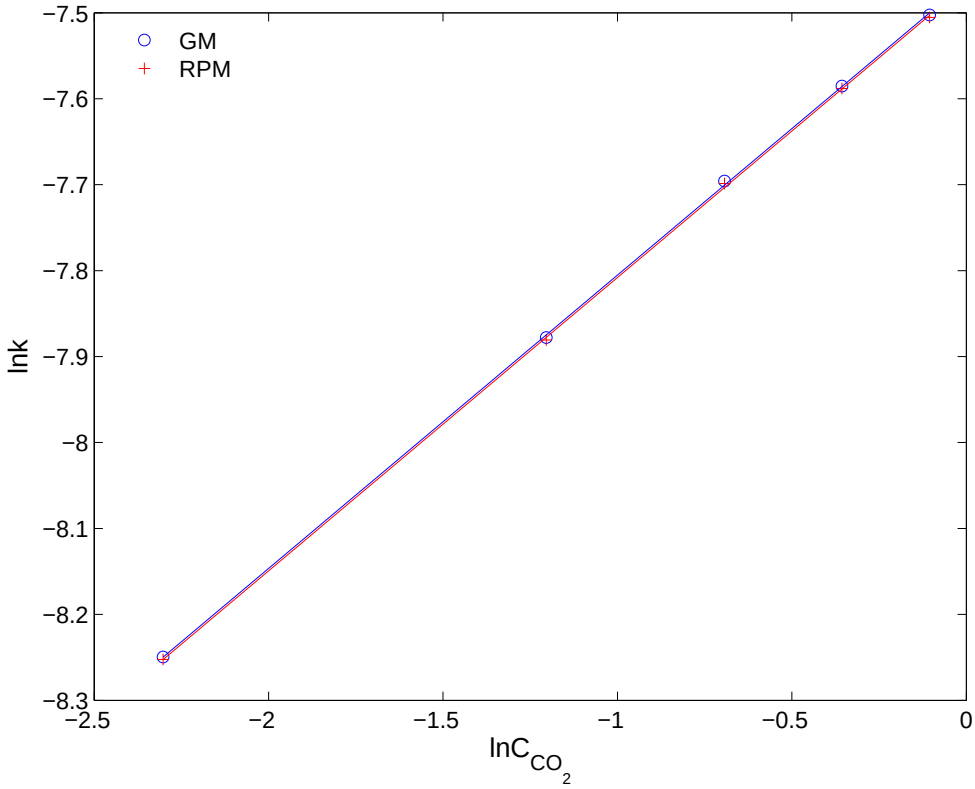

FIGURE 7.7: Dependence of reaction rate on CO_2 concentrations

There are few postulated mechanisms for carbon-CO_2 reaction [2, 8, 9]. All these mechanisms suggest that the reaction order with respect to CO_2 should be in between 0 and 1. Previous studies have suggested, the order can be anywhere within this range and varies with temperature, pressure, nature of purity of the carbon, and geometric dimension of the sample [2]. Therefore, an order of 0.34 is consistent with the previous findings. No previous literature data is available on the reaction order of CO_2 gasification of Morwell coal char.

7.5 Effect of Catalysts on Gasification

Alkaline (K, Na) and alkaline earth (Ca, Mg) metals as well as transition (Fe, Ni) metals are known to catalyse gasification of carbon with CO_2 [10]. Morwell coal has high calcium, magnesium and iron content. At the same time, it also contains sodium and potassium in a small quantity. Presence of these metal species in Morwell coal makes it one of the most reactive coals [11]. To study the effect of inherently present metals on the gasification, Morwell coal was demineralised using a three step washing method [12]. In step 1, the sample was washed with 10% NaOH solution. Step 2 and

3 involved washing the sample with 4% sulphuric and 20% nitric acid, respectively. In between each step, the sample was washed with water to remove any unused washing solvent and the product formed during washing. The sample was then dried before starting the latter step. The resultant sample was found to have 0.3% ash content.

In addition to the demineralised coal (DEM), few more catalyst loaded samples were prepared. Acid-washed coal loaded with alkaline and alkaline metals as well as iron and nickel were studied to find the effect of their individual loading [13]. Though these studies provided important information regarding the catalytic effect and kinetics, they are not applicable in practical purposes. Demineralisation of coal followed by catalyst loading is impractical as the process is tedious and requires disposal of acidic wastes. The current study focuses more on the practical side of catalytic gasification. Therefore, catalyst loading was done on the coal sample as it is.

For catalyst loading, two different methods were applied, water soaking and physical mixing. In water soaking the salt solution was used to load the sample using incipient wetness method. Physical mixing involved, mixing salt with the coal. Physical mixing has the most ease of operation. The water soaking method is also considered. It can be practically viable if the salt is mixed with water. Traditional mining of Victorian brown coals involves water spraying because of highly reactive nature of these coals.

Out of three groups of gasification catalysts, alkaline metals were not considered for the study. Salts of alkaline metals are highly volatile and retention of these species is very low as the coal temperature goes above 700 °C [14]. Calcium and iron were selected from the alkaline-earth and transition metal groups, respectively. Both calcium and iron are the relatively inexpensive and readily available in comparison to the other members of their respective groups. Nitrate salts were used for the study. For 2% extra calcium loading both water soaking (CAL2) and physical mixing (CAL2PM) were used. CAL5 sample was prepared by water soaking and contains 5% extra calcium compared to the Morwell coal. For iron loading, 2% and 5% in excess of inherent iron content, water soaking method was used (FE2, FE5).

Several gasification runs were conducted at non-isothermal (dynamic) condition. Chars were prepared at 1000 °C. The samples were then cooled in situ to 400 °C before introducing the gasifying agent, i.e. 90% CO_2 in nitrogen. The temperature was then ramped to 1100 °C at a heating rate of 10 °C/min.

The purpose of these set of experiments was to determine the temperature for initiation of the gasification (T_S). Also the temperature for maximum reactivity (T_{MAX})

TABLE 7.3: Characteristic temperatures from the DTG curves under non-isothermal condition

Sample	T_S (°C)	T_{MAX} (°C)	T_E (°C)
MW	658	888	903
DEM	723	923	938
CAL2	658	850	892
CAL2PM	658	873	900
CAL5	658	853	888
FE2	653	877	915
FE5	658	862	900

and the temperature of complete conversion (T_E) were also determined and listed in Table 7.3. DTG curves were used to find these temperatures.

From Table 7.3, it can be concluded that the addition of calcium and iron did not affect the any of the characteristic temperatures obtained from the DTG curves. The sample without any mineral, i.e. DEM, showed a 65 °C increase in temperature. The removal of alkaline-earth metal species has caused this variation, as these metals are known to reduce the gasification temperature even up to 150 °C [15]. For DEM, both T_{MAX} and T_E also shifted towards the higher end. This finding is a clear indication of the catalytic effect of the inherently present minerals in Victorian brown coal. Among the physically mixed and water soaked 2% Ca loaded samples, the water soaked sample showed slightly better performance. This resulted from better dispersion of the calcium species during the water soaking method.

To understand the effect of demineralisation and loading with calcium and iron, gasification experiments were carried out in a TGA at temperatures between 700-1000 °C, using 90% CO_2 in N_2 as the gasifying agent. Experimental data were then fitted to random pore model to find the reaction rate constant at different temperatures. The corresponding Arrhenius plots are shown in Figure 7.8. It shows that the DEM sample showed least reactivity among all these samples. 2% Fe loaded sample showed slightly better performance than the Morwell coal at lower temperatures. However, the differences in the rate constants diminished at higher temperatures. 2% Ca loaded sample showed better performance than iron loaded sample over this temperature range.

At temperatures around or above 1000 °C, CO_2 gasification of char is no longer controlled by chemical processes alone. Though rate constants at 1000 °C are shown in Figure 7.8 (circled at the top left), they were not used for the determination of kinetic parameters. It can be seen from the plot that the data points at 1000 °C are

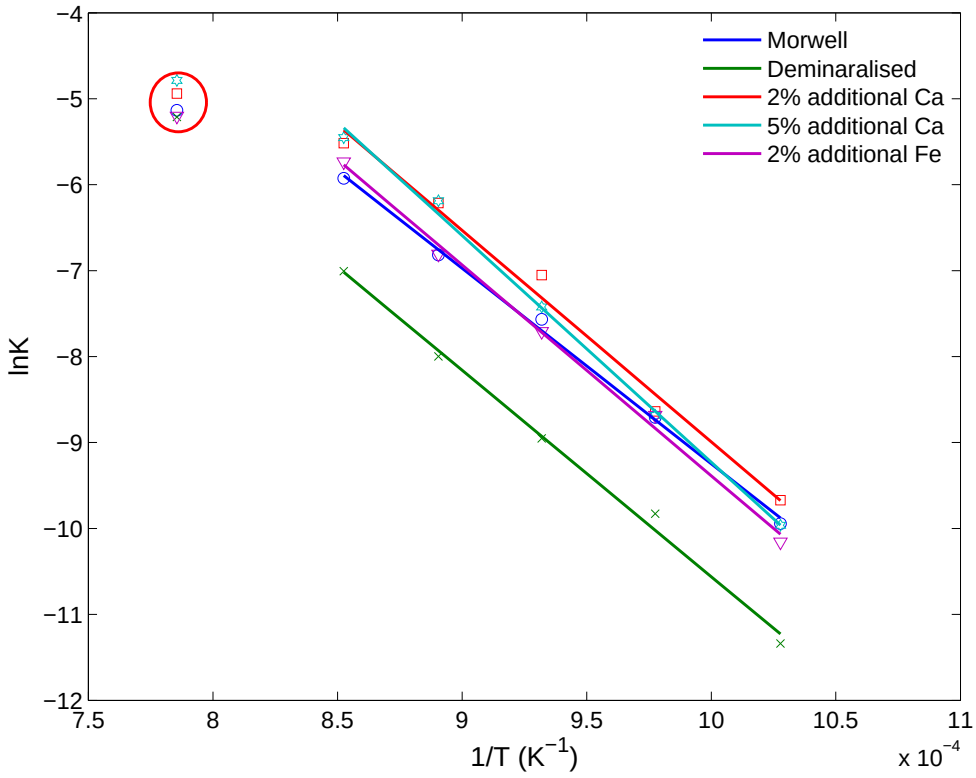

FIGURE 7.8: Arrhenius plots for demineralised and catalyst loaded samples

TABLE 7.4: Kinetic parameters for coal char gasification according to random pore model

Sample (CO_2 surface area m^2/g)	E_a	k_0	ψ
MW (190.90)	189.05	7.25 $\times 10^5$	1.32
DEM (218.25)	199.6	6.93 $\times 10^5$	10.02
CAL2 (160.31)	204.53	6.02 $\times 10^6$	0.91
CAL5 (113.25	222.28	4.38 $\times 10^7$	0.68
FE2 (173.90)	202.92	2.99 $\times 10^6$	3.3

clustered together, indicating that the rate is almost independent of surface reactions. The data points grouping together also indicate that the Arrhenius plots at higher temperature are converging and gradually approaching the isokinetic point. One major conclusion can be drawn from this finding: catalytic gasification for Morwell coal is only beneficial if the gasification temperature is maintained at or below 900 °C.

Kinetic parameters obtained from the Arrhenius plots shown in Figure 7.8 are listed in Table 7.4. It shows that the activation energy was lowest for the Morwell coal. For calcium and iron loading the activation energies were similar and slightly higher than the Morwell coal. When alkaline-earth or transition metals are loaded into coal

samples, a net decrease in surface area is observed, as some the metal atoms covers the some of the pores and make them inaccessible to the gaseous species. The CO_2 surface area determined for the samples are also shown in the first column of Table 7.4. Though surface area was lower for CAL2 and FE2 samples, the catalytic effect of Ca and Fe has increased the numbers of active sites for the reaction as indicated by the pre-exponential number. For CAL2, the increase is one order of magnitude and hence it showed better catalytic activity. DEM sample was free of inherently present minerals and therefore have larger surface area than the parent coal. Pre-exponential factor for the DEM sample also indicates that the reaction sites are less than the parent coal. So the absence of the catalytic species is the major contributing factors to the lower reactivity of this sample. For the CAL5 sample, the pre-exponential factor was higher than the CAL2 sample. However surface area was 60% of the parent coal which has resulted a decrease in specific rate constant at lower temperature. At 850 and 900 °C it was similar to that of CAL2. The activation energy was 222.28 kJ/mol for this sample.

Though Morwell parent coal is already rich in calcium, addition of 2% calcium and 5% calcium in the coal improved the gasification reactivity. However, with 5% loading there was no improvement on the reactivity compared to 2% loading.

Upon heating nitrate salt of calcium decomposes to calcium oxide, giving up two moles of NO_2 and half mole of O_2. The decomposition begins at 500 °C [16].

$$Ca(NO_3)_2 \longrightarrow CaO + 2NO_2 + 1/2O_2 \tag{R7.1}$$

CaO formed from calcium nitrate is amorphous in nature [17] and therefore ensures fine dispersion of calcium throughout the coal sample.

During pyrolysis of CAL2 and CAL5, added nitrate salt decomposed giving calcium oxide. When CO_2 was introduced into the system, calcium oxide reacted with CO_2 forming $CaCO_3$. This carbonate then reacted with carbon to form CO and calcium oxide again. The overall mechanism can be summarised as [18]:

$$CaO + CO_2 \longrightarrow CaCO_3 \tag{R7.2}$$

$$CaCO_3 + C \longrightarrow CaO + 2\,CO \tag{R7.3}$$

giving the overall gasification reaction:

$$C + CO_2 \longrightarrow 2\,CO \qquad \text{(R7.4)}$$

Since $CaCO_3$ is one of the intermediates, it can also be used as the calcium source. However, direct decomposition of $CaCO_3$ gives CaO with slightly higher crystallite size than that of nitrate [19]. Therefore, the reactivity can be lower. Even with lower reactivity $CaCO_3$ would be a preferable option compared to $Ca(NO_3)_2$, as carbonates are widely available and relatively inexpensive.

Addition of 2% Fe did not show better reactivity. Several forms of iron are known to be inactive for C-CO_2 reaction. Both hematite and magnetite are not active catalysts for this reaction. In the current experimental conditions (e.g. 90% CO_2, oxidising environment), any other forms of iron (Fe and wustite) get oxidised by CO_2 and hence forms inactive phases. The reaction at lower temperature required longer time and resulted complete oxidation. Therefore, at these temperatures the Fe-loaded sample showed lower reactivity than the parent coal.

It must be noted that the kinetics presented here were evaluated at low heating rate. The higher heating rate chars produced in a commercial gasifier will have different structure and reactivity.

7.6 Pyrolysis in an entrained flow reactor

An electrically heated, vertical furnace, with a tubular quartz reactor in the inside, was for used for the entrained flow pyrolysis and gasification experiments. The furnace is 2.0 m long and has six individually controlled heating zones allowing for a uniform gas temperature profile to be achieved over the full length of the furnace. Details of the furnace-quartz reactor arrangement can be found in Chapter 5.

For the pyrolysis runs, 90-106 μm coal sample was oven dried at 60 °C for over 1 hour. The feed was entrained with 0.5 L/min nitrogen as the purge gas and 4.5 L/min nitrogen as the preheated reactor gas. Pyrolysis experiments were conducted at furnace temperatures of 800, 900 and 1000 °C. The resultant char samples were stored at less than 4 °C to retard surface oxidation prior to further analysis and gasification experiments. The gas evolved from the pyrolysis experiments was analysed

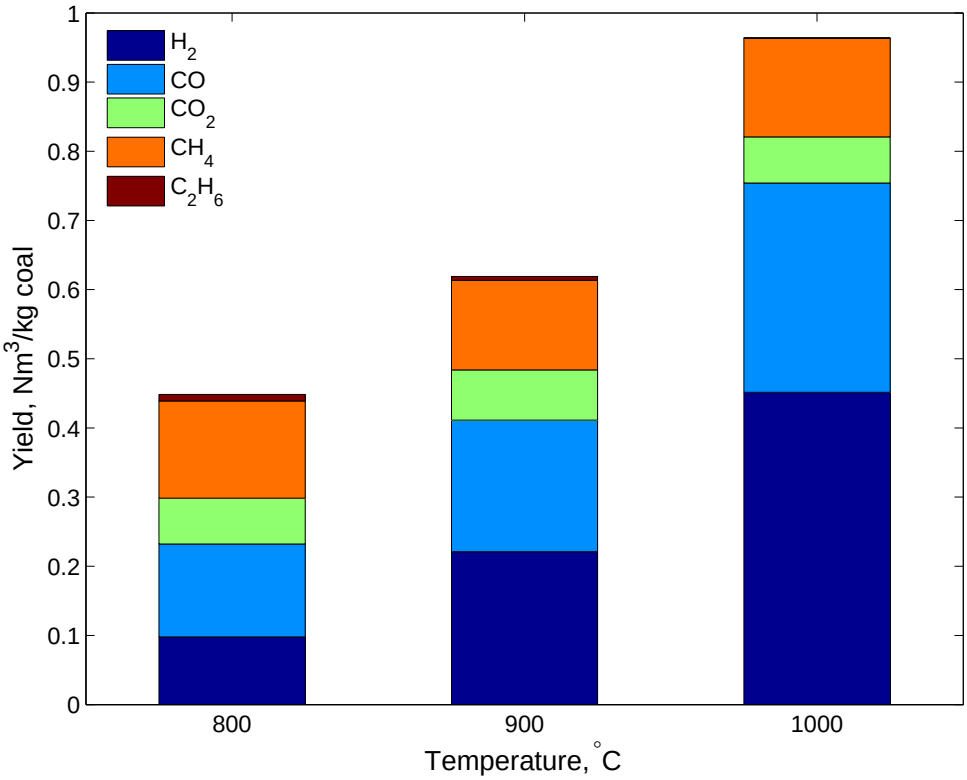

FIGURE 7.9: Components and total syngas yields from pyrolysis of Morwell coal

online using a Varian 490-GC Micro-GC equipped with Molsieve-5A and PoraPlot Q columns and a thermal conductivity detector. N_2 was used as the internal standard for calculating the gas yield. Tar analysis was performed using a Perkin Elmer Clarus 600 Gas Chromatograph coupled with a Clarus 600S Mass Spectrometer (GC-MS).

The gas yield by components for the coal pyrolysis experiments are presented in Figure 7.9. As a proportion of the total evolved gases for pyrolysis at a given temperature, hydrogen increased from 20 vol% at 1073 K to almost 50 vol% at 1000 °C while the proportion of CO remained constant at approximately 30 vol%. The proportion of CH_4 decreased from approximately 30 vol% to less than 15 vol% at 1000 °C. The CO_2 and C_2H_6 also decreased with increasing temperature.

As expected, higher pyrolysis temperatures resulted in an increase in total gas evolved from the coal samples. Part of this increase in gas yield can also be attributed to the thermal decomposition of heavier hydrocarbons in the evolved tar.

Compositions of the char samples collected after the pyrolysis are shown in Table 7.5. Pyrolysis of coal was able to convert approximately 50-53% of the solid into liquid and gaseous products. The pyrolysis conversion was slightly higher than the total volatile content of the coal. This indicates in situ gasification of the char samples in a

small extent. As the char particles are entrained in the gas containing CO_2, which is a pyrolysis product, the Boudouard reaction takes place in a smaller extent. As the rate of Boudouard reaction increases with temperature, the CO_2 concentration also slightly decreases with increasing temperature.

Table 7.5: Composition of the char samples

Temperature (°C)	800	900	1000
C (% d.a.f.)	86.06	86	92.18
H (% d.a.f.)	2.75	1.89	0.85
N (% d.a.f.)	1.64	0.95	0.21
S (% d.a.f.)	0.46	0.2	0
O (by difference)	9.09	10.96	6.76
Ash (% d.b.)	4.31	4.08	4.4
Converion(%)	52.67	50.00	53.64
Surface Area (m^2/g)	417.13	433.23	503.52

The char prepared from the Morwell coal contains mostly carbon with hydrogen and oxygen in small quantities. The surface morphology of the prepared char is shown in Figure 7.10. The release of the volatiles resulted formation of cracks and pores in the coal sample. As a result, char with surface area (400-500 m^2/g) was obtained. The char was composed of mostly Group II char [20] particles (Top inset). These particles are subspherical. Some of these particles are formed by agglomeration of smaller particles. Therefore the structure is porous and results in high surface area.

Few of Group III char [20] particles were also observed (Bottom inset). Group III particles hardly undergo any conversion during pyrolysis. The surface is non-porous. These particles are not reactive and usually formed from the woody structure present in the Victorian coals. However, number of these particles are small and the particle assay is mostly composed of Group II particle, with few exceptions.

The tars evolved from pyrolysis at 800, 900 and 1000 °C were collected by washing the tar traps with dichloromethane and analysed by GC-MS. The detected compounds are presented in Table 7.6 as a ratio of the amount collected at 800 °C to that at 900 and 1000 °C.

Tar yields were calculated by difference and decreased from 0.15 g / g coal at 800 °C to 0.05 g / g coal at 1000 °C.

Pyrolysis at 800°C resulted in the generation of both aromatic and heteroaromatic of tar compounds. The relatively small number of the compounds detected in the 900

Table 7.6: Tar components from the pyrolysis of Morwell coal

Name	Formula	MW	Pyrolysis temperature		
			800 °C	900 °C	1000 °C
Aromatic compounds					
Benzene	C_6H_6	78	trace	nd	nd
Toluene	C_7H_8	92	trace	nd	nd
Phenylethyne	C_8H_6	102	1	nd	nd
Styrene	C_8H_8	104	1	nd	nd
Xylene	C_8H_{10}	106	1	nd	nd
Indene	C_9H_8	116	1	trace	nd
Naphthalene	$C_{10}H_8$	128	1	0.02	0.08
Methylnaphthalene	$C_{11}H_{10}$	142	1	nd	nd
Biphenylene	$C_{12}H_8$	152	1	0.35	0.31
Biphenyl	$C_{12}H_{10}$	154	1	trace	trace
Acenapthene	$C_{12}H_{10}$	154	1	trace	trace
Dimethylnaphthalene	$C_{12}H_{12}$	156	trace	nd	nd
Fluorene	$C_{13}H_{10}$	166	1	0.12	nd
Phenalene	$C_{13}H_{10}$	166	1	trace	trace
Diphenylmethane	$C_{13}H_{12}$	168	trace	nd	nd
Phenanthrene	$C_{14}H_{10}$	178	trace	nd	nd
Diphenylethyne	$C_{14}H_{10}$	178	1	0.37	0.21
Methylfluorene	$C_{14}H_{12}$	180	trace	trace	nd
Methylphenanthrene	$C_{15}H_{12}$	180	1	trace	trace
Methylenephenanthrene	$C_{15}H_{10}$	190	1	0.13	nd
Methylanthracene	$C_{15}H_{12}$	192	trace	nd	nd
Pyrene	$C_{16}H_{10}$	202	1	0.31	0.4
Fluranthene	$C_{16}H_{10}$	202	1	0.23	nd
Phenylnaphthalene	$C_{16}H_{12}$	204	1	trace	trace
Methylpyrene	$C_{17}H_{12}$	216	1	trace	nd
Benzofluorene	$C_{17}H_{12}$	216	1	0.08	nd
Benzofluoranthene	$C_{18}H_{10}$	226	1	nd	nd
Triphenylene	$C_{18}H_{12}$	228	trace	nd	nd
Chrysene	$C_{18}H_{12}$	228	trace	trace	nd
Naphthacene	$C_{18}H_{12}$	228	1	0.6	0.56
Dihydronaphthacene	$C_{18}H_{14}$	230	1	nd	nd
Methyl Chrysene	$C_{19}H_{14}$	242	1	trace	trace
Benzopyrene	$C_{20}H_{12}$	252	1	trace	trace
Oxygen containing species					
Phenol	C_6H_6O	94	1	nd	nd
Cresol	C_7H_8O	108	trace	nd	nd
Benzofuran	C_8H_8O	118	1	nd	nd
Methylbenzofuran	C_9H_8O	132	trace	nd	nd
Dibenzofuran	$C_{12}H_8O$	168	1	0.16	nd
Fluorenone	$C_{13}H_8O$	180	1	0.12	nd
Fluorenol	$C_{13}H_{10}O$	182	1	nd	nd
Anthracenemethanol	$C_{15}H_{12}O$	208	trace	nd	nd
Hydroxypyrene	$C_{16}H_{10}O$	218	1	trace	nd
Nitrogen containing species					
Benzonitrile	C_7H_5N	103	1	nd	nd
Indole	C_8H_7N	117	1	nd	nd
Quinoline	C_9H_7N	129	trace	trace	trace
Carbazole	$C_{12}H_9N$	167	1	trace	nd
Phenanthridine	$C_{13}H_9N$	179	trace	nd	nd
Nitropyrene	$C_{16}H_9NO_2$	247	1	nd	nd

nd: not detected

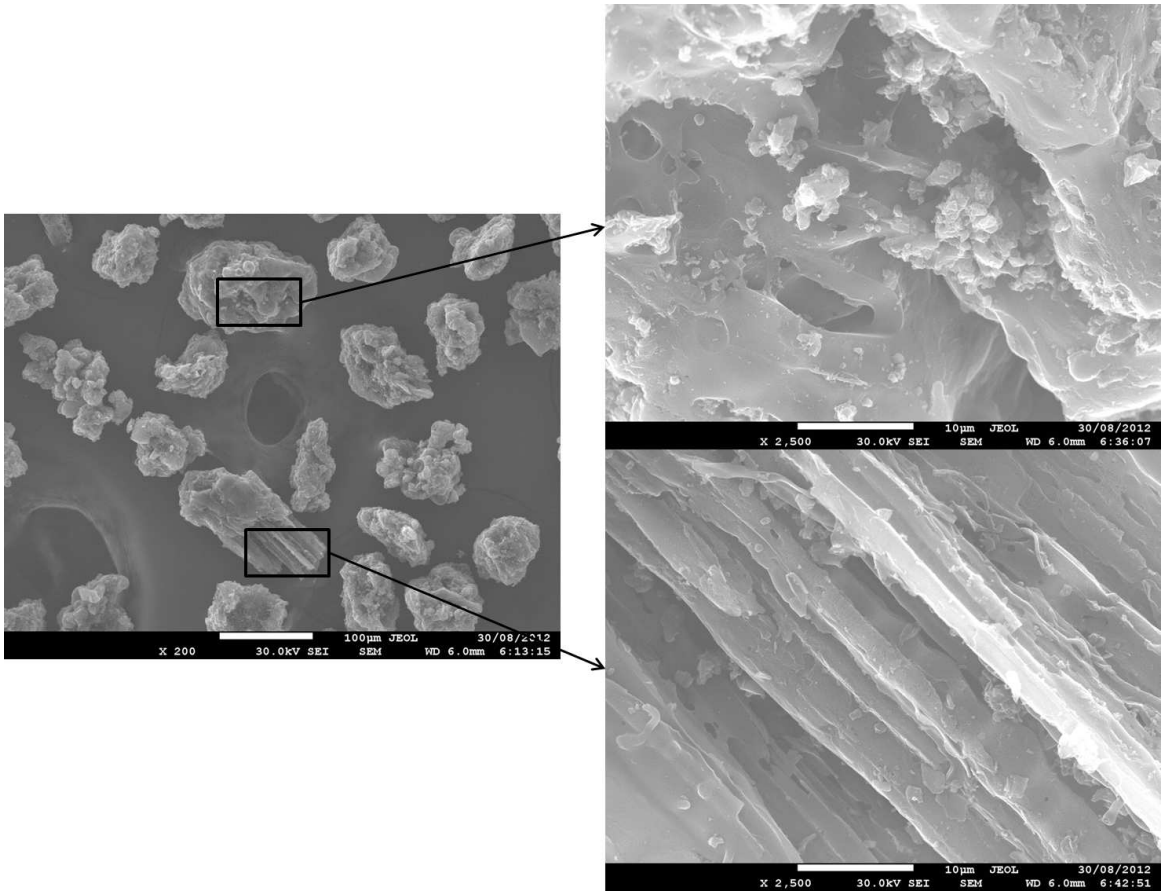

FIGURE 7.10: SEM images of the char prepared at 1000 °C

and 1000 °C tar is due to the increase in tar decomposition at higher temperatures prior to exit from the furnace. Smaller molecules (C6 to C9) underwent thermal degradation forming C1 and C2 compounds and hence were not detected at 900 and 1000 °C. A decreasing trend in the relative abundance of larger molecules was observed with increasing temperature.

The majority of the nine oxygen containing species detected in the tar collected from pyrolysis at 800 °C were phenolics, aromatic alcohols and heterocyclic compounds. Of these, only three were detected in tar collected from pyrolysis at 900 °C while no oxygen containing species were detected in the 1000 °C pyrolysis tars.

Six nitrogen containing species were detected in the tar collected from pyrolysis at 800 °C. Of these, only two were detected at 900 °C and one at 1000 °C. This decreasing trend in tar-N can be attributed to formation of gaseous species such as NH_3 and HCN. The extent of NH_3 and HCN could not be determined in the gas phase due to low sensitivity of the analysis instrument to these gases.

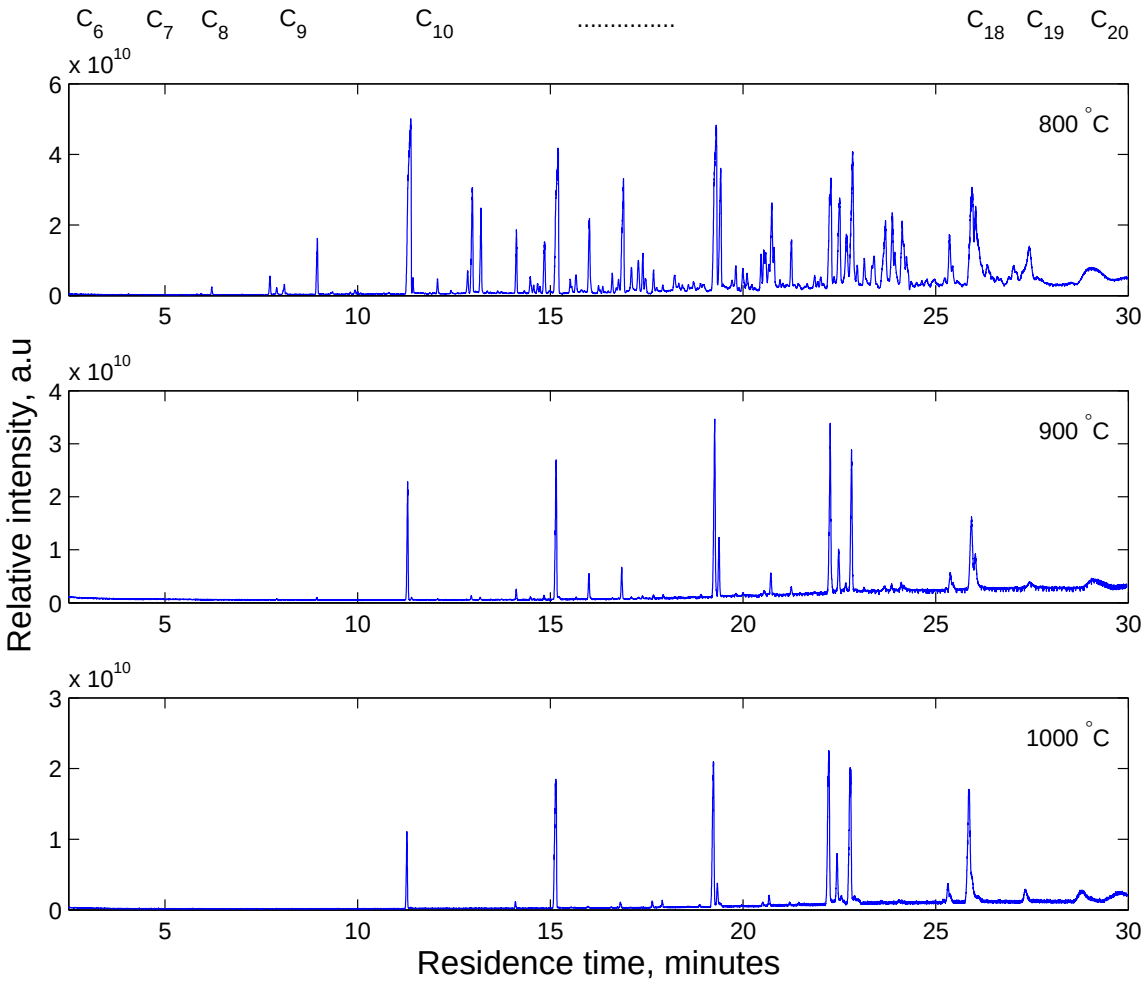

FIGURE 7.11: Mass spectroscopy of the tar samples

Two sulphur containing species were detected in trace amount for tar samples collected at 800, 900 and 1000 °C.

7.7 Entrained flow CO_2 gasification of Morwell char

5%, 10% and 20% CO_2 in N_2 were used to determine the effect of CO_2 concentration on Morwell char gasification. The results are shown in Figure 7.12. As CO2 concentration increased from 5 % to 20 % at 1000 °C, char conversion increased from 40% to 55%.

Effect of temperature on char conversion is shown in Figure 7.13. The char conversion was low at 800 °C and only 10%. At 900 °C and 1000 °C the char conversion was 21% and 55%, respectively. This indicates that temperature has a much greater influence on char-CO_2 gasification reactivity than reagent concentration over these ranges.

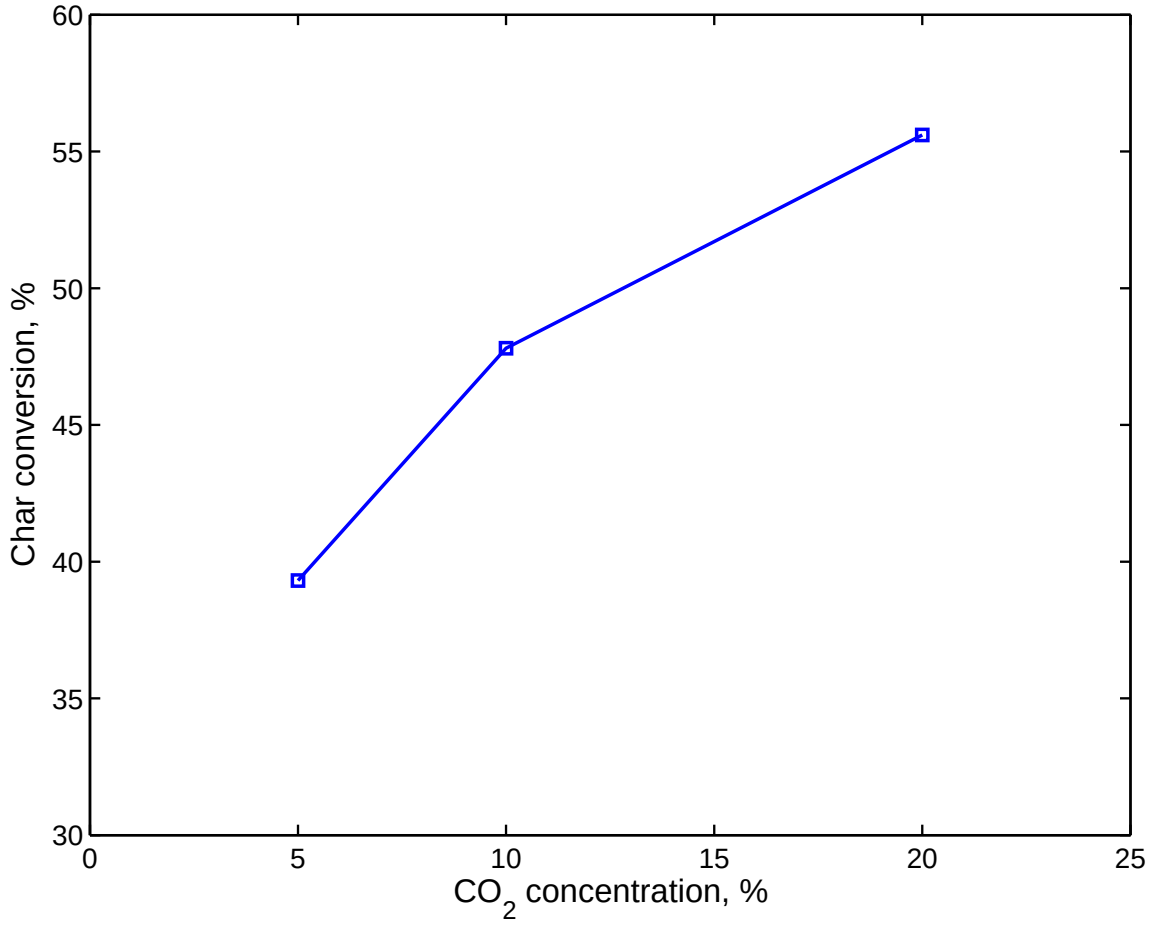

FIGURE 7.12: Variation in char conversion with reactant concentration at 1000 °C

The yield of CO and H_2 from CO_2 gasification under varying reactant concentrations at 1000 °C is shown in Figure 7.14. Both CO and H_2 yield increased with increasing CO_2 concentration. CO is a direct product Boudouard reaction and the yield increased with higher partial pressure of the reactant (e.g. CO_2) . Therefore, CO is the major gasification product. H_2 is not a direct product of the Boudouard reaction and its evolution is attributed to the liberation of residual hydrogen in the coal structure. The H_2 trend tracks that of CO evolution, but is an order of magnitude lower as no additional hydrogen is added to the system.

The gasification results are supported by the chemical analysis, presented in Table 7.7, of the char before and after gasification under various conditions. The data has been normalised for ash content, and shows that gasification under increasing CO_2 concentration at 1000 °C results in little variation in the composition of the remaining carbonaceous material. It is therefore only the conversion which appears to be affected by altering the reagent concentration. Gasification at 800 °C, 900 °C and 1000 °C under 20% CO_2 also results in similar normalised composition of the char residue,

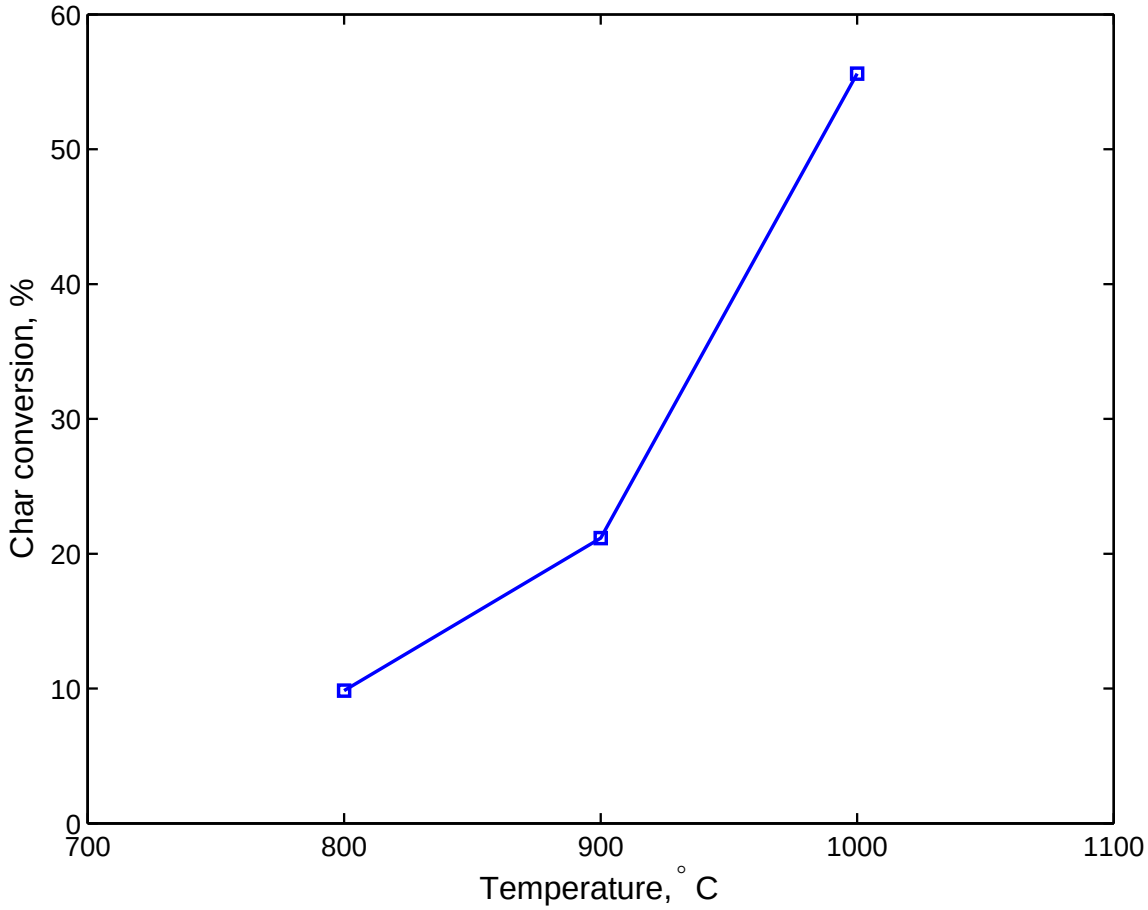

FIGURE 7.13: Variation in char conversion with temperature under 20% CO_2 gasification

indicating that the Boudouard reaction appears to proceed at increasing rates with increasing temperature, but has little impact on the remaining nitrogen and sulphur in the char.

TABLE 7.7: Composition of char gasification residues

Experimental conditions					
Atmosphere	5% CO_2/N_2	10% CO_2/N_2	20% CO_2/N_2	20% CO_2/N_2	20% CO_2/N_2
Temperature, °C	1000	1000	1000	900	800
Conversion, %	39.31	47.74	55.6	21.15	9.84
Ash (% db)	7.25	8.42	9.91	5.58	4.88
C (% daf)	88.05	91.17	88.06	90.88	91.37
H (% daf)	1.18	1.15	1.05	1.06	1.07
N (% daf)	0.93	0.9	1.04	0.8	0.78
S (% daf)	0.25	0.21	0.85	0.16	0.15
O (by difference)	9.59	6.58	9	7.1	6.62

db = dry basis; daf = dry ash free basis

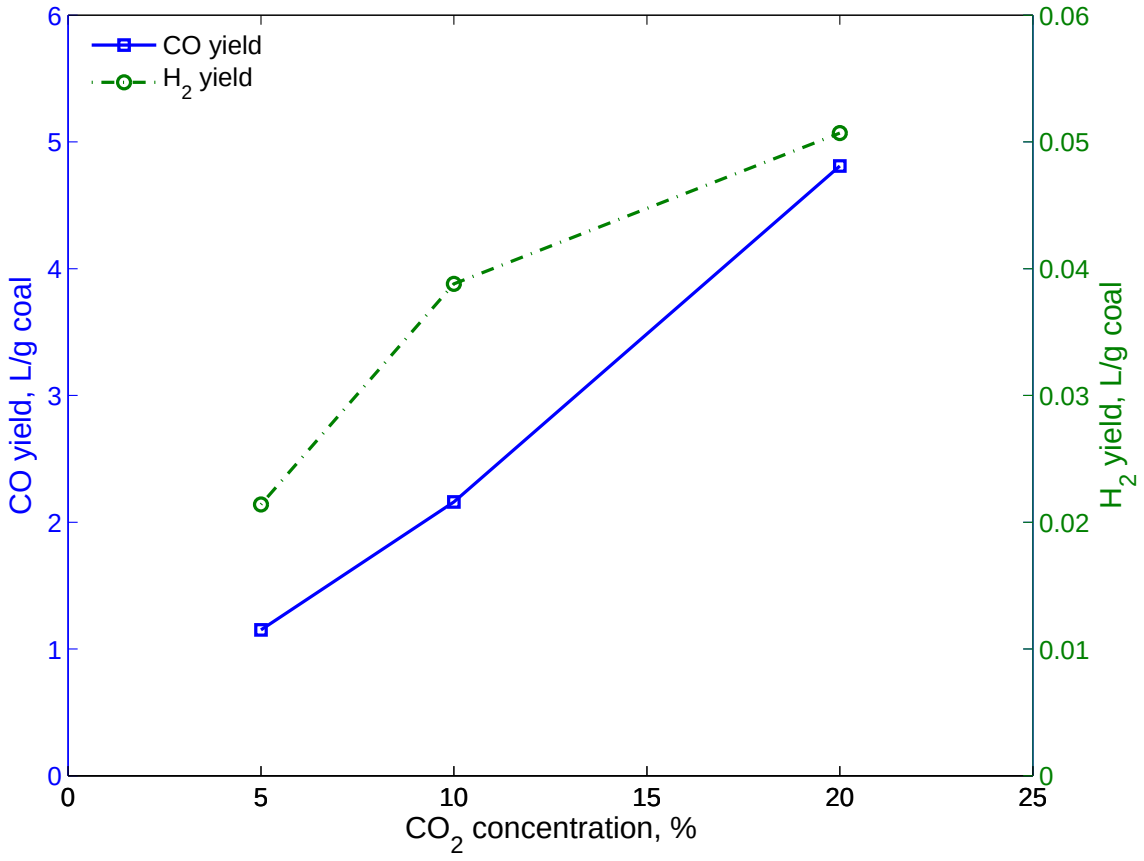

FIGURE 7.14: Variation in syngas component yield from CO_2 gasification under varying reactant concentrations at 1000 °C

Entrained flow gasifiers operate with particle sizes in the range of hundreds of microns to maximise throughput and minimise the gas flowrate required for particle entrainment . To compensate for the consequently low residence times, they therefore require higher operating temperatures, typically 1200 °C to 1600 °C, than fixed and fluidised bed technologies which operate with larger particle sizes. From the gasification experiments reported here, it is clear that the most favourable operating conditions used in this study, being 1000 °C, 20% CO_2 and a 6 s residence time, are insufficient for complete conversion of Morwell char. However, now that the potential for entrained flow gasification of Victorian brown coals has been established, this investigation will be extended to higher temperatures and longer residence time in order to establish the maximum possible char conversion and corresponding process parameters.

7.8 Conclusion

Pyrolysis and gasification of Morwell (Victorian) brown coal were studied using thermogravimetry as well as an entrained flow reactor. The entrained flow reactor was used to simulate conditions similar to those in a fluidised bed. TGA studies were focused on the determination of intrinsic kinetics of char gasification. Two well-established kinetic models, namely grain and random model, were used to determine the kinetic parameters. Both models showed acceptable performance, but the random pore model showed better performance predicting the experimental data. Activation energy for the parent Morwell coal, according to, was found to be 189.05 kJ/mol. The reaction order with respect to CO_2 concentration was found to be 0.34.

Demineralised coal char showed lower reactivity since the catalytic species were removed. At the same time the washing steps also had an adverse effect on the pore structure, as indicated by the reduction in surface area. Although, Morwell parent coal char already has high calcium, addition of 2% Ca significantly improved the gasification reactivity. However, the level-off effect was observed when the loading was increased to 5%.

From the results of the entrained flow pyrolysis and gasification, the following conclusions may be drawn:

1. Few tar compounds, which can be detrimental to the operability and efficiency of the entrained flow gasification process, are expected to be generated during entrained flow pyrolysis or gasification of Victorian brown coal above 1000 °C due to decomposition of functionalised groups to permanent gases and subsequent crosslinking of the majority of remaining hydrocarbon fragments prior to volatilisation and release

2. As gasification temperature increases, the yield of hydrocarbon contaminants in the product syngas will be reduced, increasing conversion efficiency and resulting in a cleaner syngas product requiring less conditioning prior to subsequent use

3. The most favourable reaction conditions used in the reported gasification experiments, 1000 °C, 20% CO_2 and a 6 s residence time, are insufficient for complete conversion of Morwell char.

The entrained flow gasification was performed only on the parent coal char. Further study on the loaded coal in such condition would provide a more conclusive idea whether the catalytic gasification can be applied in industrial conditions. Study on the recoverability of the catalyst is also required to find out the economics and other logistics associated with the catalytic gasification of Victorian brown coal.

References

[1] Bell DA, Towler BF, 2011, Coal Gasification and Its Application. William Andrew Publishing, Boston

[2] Walker Jr PL, Rusinko Jr F, Austin LG, 1959, *In:* Advances in catalysis, Vol. 11, 133–221, Academic Press, New York

[3] Lu GQ, Do DD, 1994, Carbon, **32**: 247–263

[4] Wen C, Dutta S, 1978, *In:* Coal Processing Technology Vol. 4, 40–51, AIChE, New York

[5] Kwon TW, Kim SD, Fung DP, 1988, Fuel, **67**: 530–535

[6] Szekely J, Evans JW, 1970, Chemical Engineering Science, **25**: 1091–1107

[7] Bhatia SK, Perlmutter DD, 1980, AIChE Journal, **26**: 379–386

[8] Reif AE, 1952, The Journal of Physical Chemistry, **56**: 785–788

[9] Gadsby J, Long FJ, Sleightholm P, Sykes KW, 1948, Proceedings of the Royal Society of London. Series A. Mathematical and Physical Sciences, **193**: 357–376

[10] Nishiyama Y, 1991, Fuel Processing Technology, **29**: 31–42

[11] Takarada T, Tamai Y, Tomita A, 1985, Fuel, **64**: 1438 – 1442

[12] Yang RT, Das SK, Tsai B, 1985, Fuel, **64**: 735–742

[13] Li CZ, 2007, Fuel, **86**: 1664–1683

[14] Li CZ, Sathe C, Kershaw J, Pang Y, 2000, Fuel, **79**: 427–438

[15] Ohtsuka Y, Asami K, 1995, Energy & Fuels, **9**: 1038–1042

[16] Laue W, Thiemann M, Scheibler E, Wiegand KW, 2002, *In:* Ullmann's Encyclopedia of Industrial Chemistry, 149–176, Wiley-VCH, Weinheim

[17] Ohtsuka Y, Tomita A, 1986, Fuel, **65**: 1653 – 1657

[18] McKee DW, 1980, Fuel, **59**: 308–314

[19] Ohtsuka Y, Tomita A, 1986, Fuel, **65**: 1653–1657

[20] Benfell KE, Liu GS, Roberts DG, Harris DJ, Lucas JA, Bailey JG, Wall TF, 2000, Proceedings of the Combustion Institute, **28**: 2233–2241

This page intentionally left blank

Chapter 8

Performance of Commercial Catalysts

8.1 Introduction

Currently, there are no commercial catalysts available for single step synthesis of DME from syngas. However, catalysts for syngas to methanol and methanol to DME are readily available. All the commercially available catalysts for methanol synthesis from syngas are copper based, and usually contain oxides of copper, zinc and aluminum. Some catalysts also contain refractory oxides (e.g. magnesium oxide) to improve their thermal stability. Methanol dehydration catalysts are usually solid acids, such as γ-alumina and zeolites.

In absence of any commercial catalyst for direct DME synthesis, bi-functional catalysts were prepared by physical mixing of two commercial catalysts. The catalysts were characterised using analytical techniques: physisorption, chemisorption, x-ray diffraction (laboratory based) and electron microscopy. The catalyst was also characterised in situ using synchrotron radiation XRD to study the phase changes during reduction and synthesis reaction. The catalyst mixtures were then used in the high pressure fixed-bed reactor to determine the conversion, product yields and selectivities. A conclusion based on the catalyst performance was drawn, to establish the optimum condition for syngas to DME synthesis.

8.2 Preparation of Bi-functional catalyst

A commercial methanol synthesis catalyst (CuO-ZnO-Al_2O_3-MgO) and a commercial methanol dehydration catalyst (γ-Al_2O_3) were used in the current study. The catalysts will be mentioned as MSC-1 and ALU-1 in this chapter. Bulk composition of the catalysts are shown in Table 8.1.

Table 8.1: Bulk composition of the methanol synthesis and methanol dehydration catalysts (wt%)

	CuO	ZnO	Al_2O_3	MgO	C
MSC-1	63.6	24.8	10.3	1.3	-
ALU-1	-	-	96.5	-	3.5

Table 8.2: Composition of physically mixed bi-functional catalysts

Sample name	MSC-1	ALU-1
M5A1	83.3%	16.7%
M3A1	75.0%	25.0%
M2A1	66.7%	33.3%
M1A1	50.0%	50.0%
M1A2	33.3%	66.7%
M1A5	16.7%	83.3%

The bi-functional catalyst for syngas to DME synthesis was prepared by physically mixing the commercial catalysts. Both catalysts were purchased in pellet forms (5.3 mm pellet for methanol synthesis catalyst and 3.2 mm pellet for methanol dehydration catalyst). The catalysts were crushed and sieved. Only particles between 20- and 40-mesh (425-850 μm) were used for the study. Bi-functional catalyst was prepared by mixing MSC-1 with ALU-1 in different proportions. Compositions of the tested catalysts are shown in Table 8.2.

8.3 Characterisation of the catalysts

The catalysts were characterised using various laboratory based techniques: TGA, chemisorption (NH_3-TPD and H_2-TPR) and electron microscopy. In addition to that, synchrotron based XRD radiation was used for in situ characterisation of the catalysts.

8.3.1 X-ray diffraction

The bulk structure of methanol synthesis and bi-functional catalysts was studied by in situ synchrotron XRD under reduction and DME synthesis conditions. The XRD patterns for bi-functional catalyst are shown in Figure 8.1. The first diffractogram for the fresh catalyst indicates presence of CuO, ZnO, and γ-alumina. The catalyst also showed the presence of a small amount of malachite as indicated by the small peaks

at lower 2θ values. In the diffraction patterns, the peaks corresponding to CuO and Cu are highlighted. At 100°C, catalyst structure was unchanged. As the temperature was increased to 250°C in flowing H_2/He, the CuO was fully reduced to CuO. The reduction of copper oxide to copper is believed to be a single step process according to the following reaction:

$$CuO + H_2 \longrightarrow Cu + H_2O \tag{R8.1}$$

At the end of the reduction, CuO or Cu_2O phases were not detected, while metallic phase of copper was observed.

At 250°C, the gas was switched from H_2-He to CO-H_2-CO_2 mixture for the rest of the experiment. The catalyst did not show any new phases during the course of the reaction. However, the copper peak intensities gradually increased with longer exposure of the catalyst to the synthesis gas at 250°C or higher temperatures.

The XRD patterns for the MSC-1 catalyst showed similar phase changes as the bi-functional catalyst at temperatures up to 300°C (Figure 8.2). A crystalline and un-strained phase was observed for the MSC-1 sample above 300°C which was found to increase at higher temperature. The observed phase has reflections at 21.9, 25.4, 36.2, 42.8, 44.7, 52.1, 58.8, 65.1 and 69.6°. It can be fit with a cubic Fm3m unit cell with a lattice constant of 3.539 Å at 300°C and = 3.546 Å at 500°C. This peak positions match with crystalline phase is metallic nickel. However, the sample did not contain any nickel as indicated by the previous diffraction patterns (dataset 1-8). These anomalous peaks are attributed to the flow cell interacting with the X-ray beam alongside the sample because of slight misalignment of the sample holder. When the residual sample from these measurements was latter tested in a lab-based XRD (Rigaku MiniFlex 600), none of the nickel diffraction peaks were observed.

Diffraction patterns for ALU-1 are shown in Figure 8.3. The catalyst is composed of amorphous γ-Al_2O_3 with small amount of carbon (Rhombohedral graphite). The XRD pattern did not show any change in the crystalline phase of the γ-Al_2O_3 during the experiment. However, crystalline graphite phase showed directional growth on plane (100) at $2\theta = 21.4°$ and plane (221) at $2\theta = 30.8°$. These peaks indicate the coke formation on the catalyst surface at higher temperatures. In fact, CO hydrogenation can occur on γ-Al_2O_3 surface, in absence of MSC-1. The CO conversion is low and the

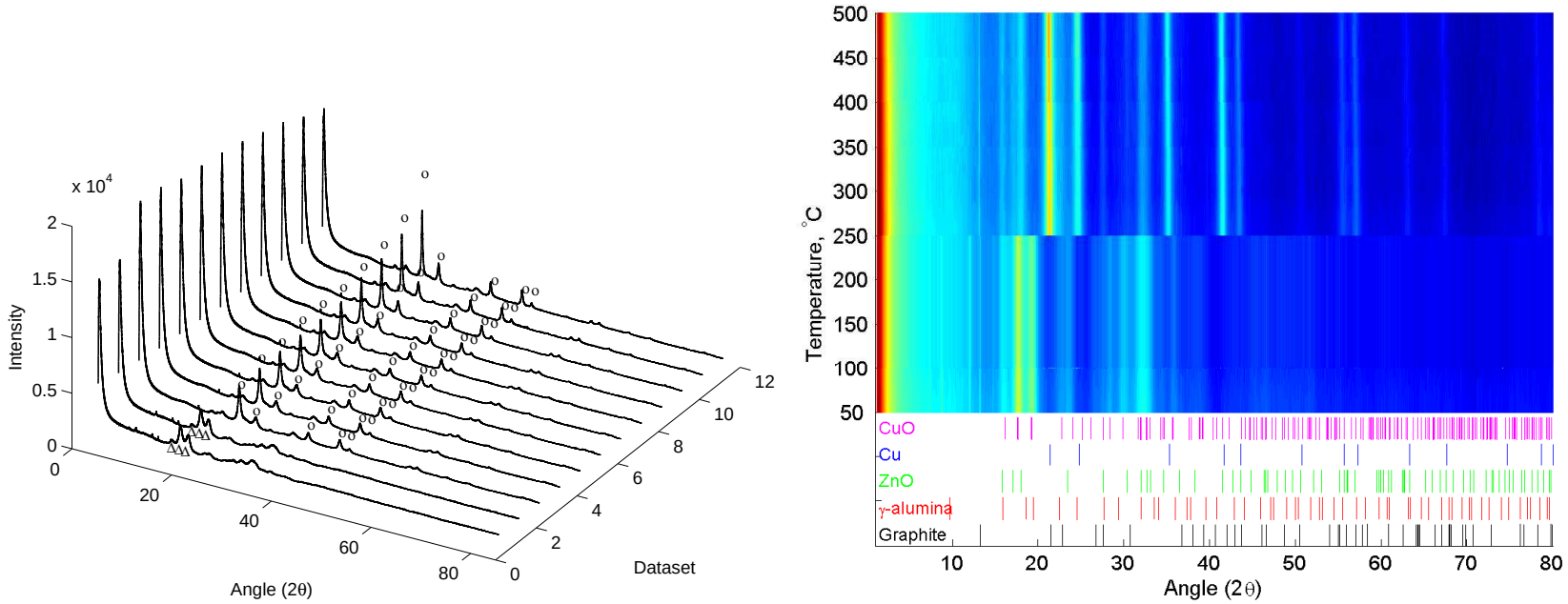

(a) (b)

FIGURE 8.1: Diffraction pattern for bi-functional catalyst. (a) 3D plot (only copper oxide and copper phases are shown; △-CuO; ○-Cu) (b) 2D projection (phase reflections are shown as tick marks at the bottom of the figure)

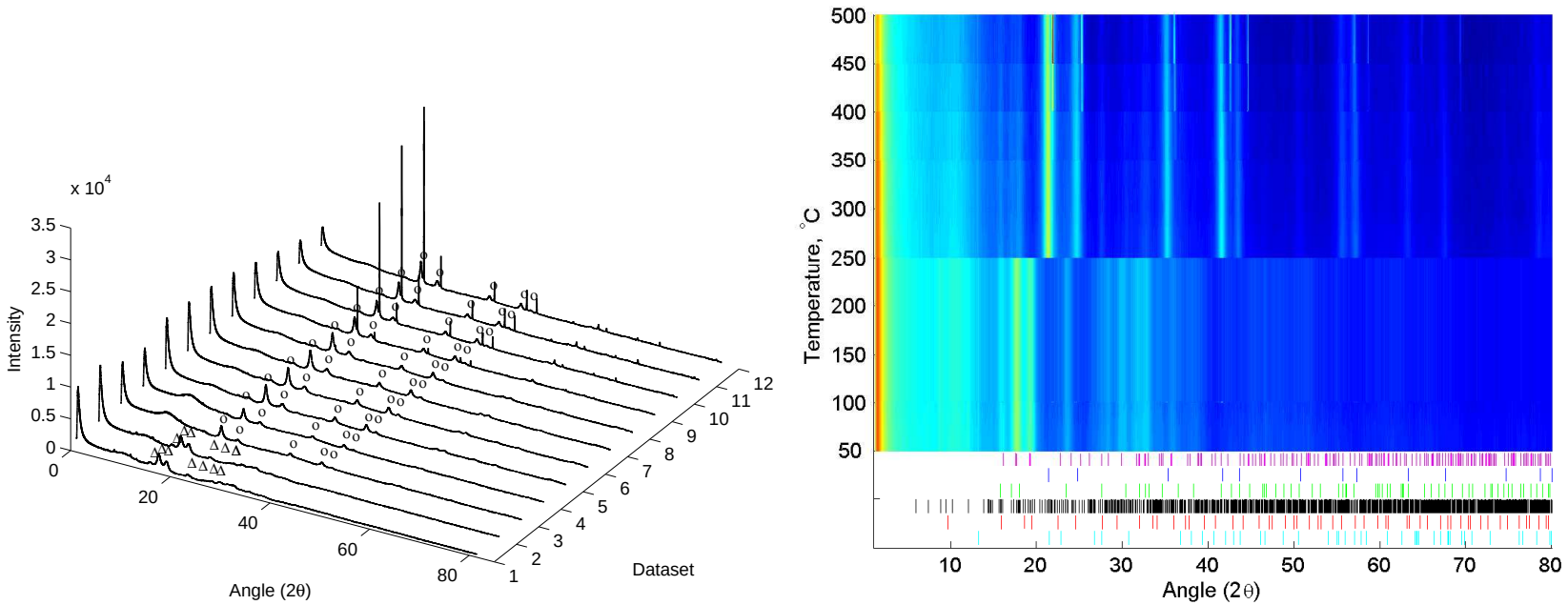

(a) (b)

FIGURE 8.2: Diffraction pattern for MSC-1. (a) 3D plot (only copper oxide and copper phases are shown; △-CuO; ○- Cu) (b) 2D projection (phase reflections are shown as tick marks at the bottom of the figure)

Table 8.3: Summary of Rietveld refinement

Temperature	MSC-1		Bi-functional catalyst	
	G	R_{exp}	G	R_{exp}
250	2.585	4.009	2.576	4.236
300	2.491	4.076	2.586	4.26
350	2.496	4.166	2.584	4.285
400	2.657	4.261	2.617	4.272
450	2.839	4.29	2.714	4.227
500	3.061	4.28	2.75	4.191

products are hydrocarbons [1]. Coke formation on the surface occurs by condensation of these hydrocarbons on the surface [2].

The XRD patterns for all three samples also showed the presence of structures below the XRD cutoff, which is usually less than 2-3 nm [3]. The presence of nano-crystallites (particles below XRD cutoff) is indicated by the first peak in each XRD, at approximately 2θÿ of 2, indicated by the red pattern in Figures 8.1, 8.2 and 8.3.

Structural parameters of the crystalline copper were obtained after Rietveld refinement of the XRD data using TOPAS [4]. The weighted profile R-factor (R_{exp}) and goodness of fit (G) for the refinement is shown in Table 8.3. Changes in the lattice parameter for MSC-1 and bi-functional catalyst are shown in Figure 8.4. The lattice parameters increased with temperature in line with the expected thermal expansion.

Copper crystallite size in (111) direction was calculated using the Scherrer equation [5]:

$$L = K\lambda / B\cos\theta \tag{8.1}$$

where B is the full width at half maximum (FWHM) of the peak profile, L is the volume average of crystal thickness in direction normal to the reflection plane, K is the constant of proportionality, θ is the angle of the reflection and λ is the wavelength.

Change in copper crystallite size as a function of temperature is shown in Figure 8.5. For both MSC-1 and bi-functional catalysts, the size of the copper crystal increased with temperature and on-stream time. Variation in the crystal size is insignificant between 250 and 300 °C. However, rapid growth in crystal size was observed above 300 °C.

The activity of a catalyst is dependent on the crystallite size of the active components [6], in this instance copper. The activity of the catalyst is inversely related to the

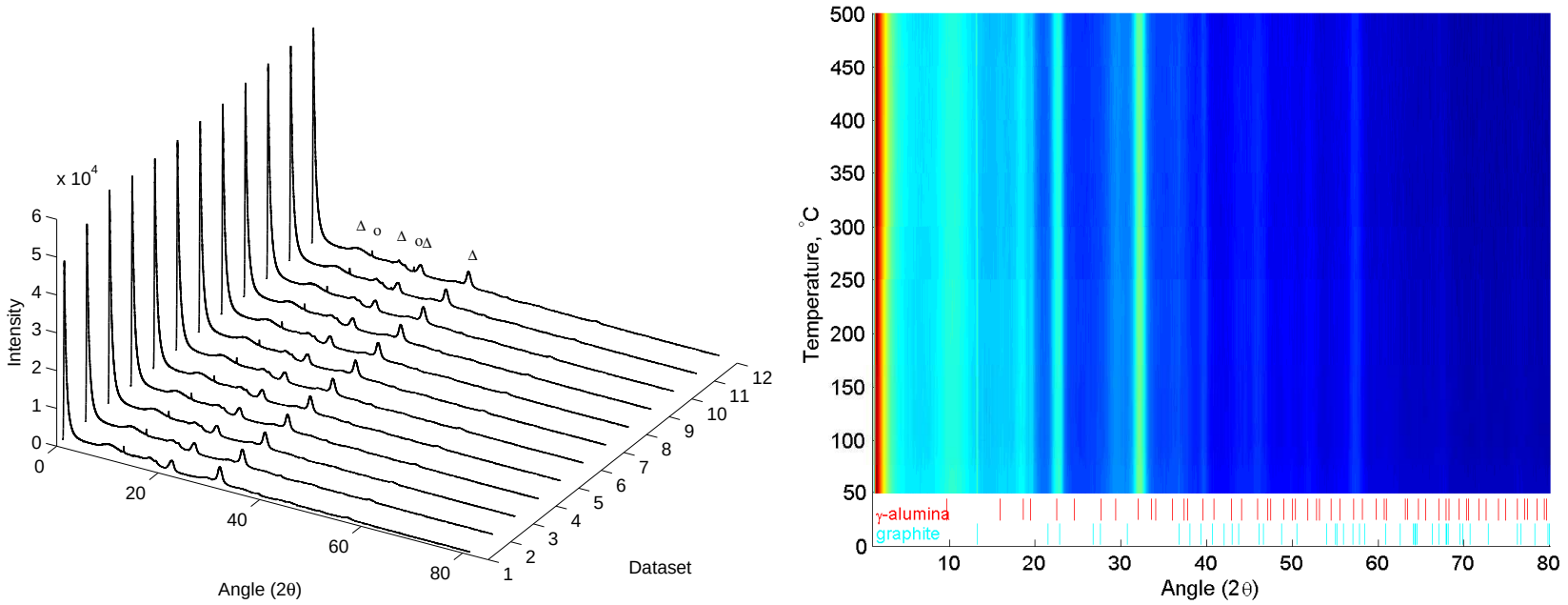

(a) (b)

FIGURE 8.3: Diffraction pattern for ALU-1. (a) 3D plot ($\triangle$-γ-Al_2O_3; $\circ$- graphite) (b) 2D projection (phase reflections are shown as tick marks at the bottom of the figure)

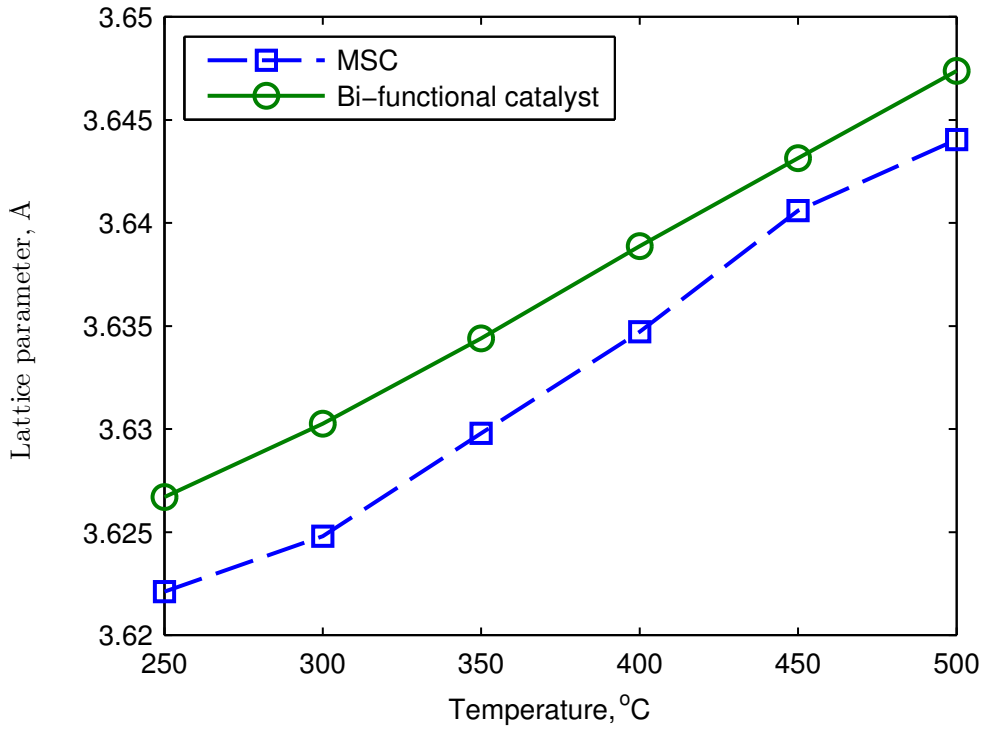

FIGURE 8.4: Lattice parameter of Cu for MSC-1 and bi-functional catalysts

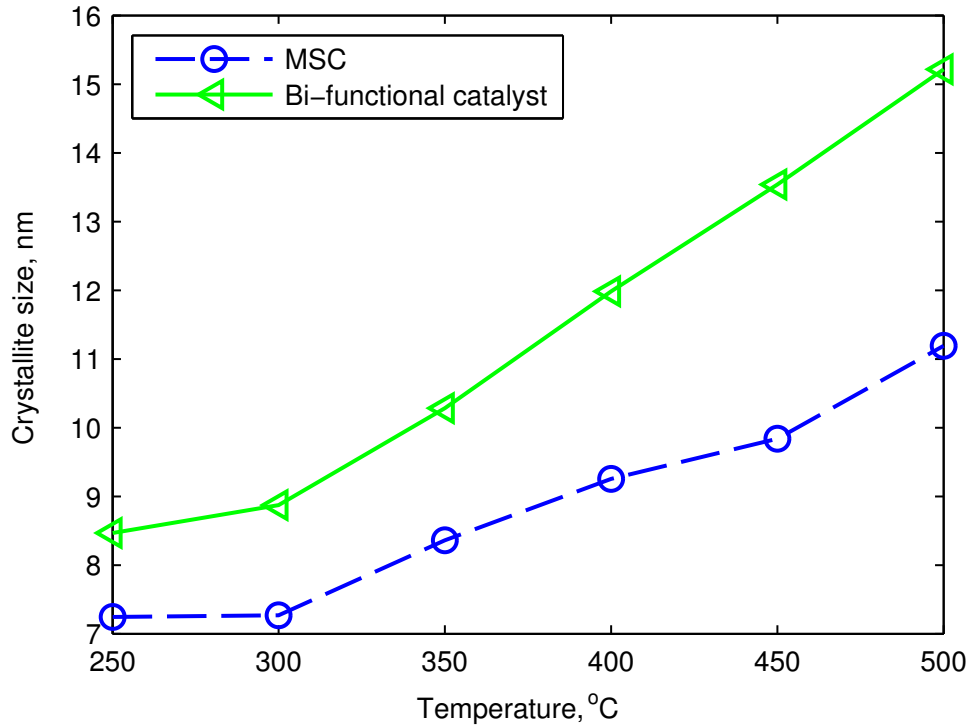

FIGURE 8.5: Variation of copper crystallite size in (111) direction with temperature

copper crystallite size. The change in the metallic Cu crystallite size as a function of temperature is shown in Figure 8.5. The results show that the crystallite size of both MSC-1 and the bi-functional catalyst on freshly reduced catalyst is 7.2 nm and 8.5 nm, respectively, at 250 °C. The introduction of syngas at 250 °C and heating up to 300 °C did not show a significant effect on the Cu-crystallite size, suggesting the stability of the catalysts in this temperature range. However, when the reaction temperature increased beyond 300 °C, the crystallite size of Cu increased rapidly and reached 11.1 nm and 14.2 nm at 500 °C for MSC-1 and bi-functional catalysts, respectively. The results suggest agglomeration of the crystallites or thermal sintering at higher temperatures. However, thermal sintering should not occur below the Tammann temperature ($\approx 0.5T_{melting} = 682.5$ K), sintering can occur above Hütting temperature ($\approx 0.33T_{melting} = 455$ K) by release of atomic or molecular species from crystallites [7]. The results also indicate that the increase in crystallite size for the bi-functional catalyst is relatively more than compared to the MSC-1 catalyst. Presence of moisture or high CO_2 in the gas phase also accelerates sintering as these gases hinder stabilisation of Cu/ZnO by the alumina phase. The crystallite sizes calculated from the XRD data clearly indicate that crystallite sizes are larger for the bi-functional catalyst. When γ-Al_2O_3 is used in conjunction with MSC-1 for syngas to DME synthesis, the dehydration and water gas shift reaction produces H_2O and CO_2 respectively. Therefore, the deactivation process of the bi-functional catalyst is faster than that of the MSC-1.

8.3.2 Thermogravimetric analysis

Thermogravimetric analysis was performed on the bi-functional catalyst under the same conditions as the in situ XRD studies (Figure 8.6). The catalyst was heated from room temperature in a 5% H_2 in He environment. The sample is heated to 100 °C and held at 100 °C for 30 minutes. At this temperature, the sample lost approximately 2% mass due to moisture loss. After this holding period, the sample was heated again to 250 °C. The catalyst exhibited a sudden drop in mass from 180 °C due to the reduction of the copper oxide phase to Cu by H_2 present in the reducing gas. The reduction was completed before 250 °C beyond which there was no significant change in the mass of the sample. The TGA results complements well with XRD results, where diffraction patterns show the formation of metallic Cu peaks at 250 °C and disappearance of CuO peaks.

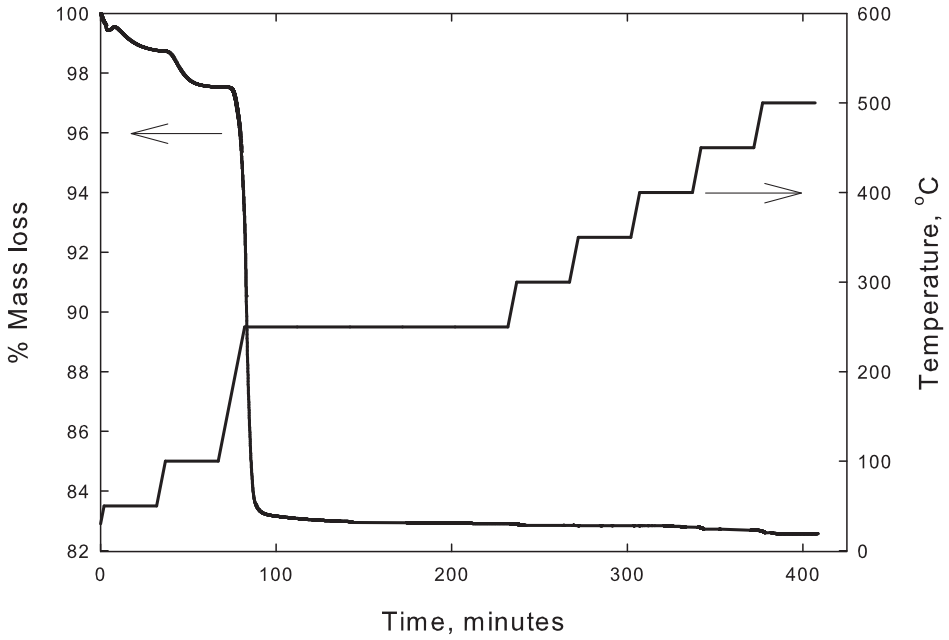

FIGURE 8.6: Thermogravimetric analysis of the bi-functional catalyst

After the reduction was complete, the gas was changed to a mixture of CO, CO_2 and H_2. No further change in the sample mass was observed. Total weight loss observed during the reduction step, according to the TG curve, corresponds to the loss of oxygen atom from copper oxide. XRD patterns were not collected continuously, so the start and end of the reduction of CuO could not be exactly determined. However, TGA results show the start and end of the reduction.

The corresponding first derivative (DTG) plot is shown in Figure 8.7. DTG curve shows peaks, at approximately 45 minutes and 85 minutes. The first peak corresponds to the moisture loss at 100 °C. The second one was observed for the fast reduction process which peaks at 250 °C.

The rate of reduction of the copper-based catalyst is a function of temperature and increases with temperature. However, the faster reduction of the catalyst comes at a price of higher copper crystallite size and results lower catalyst activity. A lower temperature reduction process has also been studied, at 190 °C. The TG and DTG curves for reduction at 190 °C is shown in Figure 8.8. The reduction completes in approximately 9 hours. The maximum rate of reduction is 0.239 at 190 °C compared to 13.241 for that at 250 °C.

The reduction process takes longer at lower temperature, as it occurs at a very slow rate. Therefore, lower reduction temperature is preferable to achieve catalyst with

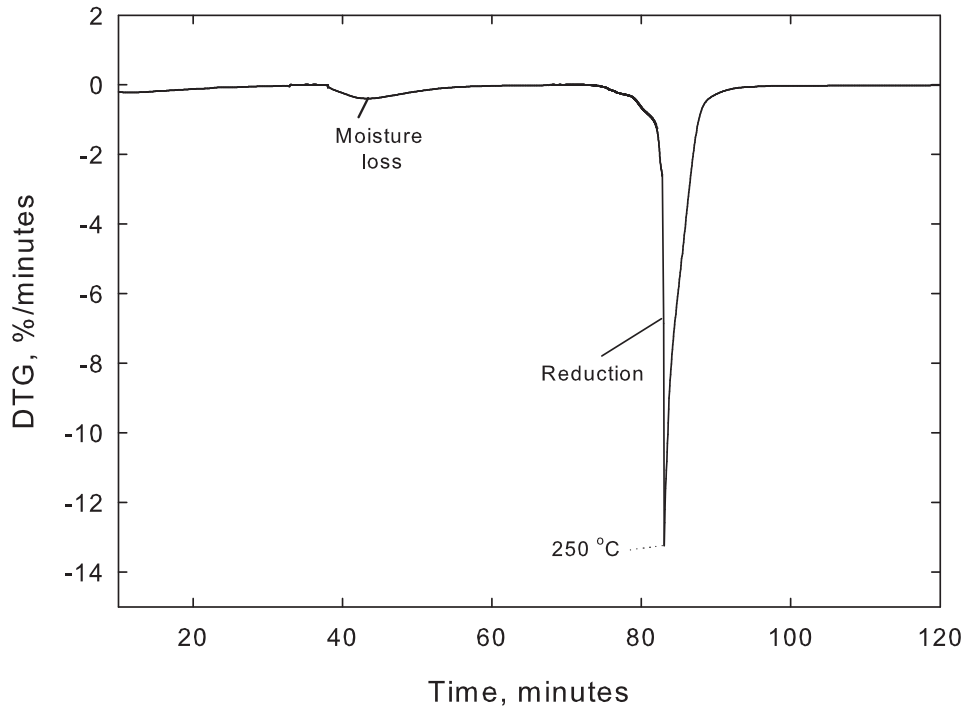

FIGURE 8.7: DTG curve of the catalyst reduction

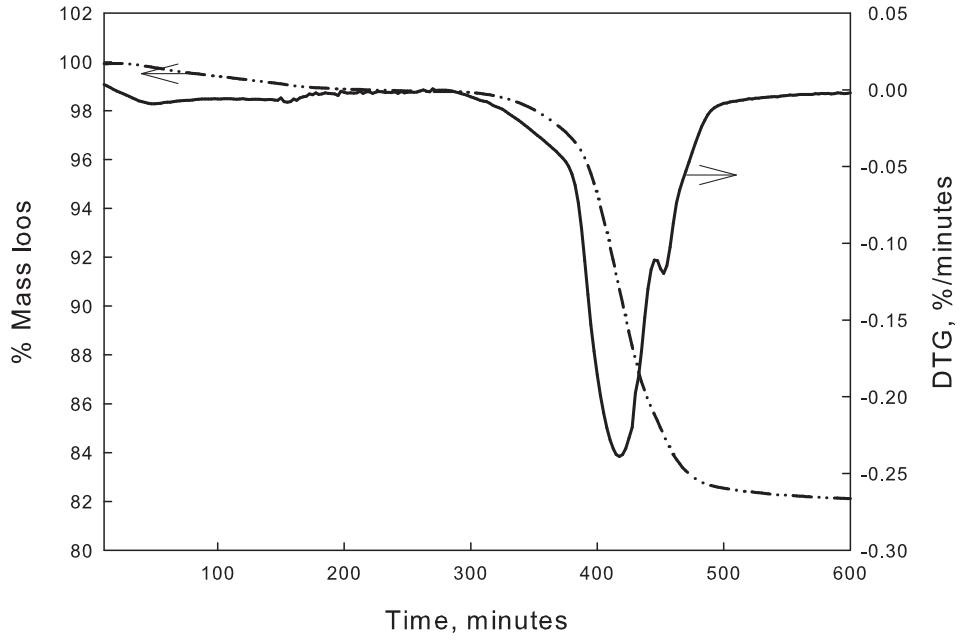

FIGURE 8.8: Thermogravimetric analysis of the bi-functional catalyst at 190 °C reduction temperature

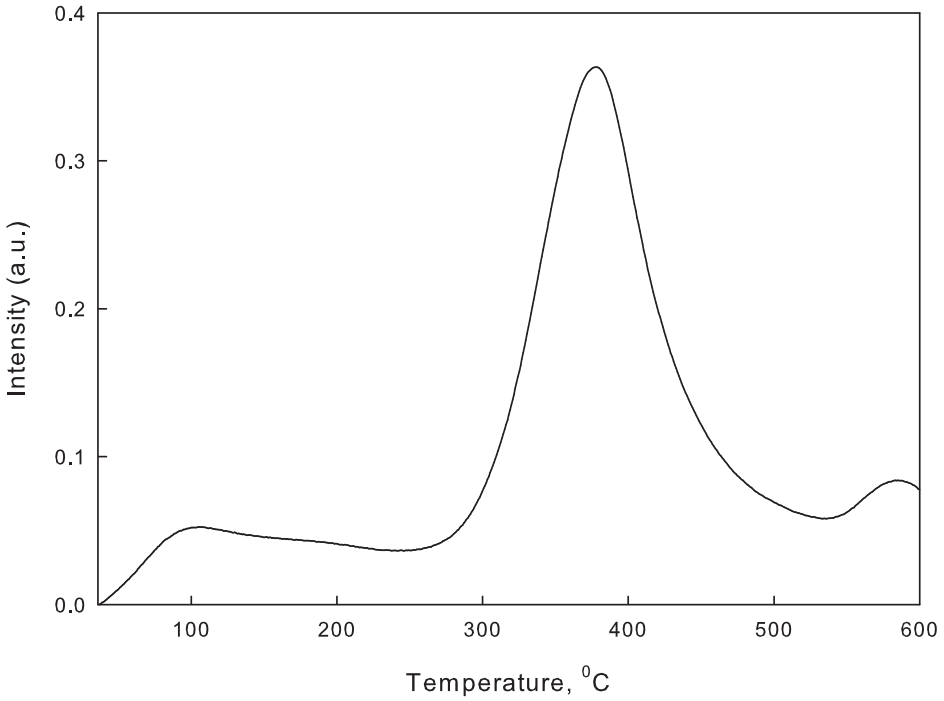

FIGURE 8.9: NH_3 TPD for the MSC-1

lower copper crystallite size [8] and higher catalyst activity.

8.3.3 Chemisorption: NH_3-TPD and H_2-TPR

Temperature programmed desorptions (TPD) were performed to study the surface acidity of the catalysts. NH_3-TPD for the MSC is shown in Figure 8.9. Three peaks were observed for the MSC. The low temperature peak at 98 °C indicates the amount of NH_3 desorbed at lower temperature from the weak acidic site. The absorbed ammonia mostly desorbed at 377 °C, which indicates moderate to high strength acidic sites. The catalyst also desorbed small amount of NH_3 at 586 °C.

Figure 8.10 shows the NH_3 desorption curve for ALU-1. ALU-1 has mostly low strength acidic sites, as indicated by the largest peak at 132 °C. The catalyst also showed a small peak at 496 °C and two shoulders at 405 and 595 °C.

Since the bi-functional catalysts discussed in this chapter were prepared by physically mixing MSC-1 with ALU-1, the surface acidity of the bi-functional catalysts depend on the fraction of each individual components present. A higher acidic catalyst would break down the product (e.g. DME) further down to the hydrocarbons. On the other

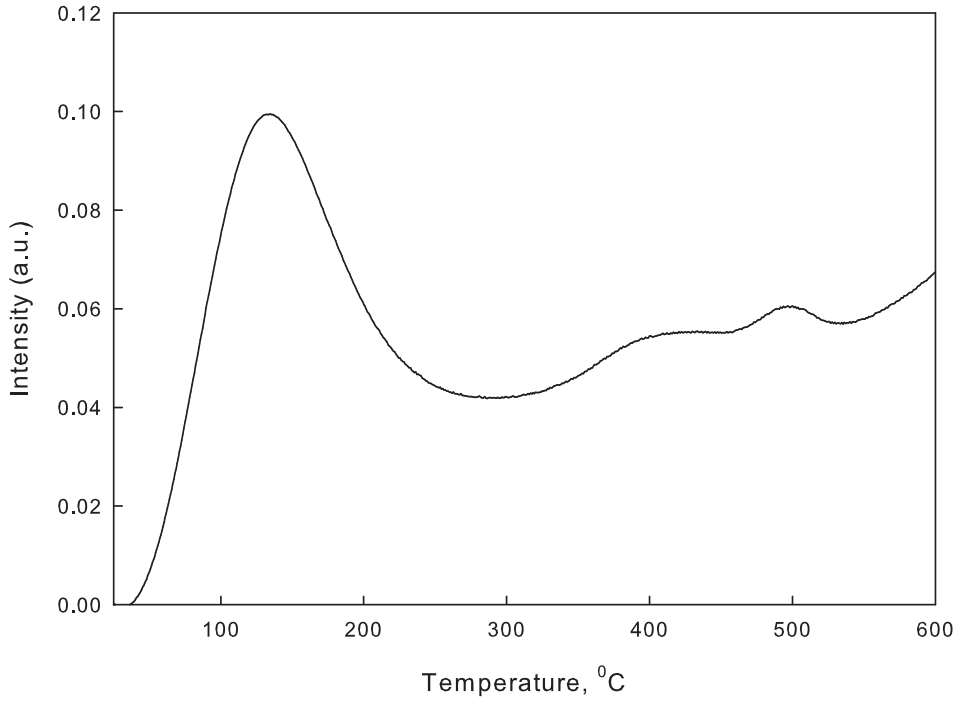

FIGURE 8.10: NH_3 TPD for the ALU-1

hand, if the catalyst has low surface acidity the dehydration reaction will not go to completion. The effect of different bi-functional catalysts and their surface acidity on the products is further discussed in the latter section, with discussion on conversion and product selectivity.

The reducibility of the MSC catalyst was studied by temperature programmed reduction (H_2-TPR) and shown in Figure 8.11. The reduction of the catalyst started at temperatures as low as 115°C at a very slow rate. The reduction curve shows a shoulder close to 190 °C. At temperatures above that, the reduction process proceeded at a very high rate and peaked at 256 °C. The reduction was completed at temperature close to 330 °C.

The observation made from the TPR along with the findings from the TG/DTG studies shows that the reduction process is dependent on both the heating rate and the reduction temperature. Reduction at lower temperature with a slower ramp rate will produce lower copper crystallite size [8] and hence preferable. Therefore, a temperature of 190 °C was selected for reducing the catalysts.

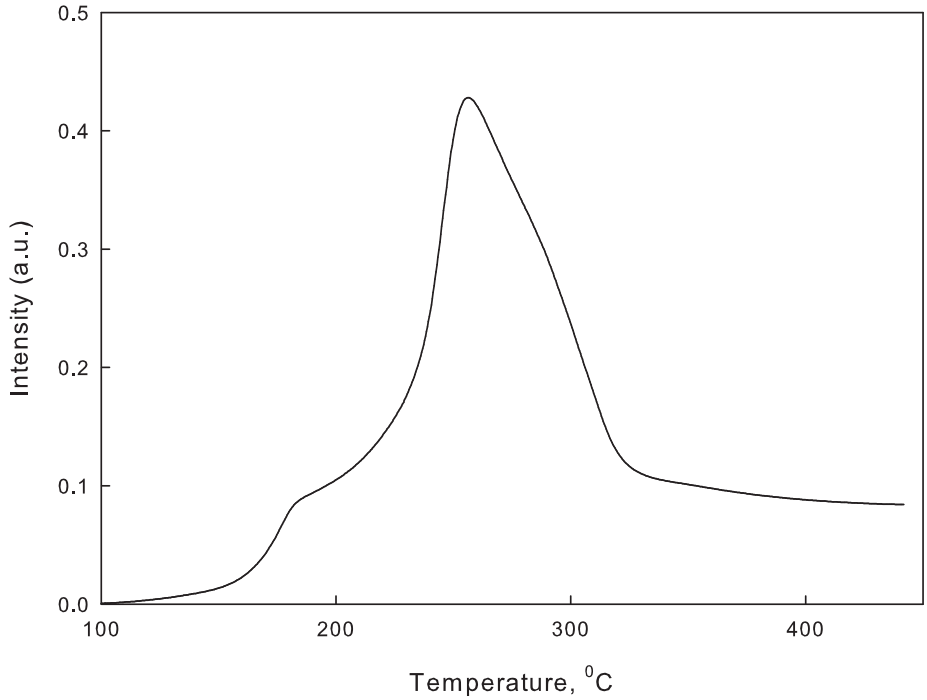

FIGURE 8.11: H_2-TPR for the ALU-1

8.3.4 Electron Microscopy

Changes in the surface morphology for MSC before and after use are shown in Figure 8.12. The catalyst before reduction showed surface morphology without any significant features. The surface was found to be non-porous. In contrast, a few narrow cracks developed on the surface of the catalyst during thermal treatment in reducing environments. The point composition measurements using EDS technique for the fresh and used catalyst also showed significant changes for Cu and Al. The surface of the used catalyst is found to have more Al than the fresh catalyst, while the fresh catalyst had more copper than the used one. Zinc and magnesium concentration on the surface found to be similar for both fresh and used catalyst. The variation in surface composition is shown in Table 8.4. The final temperature was high enough to make the atoms or ions present in the bulk phase migrate to the surface of the catalyst. Mobility of the bulk phase therefore can be attributed to the change in the surface composition.

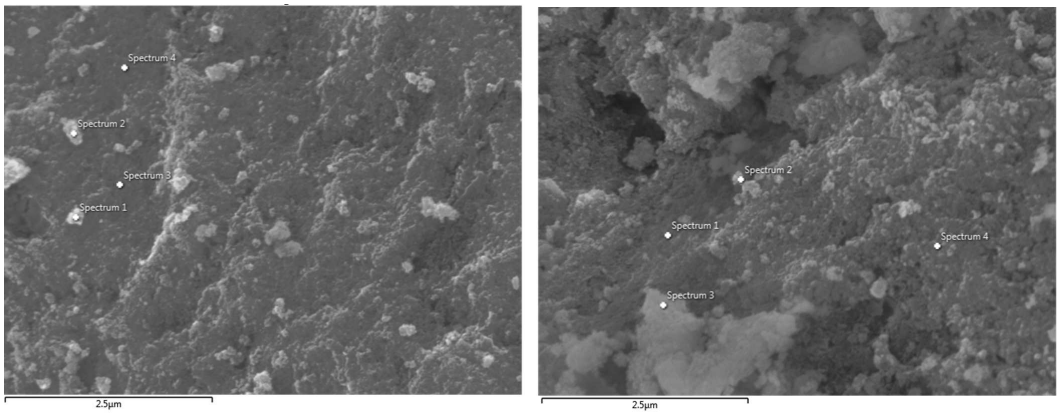

(a) (b)

FIGURE 8.12: Secondary electron images of the fresh (left) and used (right) catalyst

TABLE 8.4: Point composition of the fresh and used catalysts

Elements	Fresh MSC				Used MSC			
	Spectrum				Spectrum			
	1	2	3	4	1	2	3	4
Cu	47.4	47.3	48.8	48.3	36.1	36.8	38.8	33.5
Zn	24.5	24.2	25	23.8	24.6	24.7	24.2	26.2
Al	1.33	1.51	1.11	1.42	7.84	7.61	6.39	8.61
Mg	0.99	1.01	-	0.99	1.08	1.06	1	1.37
O	25.8	26.1	25.1	25.5	30.4	29.8	29.6	30.4

8.4 Effect of operating variables on catalyst performance

Activity of the catalyst was studied in the high pressure DME synthesis reactor. The catalyst was loaded in the reactor. For reduction of the catalyst, 5% H_2 in N_2 was used. The internal temperature of the reactor and the catalyst bed was set to 100 °C and kept for two hours, to remove moisture from the catalyst. The bed temperature was then increased to 190 °C. The catalyst bed is left at this condition for 8 hours for the completion of the reduction process. The reactor was kept at atmospheric pressure during the reduction process.

The reactor was then pressurized to 5 MPa using N_2. At the same time, the reactor was also heated to the desired reaction temperature. When the reactor pressure and temperature were achieved,the gas was changed to a mixture of CO and H_2 with a

H_2 to CO ratio 1. A space velocity of 2000 mL g_{cat}^{-1} was maintained for the activity study.

With the introduction of the synthesis gas, the following desirable reactions are expected to occur in presence of the catalysts:

$$CO + 2H_2 \longrightarrow CH_3OH \tag{R8.2}$$

$$CO_2 + 3H_2 \longrightarrow CH_3OH + H_2O \tag{R8.3}$$

$$2\,CH_3OH \longrightarrow C_2H_6O + H_2O \tag{R8.4}$$

$$CO + H_2O \longrightarrow CO_2 + H_2 \tag{R8.5}$$

In addition to these reactions, several undesirable reactions also occur inside the reactor, leading to the formation of methane and other hydrocarbons.

The conversion, yield and selectivity are defined by the following equations:

$$\%COconversion = \frac{(n_{CO,in} - n_{CO,out})}{n_{CO,in}} \times 100 \tag{8.2}$$

$$DMEyield = \frac{2n_{DME}}{n_{CO,in}} \times 100 \tag{8.3}$$

$$DMEselectivity = \frac{2n_{DME}}{n_{\mathrm{CH_4}} + n_{\mathrm{CH_3OH}} + n_{\mathrm{CO_2}} + \sum m \times n_{\mathrm{C_m}}} \times 100 \tag{8.4}$$

Effect of temperature on DME and methanol yield and selectivity is shown in Figure 8.13. CO conversion, DME+methanol yield and selectivity are determined at 190, 240, 280, 340 °C. CO conversions were found to be 2.61, 27.45, 57.32 and 40.96%, respectively. At low temperature (e.g. 190 °C), the catalyst activity is very low, as indicated by the conversion of CO. However, at low temperature, side reactions have negligible contribution, as indicated by the DME+methanol yield. With an increase in temperature, the CO conversion increased, with acceptable yield of DME until 280 °C. The selectivity towards DME+methanol also decreased , as secondary reactions like water gas shift reaction increases with temperature producing more CO_2. The results also show increase in CH_4 concentration due to CO-hydrogenation to methane at elevated temperatures. As the temperature was further increased beyond 300 °C , CO conversion, DME+methanol yield and selectivity decreased due to deactivation of the copper-based catalyst at temperatures above than 300 °C. At this temperature,

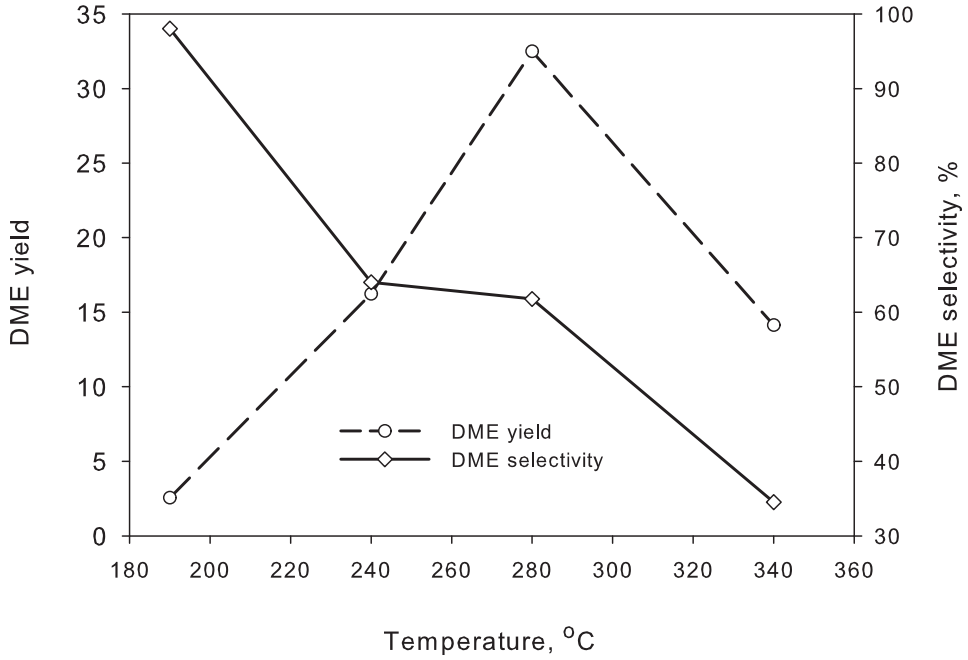

FIGURE 8.13: Effect of temperature on DME yield and selectivity

CH_4 selectivity increased since higher temperature is favourable for this side reaction. The major calculation that can be drawn from this experiment is the optimum reaction temperature to be used to obtain DME from CO with high selectivity, which is 280 °C. As a re sult, all the following results presented here were performed at 280 °C. A space velocity 2000 mL g_{cat}^{-1} was used.

Variations in CO conversion for different bi-functional catalysts and H_2/CO ratio are shown 8.14. CO conversion occurs at the metallic copper sites. Therefore, having more copper sites (i.e. the methanol synthesis component) should increase CO consumption by both hydrogenation and water gas shift reactions. However, presence of acidic active sites (i.e. methanol dehydration component) dehydrate the produced methanol and hence also improves CO conversion by removing the products in situ. This is evident from a significant increase in conversion from M5A1 to M2A1 catalyst. After a certain composition, adding more acidic components do not improve the catalyst performance in terms of CO conversion. Adding more acidic component means reducing the active metallic sites. In absence of necessary active copper sites, effect of additional acidic component was therefore proved not to be beneficial for M1A1, M1A2 and M1A5. The trend was found to be similar for different H_2/CO ratio.

DME yield is also a function of the catalyst composition as well as the H_2 to CO

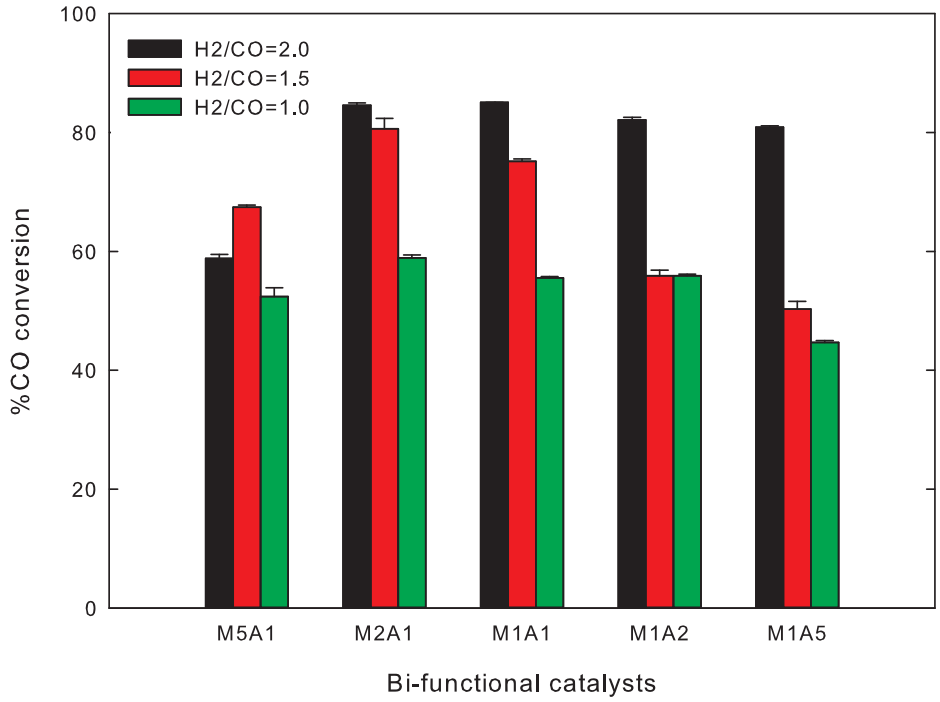

FIGURE 8.14: % CO conversion for different bi-functional catalysts

ratio. The trend is similar to that for the CO conversion. With an increase in the acidic component synergistic effect of the reactive system improves and hence the DME yield. However, excessive acidic component in the catalyst limit the number of hydrogenation sites available for reaction. With a H_2 to CO ratio of 2.0, the yield was similar for M2A1, M1A1 and M1A2 catalysts. For M5A1 the acidic sites are lesser in numbers for methanol dehydration. On the other hand, for M1A5, there are too many acidic sites, which might cause further dehydration of DME to smaller hydrocarbons. For a H_2 to CO ratio of 1.0 the DME yield was less sensitive to catalyst composition. Feed gas with that ratio were rich in CO, which makes the DME yield calculated from Equation 8.3 less sensitive with variation in catalyst. However, the trend is the same as observed for the other syngas compositions.

While synthesizing DME from CO and H_2, other carbon based products are CH_4, CO_2 and CH_3OH. The selectivity of DME depends on the extent of water gas shift reaction as well as the extent of side reactions producing methane and other hydrocarbons. Since the copper-based catalyst is also a water gas shift catalyst, DME synthesis from syngas also yield CO_2 at a high concentration. Usually the 30-40% of the carbon from converted CO would form CO_2. CH_4 is also formed since the temperature and pressure inside the reactor is favourable for the reaction. Also presence of strong acidic sites

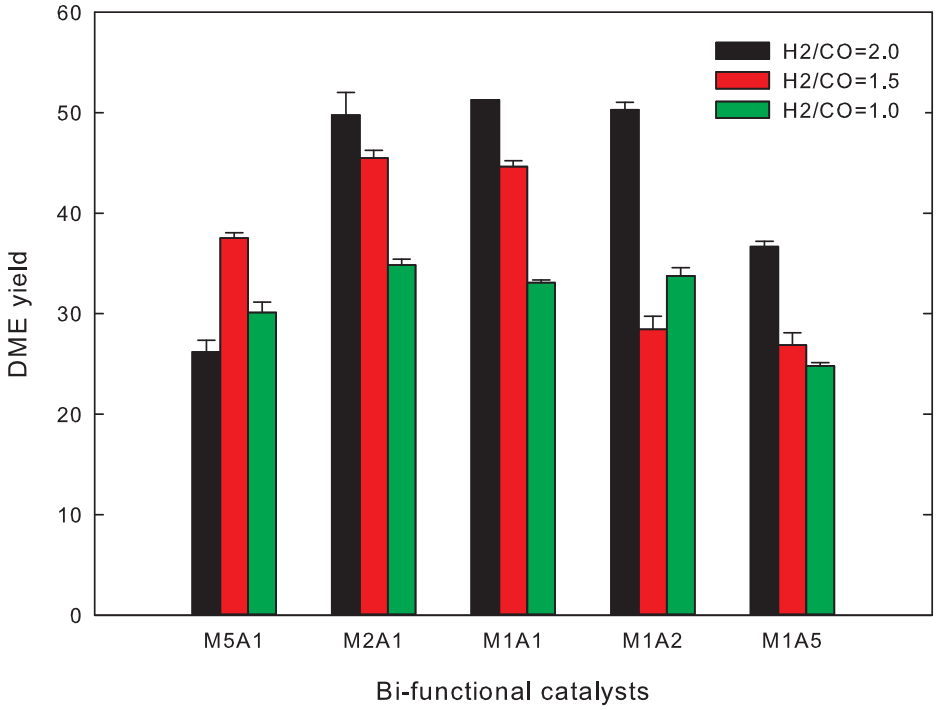

FIGURE 8.15: DME yield for differnt bi-functional catalsysts

can break down DME and methanol into smaller hydrocarbons. Presence of excessive H_2 in the feed gas also favours formation of hydrocarbons So a proper balance between the two catalyst components along with optimum syngas composition is necessary to obtain high DME yield.

With M5A1 catalyst and a H_2 to CO ratio of 2.0, the DME selectivity was only approximately 45%. The catalyst has more of the copper based catalyst, therefore resulting more CO_2. For M1A5, a higher selectivity of CH_4 was observed. For other catalysts, the selectivity was close to 60%. For H_2 to CO ratio of 1.0 and 1.5, DME selectivity did not change much with different catalyst except for the case of M1A5. Products observed for this catalyst were high in CH_4, because of the presence of more acidic sites.

For Figures 8.14 and 8.15, the conversion and yield was calculated on the basis of available CO in the feed gas, and not only the basis of total reacting gases. Since gases with higher H_2 to CO ratio had less CO in the feed gas, the conversion achieved was found to be higher than the H_2 to CO ratio of 1.0. However, if the conversion and yield are calculated based on total feed gas, the numbers will look different from the presented ons. Therefore, both CO conversion and DME yield numbers are required

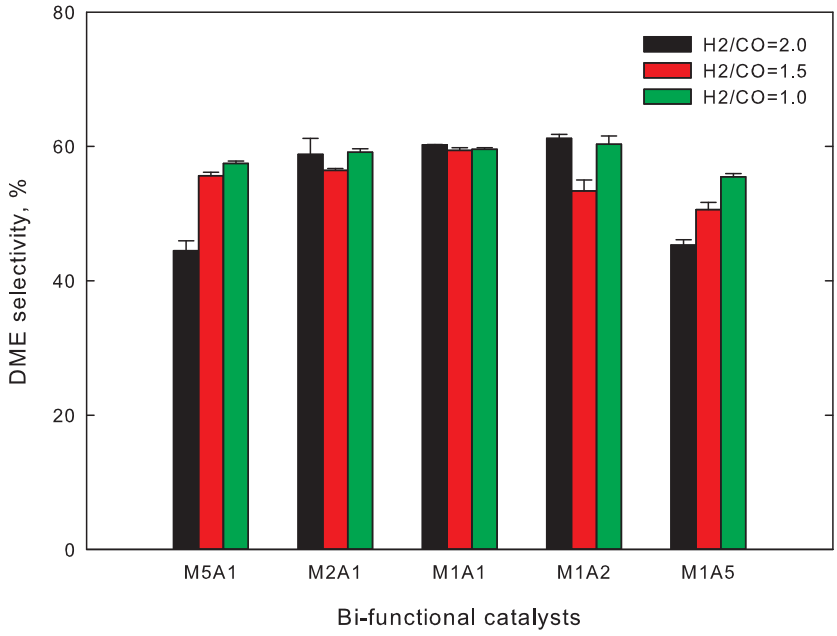

FIGURE 8.16: DME selectivity for differnt bi-functional catalysts

to be normalised so that they can be compared to find the best operating condition for DME synthesis. In the following section, a factorial experimental design and analysis was performed using the normalised values of DME yield.

8.5 Factorial analysis and optimum reaction conditions

A 3^2 factorial design of experiments were performed: with 2 factors (catalyst and syngas ratio), each at three levels (Catalysts: M5A1, M1A1 and M1A5; H_2 to CO ratio: 1.0, 1.5 and 2.0). The coded variables are defined as follows:

$$x_1 = \frac{\%MSC - (\%MSC_{low} + \%MSC_{high})/2}{(\%MSC_{high} - \%MSC_{low})/2} \tag{8.5}$$

$$x_2 = \frac{\mathrm{H_2}/CO - (\mathrm{H_2}/CO_{low} + \mathrm{H_2}/CO_{high})/2}{(\mathrm{H_2}/CO_{high} - \mathrm{H_2}/CO_{low})/2} \tag{8.6}$$

where, x_1 is the coded catalyst composition, x_2 is the coded syngas ratio. DME yield, adjusted for the total feed gas, was used as the response variable, y for the regression

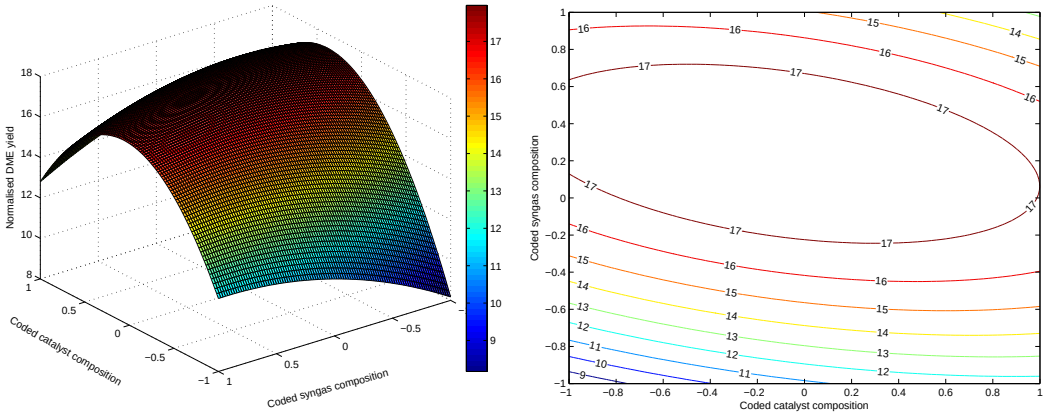

(a) The response surface plot (b) The contour plot

FIGURE 8.17: Response surface and contour plot for the model

model. The adjusted DME yield is defined as:

$$Yield_{adj} = \frac{DME - yield \times n_{CO}}{n_{total}} \tag{8.7}$$

where, DME-yield is the yield calculated from Equation 8.3, n_{CO} is the CO flow rate in the feed gas and n_{total} is the total feed gas flow rate. The adjusted yield values are shown in Table 8.5. The regression model representation of the two-factor, three level experiment could be written as:

$$y = \beta_0 + \beta_1 x_1 + \beta_2 x_2 + \beta_3 x_1 x_2 + \beta_4 x_1^2 + \beta_5 x_2^2 + \beta_6 x_1^2 x_2 + \beta_7 x_1 x_2^2 + \epsilon \tag{8.8}$$

where y is the response, the β's are model parameters, x_1 and x_2 are the coded variables, and ϵ is a random error term. The used model assumes interaction between the two factors. $x_1 x_2$ is the first order interaction, while $x_1^2 x_2$ and $x_1 X - 2^2$ are the second order interaction terms considered for the model.

The least square fit, with the regression coefficients reported to two decimal places, is as follows:

$$y = 17.72 + 2.13x_1 + 0.19x_2 - 1.53x_1x_2 - 4.78x_1^2 - 0.93x_2^2 - 1.87x_1^2x_2 - 2.33\beta_7 x_1 x_2^2 \tag{8.9}$$

The coefficient of multiple determination R^2 was found to be 0.9925. The adjusted R^2 was 0.9897, which is very close to the ordinary R^2.

The three dimensional response surface plot is shown in Figure 8.17(a). Figure 8.17(b) shows the contour lines of constant response y in the x_1, x_2 plane. Since the response

Table 8.5: Flow rate adjusted DME yield

	Process variables		Coded variable		$Yield_{adj}$
Run	Catalyst	H_2/CO ratio	x_1	x_2	
1	M5A1	2.0	1	1	8.22
2	M5A1	2.0	1	1	8.98
3	M5A1	2.0	1	1	8.71
4	M1A1	2.0	0	1	16.92
5	M1A1	2.0	0	1	16.92
6	M1A1	2.0	0	1	16.91
7	M1A5	2.0	-1	1	12.29
8	M1A5	2.0	-1	1	12.07
9	M1A5	2.0	-1	1	11.94
10	M5A1	1.5	1	0	15.20
11	M5A1	1.5	1	0	15.04
12	M5A1	1.5	1	0	14.77
13	M1A1	1.5	0	0	18.04
14	M1A1	1.5	0	0	17.92
15	M1A1	1.5	0	0	17.60
16	M1A5	1.5	-1	0	10.44
17	M1A5	1.5	-1	0	10.50
18	M1A5	1.5	-1	0	11.30
19	M5A1	1.0	1	-1	14.81
20	M5A1	1.0	1	-1	15.66
21	M5A1	1.0	1	-1	14.72
22	M1A1	1.0	0	-1	16.65
23	M1A1	1.0	0	-1	16.40
24	M1A1	1.0	0	-1	16.56
25	M1A5	1.0	-1	-1	12.58
26	M1A5	1.0	-1	-1	12.26
27	M1A5	1.0	-1	-1	12.37

$x_1 = \frac{\%MSC - 0.5}{0.33}$, $x_2 = \frac{H_2/CO - 1.5}{0.5}$

is a concave function of the factors, the contour plot contains elliptical shapes. The response surface and contour plot shows a maximum for DME yield at a certain location, indicating the optimum operational conditions. The optimum conditions was obtained by finding the global maximum for the response at $x_1 = 0.2460$ and $x_2 = -0.1010$. These values corresponds to the catalyst containing 58.2% MSC component and a H_2 to CO ratio of 1.45. The H_2 to CO ratio found here is consistent with the H_2 to CO ratio obtained from the Aspen Plus simulation (Chapter 6).

8.6 Conclusion

Two commercial catalysts, one methanol synthesis and one methanol dehydration catalyst, were used for the study. The catalysts were physically mixed to prepare the bi-functional catalyst for DME synthesis from syngas containing CO and H_2. The catalysts were characterised using analytical techniques such as XRD, TG, physisorption, chemisorption and electron microscopy. The analysis results were used to find the appropriate reduction temperature for the catalysts. 280 °C was found to be the optimum temperature, since it yielded the maximum amount of DME. A three level, two factor factorial design was used to find out the optimum syngas ratio and catalyst composition. For these commercial catalysts, a H_2 to CO ratio of 1.45 and a catalyst with 58.2% MSC component was found to yield maximum DME. The obtained H_2 to CO ratio was consistent with the ratio obtained from the Aspen Plus process model.

8.6.1 Further work

The optimum reaction conditions have been established using the experimental data obtained from the commercial catalysts mixtures. Based on the information, bi-functional catalysts for syngas to DME will be prepared. The prepared catalysts will be characterised and used in the synthesis reactor to determine the conversion, yield and selectivity.

References

[1] Zhang W, Yang H, Wang X, Su G, Gao R, Yin Y, 1994, Catalysis Letters, **30**: 113–122

[2] Sarbak Z, 2005, *In:* Sustainable strategies for the upgrading of natural gas: fundamentals, challenges, and opportunities, Derouane EG, Parmon V, Lemos F, Ramoa Ribeiro F, editors, 1st ed., 359–364, Springer, Dordrecht

[3] Clausen BS, Topsøe H, Frahm R, 1998, *In:* Advances in catalysis, Vol.42, 315–344, Academic Press, New York

[4] Bruker AXS, 2004, TOPAS V3.0: General profile and structure analysis software for powder diffraction data. Karlsruhe, Germany

[5] Mittemeijer EJ, Welzel U, 2008, Zeitschrift für Kristallographie, **223**: 552–560

[6] Meyers R, 1984, Handbook of synfuels technology. McGraw-Hill, New York

[7] Trimm D, 1991, *In:* Studies in Surface Science and Catalysis, Vol. 68: Catalyst Deactivation 1991 Proceedings of the 5th International Symposium, Bartholomew CH, Butt JB, editors, 29 – 51, Elsevier

[8] Quincoces C, Amadeo N, Gonzalez M, 1997, *In:* Studies in Surface Science and Catalysis, Vol. 111: Catalyst Deactivation Proceedings of the 7th International Symposium, Bartholomew C, Fuentes G, editors, 535 – 541, Elsevier

Chapter 9

Performance of Developed Catalysts

9.1 Introduction

Four bi-functional catalysts were prepared for syngas to DME synthesis in single step. The performance of the commercial catalyst (Chapter 8) was used as the basis for the development of the composition of the new catalysts. Firstly, a methanol synthesis catalyst and two alumina-based dehydration catalysts were prepared. A bi-functional catalyst was prepared by physically mixing methanol synthesis catalyst with the dehydration catalyst. Later, co-precipitation impregnation method was used to prepare three more bi-functional catalysts. The catalysts were characterised using XRD, chemisorption (NH_3-TPD and H_2-TPR) and physisorption. Then, the catalysts were used in a high pressure reactor for single-step synthesis of DME from syngas to asses their performance - conversion, activity and selectivity. The performance of the prepared catalysts were analysed and then compared with each other, and also with that from the commercial catalyst.

9.2 Preparation of the catalysts

A methanol synthesis catalyst and two alumina catalysts were prepared. A bi-functional catalyst was prepared by mixing them one of the aluminas with the methanol synthesis catalyst. Co-precipitation impregnation method was used to prepare three more bi-functional catalyst.

9.2.1 Preparation of methanol synthesis catalysts

Copper-based methanol synthesis catalyst was prepared using nitrate salts of copper, zinc and aluminium. A 0.3 M solution was made using nitrate salts with an atomic

ratio copper, zinc and aluminium of 6:3:1. 0.4 M sodium nitrate solution was used as the precipitating agent.

200 mL of water was heated to 70 °C while stirring. The solutions were then added drop by drop to the flask. A blue precipitate was formed. The precipitate was aged at 70 °C for 4 more hours. The precipitate was then filtered, washed and dried overnight.

The catalyst precursor containing copper, zinc and aluminium was then calcined at 550 °C in air, with a heating rate of 2 °C. min^{-1}. The isothermal period for calcination was 6 hours. The catalyst prepared will be called MSC-A from here onwards.

9.2.2 Preparation of alumina

γ-Al_2O_3 was obtained by the thermal decomposition of the alumina precursor containing boehmite (γ-AlOOH) at 550 °C. To prepare the alumina precursor, initially aluminium nitrate nonahydrate [$Al(NO_3)_3 \cdot 9\,H_2O$; Sigma Aldrich 237973] was dissolved in demineralised water to produce $\sim$ $.25M$ solution. Two different alumina samples were prepared: one using aqueous ammonia and the other using Na_2CO_3 as the precipitating agents.

A 2-L three-neck round bottom flask with 200 mL of demineralised water was placed in a magnetic stirrer hotplate. The content of the flask was heated to 70 °C while heating continuously. The aluminium nitrate and the base solutions were then added drop by drop to the stirred solution in the flask in a manner that the pH of the solution stays close to 8. The precipitate was aged at 70 °C for 4-hours. After that, the precipitate was filtered, washed and dried at 105 °C overnight. The solid is the alumina precursor.

The alumina precursor was then calcined in air from room temperature to 550 °C with a heating rate of 2 °C. min^{-1}, and kept at this temperature for 6 hours.

The catalyst prepared using aqueous ammonia and Na_2CO_3 were named as ALU-A and ALU-S, respectively.

9.2.3 Preparation of bi-functional catalysts

Bi-functional catalysts were prepared using two different methods: physical mixing and co-precipitation impregnation.

Table 9.1: List of prepared bi-functional catalysts

Name	Preparation method
DSC-1	Coprecipitation impregnation using ALU-A
DSC-2	Coprecipitation impregnation using ALU-S
DSC-M	Physical mixing of MSC-A and ALU-A
DSC-1-PRE	Coprecipitation impregnation using ALU-A precursor

MSC-A: prepared methanol synthesis catalyst
ALU-A: Alumina prepared using aqueous ammonia
ALU-S: Alumina prepared using Na_2CO_3

For physical mixing preparation, methanol synthesis catalyst and alumina prepared according to section 9.2.1 and 9.2.2 were used. The samples were pelletised, crushed and sieved to 20-40 mesh size. The prepared catalysts were then mixed with each other to make the bi-functional catalyst.

In the coprecipitation-impregnation method, a suspension of alumina was placed in a round bottom flask. The suspension was heated up to 70 °C. The suspension was stirred continuously, while the solutions of nitrate salts and sodium carbonate were added to drop wise. The final pH of the solution was kept close to 7. The precipitation was aged for 4 hours, filtered, washed and dried at 105 °C overnight. The dried solid was then calcined at 550 °C for 6 hours.

A variation of coprecipitation-impregnation method was also used to prepare one bi-functional catalyst. Instead of using alumina in the suspension, the alumina precursor was used. The alumina precursor was prepared according to section 9.2.2 with aqueous ammonia as the precipitating agent. The following steps were the same as the coprecipitation-impregnation method.

9.3 Characterisation of the catalysts

The catalysts were characterised using physisorption, chemisorption (NH_3-TPD and H_2-TPR) and XRD.

9.3.1 Physisorption

The surface area of the catalyst samples were measured by using N_2 adsorption at 77 K. The quantity adsorbed gas at different pressure ratio was then fitted to the

Brunauer-Emmett-Teller (BET) model to find the surface area. The BET surface area for various catalyst samples are listed in Table 9.2.

Table 9.2: BET surface area for catalyst samples

Catalyst	Surface area m^2/g	Pore volume, cm^3/g	Pore diameter Å
Methanol synthesis catalyst			
MSC-A	50.21 ± 0.19	0.142	110.38
Methanol dehydration catalysts			
ALU-A	240.03 ± 2.57	0.653	94.67
ALU-S	252.03 ± 3.07	0.559	79.48
Bi-functional catalysts			
DSC-1	105.40 ± 1.06	0.260	85.64
DSC-2	107.31 ± 0.99	0.296	99.39
DSC-M	126.14 ± 1.14	0.357	100.25
DSC-1-PRE	159.00 ± 1.50	0.398	102.35

9.3.2 X-ray diffraction

X-ray diffraction pattern for both alumina precursors, namely ALU-A and ALU-S, are shown in Figure 9.1. ALU-A precursor showed presence of boehmite as well as bayerite, as shown by line (a). On the other hand, only boehmite was present in the ALU-S precursor, line (b).

Boehmite, or aluminium oxyhydroxide (γ-AlO(OH)), is alumina precursor and can be used to prepare different phases of alumina according to Reaction R9.1.

$$\gamma\text{−AlO(OH)} \rightarrow \gamma\text{−}Al_2O_3 \rightarrow \delta \rightarrow \theta \rightarrow \alpha \tag{R9.1}$$

However, the transition forms of alumina are more important in terms of their industrial applications.

Bayerite is another form of aluminium hydroxide with a chemical formula of $Al(OH)_3$. It has a monoclinic crystal structure and is a precursor for η-Al_2O_3.

The precursors were calcined in air at 550 °C. The XRD profiles for the calcined catalysts are shown in Figure 9.2. Both the profiles show peaks for same 2θ values. However, the bottom line showing XRD profile for ALU-S shows presence of γ-Al_2O_3 only. γ-Al_2O_3 has a simple cubic structure with $D1 \approx 2.39$Å.

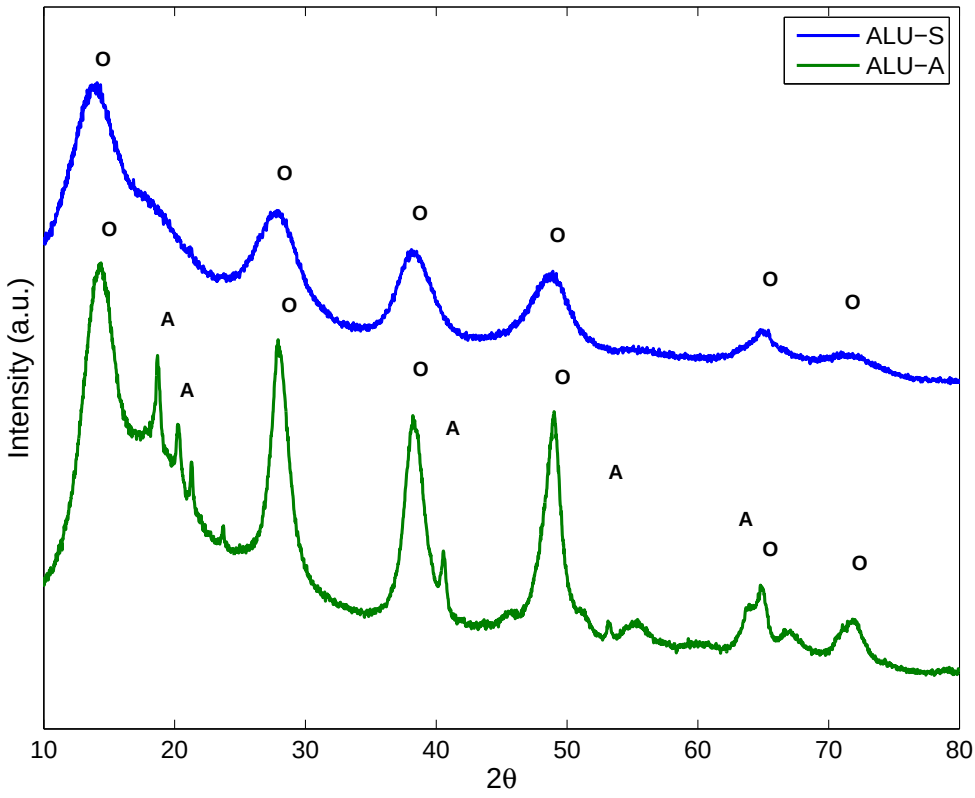

FIGURE 9.1: XRD patterns for alumina precursors (a) ALU-A, (b) ALU-S [O - Boehmite; A - Bayerite]

ALU-A sample showed presence of both γ- and η-alumina. The presence of η-Al_2O_3, in addition to γ-Al_2O_3, was confirmed by the presence of higher intensity peaks at high angles, since it has the first diffraction line at $D1 \approx 1.39$Å.

Presence of different phases in the final catalyst can be explained from the phases present in the catalyst precursor. When calcined at 550 °C, the boehmite phase completely transformed into γ-Al_2O_3 and the bayerite phase transformed into η-Al_2O_3.

The precursor of the bi-functional catalysts mostly consists of hydroxycarbonates of copper and zinc. The major mineral phases present are rosasite, aurichalsite and malachite. The precursor also showed presence of boehmite. The diffraction pattern is shown in Figure 9.3. Most importantly, the XRD confirmed that absence of gerhardite, which can lead to formation of less active catalysts [1].

The powder diffraction pattern for the MSC-B and bi-functional catalysts are shown in Figure 9.4. The calcined catalysts showed three oxide phases only, tenorite, zincite and alumina.

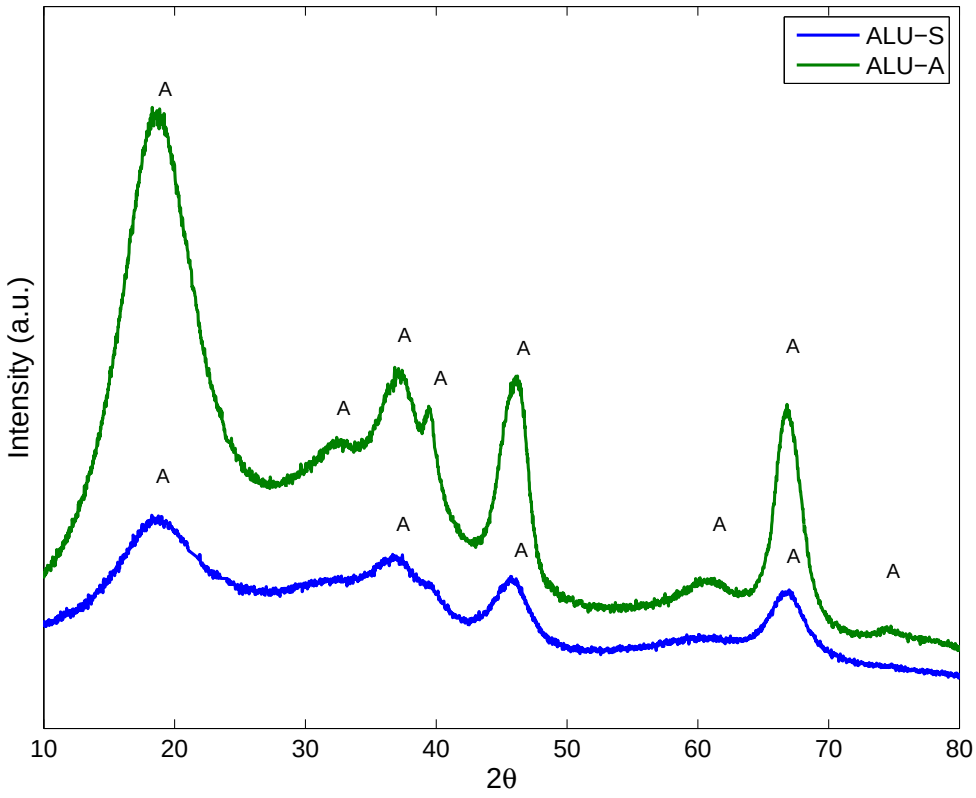

FIGURE 9.2: XRD patterns for alumina [A - Alumina]

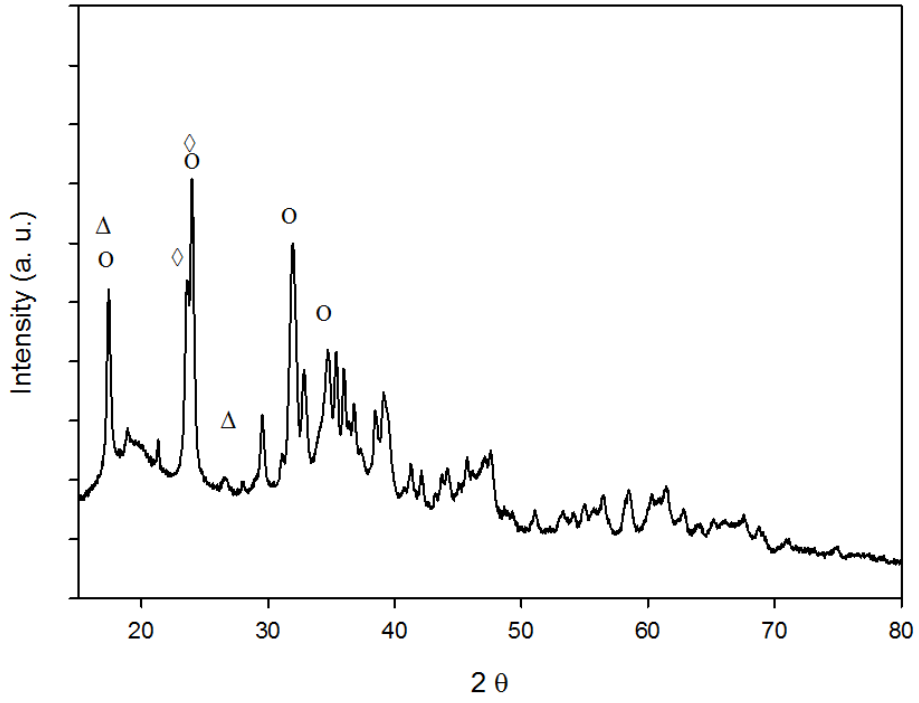

FIGURE 9.3: XRD patterns for the MSC and the bi-functional catalysts[○-rosasite;◊-aurichalsite;△-malachite]

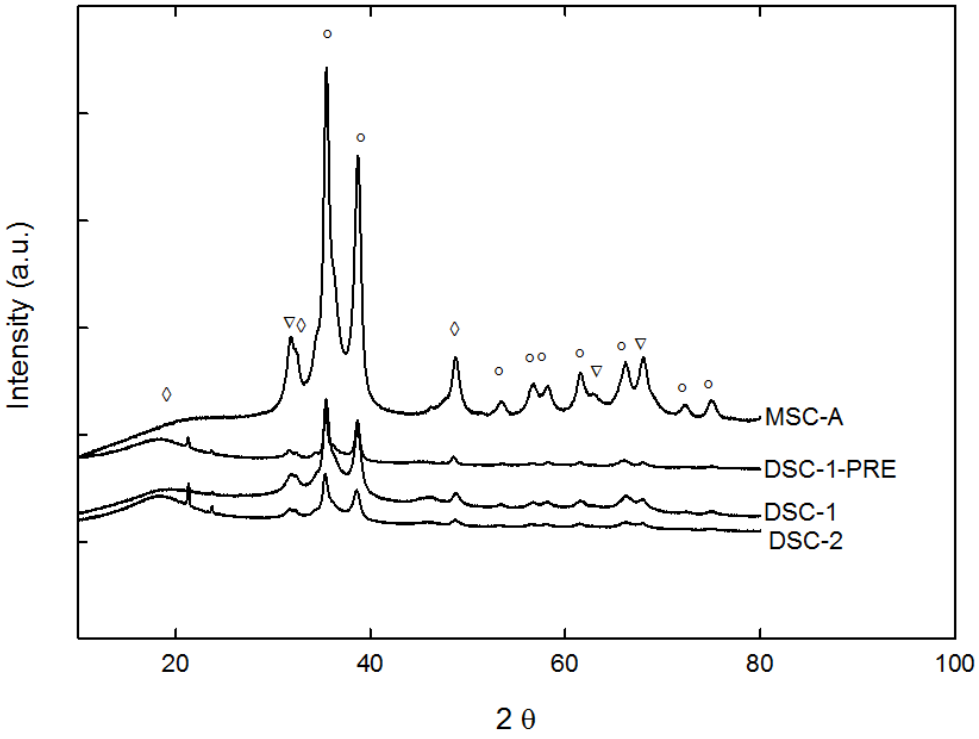

FIGURE 9.4: XRD patterns for the MSC and the bi-functional catalysts[o-CuO;◊-γAl_2O_3; ▽-ZnO]

9.3.3 Chemisorption

Figure 9.5 shows the NH3-TPD profiles for the two prepared alumina catalysts. For both the samples, three peaks were observed. Theses peaks were at 137, 273 and 394 °C for the ALU-A sample. This sample has mostly low to moderate acidity. On the other hand, ALU-S showed desorption peaks at 170, 295 and 465 °C. The acidity of this sample is similar to that of ALU-S. The amount of NH_3 desorbed from the ALU-A and ALU-S are 0.50 and 0.48 mmolo/g, respectively.

Figure 9.6 shows the temperature programmed reduction patterns for three prepared bi-functional and one methanol synthesis (MSC-A) catalysts. The intensity for each of these samples were normalised for the same mass of the catalyst. MSC-A sample does not contain any dehydration component, while the three bi-functional catalysts have γ-Al_2O_3 included in the preparation. The effect of dehydration component on the H_2 consumption, corresponding to the area under the peak, is visible from the graphs. Less amount of copper oxide in the catalyst resulted less H_2 consumption for the bi-functional catalysts. For all the samples, only one broad reduction peak was observed in the range of 150-300 °C.

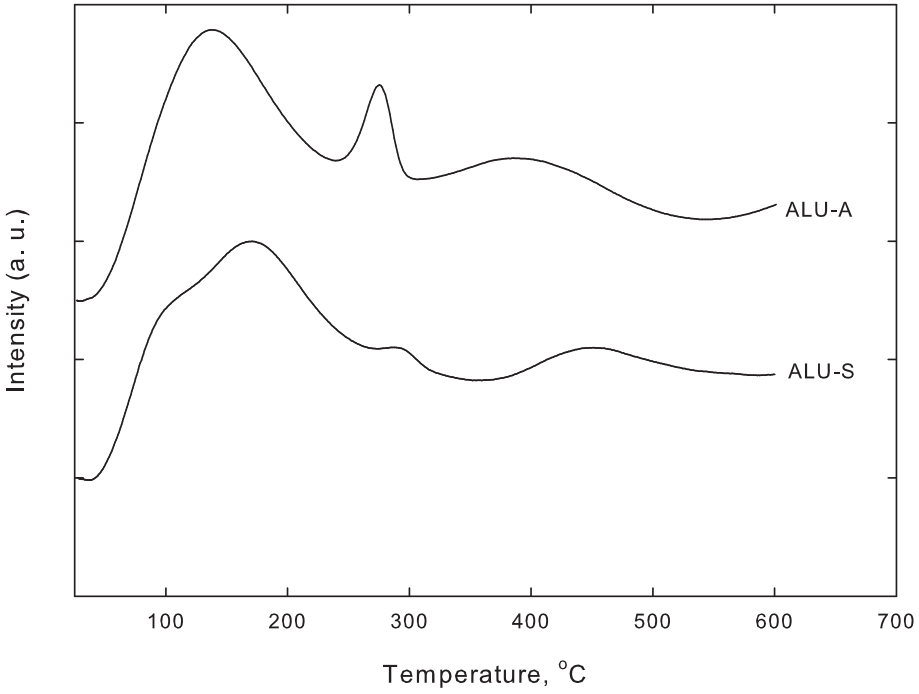

FIGURE 9.5: NH_3-TPD profiles for the prepared alumina samples

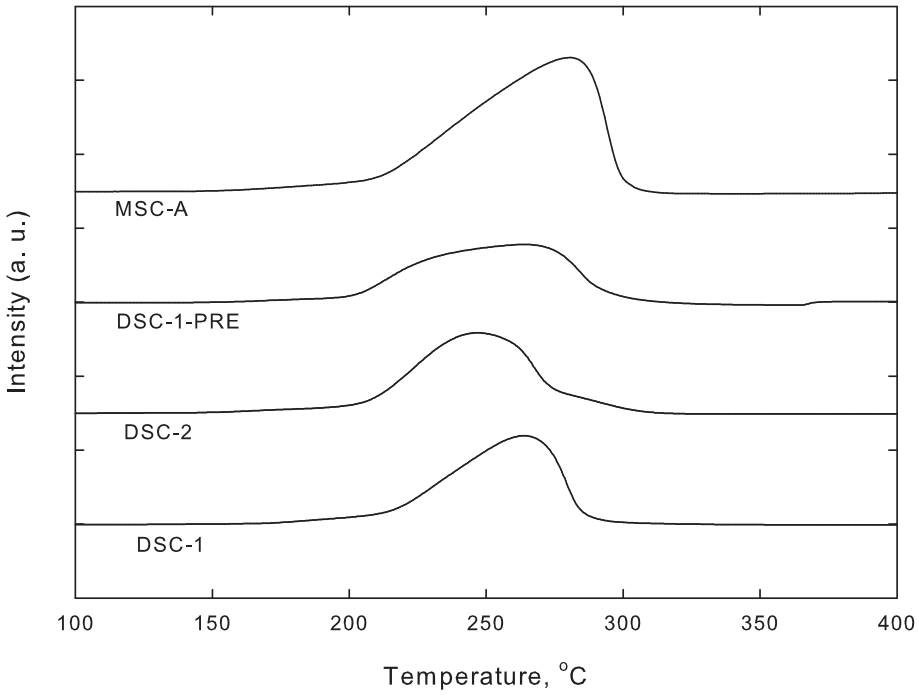

FIGURE 9.6: Temperature programmed reduction patterns for bi-functional catalysts

9.4 Performance of the catalysts

Four bi-functional catalysts were used in the high pressure DME synthesis reactor. The catalyst was loaded in the reactor and reduced at 190 °C in 5% H_2 in N_2 for eight hours. At the end of the reduction period, the reactor temperature and pressure were increased to 280 °C and 5 Mpa in N_2. The gas flow was then changed from N_2 to a H_2+CO. The H_2 to CO ratio for these runs was maintained at 1.45, since it was found the optimum H_2 to CO ratio for direct synthesis of DME from syngas, as shown in Chapter 8.

The conversion, yield and selectivity are defined by the following equations:

$$\%\text{CO conversion} = \frac{n_{CO,in} - n_{CO,out}}{n_{CO,in}} \times 100 \tag{9.1}$$

$$\text{DME yield} = \frac{2n_{DME}}{n_{CO,in}} \times 100 \tag{9.2}$$

$$\text{DME selectivity} = \frac{2n_{DME}}{n_{\text{CH}_4} + n_{\text{CH}_3\text{OH}} + n_{\text{CO}_2} + \sum m \times n_{\text{C}_\text{m}}} \times 100 \tag{9.3}$$

$$\text{CH}_3\text{OH selectivity} = \frac{n_{\text{CH}_3\text{OH}}}{n_{\text{CH}_4} + n_{\text{CH}_3\text{OH}} + n_{\text{CO}_2} + \sum m \times n_{\text{C}_\text{m}}} \times 100 \tag{9.4}$$

$$\text{CO}_2\text{ selectivity} = \frac{n_{\text{CO}_2}}{n_{\text{CH}_4} + n_{\text{CH}_3\text{OH}} + n_{\text{CO}_2} + \sum m \times n_{\text{C}_\text{m}}} \times 100 \tag{9.5}$$

$$\text{CH}_4\text{ selectivity} = \frac{n_{\text{CH}_4}}{n_{\text{CH}_4} + n_{\text{CH}_3\text{OH}} + n_{\text{CO}_2} + \sum m \times n_{\text{C}_\text{m}}} \times 100 \tag{9.6}$$

$$\text{C}_2\text{H}_6\text{ selectivity} = \frac{2n_{\text{C}_2\text{H}_6}}{n_{\text{CH}_4} + n_{\text{CH}_3\text{OH}} + n_{\text{CO}_2} + \sum m \times n_{\text{C}_\text{m}}} \times 100 \tag{9.7}$$

where n is the molar flow of the components in the feed (in) or product (out) streams.

Summary of the results obtained from the synthesis experiments are shown in Table 9.3. Maximum CO conversion was obtained for the DSC-1 catalyst, 67-70%. DSC-2 and DSC-M showed similar conversion. The CO conversion for DSC-1-PRE is very low compared to the other catalysts and was only 11-12%.

Similar trend was observed for DME yield. DSC-1 had the maximum yield with 36-40% of CO in the feed gas getting converted to DME. DSC-2 and DSC-M had similar but slightly lower DME yield than DSC-1. DSC-1-PRE had very low DME yield, only up to 1.5%.

Table 9.3: Conversion, activity and selectivity of the catalysts

Catalyst	CO conversion (%))	DME yield	Selectivity (%)				
			DME	Methanol	CO_2	CH_4	C_2+
DSC-1	67-70	36-40	55-59	∼0.02	34-36	4-5	∼1
DSC-2	58-61	32-36	55-59	∼0.02	34-38	4-6	∼1
DSC-M	55-60	33-37	60-65	∼0.02	32-34	3-4	∼1
DSC-1-PRE	11-12	1-1.5	9-12	∼0.20	55-56	24-26	6-7

The product selectivities are also presented in Table 9.3. For DSC-1, DSC-2 and DSC-M, major carbon products are DME and CO_2, with small amount of methane. DSC-M showed better DME selectivity than the other two catalysts. DSC-1-PRE proved not to be a good DME synthesis catalyst. Like the conversion and yield, DME selectivity was low, only 9-12%. Major carbon products are CO_2, and CH_4 and other hydrocarbons. The catalyst seems to favour methanation and water gas shift reaction more than methanol formation.

Results obtained from all these catalysts, show very low methanol selectivity, indicating that the dehydration component is effectively converting methanol to DME.

The synthesis experiments were continued up to 50 hours to see the effect of time on the performance on the catalysts. Changes in CO conversion are shown in Figure 9.7. For DSC-1 and DSC-1-PRE, CO conversion did not vary much with time. However, the conversion was very low for DSC-1-PRE. For DSC-2 and DSC-M, the conversion slightly varied with time. The trend shows that the conversion went down slightly with time. This indicates slow but gradual deactivation of the catalyst. As shown, the deactivation in lower for DSC-1. This slow deactivation is due to highly reducible condition, containing only CO and H_2, with the introduction of the feed gas after the reduction period. As soon as the feed gas was introduced, the catalyst surface interacts with the reducing gases, which gradually increases the copper crystallite size. However, this gradual degradation only happens during the initial period of feed gas introduction. The catalyst performance stabilises after a certain period of time. For Figure 99.7, it can be concluded that after approximately 40-50 hours the catalysts showed invariable CO conversion. To compare the performance of the prepared catalysts with the commercial catalyst mix, results obtained for M1A1 (defined in Table 8.2) catalyst is also shown in the Figure 9.7. After the initial stabilisation period, DSC-1, DSC-2 and DSC-M showed better or similar CO conversion compared to that of the M1A1 catalyst.

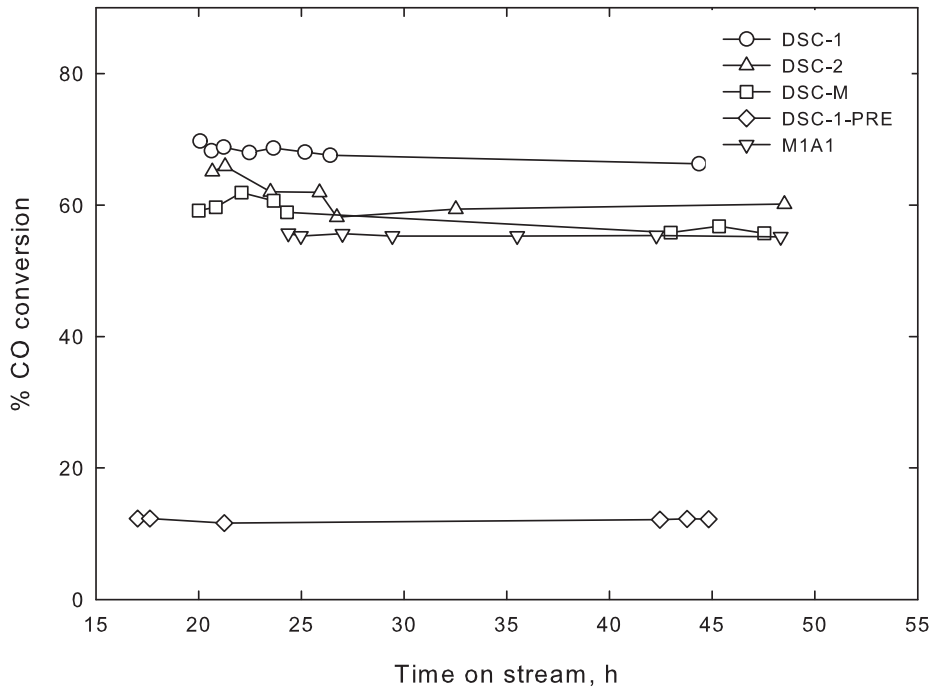

FIGURE 9.7: Effect of time on steam on CO conversion

Effect of time on DME yield and selectivity are shown in Figures 9.8 and 9.9. Trends are similar to that observed for the CO conversion. In terms of DME yield, DSC-1 and DSC-M showed slightly better performance than M1A1. On ther other hand, only DSC-1 showed better DME selectivity than M1A1, while the other catalysts had lower DME selectivity compared to M1A1.

Another mentionable observation about the commercial catalyst mix is that the variation in coversion, yield and selectivity were not seen after 25 hours on stream. The commercial catalyst therefore has shown to reach to its stabilised performance faster than the commercial catalysts.

In addition to the initial effect of the reducing environment on the catalyst, coke formation also occurs on the catalyst surface. All of these catalysts show presence of some strong acidic sites, as indicated by a small peak in the NH_3-TPD for the alumina samples. Hydrocarbons are formed at these sites as methanol/DME breaks further down. Coke is then formed by condensation of hydrocarbons on catalyst surface [2]. Coke can deposit on either acidic or metallic site. As the surface sites get covered, they are no longer accessible to the reacting gases.

The performance of the DSC-1-PRE catalyst was very different from the other catalyst. The reason is the preparation technique used for this catalyst. For DSC-1 and

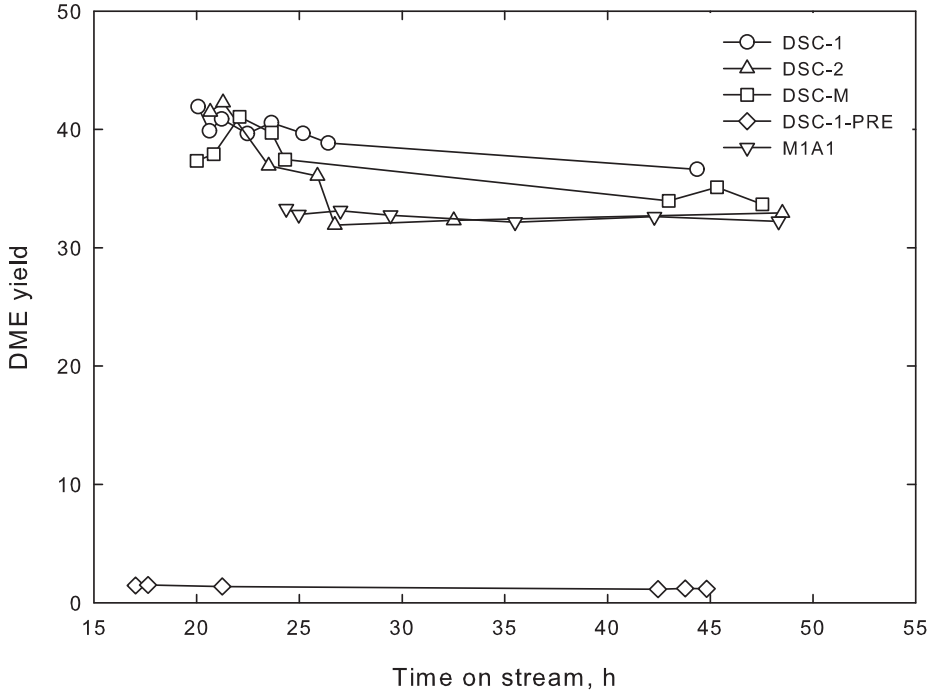

FIGURE 9.8: Effect of time on stream on DME yield

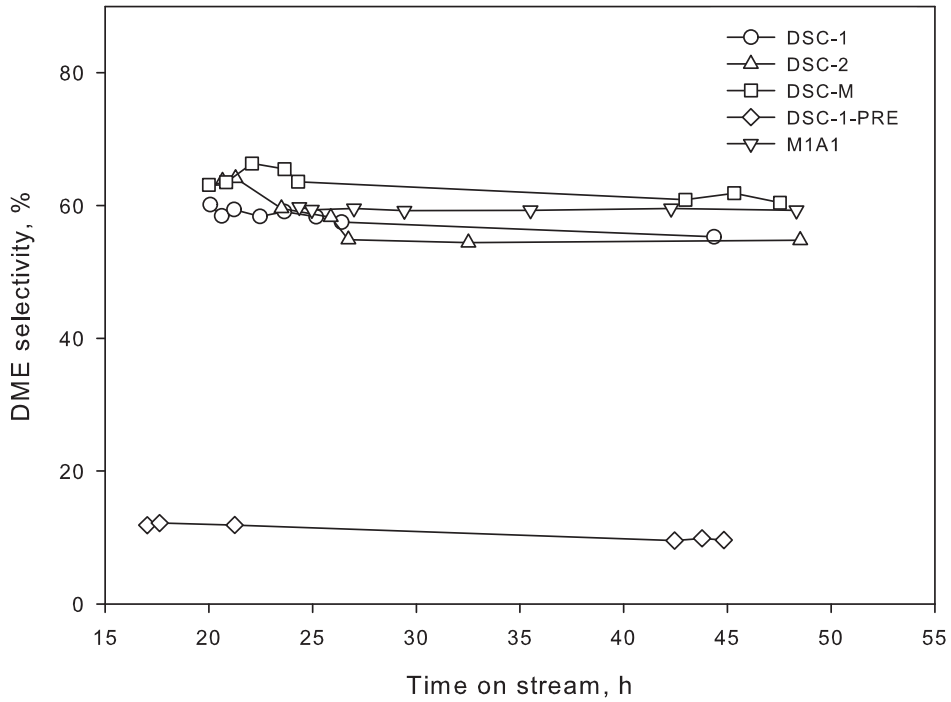

FIGURE 9.9: Effect of time on steam on DME selectivity

DSC-2, calcined alumina was impregnated with the mixed salts of Cu, Zn and Al. Therefore, the catalyst had both moderate acidic and methanol synthesis sites. On the other hand, for DSC-1-PRE boehmite was impregnated with precipitates from mixed nitrate salts. The resulted catalyst had stronger acidic sites and hence acted as a methanol reforming catalyst. The products are mostly hydrocarbons.

DSC-1 showed slightly better performance DSC-2. For this catalyst only the dehydration catalyst was different. ALU-A sample contained a mixture of γ and η-Al_2O_3. On the other hand, only γ-Al_2O_3 was present in ALU-S. Since η-Al_2O_3 is a better dehydration catalyst than γ-Al_2O_3 [3], better performance of the DSC-1 catalyst can be attributed to this feature of the catalyst.

Another noticeable feature is the correlation of the catalyst performance with the surface area of the catalyst. Both DSC-1 and DSC-2 had similar surface areas and showed almost identical performance. DSC-1-PRE, with a surface area of 159, showed the worst performance among all these catalysts. Since this variation in surface area is because of the alumina present in the catalyst, it can be concluded both the type and surface area of the dehydration component plays a very important role in the catalyst performance. In addition to the deactivation that occurs to the copper sites, alumina is responsible for coke formation. Also alumina is known to absorb moisture. Hence an alumina component with high surface area can hinder the CO conversion and DME yield, as observed for this catalyst.

DSC-M had slightly higher surface area than these two catalysts and also showed similar performance. Since DSC-M is prepared by physical mixing, the number of metallic sites next to acidic sites is less than that for the impregnated catalysts. Hence, the effect of higher surface area did not show the same trend for this catalyst. At the same site, presence of η-Al_2O_3 also aided to the better catalyst activity.

9.5 Effect of space velocity

Figure 9.10 shows effect of space velocity on the CO conversion and DME yield and DME selectivity for DSC-1 catalyst, at 280°C and 5 Mpa. When the space velocity was increased from 2000 to 4400 ml/g_{cat}.h CO conversion decreased from 68% to 53%. Convesion was 47% when the space velocity was 7350 ml/g_{cat}.h.

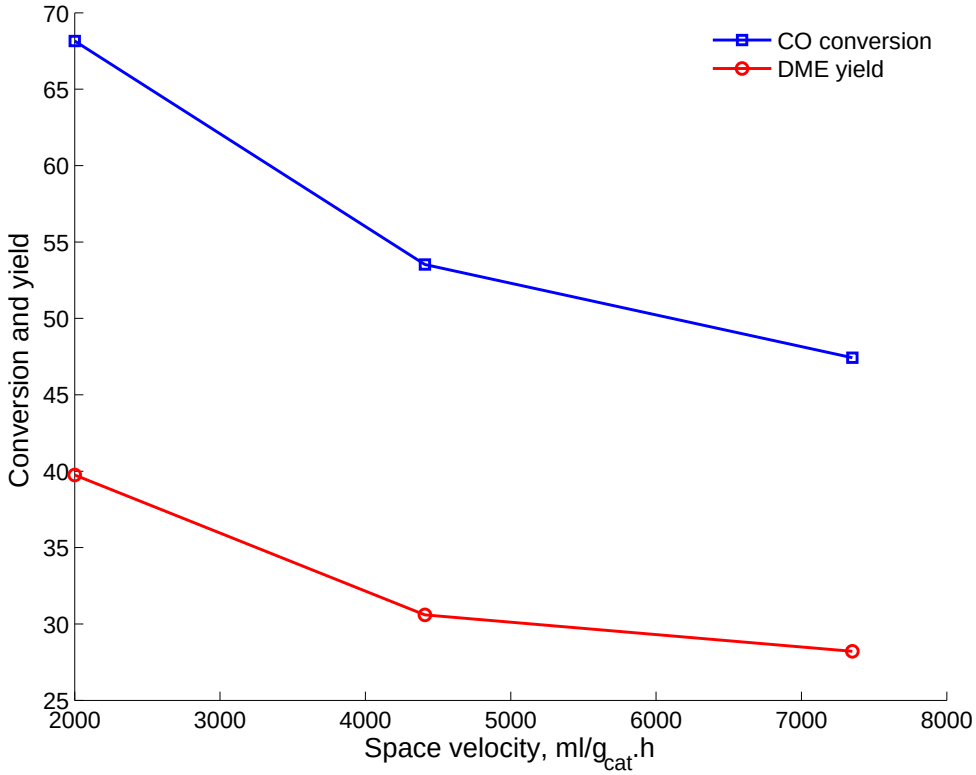

FIGURE 9.10: Effect of space velocity on CO conversion and DME yield

A similar trend was observed for DME yield, For 2000, 4400 and 7350 ml/g_{cat}.h space velocity, 40, 31 and 28% of carbon (in the feed) was converted to DME. For both conversion and yield, the space velocity has an asymptotic effect.

Figure 9.11 shows the effect of space velocity on DME, CO_2 and CH_4 selectivity. Changes in space velocity did not show noteworthy changes in DME or CO_2 selectivity. DME and CO_2 are produced from the methanol dehydration and water gas shift reactions. Both these reactions are desirable for the synergy of the reactive system. Even though the conversion went down with sapce velocity (Figure 9.10), the selectivity remained almost unchanged. On the other hand, CH_4 is a secondary and undesirable product, formed either by direct hydrogenation or by further break down of DME/methanol. Therefore, when space velocity was decreased CH_4 selectivity went down, as the reactant gases had to spend less time in the reactor. The CH_4 selectivity went down from 4.75 to 1.53 when the space velocity increased from 2000 to 4400 ml/g_{cat}.h. A further increase in space velocity showed little variation in the CH_4 selectivity.

The observations made on the conversion, yield and selectivity are consistent with previously reported results [4].

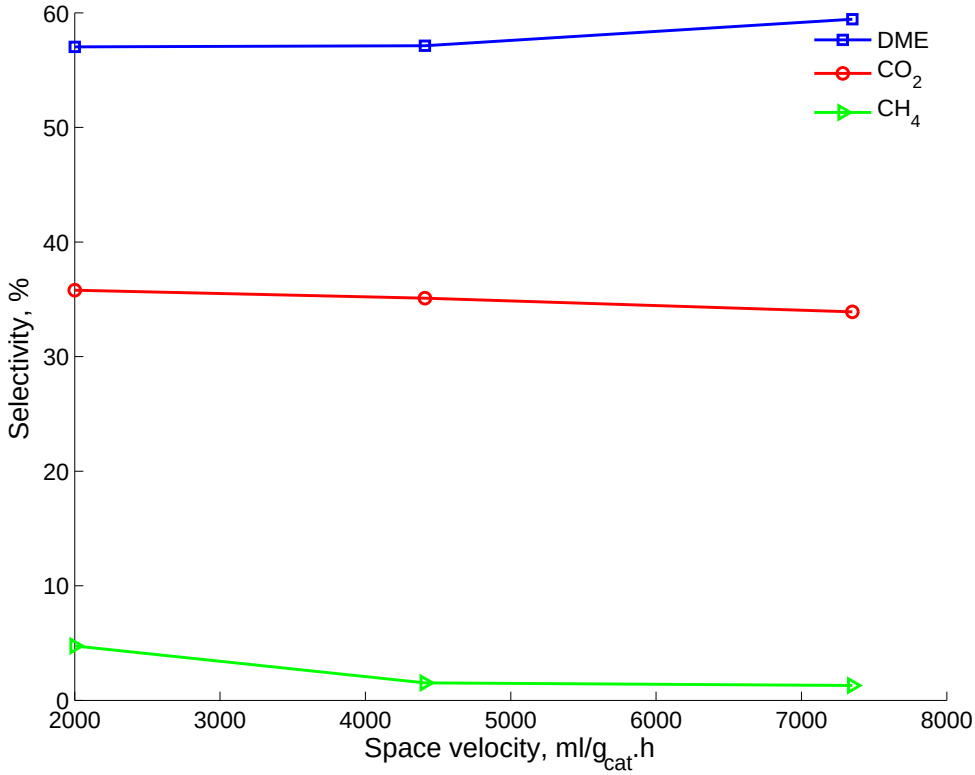

FIGURE 9.11: Effect of space velocity on selectivity

9.6 Conclusions

Four bi-functional catalysts were prepared for direct DME synthesis. Three of the catalysts, namely DSC-1, DSC-2 and DSC-M, showed better or similar performance than the M1A1 commercial catalyst mixture in terms of conversion, yield and selectivity. The performance of the catalysts was found to be stable with time on stream. DSC-1-PRE catalyst performed poorly as a bi-functional catalyst with mostly hydrocarbons as the carbon products. The catalysts used for the current study can be ranked according to their performance as follows:

$$\text{DSC-1} > \text{DSC-M} > \text{M1A1} > \text{DSC-2} >> \text{DSC-1-PRE} \tag{9.8}$$

The CO conversion and DME yield was lower for higher space velocities as the contact time between the catalyst and the reactants were less. The selectivity of the hydrocarbon bi-product, especially CH_4, also decreased with increasing space velocity.

9.6.1 Further work

Victorian brown coal syngas contains sulphur species: H_2S, COS. The effect of the sulphur poisoning on the CO conversion, and DME yield and selectivity will be evaluated. Using FTIR and XRD the possibility of formation of surface species on the catalyst surface will be investigated.

References

[1] Hansen JB, Nielsen PEH, 2008, *In:* Handbook of heterogeneous catalysis, 2920–2949, Wiley-VCH, Weinheim

[2] Aguayo AT, Ereña J, Sierra I, Olazar M, Bilbao J, 2005, Catalysis today, **106**: 265–270

[3] Seo CW, Jung KD, Lee KY, Yoo KS, 2008, Industrial & Engineering Chemistry Research, **47**: 6573–6578

[4] Sofianos AC, Scurrell MS, 1991, Industrial & engineering chemistry research, **30**: 2372–2378

Chapter 10

Sulphur Poisoning of the Catalysts

10.1 Introduction

As shown in Table 6.1 and 7.1 Victorian brown coal contains sulphur, chlorine and nitrogen in small amounts. The fate of these species depends on the type of thermal treatment of coal. During gasification, sulphur in coal is converted to H_2S and COS. Chlorine usually forms hydrogen chloride while ammonia and hydrogen cyanide are the nitrogen containing species. Concentrations of sulphides (H_2S+ COS), NH_3 and HCl in the Victorian brown coal syngas can be up to 100, 1370 and 10 ppm, respectively [1]. HCN concentration is usually 5 ppm or below [1].

All these gaseous species evolving from sulphur, chlorine and nitrogen are considered as pollutants. However, not all of them are responsible for catalyst poisoning. HCN was found to be non-poisonous to methanol synthesis catalyst [2]. NH_3 is responsible for moderate reversible poisoning [3]. Sulphur and chlorine containing species are severe poisons. Among them HCl is relatively easier to remove by quenching the gas and the HCl vapour concentration can be rapidly reduced to less than 1 ppmv [4]. Therefore, the sulphur species (e.g. H_2S and COS) are considered as major threats to the activity and stability of the catalysts used for syngas to DME synthesis.

Preliminary studies on the effect of sulphur exposure on the catalysts are discussed in this chapter. The samples were exposed to sulphur containing gases for up to 10 hours. The poisoned catalysts were then characterised using IR and X-ray diffraction spectroscopy.

10.2 Preparation and treatment of the catalyst samples

A bi-functional catalyst (DSC-1) was used to study the effect of sulphur containing gases on the catalyst. A small quartz reactor was used for the preparation of the samples. For each experiment, ca. 100 mg of catalyst was loaded in the quartz reactor. The catalyst was then reduced at 190 °C with 5% H_2 in N_2. The quartz reactor was then heated to 280 °C in an inert environment (e.g. N_2). When the temperature was achieved, the gas was changed to H_2S/N_2 (containing 102 ppm H_2S) or COS/N_2 (containing 530 ppm COS). A space velocity of 2000 mL.g_{cat}.h^{-1} was maintained throughout the experiment. The catalyst samples were treated with these gases for different time durations (e.g. 1, 5 and 10 hours). The sulphur exposure experiments were carried out at ambient pressure. At the end of exposure period, the reactor was cooled down and the samples were collected for characterisation.

10.3 Infra-red transmission spectroscopy using synchrotron radiation

The IR measurement experiments were carried out using the Infrared Microspectroscopy (IRM) Beamline at Australian Synchrotron, Melbourne, Australia. The IRM beamline combines the high brilliance and high collimation of the synchrotron beam with a Bruker V80v FTIR spectrometer. A CaF_2 window was used for these experiments. The measurements were done at room temperature.

In a typical experiment 0.2 mg sample of < 100 μm was used for the measurement. A narrow-band, high sensitivity, liquid nitrogen cooled Mercury Cadmium Telluride (MCT) detector was used for measurements. Data collection was carried out at a wavelength range of 3800-900 cm^{-1} with a 4 cm^{-1} resolution.

IR spectra obtained for the H_2S and COS treated samples are shown in Figures 10.1 and 10.2. . For these samples, the obtained spectra are featureless. The samples show absorption band at the higher end (3500-3200 cm^{-1}) which has resulted from $-OH$ stretch. The absorption band between 2000-1400 cm^{-1} was due to COO^- and C=O strech [5]. The CO_2 doublets resulted from the gas phase CO_2 were also observed at around 2350 cm^{-1}. Another absorption band was observed between 2970-2950 cm^{-1}.

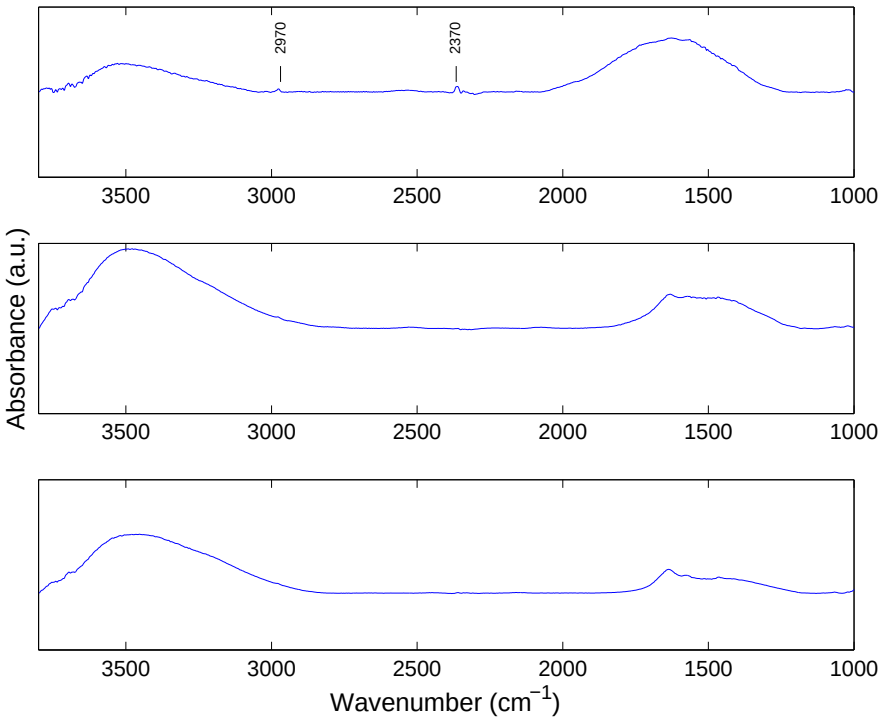

FIGURE 10.1: Infra-red spectra obtained for H_2S treated gases (Bottom- 1 hour; middle - 5 hours; top- 10 hours)

When copper-based catalyst samples are treated with H_2S or COS the sulphur compounds react with copper and zinc forming Cu_2S and ZnS. For ZnS, the fingerprint absorption band is at 300 cm^{-1} which is outside the current measurement range. Weak bands can also be observed at 720, 1350, 1730 and 2350 cm^{-1} [6]. The peak at 720 is also out of the measurement range, while the rest are either masked by the atmospheric CO_2 or adsorbed water bands. Hence, the FTIR measurements were not conclusive to identify ZnS on the catalyst surface.

Cu_2S only gives weak absorption bands at 960, 1340 and 2950 cm^{-1} [6]. The first two bands for this case are expected to be masked by the moisture bands. The obtained spectra showed a peak at around 2960-2970 cm^{-1}. Since the catalyst consists of inorganic species, presence of C-H groups at this location can be ruled out. The absorption band observed here can be an indication of the formation of Cu_2S.

10.4 X-ray diffraction

X-ray diffraction of the H_2S treated samples are shown in Figure 10.3.

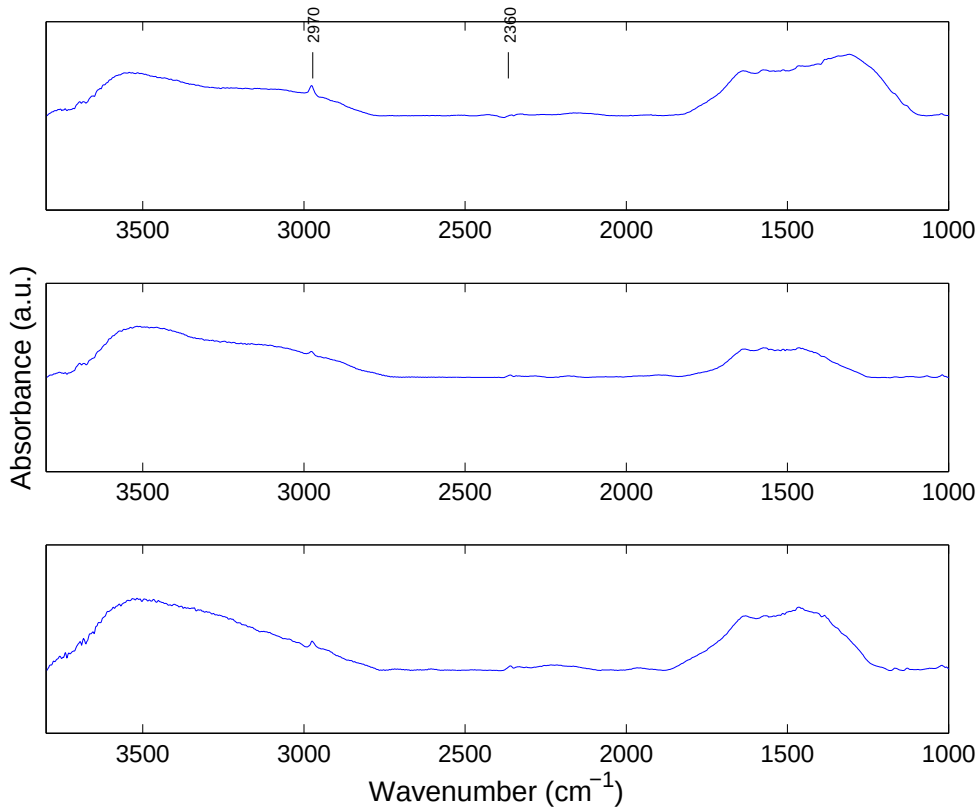

FIGURE 10.2: Infra-red spectra obtained for COS treated gases (Bottom- 1 hour; middle -5 hours; top- 10 hours)

Freshly reduced catalyst samples contain three phases only: Cu, ZnO and γ-Al_2O_3. When the catalysts were treated with H_2S, both copper and zinc oxide reacted to form Cu_2S and H_2S through the following reactions:

$$2Cu + H_2S \longrightarrow Cu_2S + H_2 \tag{R10.1}$$

$$ZnO + H_2S \longrightarrow ZnS + H_2O \tag{R10.2}$$

The 1hour treated sample did not show presence of ZnS, but confirmed presence of Cu_2S. In the 5-hour and 10-hour samples ZnS was also observed in addition to Cu_2S. The observed zinc sulphide is sphalerite (β-ZnS), which is the stable form of zinc sulphides . Presence of these phases indicates the severity of the deactivation caused in presence of H_2S. It reacts with the active catalyst component (e.g. copper). At the same time, it also destroys the ZnO support of the catalyst

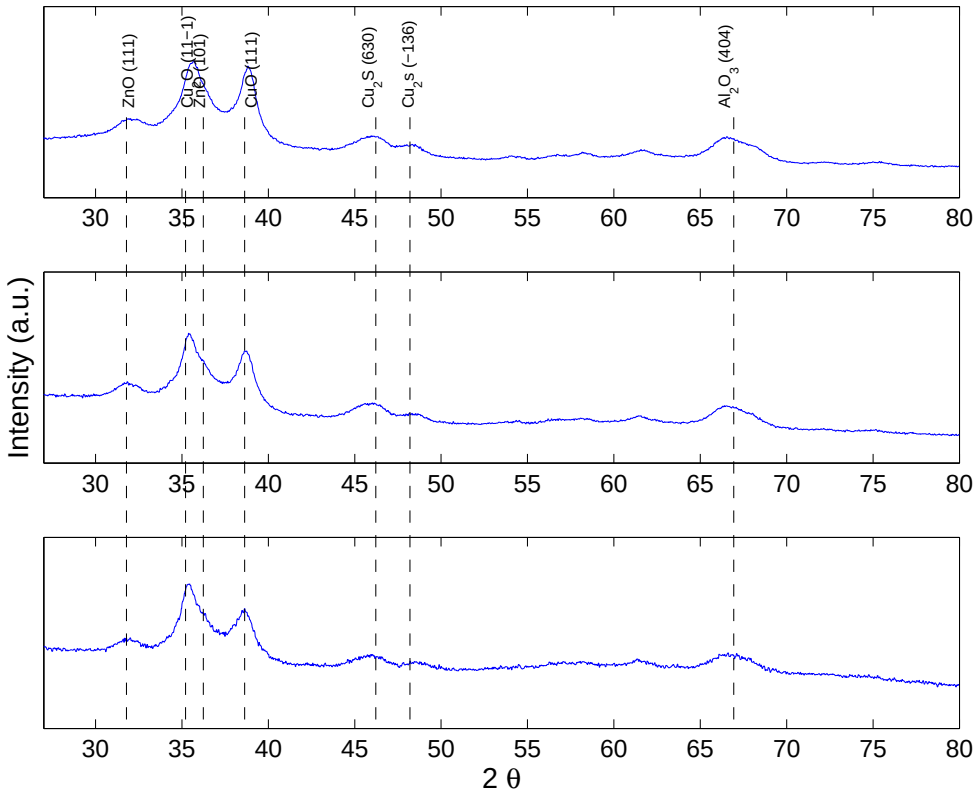

FIGURE 10.3: IXRD of H_2S treated samples ((Bottom- 1 hour; middle - 5 hours; top- 10 hours)

Diffraction patterns for COS treated samples are shown in Figure 10.4. The samples showed presence of only one sulphide. Cu_2S is formed through the following reaction:

$$2\,Cu + COS \longrightarrow Cu_2S + CO \tag{R10.3}$$

Zinc oxide does not directly react with COS [3] and hence zinc sulphide was not observed in these samples. However, in real life synthesis conditions (with CO and H_2 in the feed gas), the following reactions will eventually lead to the formation of zinc sulphide:

$$Cu_2S + H_2 \longrightarrow 2\,Cu + H_2S \tag{R10.4}$$

$$ZnO + H_2S \longrightarrow ZnS + H_2O \tag{R10.5}$$

As shown by the diffraction studies, both COS and H_2S causes net deactivation of the catalysts by sulphur deposition on copper and zinc sulphide formation. It was found, empirically, that the gas-phase sulphur concentrations should be kept below 1 ppmv and preferably below 0.1 ppmv [7].

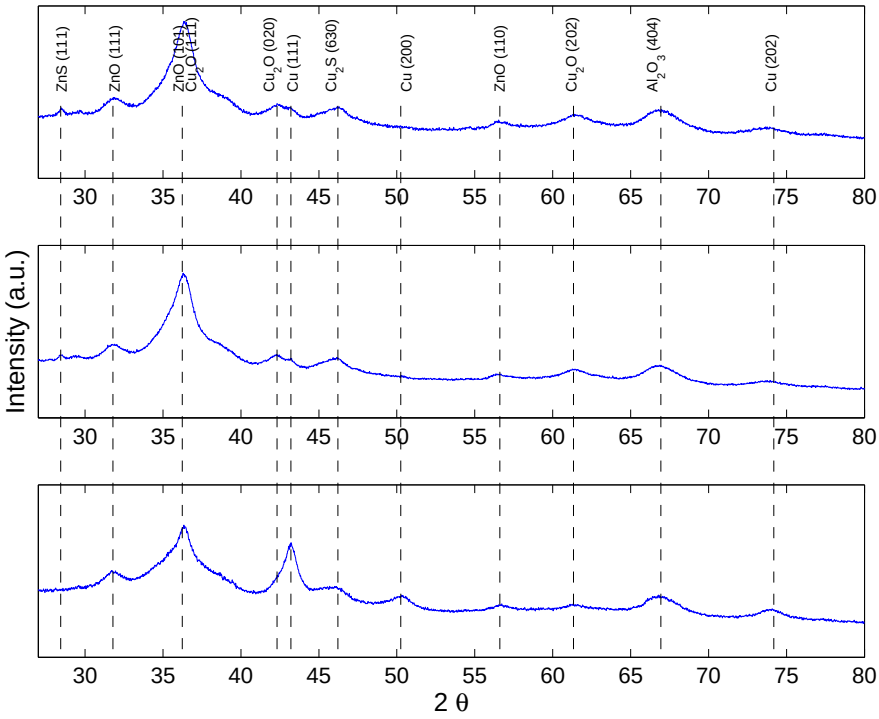

FIGURE 10.4: XRD of H_2S treated samples ((Bottom- 1 hour; middle - 5 hours; top- 10 hours)

Regeneration of deactivated copper catalysts is not practically viable. The required temperature to remove adsorbed sulphur from the spent catalyst at a reasonable time is well above normal operating temperature and results in sintering of the catalyst. Hence, it is essential to remove the sulphur containing gases before feeding to the synthesis reactor.

10.5 Effect on yield, conversion and selectivity

To study the effect of H_2S poisoning on the catalyst performance, freshly reduced DSC-1 catalyst was exposed to 102 ppm H_2S in N_2 for 10 hours. The space velocity was maintained at 2000 ml/g_{cat}.h. Then, the syngas of the same space velocity was introduced in the reactor. The effluent gases from the reactor was analysed as usual. This experiment was continued for 6 hours.

The performance of the poisoned catalyst is shown in Table 10.1. Performance of the unpoisoned DSC-1 (for first 6 hours) catalyst is also listed here.

Table 10.1: Performance of the poisoned and unpoisoned DSC-1 catalyst

	CO conversion %	DME yield %	DME selectivity %
Poisoned	55-60	30-34	55-56
Unpoisoned	68-70	40-41	58-60

The poisoned catalyst showed lower conversion and DME yield. This has resulted from the irreversible poisoning of the active component (Cu) and the support (ZnO). The poisoned catalyst had less active sites and hence lost some of its activity, even after 10 hour exposure to the H_2S containing gas. Changes in the selectivity was not significant. Poisoning has effect on the number of active reaction sites, but does not affect the performance of unpoisoned site. Therefore, the selectivity for both the poisoned and unpoisoned catalysts were similar.

10.6 Discussion on other catalyst poisons

Nitrogen containing species, such as HCN, CH_3NH_2 and CH_3CN, are found not to cause deactivation of the catalyst. Very little or no cyanide was deposited on the exposed samples, even when the level of exposure was extremely high [2]. Poisoning by ammonia has been found to be reversible [3].

Chlorides and other halides cause severe deactivation of the copper based catalysts. When exposed to halide gases, copper and zinc react with the gas phase forming halides. Halides have lower melting point than copper, and zinc oxide [7, 8]. Therefore, small amount halides are sufficient to result in mobile species leading to rapid sintering. Also, mobility of copper (I) chloride exacerbates sulphur poisoning of copper [7]. The HCl limit to avoid poisoning is more severe than thay of H_2S, and is of the order of 1 ppbv [9].

Iron and nickel carbonyls, generated within the synthesis loop from the steel, are also considered as catalysts poison. The metal carbonyls decompose in metal forms over the catalyst and block the active catalyst sites. The recommended level of Fe and Ni carbonyls are 0.005 ppmv [10].

10.7 Concluding Remarks: Practical implication for Victorian brown coal syngas

Victorian brown coal syngas contains sulphur species such as H_2S and COS up to 100 ppm. This is far above the recommended sulphide concentration. When the catalyst samples were treated with these gases, sulphur was found to condense on the catalyst surface forming Cu_2S and ZnS. Formation of sulphides causes deactivation by permanently blocking the active catalyst sites. Hence, gas cleaning is necessary to reduce the sulphur species composition below the recommended level by using a catalytic bed with can hydrolyse COS producing H_2S and CO_2. H_2S can then be removed using any of the available acid gas removal technologies.

In addition to acid gas removal, a guard bed containing appropriate chemicals can be used before the feed gas reaches the main catalyst bed. Zinc oxide beds have been used for desulphurization while alkalised alumina has been used in the guard for removal of chloride gases [11]. This protective measure will make sure that the synthesis catalyst bed is protected from deactivation from poisoning by sulphur or chlorine containing species.

10.7.1 Further work

The current study was carried out on a small scale and only for H_2S and COS. Further studies can be conducted for other impurities (e.g. HCl, NH_3) present in Victorian brown coal syngas. The maximum tolerance for these impurities for the catalysts should be determined by performing experiments with varying concentrations of polluting gases. Also, the effect of poisoning on conversion, yield and selectivity will provide more in-depth knowledge for brown coal to DME production plants.

References

[1] Bhattacharya S, Beaupeurt I, Topping B, 2006, *Gasification Tests in a Pressurised Fluidised Bed Gasifier-Process Development Unit Using Air/Oxygen and Steam as Reactants*

[2] Quinn R, Dahl TA, Toseland BA, 2004, Applied Catalysis A: General, **272**: 61–68

[3] Hansen JB, Nielsen PEH, 2008, *In:* Handbook of heterogeneous catalysis, 2920–2949, Wiley-VCH, Weinheim

[4] Dou B, Wang C, Chen H, Song Y, Xie B, Xu Y, Tan C, 2012, Chemical Engineering Research and Design, **90**: 1901–1917

[5] Socrates G, 2004, Infrared and Raman Characteristic Group Frequencies: Tables and Charts. 3rd ed., Wiley, New York

[6] Nyquist RA, Kagel RO, 1997, The handbook of infrared and raman spectra of inorganic compounds and organic salts: Vol. 4, Infrared spectra of inorganic compounds. Academic Press, San Diego

[7] Twigg MV, Spencer MS, 2003, Topics in Catalysis, **22**: 191–203

[8] Campbell JS, 1970, Industrial & Engineering Chemistry Process Design and Development, **9**: 588–595

[9] Twigg MV, Spencer MS, 2001, Applied Catalysis A: General, **212**: 161–174

[10] Kung HH, 1992, Catalysis today, **11**: 443–453

[11] Woolcock PJ, Brown RC, 2013, Biomass and Bioenergy, **52**: 54–84

This page intentionally left blank

Chapter 11

Conclusions and Recommendations

This is the first ever study on DME synthesis from fuel gas produced via gasification of Victorian brown coal. This study has generated considerable information regarding gasification temperature, need for gas cleaning, catalyst property, and most importantly gas conversion, DME yield and DME selectivity. Findings from this study outlines areas of future research for liquid fuel production from brown coal and brown coal derived CO_2.

11.1 Conclusions

Conclusions drawn from the process simulation, coal gasification and DME synthesis experiments are discussed below:

11.1.1 Equilibrium modelling and process simulation

Thermodynamic calculations were performed for synthesis of DME from CO and H_2. CO and CO_2 hydrogenation are non-spontaneous reactions at temperatures above 150 °C, while water gas shift and methanol dehydration reactions occur with spontaneity.

These reactions are exothermic. Also the hydrogenation reactions show reduction in number of gas molecules. Therefore, high pressure and low temperature would increase the equilibrium yield.

The DME synthesis reactor can be operated at low temperatures as the rate of reaction is insignificant. A process model was developed that includes drying and gasification of Victorian brown coal, and DME production from coal syngas. Low temperature gasification at 900 °C was found to produce syngas with appropriate H_2 to CO ratio

for DME synthesis. Simulation results showed a maximum DME yield for a H_2 to CO ratio of 0.81 at the gasifier outlet and 1.41 at the DME reactor inlet.

Considering the base process condition for the simulation study (Coal drying with steam; Gasification temperature 900 °C, pressure 30 bar; DME synthesis temperature 240 °C, pressure 60 bar) the overall process efficiency is ∼32% considering energy penalty for CO_2 separation. The net CO_2 generation is 2.91 kg/ kg of DME or 0.37 tonnes/MW.

The simulation studies provided the basis for the gasification at low temperature and use of catalyst for complete conversion.

11.1.2 Gasification of Victorian brown coal

Gasification of Victorian brown coal from Morwell mine was studied using a thermogravimetric analyser (TGA) and an entrained flow reactor (EFR).

Kinetics of the gasification of char was studied using TGA. The char was prepared in the TGA at 1000 °C in a 100% N_2 environment. The results were fitted to grain model and random pore model. Random pore model fitted the experimental data better than the grain model. The activation energy for the Morwell coal was calculated to be 189.05 kJ/mol. The reaction order was 0.34 with respect to CO_2 concentration. Although, Morwell coal is rich in calcium, addition of 2% Ca to the parent coal improved gasification reactivity. The low surface area of the Ca-loaded Morwell coal char had higher activation energy (204.53 kJ/mol). However, inclusion of Ca in the coal increased the number of reaction sites, as indicated by the pre-exponential factor, and hence increased the reactivity.

The results also indicated that the effect of minerals is insignificant at 1000 °C or above, as the kinetics is no longer chemically controlled. Therefore, catalytic gasification would be only beneficial at temperatures below 1000 °C.

Pyrolysis experiments were carried out in the EFR to prepare char. gasification Pyrolysis in an EFR, shows that the major pyrolysis gas products are CO, H_2 and CH_4. The tar yield significantly decreased with increasing temperature. The char gasification results show that complete char conversion was not possible at 1000 °C with 20% CO_2 as the gasifying agent. EFR gasification experiments were not performed on the catalyst loaded coal samples.

11.1.3 DME synthesis

Initial screening experiments of DME synthesis were performed using commercial catalysts (one methanol synthesis and one methanol dehydration). Bi-functional catalysts were prepared by physically mixing these two catalysts in different proportions.

Three catalysts (methanol synthesis, methanol dehydration and bi-functional catalyst) were studied in situ using synchrotron radiation XRD. The copper crystallite size increased slightly as the temperature was increased from 250 to 300 °C. However, at temperature above 300 °C there was a significant increase in the copper crystallite size. The change in the copper crystallite size with temperature was greater for the bi-functional catalyst than that of the methanol synthesis catalyst. This indicates that the deactivation is faster for the bi-functional catalysts than the methanol synthesis catalyst. At temperatures above 300 °C, phase mobility and thermal sintering of the catalysts were observed. Therefore, the synthesis of DME should be carried out below 300 °C to ensure longer catalyst life.

When the DME synthesis experiments were carried out at low temperature, a low CO conversion and high DME selectivity were observed. At lower temperatures, side reactions were not significant and hence showed high DME selectivity. Both the CO conversion and DME yield increased with increasing temperature. However, DME selectivity reduced as rate of side reactions also increased. The optimum reaction temperature was found to be 280 °C.

A factorial experimental design was used to study the effect of catalyst composition and H_2 to CO ratio. A H_2 to CO ratio of 1.45 gave the maximum DME yield. This is very close to the H_2 to CO ratio obtained from the simulation, which was 1.41. A catalyst with 58% methanol synthesis component also gave the maximum DME yield.

Four bi-functional catalysts were prepared using physical mixing and co-precipitation impregnation. Three of these catalysts performed similar or better than the commercial catalysts when tested in the DME synthesis reactor.

An increase in space velocity (2000-7350 ml g_{cat} h^{-1}) showed a decrease in CO conversion (68% to 47%) and DME yield (40% to 28%) . However, the effects on DME and CO_2 selectivity were insignificant.

Sulphur containing gases (e.g. 500 ppm COS and 103 ppm H_2S) caused deactivation of the catalyst as both of them reacted with copper and/or zinc oxide. The deactivation was indicated by reduction in CO conversion and DME yield by 12% and 15%, respectively, after 10 hour exposure to H_2S.

The performance of the DSC-1, prepared using co-precipitation impregnation, catalyst was better than the other prepared catalysts. Performance of this catalyst was also better than the commercial catalyst mixtures in terms of CO conversion (67-70% vs 58-60%) and DME yield (36-40% vs 35-38%).

11.2 Practical Implications

This is an exploratory research project assessing the production of DME from Victorian brown coal following gasification. The practical implications for the current study are as follows:

- Process simulation provides an insight into the overall production train starting from as-mined coal to DME. The process simulation results were used to set the conditions of the initial experiments.
- The kinetics of non-catalytic and catalytic gasification of char were evaluated. This information can be used in the gasifier design.
- The tar yield considerably dwindled as the gasification temperature was increased. This indicates that tar generation will not cause any mentionable operating issues for such a process.
- The optimum operating conditions for converting syngas to DME has been identified, using commercial catalyst mixtures. Maximum DME yield was obtained for a H_2 to CO ratio of 1.45 and at 280 °C.
- Sulphur containing gases such as H_2S and COS rapidly deactivates the catalyst. Therefore, removal of sulphur species and use of guard bed are necessary to ensure longer catalyst life.

The study as a whole shows that the production of DME can be accomplished using Victorian brown coal. Some of the key issues were addressed. As this is more of an

exploratory work, this also identifies the focal points for future research in the next section.

11.3 Recommendations for future work

Based on the findings of this study, the following suggestions were made for future work:

- Current synthesis studies did not provide DME synthesis kinetics for the catalyst. The diameter and the length of the reactor used for the current study is not suitable for kinetic study. A smaller scale reactor would permit determination of the kinetic parameters that can be used for reaction design.
- During this study, prepared catalysts included similar methanol synthesis component and only the dehydration component was varied. Changes in the methanol synthesis component should be incorporated in future studies to study the effect on conversion and yield. Effect of small additives (e.g. Pd) should also be studied. Different solid acids should also be assessed as the dehydration component.
- Theoretical catalyst design techniques such as density functional theory (DFT) calculations can be employed for further development of the novel catalysts.
- The current study only focused on synthesis from CO and H_2 mixture. Industrial syngas also contains CO_2. Effect of CO_2 containing syngas on the performance of the catalysts shall be assessed. Also, the synthesis of DME from brown coal derived CO_2 and H_2 with the current catalysts and developed catalysts can be studied.
- As brown coal syngas contains polluting species (e.g. H_2S, COS, HCl), also known for their capability to poison the catalysts, some experiments with H_2S and COS were performed. Formation of surface species and decrease in the yield and conversion indicates rapid catalyst deactivation. Therefore, gas cleaning would be critical for the catalyst's active life and the process economics. The critical concentration of this gaseous species could not be determined during this study. Further experiments to determine the exposure limit and the deactivation kinetics are necessary. This would also set the extent of syngas cleaning for Victorian brown coal syngas.

- Process economics of direct synthesis of DME from Victorian brown coal, including drying, gasification and synthesis steps, needs to be evaluated.

Appendix A

List of Publications

A.1 Journal Articles

1. Bhattacharya S, Kabir KB and Hein K, Dimethyl Ether Synthesis from Victorian Brown Coal Through Gasification - Current Status, and Research and Development Needs, Progress in Energy and Combustion Sicence, 2013. 39: pp. 577-605

2. Kabir KB, Hein K and Bhattacharya S, Process modelling of Dimethyl Ether (DME) production from Victorian brown coal - integrating drying, gasification and DME synthesis processes, Computers & Chemical Engineering, 2013. 48: pp. 96-104

3. Kirtania K, Tanner J, Kabir KB, Rajendran S and , Bhattacharya S, In situ synchrotron IR study relating temperature and heating rate to surface functional group changes in biomass, Bioresource Technology, 2014. 151: pp.36-42

4. Kabir KB, Maynard-Casely HE and Bhattacharya S, In situ studies of structural changes in DME synthesis catalyst with synchrotron powder diffraction, Submitted to Applied Catalysis A

A.2 Manuscripts in Preparation

1. Tanner J, Kabir KB and Bhattacharya S, Low temperature entrained flow pyrolysis and gasification of a Victorian brown coal

2. Kabir KB and Bhattacharya S, Optimisation of direct DME synthesis catalyst using factorial experimental design

3. Kabir KB and Bhattacharya S, Kinetics of catalytic gasification of Morwell brown coal

4. Kabir KB, Tanner J, Xu T, Dayal S and Bhattacharya S, Review on Victorian brown coal gasification: Research & development needs

A.3 Conference Papers

1. Islam MS, Kabir KB, Wijayanta AT, Nakaso K, Fukai J and Bhattacharya S, Investigation of Brown Coal Char-CO_2 Gasification in a Laboratory Scale Drop Tube Furnace, AIChE Annual Meeting, 2012, Pittsburgh, USA.

2. Kabir KB, Moore J, Hein K and Bhattacharya S, Low temperature pyrolysis of a Victorian brown coal, 2nd Annual Monash University Chemical Engineering Conference, 2012, Melbourne, Australia

3. Kabir KB, Grills G, Walter J and Bhattacharya S, Dimethyl ether production from Victorian brown coal and biomass: A comparative process modelling study, International Conference on Coal Science & Technology (ICCS&T), 2011, Oveido, Spain

4. Kabir KB and Bhattacharya S, Dimethyl ether production from gasification of victorian brown coal - process model and related preliminary experiments, Chemeca2011, Sydney, NSW, Australia

5. Kabir KB and Bhattacharya S, A Process Model for DME production from Victorian Brown Coal: Integration of Drying, Gasification and DME synthesis Processes. 2011, 36th International Technical Conference on Clean Coal & Fuel Systems, Clearwater, Florida, USA